Polyoxometalate as Building Units to Design Functional Metal Organic Hybrid Materials

Chandan Kumar Dey

AcSIR

Academy of Scientific & Innovative Research

Polyoxometalate as Building Units to Design Functional Metal Organic Hybrid Materials

A Thesis Submitted
in Partial Fulfillment of the Requirements
for the degree of

DOCTOR OF PHILOSOPHY
by
Chandan Dey

Dr. Rahul Banerjee
(Supervisor)

Physical Chemistry Division

CSIR-National Chemical Laboratory

Pune-411008, India

Researcher Information

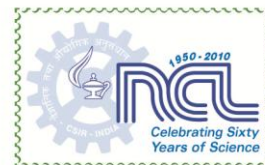|	
Name	Chandan Kumar Dey
Date of Birth	1983-05-04
Roll	10893
AcSIR Roll	10CC11J26025
Division	Physical & Materials Chemistry
Faculty	Chemical Sciences
Date of Joining	2009-01-01
Supervisor	Dr. Rahul Banerjee
Research Topic	Polyoxometalate as Building Units to Design Functional Metal Organic Hybrid Materials

CERTIFICATE

It is certified that the work **"Polyoxometalate as Building Units to Design Functional Metal Organic Hybrid Materials"** submitted to Academy of Scientific & Innovative Research (AcSIR) for the degree of Doctor of Philosophy was carried out by **Chandan Kumar Dey** at the CSIR-National Chemical Laboratory, Pune under my supervision. Such material has not been submitted elsewhere for a degree.

Dr. Rahul Banerjee,   **Date: 15/09/2014**

(Thesis Supervisor)

Physical and Materials Chemistry Division,

CSIR-National Chemical Laboratory,

Pune-411008.

DECLARATION

I hereby declare that the thesis entitled "**Polyoxometalate as Building Units to Design Functional Metal Organic Hybrid Materials**" submitted for the award of degree of Doctor of Philosophy in Chemical Sciences to Academy of Scientific & Innovative Research (AcSIR), was carried out by me at the CSIR-National Chemical Laboratory, Pune, India, under the supervision of Dr. Rahul Banerjee. This work has not been submitted by me to any other institution or university for Ph.D. degree.

Chandan Kumar Dey   Date: 15/09/2014
CSIR-National Chemical Laboratory,
Pune-411008.

Dedicated to.........
My Parents and Brother

Acknowledgements

Table of Contents

ABSTRACT

The thesis entitled **"Polyoxometalate as Building Units to Design Functional Metal Organic Hybrid Materials"** has been divided into seven chapters.

CHAPTER I: Introduction to Polyoxometalates

Polyoxometalate (POM) being an important class of inorganic cluster have potential application in catalysis, sorption, separation, photochemistry, proton conductivity, medical biology, etc. Polyoxometalate are accumulation of metal oxide units linked via oxide linker to built three dimensional clusters. Polyoxometalate chemistry stays one of the most diverse growing field in current Inorganic chemistry and the durable interest in the domain is unquestionably highlighted by the large number of varying POM species (isopolyoxometalates and heteropolyoxometalates) which have been discovered recently. Since the first report of POM by Berzelius in 1826, the field has grown tremendously not only in the novelty and diversity of compounds, but also in many attractive properties which make them suitable for application, ranging from catalysis to magnetism, sensing and in therapeutics. In this work we have focused in designing functional hybrid material using polyoxometalate as building units.

CHAPTER II: Room Temperature Synthesis of Polyoxometalate Based Hybrid Salts

The construction of the isolable POM-based compounds and finally their potential evolving property of the material created by the POM clusters have increasingly became apparent. The key characteristic have been utilized frequently over the last few years, the connection between the POM cluster generated from monomeric metal oxide salt and intermediate metal-oxide/metal complex building blocks, resulted to be a vitally new approach to adopt and enable control over new structure, engineer properties. POM units are composed of metal ions (M = W, Mo, V, Nb, etc.) and oxo ligands. Organic moieties can be attached via addenda compounds to lacunary POM clusters. The reaction of Keggin-type and Dawson-type lacunary clusters with organosilicon, organotin, organogermanium compound leads to the formation of stable covalent bonded POMs and organic composite. Anderson clusters and Dawson can be tailored with tris-alkoxo ligands by replacement of the oxo ligands with alkoxo groups. Cronin *et al.* successfully organized a covalently modified Anderson-based scaffold by grafting pyrene moieties onto the Anderson POMs. The resulting materials show typical physical properties that are essentially different the parent POM cluster. Additionally,

covalently modified POMs can be connected further through non-covalent interactions. According to the available literature POM based hybrid can classified in six different categories, depending on the type of interaction POM with organic constituent and the arrangement of POM in hybrid matrix, (i) POM based ionic composites (ii) POM polymer hybrid (iii) POM incorporated MOFs (POM encapsulated inside the cavity of MOFs) (iv) POM based coordination polymer (v) POM based architecture (vi) POM-graphene composites. In this chapter we have focused in preparing ionic salts using $[Co(en)]^{3+}$ and different POM anions. The salts were characterized by single crystal X-ray diffraction and studied for gas adsorption experiments.

CHAPTER III: Synthesis and Morphological Study of Polyoxometalate (POM) Based Hybrid Materials

Researchers attempted to introduce POMs inside the metal organic frameworks (MOFs) to introduce not only functionality inside the structure but also enhance the thermal stability of the network. Polyoxovanadates (POVs) are an important class of polyoxometalates which has a unique ability to adopt different oxidation state. Morphology of a material plays a crucial role in determining the properties and makes them suitable for various applications. In this chapter synthesis of rarely observed vanadium cubane based MOF have been discussed which shows simultaneous occurrence of two morphologies of same phase at same reaction condition.

CHAPTER IV: Synthesis and Proton Conductivity Measurement of Polyoxometalate (POM) Based Composites

Proton conductivity in solid state has caught much attention due to its potential application in fuel cells, batteries and chemical sensors. Proton conducting material plays a crucial in fuel cell, a promising energy conversion means for automobiles and portable electronic devices. Nafion is the standard as proton conductor in fuel cell application and shows excellent activity at low temperatures and high levels of hydration. $MgCrO_4$-TiO_2, ZrO_2-MgO, $Ba_{0.5}Sr_{0.5}TiO_3$, TiO_2-$K_2Ti_6O_{13}$, $HZr_2P_3O_{12}$ oxides are known for their proton conducting property at humidification condition. Nanocomposite membranes consist of hydrophilic inorganic nanoparticles and polyelectrolyte collected considerable attention due to their proton conducting nature at high temperature. Organic sulfonic and phosphonic acid functionalized mesoporous silica and zeolite are also rectified for proton conduction. In this work we studied proton conductivity in POM based coordination polymer.

CHAPTER V: Incorporation of Metal Oxide Sites in Metal Organic Frameworks (MOFs)

Metal Organic Frameworks (MOFs) are formed by the linkage of organic ligands to metal atoms to built extended structures. MOFs are well known for last two decades due to adsorption property in their porous network. MOFs are advantageous over other porous materials due to systematic arrangement of pores in the network and their ability to change pore size by changing the metal ions or ligands. Although MOFs have shown some activity on catalysis, magnetism, ion exchang etc, but major activity of MOFs are still limited in the area of absorption. The aim of this work is to incorporate functionality inside MOFs by introducing Polyoxometalates (POMs) in the network. POMs have the potential to link metal ions via its peripheral oxygen to form network structures. POM incorporated networks not only introduce functionality inside the structure, but also enhance their thermal stability. Recent investigation on POM based covalently linked transition-metal complex frameworks has received considerable attention. There are three ways to introduce POMs inside extended network (i) building up of MOFs keeping the POMs inside the pores of MOFs, (ii) coordination of oxygen atom of polyoxometalate to hetero metal ions to form extended structure, (iii) replacing the oxygen atom of POMs via organic ligands to join them in one, two or three dimensional fashion (1-D, 2-D or 3-D). In our work we have used first approach to incorporate POM incorporated Metal Organic Framework (MOF).

CHAPTER VI: POM Catalyzed *in situ* Ligand Synthesis to Prepare Coordination Polymer

Combination of multiple reagents in a vessel for the easy access of the products in single step reduce the time of the reaction and avoid difficulties of separating the products in each steps of reaction. It sometime minimizes the difficulties of using hazardous chemicals, like azide, cyano etc. *In situ* ligand synthesis not only provides a synthetic root for organic ligands which are not readily accessible but also represents a potential new direction for construction of novel inorganic–organic hybrid network construction through crystal engineering. Current studies prove that hydrothermal synthesis under high pressure and moderate temperature (~ 150 °C) is an effective method for *in situ* ligand generation. Various methods like hydrolysis of -CN and -COOR groups, reduction of -COO-, hydroxylation, C-C bond formation by reductive or oxidative coupling, and cleavage and formation of disulfide bonds, etc. were used while *in situ* ligand formation. Coordination Polymers (CPs) being a new class of hybrid

network solids, have potential applications in separation, storage and controlled drug delivery. One-pot synthesis of CPs using mixture of ligand and metal salt is routine process but preparation of ligand from ligand precursor during formation of CPs is still challenging. Recently click chemistry process was utilized with various metal ions such as Zn(II), Cd(II), Cu(I)/Cu(II), and Ag(I) in the construction of CPs. The example of *in situ* oxidation during formation of CP is very rare. *In situ* selective oxidation of one or two methyl groups of neocuproine in presence $Ni(NO_3)_2$ or $Cu(NO_3)_2$ and HNO_3 were reported in literature. In this work, we have used oxidation of neocuproine to form coordination complex as well as coordination ploymer in presence Cu^{2+} and conc. HCl using Na_2MoO_4/MoO_3 as catalyst.

Chapter VII: Conclusion and Future Directive

In last chapter I have summarised the results of all previous chapter. Based on the obtained results I have also proposed three new ideas, (i) Incorporation of POM inside metal organic framework; (ii) Incorporation of POM inside covalent organic frameworks (COFs), (iii) POM Catalysed in situ complex ligand synthesis to form new MOF architectures, which will be fruitful for future applications.

Introduction to Polyoxometalate

1.1 Introduction

Polyoxometalates (POMs) are a large family of inorganic cluster compounds; containing bridging oxygen atoms between two or more metal ions [1.1]. These are polyatomic ionic species that consist of at least two but usually three or more transition metal oxyanions that are linked together by shared oxygen atoms to form large and closed three-dimensional clusters. Most of the elements in the periodic table can be incorporated into the POM framework and this leads to an overwhelming diversity of structures and properties [1.2]. Usually group V and group VI transition metal elements in their higher oxidation state with d^0 or d^1 electronic configuration are suitable for POMs. Higher the positive charge easier the proton from oxo-ligands of the monomer units to dissociate, therefore, highly charged metals [vanadium (V), molybdenum (VI), etc.] of group V and VI form stable complexes with oxo-ligand. The condensation reaction takes place upon acidification in aqueous solution forming M-O-M bridges [1.3]. The metal atoms that make up the cluster are called addenda atom, if more than one such element is present it is called mixed addenda clusters. They have the general formula $[X_xM_mO_y]^{q-}$, where X is the hetero atom such as P, Si, As, Co, Zn, etc. M is addenda atom, q is the charge which varies from -3 to -28 [Figure1.1] [1.4].

1.2 Development of polyoxometalates

Various applications of polyoxometalates are based on their physicochemical properties. These include large anion size and mass, electron and proton transfer abilities, high Bronsted acidity of the corresponding acids, solubility and extractability, etc. Another important property of these metal oxide clusters is their ability to undergo reversible multi-valence reduction processes forming mixed valence species [1.5]. These properties made POMs very useful in the preparation of modified electrodes and brings in favorable catalytic properties [1.5d]. POMs display very strong Brønsted acidity which makes them efficient acid catalyst for certain reaction such as esterification, hydrolysis, Friedel-Crafts alkylation and ring opening polymerization of tetrahydrofuran [1.6]. In addition, reversible transformations under UV irradiation or electric field make polyoxometalate applicable as optical switches or other electronic devices [1.7]. The vacant sites of POMs can accommodate transition or rare earth

elements through coordination interaction that can endow magnetic, luminescent and other unique properties [1.8]. POMs also have shown their potential in various applications, such as catalysis, sorption, separation, photochemistry, proton conductivity, medical biology, etc [1.9]. POM chemistry is one of the most diverse growing field in current inorganic chemistry and the durable interest in the domain is unquestionably highlighted by the large number of varying POM species (isopolyoxometalates and heteropolyoxometalates) which have been discovered recently.
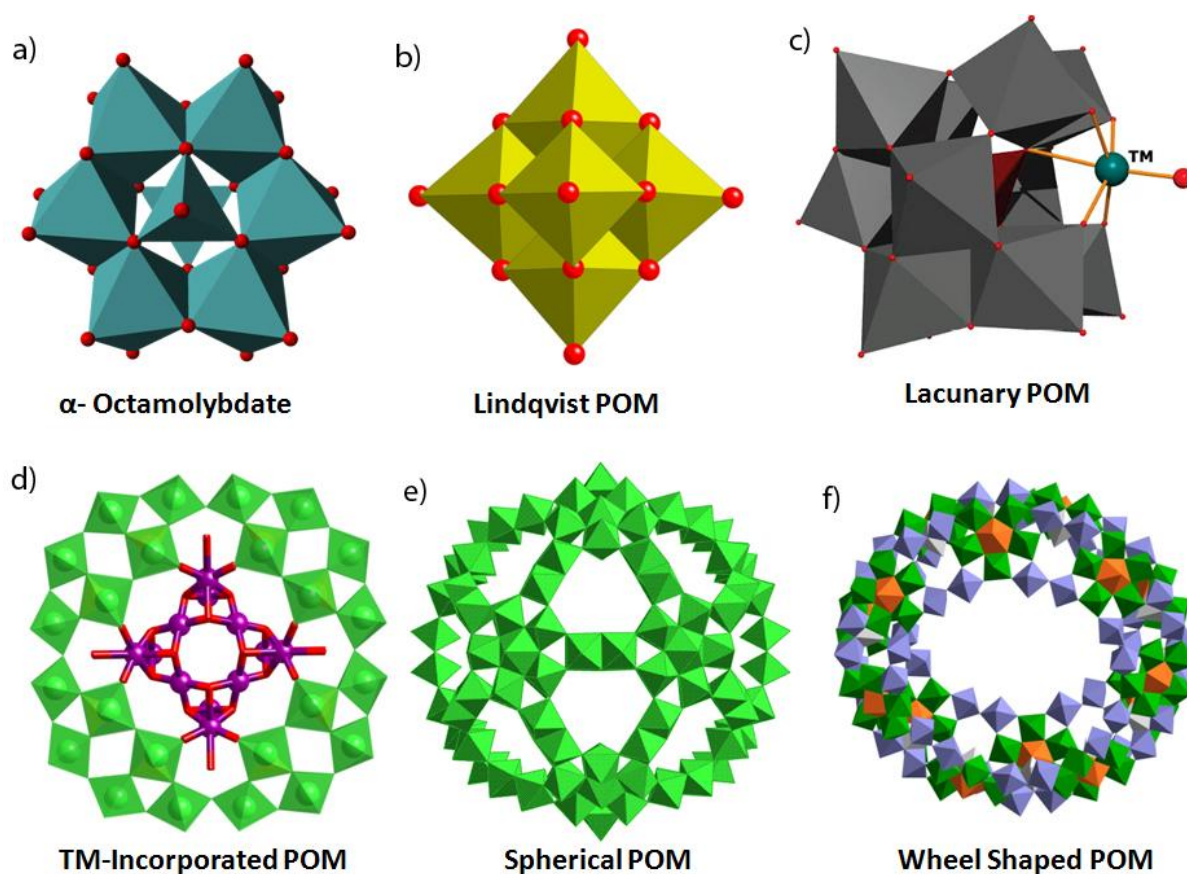
Figure 1.1: (a) Crystal structure of *α*-octamolybdate. (b) Lindqvist structure, an example of homopolyoxometalate. (c) In lacunary POM one of the metal centre is substituted by hetero metal (transition metal). (d) Transition metal cluster has been stabilized inside POM cluster. (e) Spherical cluster of Mo132. (f) Wheel shape cluster of Mo154 (diameter of the wheel: 3.6 nm).

1.3 Synthesis of different types of POM clusters

Since the first report of POM by Berzelius in 1826, the field has grown tremendously not only in the novelty but also on the diversity of compound synthesis [1.10]. General approach

used to fabricate POM based clusters are quite simple, requiring few number of steps, or sometimes just one step (one-pot method), through which acidification of a solution containing the appropriate salt of molybdates, tungstates, vanadates, etc results the condensation process and encourages the aggregation of metal oxide units towards the formation of precise archetypes. The aggregation routes to design defined architecture are controlled by many experimental variables, such as: (1) type and concentration of metal oxide, (2) pH of the medium, (3) ionic strength of medium, (4) presence of heteroatom, (5) presence of different ligands, (6) diverse redox environment, (7) temperature and pressure, and (8) types of counter-ion [1.11]. The huge growth in the numbers POM based assembled clusters may be attributed to many possible hybrid structure types, in which individual building block can adopt itself to a range of potential isomers. Moreover, the progress of the POM chemistry has directed to the realization that the isolated clusters could act as a building blocks that can be constantly utilized in the formation of new architectures [1.12].

1.3.1 Isopolyanions

When the POM contains only one type of metal oxide unit without any hetero atom they are called 'Isopolyanion'. The synthesis of isopolyanion clusters of $V^{5+,}$ Mo^{6+} and W^{6+} starts with the water soluble salts of the oxoanion monomeric unit; VO_4^{3-}, MoO_4^{2-} and WO_4^{2-}, etc. The pH of the solution goes up (normally above 12) in water, due to protonation of the oxo-ligands of the monomeric units. These oxoanions concurrently expand their coordination environment by binding to water. Successive addition of acid outcomes the hydrolysis and condensation reactions to result in soluble, discrete anionic POM clusters [1.13]. The size, shape and monodispersity of the POM clusters that generated is dependent on many factors including pH, concentration of the POM forming metal, solvent, temperature, etc. α-Octamolybdate [Figure 1.1a], Lindqvist type POM [Figure 1.1b], β-ocatbolybdate are the examples of isopolyanion [1.14].

1.3.2 Heteropolyanions

Hetropolyanions are the class of POMs which contain one or more than one addenda atoms inside the metal oxide cluster. Due to the presence of different addenda atoms, they show interesting properties [1.8] which can be tuned by changing addenda atoms and location of the addenda atom in the clusters. This type of POMs is catalytically more active compare to the isopolyanion. Keggin POM is an example of heteropolyanion, where one PO_4 (hetero

atom) is surrounded by 12 MO_6 units [Figure 1.2] [1.15]. Dawson type POM is another example of heteropolyanions [1.16].

$$12WO_4^{2-} + PO_4^{3-} + 24H^+ \longrightarrow [PW_{12}O_{40}]^{3-} + 12H_2O$$
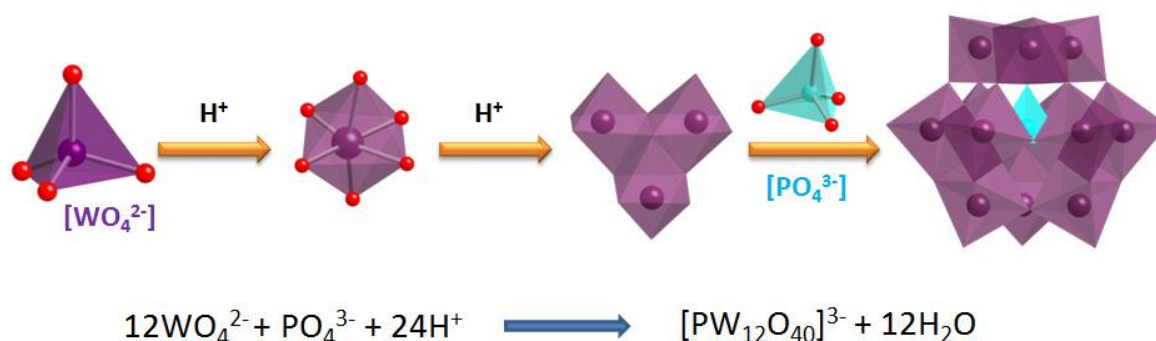
Figure 1.2: Top image shows the steps involve during formation of Keggin anion. Step 1: Proton mediated coordination sphere expansion form tetrahedral to octahedral, Step 2: Self aggregation of octahedral units to form triad Mo_3O_{13} secondary building units. Step 3: $[PO_4]^{3-}$ templated formation of Keggin, $[PW_{12}O_{40}]^{3-}$ anion. Bottom scheme shows the stiocheometry of Keggin anion formation.

1.3.3 Lacunary anions

Lacunay species can be build form POM cluster by removing at-least one metal oxide (M=O) unit by addenda metal centre [Figure 1.1c]. Most of the known lacunary anions have been derived form Keggin or Well-Dawson POM clusters [Figure 1.3]. The focus to create lacunary anion is for their application in catalysis and magnetism [1.17]. 4f-metals are more suitable than 3d-metal as addenda atom in lacunary species due to their oxophilicity. Merca *et al.* have prepared $[(VO)_2\{Dy(H_2O)_4\}(AsW_9O_{33})_2]^{11-}$ sandwich type POM by instantaneous addition of $(VO)SO_4$ and $DyCl_3$ into acidified solution of Na_2WO_4 and As_2O_3, which was followed by addition of KCl [1.18]. Wang and co-workers have synthesized the $[K\{Ce(H_2O)_2(AsW_{10}FeO_{38})\}_3]^{14-}$ cluster by addition of Fe^{3+} and Ce^{3+} ions to an acidified aqueous solution of Na_2HAsO_4 and Na_2WO , followed by addition of KOH (pH = 4–5) [1.19]. Reaction of the heterometallic cuboidal clusters $[Mo_3S_4Pd0(H_2O)_9Cl]^{3+}$ and the tri-vacant $[AsW_9O_{33}]^{9-}$ ion in aqueous media results in the four-lobed assembly $[(H_2AsW_9O_{33})_4\{Mo_3S_4Pd0(H_2O)_5\}_2]^{20-}$. The vanadopalladate(II) anion, $[Pd(II)V_6O_{18}]^{4-}$ was prepared in acetonitrile solution, has a boat conformation of the hexametavanadate ring stabilized by the attachment of the Pd(II) center [1.20].
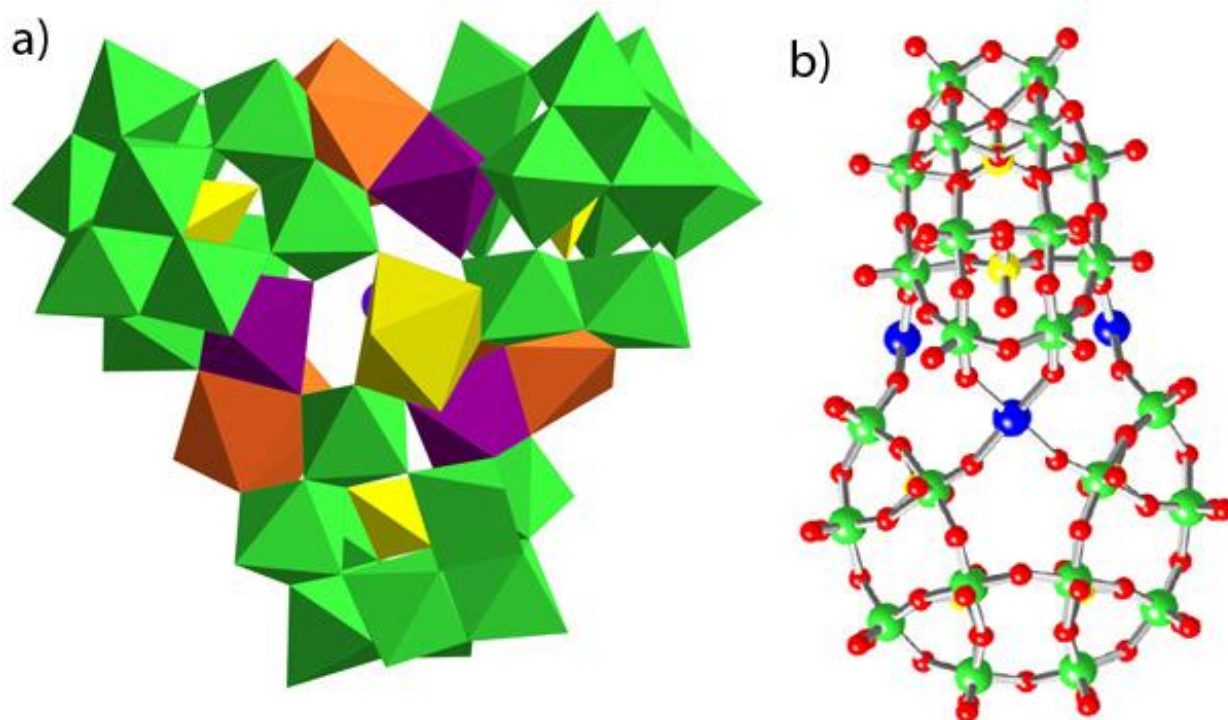
Figure 1.3: (a) three lacunary {α-AsW$_{10}$O$_{38}$} fragments are bridged by three {Fe–(μ$_3$-O)$_3$–Ce} heterometallic clusters to build the aggregated cluster (Ref No. 17f). (b) Ball and stick representations of [{Sn(CH$_3$)$_2$}$_4$(H$_2$P$_4$W$_{24}$O$_{92}$)$_2$]$^{28-}$ The color code is as follows: tungsten (green); oxygen (red); phosphorus (yellow); tin (blue) (Ref No. 1.17g).

1.3.4 Giant POM clusters

Polyoxometalates are an important class of clusters which has a unique ability to adopt different coordination geometries such as tetrahedral, square-pyramidal and octahedral. These clusters can be joined either by edge share, face share or corner share to form extended structure. The giant POM clusters are an important family of POMs, most of them have been discovered by Müller and co-workers, could be the potential candidates in cluster chemistry. These clusters could also be classified as reduced POM clusters and can be prepared by simple protocol with careful maintenance of pH and concentration of reagents. Development of the field of POMs discovered several giant POMs which include 'big wheel' (Mo154) 'hedgehog' (Mo368), 'icosahedral' (Mo132), 'capped cyclic' (Mo248), 'basket' (Mo116), etc [1.21]. The specific example of one such cluster is Mo$_{132}$ sphere [Figure 1.1e], which was prepared by acidification of aqueous solution of Na$_2$MoO$_4$·2H$_2$O in presence L-cysteine hydrochloride monohydrate at room temperature [1.21a]. Similarly the Bielefeld giant wheel

Mo_{154} can be prepared by reduction of acidified solution of Mo(VI) according to following reaction scheme [1.22].

$$154\ MoO_4^{2-} + 14\ S_2O_4^{2-} + 322\ H^+ \rightarrow [Mo^{VI}_{126}Mo^{V}_{28}O_{462}H_{14}(H_2O)_{70}]^{14-} + 28\ SO_2 + 84\ H_2O$$
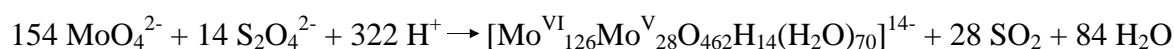
1.3.4 Post synthetic modification of POM clusters

Post-synthetic modification of POM cluster or architecture is a crucial step ahead in designing POM based hybrid materials. By this method not only functional group can be incorporated inside the materials but also the polarity and stability of the materials can be change. The example of one such synthesis is acetic acid functionalization of Mo_{132} sphere, which have been prepared by the following reaction scheme [1.23].

$$132MoO_4^{2-} + 15N_2H_6^{2+} + 30CH_3COOH + 192H^+ \rightarrow [Mo^{VI}_{72}Mo^{V}_{60}O_{372}(CH_3COO)_{30}(H_2O)_{72}]^{42-} + 15N_2 + 84H_2O$$

Cystein functionalized Mo_{154} cluster can also be prepared by addition of cysteine hydrochloride monohydrate into the acidified (HCl) aqueous solution of $Na_2MoO_4 \cdot 2H_2O$ [1.24].

1.4 Application of POMs

By gradual development of the field, the POM clusters have been decorated and modified with various organic group and transition, lanthanide metal ions, which enrich POM for their potential application in magnetism, photochemistry, catalysis, therapeutics, etc.

1.4.1 Magnetism

An important discovery in molecular magnetism is the preparation and characterization of single-molecule magnets (SMM) which shows slow magnetic relaxation and quantum effects at low temperatures, could be potential candidate in memory device applications. POMs possess huge variety in both shape and size and therefore provide access to a vast family of Inorganic cluster which can be interconnected by electrophilic centres. Hence POMs can incorporate and stabilize magnetically active metal ions or clusters. POMs can act as ligand, diamagnetic separator, trapping substrate inbetween magnetically active ions or clusters. POMs could be useful to deconvolute magnetic interaction in single-molecule magnets (SMMs) to remove unwanted dipolar interactions. The first Mn(II)/Mn(III) based SMM material with lacunary $\{B\text{-}a\text{-}SiW_9O_{34}\}^{10-}$ polyanions has been reported by Cronin and co-

6

workers[1.25a]. In 2011 Kortz's group has reported the synthesis and characterization of tetrameric $[\{Co_4(OH)_3PO_4\}_4(PW_9O_{34})_4]^{28-}$ cluster which entrapped a $\{Co_{16}\}$ magnetic core [1.25b]. The use of lacunary POM fragments have also been used as multidentate stout ligand to entrap polynuclear paramagnetic cores of $\{W_{18}Cu_6\}$[1.26] and $\{W_{48}Cu_{20}\}$ [1.27].

1.4.2 Catalysis

POMs have been extensively applied for industrial catalysis. Catalysis POMs, especially heteropolyanions (HPAs), persists to attract extensive interest during recent years. The properties of POMs such as (i) very strong Brønsted acidity; (ii) very fast reversible redox transformations under mild conditions; (iii) tunable redox properties, (iv) good solubility in polar solvents, and (v) high proton mobility in solution, made them suitable candidate for catalysis. POMs have been used in solution phase as well as in solid state as acid catalysts and oxidation catalysts [1.28]. Dispersed POMs on solid support with higher surface areas are important for catalytic application since the surface areas of unsupported POMs are comparatively low. Enhanced catalytic activity of heteropoly acids (HPAs) was observed when the HPAs were supported on strongly acidic ion-exchange resins, such as Amberlyst-15 [1.29]. The rate of oxidation of CO by solid salt or acid of $PMo_{12}O_{40}$ is found to be proportional to specific surface area of the catalyst [1.30]. Insoluble POM catalysts to replace soluble catalysts are advantageous for making the catalytic processes environmentally benign [1.31]. For this purpose cesium, ammonium, and cerium salts of POM in silica matrix have been projected. The preparation methods as well as characteristics of POM-based heterogeneous catalysts are different from conventional supported metal catalysts [1.32]. Homogeneous POM catalysts are functionalized or grafted on solid supports to make them heterogeneous with preservation of the active sites at the molecular level. This process retains the catalytic activity of homogeneous catalyst in heterogeneous condition, but enhances the recyclability of the catalyst. Mizuno and co-workers recently proposed that, POMs with organometallic cations of appropriate charge, shape, size, and electrophilicity may lead to the formation of insoluble ionic composite due to the strong electrostatic interaction between the ionic constituents [1.33]. Inumara and co-workers prepared a water stable POM and mesoporous silica composite by immobilizing $H_3PW_{12}O_{40}$ in hydrophobic nanospaces of organomodified mesoporous silica while retaining its catalytic activity. The catalyst shows high water stability and the leaching of the POMs form the matrix was negligible (only 2% of

the loaded POMs) after a reaction time of 12 hours. Also this composite was found to enhance activity for the ester hydrolysis reaction [1.34].

1.4.3 Desulfurization using POMs

Sulfur-containing compounds are transformed to sulfooxide during combustion processes, which poison the atmosphere and causes acid rain. Hence, desulfurization has become an important charge for the petroleum refining industry. Benzothiophene (BT) and dibenzothiophene (DBT) account 75-80% of sulfur content in diesel fuel, thus, removal of these sulfides is a major challenge in petroleum industries [1.35]. Currently used industrial method is catalytic hydrodesulfurization (HDS), which require harsh operating conditions [1.36] (high pressure and temperature), hence need urgent replacement by milder reaction condition. Oxidative desulfurization with polyoxometalate/SiO_2, H_2O_2/polyoxometalates system could be the replacement for industrial purpose [1.37]. Neumann and co-workers recently studied desulfurization process of hydrocarbons through the electron transfer oxidative polymerization of sulfides using $H_2PV_2Mo_{10}O_{40}$/SiO_2 catalyst [1.38]. They have also shown that this heterogeneous catalyst is stable in solution and recyclable in nature. Song and co-workers have reported a very competent desulfurization composite consist of $Na_7H_2LaW_{10}O_{36} \cdot 32H_2O$ [bmim]BF_4 using H_2O_2 as oxidant [1.39]. Among different processes utilized for desulfurization, the later mentioned system is considered to be one of the most promising process which combines oxidative desulfurization (ODS) and subsequent extraction of sulfoxides and sulfones from solution.

1.4.4 CO_2 fixation with POM cluster

The progress of proficient catalytic conversion of CO_2 into attractive chemical products is of great interest because CO_2 is not only an profuse, inexpensive, nonflammable, renewable carbon resource, but also the principle origin of the greenhouse effect, as a result, has caught broad attention from worldwide research activities. Xu *et al.* recently described two POMs that could covalently attach CO_2 molecules and have successfully synthesized $(C_3H_5N_2)_3$-$(C_3H_4N_2)[PMo_{11}CoO_{38}(CO_2)]\cdot 4H_2O$ and $(C_3H_5N_2)_4[SiMo_{11}CoO_{38}(CO_2)]\cdot 4H_2O$ clusters respectively [1.40]. Recently Müller and co-workers have also shown that purging of CO_2 gas in the solution of Mo_{132} spherical cluster can replace inner coordinated water molecule by carbonates. Single crystal structure analysis suggests that one Mo_{132} can take 30 CO_2 molecules [Figure 1.4] [1.41].
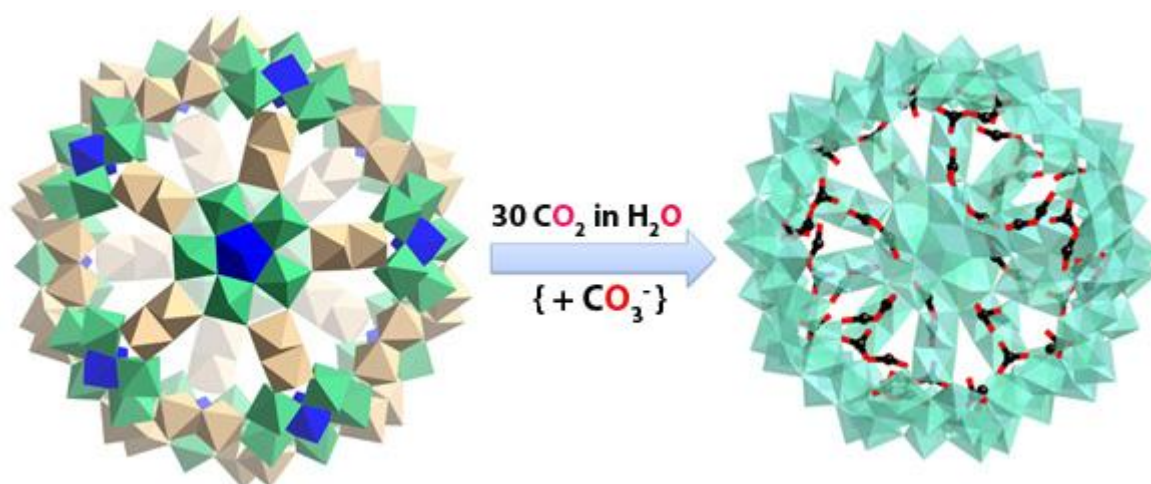
Figure 1.4: One Mo_{132} spherical cluster can reversibly take 30 molecules of carbon dioxide as carbonate inside the cluster. CO_2 gets converted to CO_3^- (carbonate) in the reaction medium, which coordinate to POM in reversible manner.
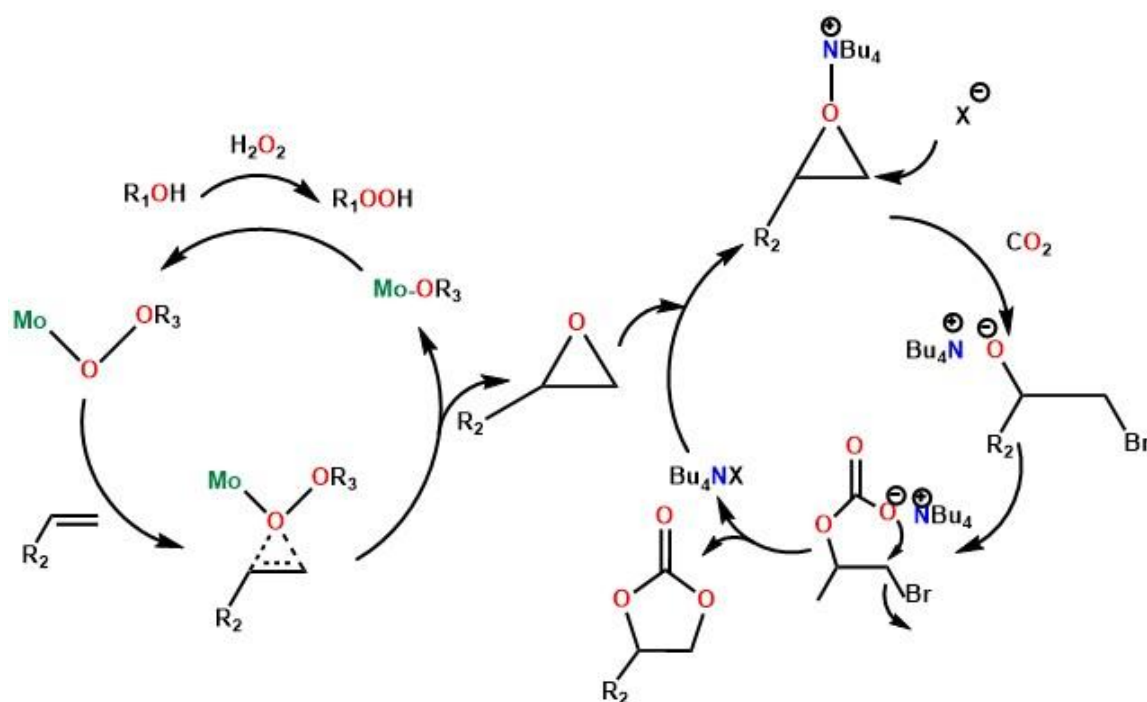
Figure 1.5: General scheme for CO_2 fixation. This strategy involves the initial epoxidation of alkenes to epoxides in presence of H_2O_2, these epoxide can further be converted to cyclic esters.

Hu and co-workers newly reported an extremely competent system for conversion of olefins and CO_2 to cyclic carbonates by using a molybdenyl acetylacetonate $[MoO_2(acac)_2]$– quaternary ammonium salt catalyst with *tert*-butyl hydroperoxide as oxidant in a one-pot

process [Figure 1.5]. This simple and cheap process can be applied to various olefins (1-octene, 1-hexene, allyl chloride, cyclohexene and styrene) to convert them to the corresponding carbonates [1.42].

1.4.5 Electrochemistry of POMs

The redox activity of polyoxometalates has drawn much attention in current years. Heteropolyanions (HPA), especially their metal-substituted derivative have valuable and interesting properties. These attribute to the high stability of redox states of HPA and increase the possibility to tune their redox potentials by changing the heteroions or addenda ions without affecting their structural feature. Although endless numbers of polyoxometalates has been synthesized and characterized, but the number of POMs used as electro-catalysts are limited. Mostly, α-Keggin-type and Dawson-type HPAs of phosphotungstate, silicontungstate, phosphomolybdate, silicomolybdate with metal-substitution are used as electro-catalysts due to their stability and ease of preparation. Nadjo and co-workers have reported the synthesis of metal nano-particles (NPs) using electrochemically reduced POMs. The preparation of Pd(0) NPs from $[PdCl_4]^{2-}$ was carried out using the α_2-$[H_4PV^{IV}W_{17}O_{62}]^{9-}$ where Wells-Dawson-type vanadium-substituted POM was used as both a reducing and stabilising agent [1.43]. The multi valence phosphomolybdate β-$H_3[H_4P(Mo^V)_4(Mo^{VI})_8O_{40}]^{3-}$, synthesised electrochemically was used as a reducing agent for the reduction of chloroauric acid at room temperature to form Au nanostructures [1.44]. Generally, POMs acts as electron transferring mediator, at the same time reversible electron storage ability of POMs by muiltistep reduction made them suitable for Li-ion batteries [1.44b-f].

1.4.6 Photochemistry of POMs

The photoreactivity of polyoxometalates is known for decades, but it is only recently the systematic study of POM for photocatalysis became an important topic. The photochemistry of POM was pioneered by the groups of Hill, Yamase and others [1.45]. The heteropolyoxometalates of the Keggin-type and the Dawson-type clusters were utilized for photo catalysis due to their high stability and ability to undertake multi-electron reversible redox processes, which made them promising prototype complex for homogeneous photochemical reactions.

The current century started feeling the fact that a shift of energy sources to renewable and sustainable systems are required to solve the problem of global warming caused by

greenhouse gases such as CO_2 [1.46]. The promising step is the use of photochemical methods to allow the conversion of sunlight to useful chemical systems. POMs have the potential for homogeneous photoreduction of CO_2 and the photocatalytic production of hydrogen from water splitting reaction [Figure 1.6] [1.47].
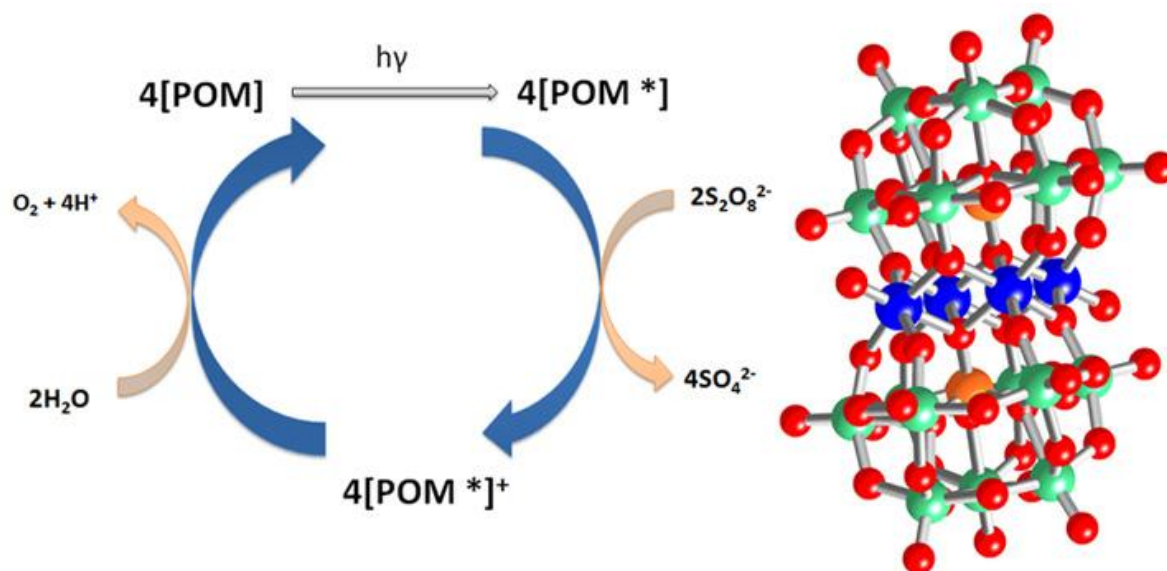
Figure 1.6: General scheme for polyoxometalate-based photocatalytic water oxidation involves the following steps (1) photo-excitation of the oxidised cluster (POM_{ox}) by light (photon) absorption; (2) light driven oxidation of POM in presence of peroxodisulphate; (3) water oxidation and electron transfer to oxidized POM.

1.4.7 Bio-medical application of POMs

POM based pharmaceuticals are less expensive and easier to scale-up than the majority of traditional organic pharmaceuticals, thus their improvement optimistically impact the large and growing markets in the upcoming world. Antiviral and antitumoral activity of POM are know in the literature. Researchers have also focused on the antiviral properties of POMs because of their non-toxicity to normal cells. Earlier POM cluster, HPA-23 formulated as $[NaSb_9W_{21}O_{86}]^{18-}$ have been studied for antiviral activity [1.48].

1.4.8 Synthesis of noble metal Nano-Particles (NPs) using POMs

In recent years, noble metal nano-particles (NPs) with well defined shape and size have received huge attention due to their unique chemical, physical and optical properties. An enormous amount of literature report is available on the preparation of metal nano-particles

(NPs) using POM as reducing, capping, and stabilising agents [Figure 1.7] [1.49]. A group of researchers have reported a basic photocatalytic method for the preparation of complex core-shell nanostructures such as Au core–Ag shell bimetallic compounds. The elegant process employed by researcher assisted the formation of Au core–Ag shell nanoparticles (NPs)

Figure 1.7: Photo excited POMs oxidise organic substrate and itself get reduced to POM_{red}. This reduced POM_{red} again comeback to its original POM_{ox} form and reduce matal ions to metal nano-particles (NPs). The re-oxidation of the POMs happen simultaneously with the reduction of M^+ metal ion to metal M^0 metal nano-particles (NPs).

using photochemically reduced phosphotungstic acid (PTA) [1.50].

1.5 Designing polyoxometalate based hybrid materials

Physical and chemical properties of POMs could be constantly modified during the process to develop sophisticated tools and devices. POMs have prospect of integrating variety of molecules to act as well-defined podium for the development of multifunctional materials. According to the interaction of POM with organic functional groups classical organic–inorganic POM based hybrids can be classified mainly two categories, non-covalently attached POM and covalently attached POMs respectively [1.51]. One of the important features of POM clusters is their unique ability to be desolved in a variety of solvents, which makes them distinct as molecular metal oxide clusters.

Based on the composition, interaction between composite, location of POM in the matrix and their application, POM hybrids have categorized and discussed as follows.

1.5.1 Non-covalently functionalized POMs

POM dissolved in suitable solvent can electrostatically interact with the cationic complexes, molecules, and polymeric material, as well as positively charged solid surfaces to form POM based composites without covalent interaction. Hydrogen bonding is governing factor to construct POM based ionic composites with cationic ammonium and protein counter parts [1.52]. These types of hybrids are easy to prepare and have potential application in sorption, separation, catalysis, conductivity, etc [1.53].

1.5.2 Covalently functionalized POM based materials

Organic moieties can be grafted to lacunary POM cluster via addenda organometallic compounds attached to POM cluster. Literature evidences suggest that the attachment of Keggin-type and Dawson-type lacunary POM clusters with organosilicon, organotin, and
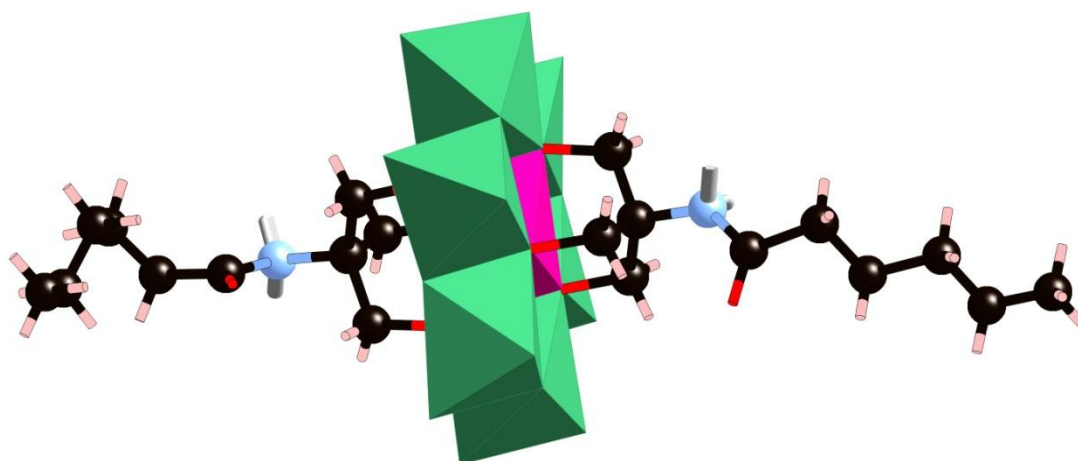
Figure 1.8: Anderson type cluster is covalently connected to two alkyl chain to prepare amphiphilic Inorganic Organic hybrid (Ref No. 1.57).

organogermanium compounds leads to the construction of stable covalently bonded POMs functionalized with organic moieties [1.54]. Zubieta and co-works first reported the organoimido derivatives of POM [1.55], since then mono to hexa amino derivative of Lindqvist POMs have been prepared [1.56]. A group of researchers successfully synthesized a covalently modified Anderson POM based hybrid material by tethering delocalized aromatic pyrene group covalently to the Mn-Anderson type POM cluster through a Tris [Tris = tris(hydroxymethyl) aminomethane] linker [1.57]. Furthermore, covalently modified hydrophilic POMs with hydrophobic organic moieties could build relatively stable POM based amphiphiles. Silicon tailor with alkyl chain attached to lacunary Keggin type POM was reported, where alkyl group was at one side of the POM cluster [1.58]. Anderson-type and

Dawson-type POM units in contrast can contain two hydrophobic tails on both sides of the cluster to prepare amphiphilic structures [Figure 1.8].

1.5.3 POM containing monolayer and thin film structures

By dropping the structural dimensions of the POMs based materials from three-dimensional to low-dimensional structures, POM hybrid can be effectively used as functional electrodes, heterogeneous catalysts, etc [1.59]. A large number of POM-based self-assembled structures have been synthesized via non-covalent and covalent interactions. POM-containing Layer by Layer (LbL) assembly composed of monolayers of POMs with alternating arrangement of organic cations and POM anion, where the thickness of the inorganic layer is controlled by the width of POM clusters. The electrostatic interaction is the governing factor which holds the LbL structure in perfect orientation [1.60]. The Langmuir–Blodgett (LB) technique can provides monolayer and multilayer films using wet techniques, and the number of layers can be adjusted from monolayer to multilayer structures [1.61]. Another different type of self assembled POM based hybrid structure was perceived during the course of the research which was termed as 'blackberry structure'. These types of structure are generally observed with giant POM cluster because of their larger size they behave differently from point charge (small anion) [1.62].

1.6 Conclusion

Polyoxometalates (POMs) have notable properties and a great potential to meet current societal demands concerning environment, health, energy and information technologies. However, execution of POMs in various functional materials and devices requires a development in processing steps. The development in POM based hybrid materials has been achieved *via* electro static interaction, immobilization of POMs on mesoporous silica and layered double hydroxide (LDH), embedding of POMs in polymers matrix. POM based coordination polymer has caught current research attention due to its porous nature, immiscibility in different solvent and recyclability after catalytic reactions. In this regard lots of studies have been cried out to prepare transition metal or lanthanide incorporated POM based coordination polymer. Since POMs are generally large anion with high negative charge, the initial strategy to organize them in three dimensional materials relies on the substitution of their counterions. Taking this strategy forward we have tried to synthesize a series of POM based ionic salts with POM anions. Being porous in nature these salts are

expected to show H_2 and CO_2 adsorption. In the next phase of our study we have prepared POM based coordination polymers with few rare POMs which for their morphology and property. Metal organic frameworks (MOFs) [1.63] are porous coordination polymers where metal nodes have been connected via organic linkers. MOFs can be used efficiently as platform for catalytic reactions. In the later stage of our studies we engaged ourselves to incorporate catalytically active metal oxide units inside MOFs. The final phase of study is involved in preparation of POM based metal organic hybrid materials using one pot methods.

1.7 References

1.1   (a) D. E. Katsoulis. *Chem. Rev.* **1998**, *98,* 359. (b) D. Barats, G. Leitus, R. Popovitz-Biro, L. J. W. Shimon, R. Neumann. *Angew. Chem. Int. Ed.* **2008**, *47*, 9908. (c) N. S. Antonova, J. J. Carbo, U. Kortz, O. A. Kholdeeva, J. M. Poblet, *J. Am. Chem. Soc.* **2010**, *132*, 7488.

1.2   (a) A. M. Khenkin, R. Neumann, *J. Am. Chem. Soc.* **2004**, *126*, 6356. (b) A. M. Douvas, E. Makarona, N. Glezos, P. Argitis, J. A. Mielczarski, E. Mielczarski. *ACS Nano,* **2008**, *2,* 733. (c) C. Zhao, Z. Huang, W. Rodríguez-Cordoba, C. S. Kambara, K. P. O'Halloran, K. I. Hardcastle, D. G. Musaev, T. Lian, C. L. Hill, *J. Am. Chem. Soc.* **2011**, *133*, 20134.

1.3   (a) K. Nomiya, Y. Sakai, S. Matsunaga. *Eur. J. Inorg. Chem.* **2011**, 179. (b) Y. P. Jeannin. *Chem. Rev.* **1998**, *98,* 51.

1.4   D. –L. Long, R. Tsunashima, L. Cronin, *Angew. Chem. Int. Ed.* **2010**, *49*, 1736.

1.5   (a) R. Neumann, M. Dahan. *Nature*. **1997**, *388*, 353. (b) J. Ettedgui, Y. Diskin-Posner, L. Weiner, R. Neumann, *J. Am. Chem. Soc.* **2011**, *133*, 188. (c) M. Natali, S. Berardi, A. Sartorel, M. Bonchio, S. Campagna, F. Scandola. *Chem. Commun*. **2012**, *48*, 8808. (d) D. –Y. Du, J. –S. Qin, C. –G. Wang, X. –C. Liu, S. –L. Li, Z. –M. Su, X. –L. Wang, Y. –Q. Lan, E. –B. Wang, *J. Mater. Chem.* **2012**, *22*, 21040.

1.6   (a) K. Kamata, T. Yamaura, N. Mizuno. *Angew. Chem. Int. Ed*. **2012**, *51*, 7275. (b) T. Hirano, K. Uehara, K. Kamata, N. Mizuno. *J. Am. Chem. Soc.* **2012**, *134*, 6425. (c) Q. Li, Y. Wei, J. Hao, Y. Zhu, L. Wang. *J. Am. Chem. Soc.* **2007**, *129*, 5810. (d) G. Absillis, E. Cartuyvels, R. V. Deun, T. N. Parac-Vogt. *J. Am. Chem. Soc*. **2008**, *130*, 17400. (e) R. Palkovits, K. Tajvidi, A. M. Ruppertc, J. Procelewska. *Chem. Commun.* **2011**, 47, 576.

1.7   (a) F. Xiao, J. Hao, J. Zhang, C. Lv, P. Yin, L. Wang, Y. Wei, *J. Am. Chem. Soc*. **2010**, *132*, 5956. (b) Y. Zhang, L. Zhang, Z. Hao, F. Luo. *Dalton Trans.* **2010**, *39*,

7012. (c) H. Naruke, J. Iijima, T. Sanji. *Inorg. Chem.* **2011**, *50*, 7535. (d) S. Chakraborty, A. Keightley, V. Dusevich, Y. Wang, Z. Peng. *Chem. Mater.* **2010**, *22*, 3995.

1.8   (a) L. E. Roy, D. Ortiz-Acosta, E. R. Batista, B. L. Scott, M. W. Blair, I. May, R. E. D. Sesto, R. L. Martin. *Chem. Commun.* **2010**, *46*, 1848. (b) L. Chen, F. Jiang, Z. Lin, Y. Zhou, C. Yue, M. Hong. *J. Am. Chem. Soc.* **2005**, *127*, 8588. (c) C. Yao, L. –K. Yan, W. Guan, C. –G. Liu, P. Song, Z. –M. Su. *Dalton Trans.* **2010**, *39*, 7645. (d) C. –G. Liu, W. Guan, P. Song, Z. –M. Su, C.Yao, E. –B. Wang. *Inorg. Chem.* **2009**, *48*, 8115. (e) A. M. Douvas, E. Makarona, N. Glezos, P. Argitis, J. A. Mielczarski, E. Mielczarski, *Acs Nano*, **2008**, *2*, 733.

1.9   (a) J. T. Rhule, C. L. Hill, D. A. Judd, *Chem. Rev.* **1998**, *98,* 327. (b) S. Uchida, R. Kawamoto, N. Mizuno, *Inorg. Chem.* **2006**, *45*, 5136. (c) C. Zhao, Z. Huang, W. Rodríguez-Cordoba, C. S. Kambara, K. P. O'Halloran, K. I. Hardcastle, D. G. Musaev, T. Lian, C. L. Hill. *J. Am. Chem. Soc.* **2011**, *133*, 20134. (d) B. Qin, H. Chen, H. Liang, L. Fu, X. Liu, X. Qiu, S. Liu, R. Song, Z. Tang. *J. Am. Chem. Soc.* **2010**, *132*, 2886.

1.10 (a) T. Yamase. *J. Mater. Chem*. **2005**, *15*, 4773. (b) J. Geng, M. Li, J. Ren, E. Wang, X. Qu. *Angew. Chem. Int. Ed*. **2011**, *50*, 4184.

1.11 (a) S. Reinoso. *Dalton Trans*. **2011**, *40*, 6610. (b) A. Müller, P. Gouzerh. *Chem. Soc. Rev.* **2012**, *41*, 7431. (c) A. Proust, B. Matt, R. Villanneau, G. Guillemot, P. Gouzerh, G. Izzet. *Chem. Soc. Rev*. **2012**, *41*, 7605.

1.12 (a) A. Müller, S. K. Das, C. Kuhlmann, H. Bögge, M. Schmidtmann, E. Diemann, E. Krickemeyer, J. Hormes, H. Modrow*,* M. Schindler. *Chem. Commun.* **2001**, 655. (b) X. Kuang, X. Wu, R. Yu, J. P. Donahue, J. Huang, C. –Z. Lu. *Nat. Chem*. **2010**, *2*, 461.

1.13   M. Nymanz, P. C. Burns, *Chem. Soc. Rev.* **2012**, *41*, 7354.

1.14 (a) X. López, I. A. Weinstock, C. Bo, J. P. Sarasa, J. M. Poblet. *Inorg. Chem.*, **2006**, *45*, 6467. (b) D. M. –L. Carey, A. Muñoz-Castro, C. J. Bustos, J. M. Manríquez, R. Arratia-Pérez *J. Phys. Chem. A*, **2007**, *111*, 6563. (c) M. R. S. A. Janjua. *Inorg. Chem.*, **2012**, *51*, 11306.

1.15 (a) E. Coronado, S. Curreli, C. Gimenez-Saiz, C. J. Gomez-Garcia, A. Alberola, E. Canadell, *Inorg. Chem*. **2009**, *48*, 11314. (b) W. Bu, S. Uchida, N. Mizuno, *Angew. Chem., Int. Ed*. **2009**, *48*, 8281. (c) C. M. Granadeiro, R. A. S. Ferreira, P. C. R.

Soares-Santos, L. D. Carlos, H. I. S. Nogueira, *Eur. J. Inorg. Chem.* **2009**, 5088. (d) T. Ito, H. Yashiro, T. Yamase, *Langmuir*, **2006**, *22*, 2806. (e) R. Cao, S. Liu, L. Xie, Y. Pan, J. Cao, Y. Ren, L. Xu, *Inorg. Chem.* **2007**, *46*, 3541. (f) D. Honda, T. Ozeki, A. Yagasaki*, Inorg. Chem.* **2005**, *44*, 9616.

1.16 (a) Y. Lu, Y. Xu, Y. Li, E. Wang, X. Xu, Y. Ma. *Inorg. Chem.* **2006**, *45*, 2055. (b) L. Cheng, J. A. Cox. *Chem. Mater.* **2002**, *14*, 6. (c) C. R. Graham, R. G. Finke. *Inorg. Chem.* **2008**, *47*, 3679. (d) Y. –W. Li, Y. –G. Li, Y. –H. Wang, X. –J. Feng, Y. Lu, E. –B. Wang, *Inorg. Chem.* **2009**, *48*, 6452.

1.17 (a) J. Kim, A. A. Gewirth. *Langmuir*, **2003**, *19*, 8934. (b) S. –T. Zheng, D. –Q. Yuan, J. Zhang, G. –Y. Yang. *Inorg. Chem.* **2007**, *46*, 4569. (c) R. Copping, L. Jonasson, A. J. Gaunt, D. Drennan, D. Collison, M. Helliwell, R. J. Pirttijarvi, C. J. Jones, A. Huguet, D. C. Apperley, N. Kaltsoyannis, I. May. *Inorg. Chem.*, **2008**, *47*, 5787. (d) N. S. Antonova, J. J. Carbó, U. Kortz, O. A. Kholdeeva, J. M. Poblet, *J. Am. Chem. Soc.* **2010**, *132*, 7488. (e) B. S. Bassil, S. S. Mal, M. H. Dickman, U. Kortz, H. Oelrich, L. Walder, *J. Am. Chem. Soc.* **2008**, *130*, 6696. (f) W. Chen, Y. Li, Y. Wang, E. Wang, Z. Zhang. *Dalton Trans.* **2008**, 865. (g) F. Hussain, U. Kortz, B. Keita, L. Nadjo, M.T. Pope. *Inorg. Chem.* **2006**. *45,* 761.

1.18 A. Merca, A. Müller, J. v. Slageren, M. Lage, B. Krebs. *J. Cluster Sci.* **2007**, *18*, 711.

1.19 W. Chen, Y. Li, Y. Wang, E. Wang, Z. Zhang, *Dalton Trans.* **2008**, 865.

1.20 (a) T. Kurata, A. Uehara, Y. Hayashi, K. Isobe, *Inorg. Chem.* **2005**, *44*, 2524.

1.21 (a) A. Müller, C. Serain. *Acc. Chem. Res.* **2000**, *33*, 2. (b) A. Müller, E. Krickemeyer, J. Meyer, H. Bögge, F. Peters, W. Plass, E. Diemann, S. Dillinger, F. Nonnenbruch, M. Randerath, C. Menke, *Angew. Chem. Int. Ed. Engl.* **1995**, *34*, 2122. (c) A. Müller, E. Krickemeyer, H. Bögge, M. Schmidtmann, F. Peters, *Angew. Chem. Int. Ed.* **1998**, *37*, 3360. (d) T. Liu, E. Diemann, H. Li, A. W. M. Dress, A. Muller, *Nature*, **2003**, *426*, 59. (e) J. Qiu, J. Ling, A. Sui, J. E. S. Szymanowski, A. Simonetti, P. C. Burns, *J. Am. Chem. Soc.* **2012**, *134*, 1810. (f) H. Imai, T. Akutagawa, F. Kudo, M. Ito, K.. Toyoda, S. Noro, L. Cronin, T. Nakamura, *J. Am. Chem. Soc.* **2009**, *131*, 13578.

1.22 (a) A. Müller, J. Meyer, E. Krickemeyer, E. Diemann, Angew. *Chem. Int. Ed. Engl.* **1996**, *35*, 1206. (b) A. Müller, S. K. Das, W. P. Fedin, E. Krickemeyer, C. Beugholt, H. Bögge, M. Schmidtmannn, B. Hauptfleisch, *Z. Anorg. All. Chem.* **1999**, *625,* 1187.

1.23 A. Müller, E. Krickemeyer, H. Bögge, M. Schmidtmann, F. Peters. *Angew. Chem. Int. Ed.* **1998**, *37*, 3360.

1.24 A. Müller, S. K. Das, C. Kuhlmann, H. Bögge, M. Schmidtmann, E. Diemann, E. Krickemeyer, J. Hormes, H. Modrowb, M. Schindler. *Chem. Commun*. **2001**, 655.

1.25 (a) C. Ritchie, A. Ferguson, H. Nojiri, H. N. Miras, Y. F. Song, D.-L. Long, E. Burkholder, M. Murrie, P. Kogerler, E. K. Brechin, L. Cronin*, Angew. Chem., Int. Ed*. **2008**, *47*, 5609. (b) M. Ibrahim, Y. Lan, B. S. Bassil, Y. Xiang, A. Suchopar, A. K. Powell, U. Kortz, *Angew. Chem., Int. Ed*. **2011**, *50*, 4708.

1.26 T. Yamase, K. Fukaya, H. Nojiri, Y. Ohshima, *Inorg. Chem.* **2006**, *45*, 7698.

1.27 (a) S. S. Mal, U. Kortz. *Angew. Chem., Int. Ed.* **2005**, *44*, 3777. (b) H. N. Miras, J. Yan, D. –L. Long, L. Cronin, *Chem. Soc. Rev*. 2012, **41**, 7403.

1.28 H. N. Miras, J. Yan, D. –L. Long, L. Cronin. *Chem. Soc. Rev*. **2012**, *41*, 7403.

1.29 (a) T. Baba, Y. Ono, T. Ishimoto, S. Morikawa, S. Tanooka, *Bull. Chem. Soc. Jpn.* **1985**, *58*, 2155. (b) T. Baba, Y. Ono. *Appl. Catal.* **1986**, *22*, 321.

1.30 N. Mizuno, T. Watanabe, M. Misono, *J. Phys. Chem.* **1985**, *89*,80.

1.31 (a) K. Bruckman, M. Che, J. Haber, J. M. Tatibouet, *Catal. Lett.* **1994**, *25*, 225. (b) C. Rocchiccioli-Deltcheff, M. Amirouche, G. Herve, M. Fournier, M. Che, I. M. Tatibouet. *J. Catal.* **1990**, *126*, 591.

1.32 N. Mizuno, K. Yamaguchi, K. Kamata, *Catal. Surv. Asia*, **2011**, *15*, 68.

1.33 (a) S. Uchida, S. Hikichi, T. Akatsuka, T. Tanaka, R. Kawamoto, A. Lesbani, Y. Nakagawa, K. Uehara, N. Mizuno, *Chem. Mater*. **2007**, *19*, 4694. (b) S. Uchida, N. Mizuno, *Chem.–Eur. J.* **2003**, *9*, 5850.

1.34 K. Inumara, T. Ishihara, Y. Okuhara, S. Yamanaka, *Angew. Chem., Int. Ed*. **2007**, *46*, 7625.

1.35 (a) P. S. Kulkarni, C. A. M. Afonsoa, *Green Chem*. **2010**, *12*, 1139. (b) Y. Chi, C. Li, Q. Jiao, Q. Liu, P. Yan, X. Liu, U. Welz-Biermann, *Green Chem*. **2011**, *13*, 1224.

1.36 A. Rothlisberger, R. Prins, *J. Catal*. **2005**, *235*, 229.

1.37 (a)Y. Shiraishi, K. Tachibana, T. Hirai, I. Komasawa, *Ind. Eng. Chem. Res*. **2002**, *41*, 4362. (b) C. Komintarachat, W. Trakarnpruk, *Ind. Eng. Chem. Res*. **2006**, *45*, 1853. (c) L. Y. Kong, G. Li, X. S. Wang, *Catal. Today*. **2004**, *93*, 341. (d) H. Li, X. Jiang, W. Zhu, J. Lu, H. Shu, Y. Yan. *Ind. Eng. Chem. Res*. **2009**, *48*, 9034. (e) A. Chica, A. Corma, M. E. Domine, *J. Catal*. **2006**, *242*, 299.

1.38 A. M. Khenkin, R. Neumann, *ChemSusChem*. **2011**, *4*, 346.

1.39 J. Xu, S. Zhao,W. Chen, M.Wang, Y. F. Song. *Chem.–Eur. J.* **2012**, *18*, 4775.

1.40 G. Gao, F. Li, L. Xu, X. Liu, Y. Yang. *J. Am. Chem. Soc.* **2008**, *130*, 10838.

1.41   S. Garai, E.T. K. Haupt, H. Bogge, A. Merca, A. Muller. *Angew. Chem. Int. Ed.* **2012**, *51*, 10528.

1.42   F. Chen, T. Dong, T. Xu, X. Li, C. Hu, *Green Chem*. **2011**,*13*, 2518.

1.43   B. Keita, I.-M. Mbomekalle, L. Nadjo, C. Haut. *Electrochem. Commun.* **2004**, *6*, 978.

1.44   (a) G. Zhang, B. Keita, R. Ngo Biboum, F. Miserque, P. Berthet, A. Dolbecq, P. Mialane, L. Catalae, L. Nadjo. *J. Mater. Chem.* **2009**, *19*, 8639. (b) M. Lira-Cantu, P. Gomez-Romero. *Chem. Mater*. **1998**, *10*, 698. (c) B. M. Azumi, T. Ishihara, H. Nishiguchi, Y. Takita, *Electrochemistry*, **2002**, *70*, 869. (d) N. Kawasaki, H. Wang, R. Nakanishi, S. Hamanaka, R. Kitaura, H. Shinohara, T. Yokoyama, H. Yoshikawa, K. Awaga, *Angew. Chem., Int. Ed*. **2011**, *50*, 3471.

1.45   (a) T. Yamase, *Chem. Rev.* **1998**, *98*, 307. (b) E. Papaconstantinou, *Chem. Soc. Rev.*, **1989**, *18*, 1.

1.46   N. S. Lewis, D. G. Nocera, *Proc. Natl. Acad. Sci. U. S. A.* **2006**, *103*, 15729.

1.47   (a) C. Streb. *Dalton Trans.* **2012**, *41*, 1651. (b) A. Mylonas, A. Hiskia, E. Androulaki, D. Dimotikali, E. Papaconstantinou, *Phys. Chem. Chem. Phys.* **1999**, *1*, 437.

1.48   J. T. Rhule, C. L. Hill, D. A. Judd. *Chem. Rev.* **1998,** *98,* 327.

1.49   (a) B. Keita, T. Liub, L. Nadjo, *J. Mater. Chem.* **2009**, *19*, 19. (b) J. Zhang, B. Keita, L. Nadjo, I.-M. Mbomekalle, T. Liu, *Langmuir*, **2008**, *24*, 5277.

1.50   (a) S. Mandal, P. R. Selvakannan, R. Pasricha, M. Sastry, *J. Am. Chem. Soc*. **2003**, *125*, 8440. (b) M. Sastry, A. Swami, S. Mandal , P. R. Selvakannan, *J. Mater. Chem.* **2005**, *15*, 3161. (c) S. Mandal, D. Rautaray, M. Sastry, *J. Mater. Chem*. **2003**, *13*, 3002.

1.51   C. Sanchez, G. J. de A. A. Soler-Illia, F. Ribot, T. Lalot, C. R. Mayer, V. Cabuil, *Chem. Mater*. **2001**, *13*, 3061.

1.52   (a) C. Sanchez, G. J. de A. A. Soler-Illia, F. Ribot, T. Lalot, C. R. Mayer, V. Cabuil, *Chem. Mater*. **2001**, *13*, 3061. (b) T. Akutagawa, F. Kudo, R. Tsunashima, S. Noro, L. Cronin, T. Nakamura, *Inorg. Chem.* **2011**, *50*, 6711. (c) Y. Zhou, L. Zheng, F. Han, G. Zhang, Y. Ma, J. Yao, B. Keita, P. de Oliveira, L. Nadjo. *Colloids Surf. A*. **2011**, *375*, 97.

1.53   (a) S. Uchida, R. Kawamoto, N. Mizuno. *Inorg. Chem.* **2006**, *45*, 5136. (b) A. M. Douvas, E. Makarona, N. Glezos, P. Argitis, J. A. Mielczarski, E. Mielczarski. *Acs. Nano.* **2008**, *2*, 733.

1.54 (a) A. Proust, R. Thouvenot, P. Gouzerh. *Chem. Commun.* **2008**, 1837. (b) G. Sazani, M. T. Pope, *Dalton Trans*. **2004**, 1989.

1.55 H. Kang, J. Zubieta, *J. Chem. Soc., Chem. Commun*. **1988**, 1192.

1.56 (a) Y. Du, A. L. Rheingold, E. A. Maatta, *J. Am. Chem. Soc.* **1992**, *114*, 345. (b) P. Gouzerh, A. Proust, *Chem. Rev.* **1998**, *98*, 77.

1.57 (a) Y.-F. Song, D.-L. Long, S. E. Kelly, L. Cronin, *Inorg. Chem.* **2008**, *47*, 9137. (b) M. H. Rosnes, C. Musumeci, C. P. Pradeep, J. S. Mathieson, D.-L. Long, Y.-F. Song, B. Pignataro, R. Cogdell, L. Cronin, *J. Am. Chem. Soc*. **2010**, *132*, 15490.

1.58 S. Landsmann, C. Lizandara-Pueyo, S. Polarz, *J. Am. Chem. Soc*. **2010**, *132*, 5315.

1.59 (a) C. Lin, W. Zhu, H. Yang, Q. An, C. Tao, W. Li, J. Cui, Z. Li, G. Li, *Angew. Chem., Int. Ed.* **2011**, *50*, 4947. (b) G. Maayan, R. Popovitz-Biro, R. Neumann, *J. Am. Chem. Soc.* **2006**, *128*, 4968.

1.60 Y. Nagaoka, S. Shiratori, Y. Einaga, *Chem. Mater.* **2008**, *20*, 4004.

1.61 M. Clemente-Leon, E. Coronado, C. J. Gomez-Garcia, C. Mingotaud, S. Ravaine, G. Romualdo-Torres, P. Delhaes, *Chem.–Eur. J*. **2005**, *11*, 3979.

1.62 T. Liu, *Langmuir*, **2010**, *26*, 9202.

1.63 (a) A. Mallick, B. Garai, D. D. Díaz, R Banerjee, *Angew. Chem.* **2013**, *125*, 14000. (b) A. Mallick, S. Saha, P. Pachfule, S. Roy, R. Banerjee, *J. Mater. Chem*. **2010**, *20*, 9073. (c) T. Panda, P. Pachfule, Y. Chen, J. Jiang, R. Banerjee, *Chem. Commun*. **2011**, *47*, 2011.

Room Temperature Synthesis of Polyoxometalate Based Hybrid Salts

2.1 Introduction

Designing novel porous crystalline materials are of current research interest because of their unique properties, which make them suitable candidates for potential application in sorption, separation, and catalysis [2.1-2.3]. Recently researchers have found interest in designing variety of porous crystalline materials by the rational synthesis of zeolites and their analogues using new building blocks [2.1], metal–organic frameworks (MOFs) [2.2], and covalent organic frameworks (COFs) [2.3]. Ionic crystals consisting of anions and cations generate strong electrostatic attraction force at the intra-crystalline region which makes them suitable for accommodating polar guests [2.4]. The coulombic potential created by the ionic constituents is isotropic in nature and decreases with increasing distances. Therefore, some ionic crystals can change their crystal phase to accommodate specific guest molecules [4.4d,e].

The construction of the isolable POM-based compounds and properties of the materials created by the POM clusters have increasingly became apparent. The key characteristic have been utilized frequently over the last few years, the connection between the POM cluster generated from monomeric metal oxide salt and intermediate metal-oxide/metal complex building blocks, resulted to be a vitally new approach to adopt and enable to control over new structure, engineer properties. POM units are composed of metal ions (M = W^{VI}, Mo^{VI}, V^{V}, Nb^{V}, etc.) and oxo ligands [2.5]. Organic moieties can be attached via addenda compounds to lacunary POM clusters [2.6]. The reaction of Keggin-type and Dawson-type lacunary clusters with organosilicon, organotin, organogermanium compound leads to the formation of stable covalent bonded POMs and organic composites [2.7]. Anderson type and Dawson type clusters can be tailored with tris-alkoxo ligands by replacement of the oxo ligands with alkoxo groups [2.8]. A group of researchers successfully organized a covalently modified Anderson-based scaffold by grafting pyrene moieties onto the Anderson type POMs. The resulting materials show typical physical properties that are essentially different than parent POM cluster. Additionally, covalently modified POMs can be connected further through

non-covalent interactions [2.9]. Neumann and co-workers have reported the synthesis of POM polymer composite which was used as biphasic catalyst for selective oxidation of aliphatic alcohol in aqueous medium [2.10]. Depending upon the type of interaction of POMs with organic constituents and the arrangement of POM in hybrid matrix, POM hybrids can be classified in six different categories, such as (i) POM based ionic composites [2.11] [Figure 2.2a], (ii) POM incorporated MOFs [2.12] [Figure 2.2b], (iii) POM based coordination polymers [2.13] [Figure 2.2c], (iv) POM-graphene composites [2.14] [Figure 2.2d], (v) POM and polymer hybrid [2.15] [Figure 2.3a], (vi) POM based porous architecture [2.16] [Figure 2.3b].
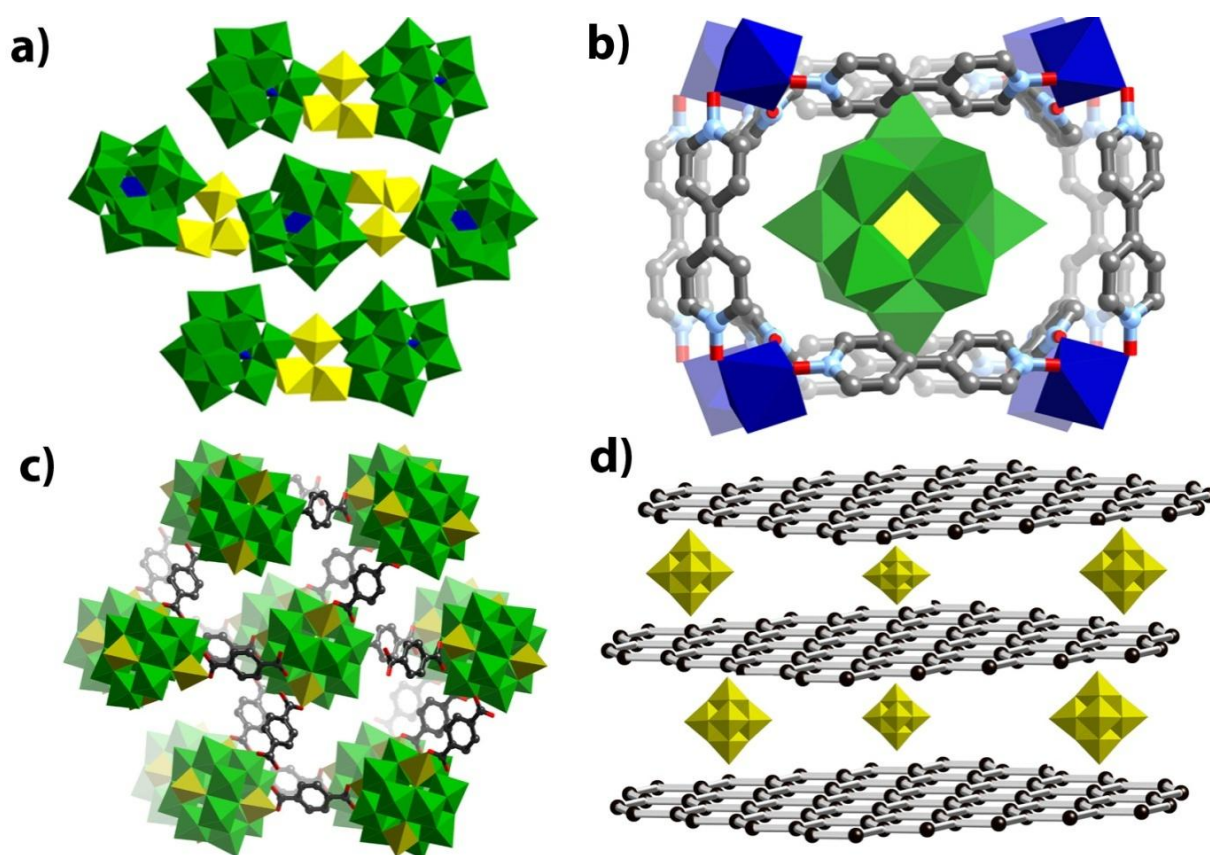
Figure 2.2: (a) Tri-chromium cation and Keggin type anion based ionic composite (Figure reproduced from ref 7). (b) Polyoxometalate incorporated 4,4′-bipyridine-*N,N*-dioxide and Co(II) based metal organic framework (Figure reproduced from ref 2.8). (c) Keggin type polyoxometalate are connected via benzene dicarboxylic acid to from coordination polymer (Figure reproduced from ref 9). (d) Layer-by-layer assembly of polyoxometalate graphene composite (Ref 10).
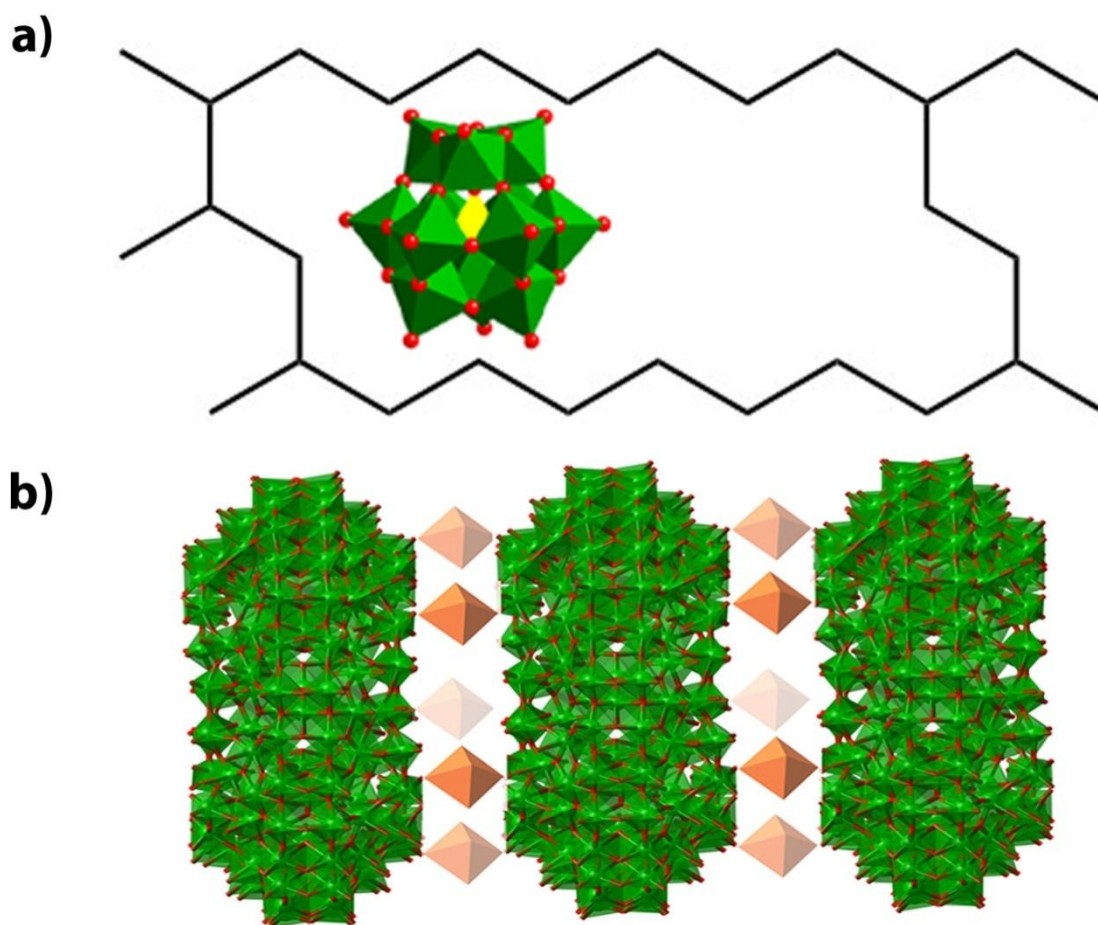
Figure 2.3: (a) POM encapsulated in cross-link polymer hybrid (Ref 2.11). (b) Polyoxometalate based extended architecture connected via hetero metallic centers (Ref 2.12).

2.2 Crystallization of POM based ionic salts for various applications

Hydrophilic macro anions of POM interact with organic cations or cationic surfactants through electrostatic interaction to build inorganic–organic hybrids. One example of such compound is the surfactant encapsulated POM clusters [2.12]. These clusters typically consist of a core–shell structure having hydrophilic POMs in the core enclosed by hydrophobic functional groups. A similar synthetic approach can be extended to fabricate POM/polymer hybrids. Mizuno and co-workers has recently developed a new class of organic macrocations and POM anion based ionic crystals. An ionic crystal, $[Cr_3O(OOCCF_3)_6(H_2O)_3]_3[\alpha\text{-}PW_{12}O_{40}]\cdot8CH_3COCH_3\cdot8H_2O\cdot CHCl_3$ have been prepared by using a fluorine-substituted macrocation with a phosphododecatungstate. This compound consists of a layered structure [interlayer distance of *ca.* 3.5 Å] where the inner surface of the layer was modified with CF_3 groups of the macrocations. Solvent molecules (acetone and

chloroform) instantly desorbed and exchanged with water in ambient condition and a hydrated phase, $[Cr_3O(OOCCF_3)\cdot6(H_2O)_3]_3[\alpha\text{-}PW_{12}O_{40}]\cdot25H_2O$ was obtained [Figure 2.4]. The H_2O molecules were partially desorbed by the treatment of hydrated phase in vacuum or under
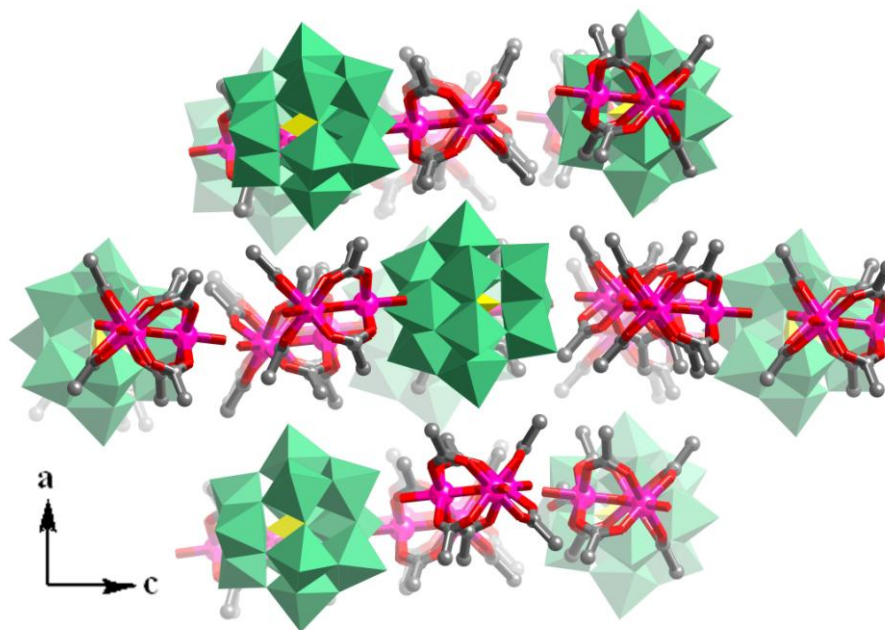
Figure 2.4: Crystal structure of $Cr_3O(OOCCF_3)_6$ $(H_2O)_3]_3[\alpha\text{-}PW_{12}O_{40}]\cdot 8CH_3COCH_3\cdot 8H_2O\cdot CHCl_3$. Green and yellow polyhedra show the $[WO_6]$, $[PO_4]$. C, O, Cr are represented in grey, red and pink colour respectively. Solvent molecules and fluorine atoms are removed for charity (Figure reproduced from ref 2.17).

inert gas flow at 298–303 K, and a partially hydrated new phase, $[Cr_3O(OOCCF_3)\cdot6(H_2O)_3]_3[\alpha\text{-}PW_{12}O_{40}]\cdot15H_2O$ was formed. The PXRD patterns of the partially hydrated phase matched well with the simulated PXRD patterns of the parent phase, which proved the retention of same crystalline phase after solvent exchange. The partially hydrate compound adsorbed CO_2 and unsaturated hydrocarbons, while it repelled saturated hydrocarbons such as ethane and methane. Acetylene/methane, CO_2/methane, and ethylene/ethane sorption ratios were calculated as 13, 15, and 4.9, respectively, at 198 K and 100 kPa [2.17].

Anionic nano-size POM clusters can form ionic crystals with unique guest sorption properties by complexation with appropriate organometallic cations (macrocations). With this ideas, a flexible organic–inorganic hybrid ionic crystal $K_2[Cr_3O(OOCH)_6(4\text{-ethylpyridine})_3]_2[\alpha\text{-}SiW_{12}O_{40}]\cdot4CH_3OH$ was prepared by complexation of macrocations $[Cr_3O\text{-}(OOCH)_6(4\text{-ethylpyridine})_3]^+$, silicododecatungstates $[\alpha\text{-}SiW_{12}O_{40}]^{4-}$, and potassium ions [Figure 2.5]. The compound shows high affinity towards CO_2 over C_2H_2, and can be used for purification of C_2H_2 form CO_2. The CO_2 sorption involves two phase transitions, while the C_2H_2 sorption

involves single phase transition. The CO_2/C_2H_2 sorption ratio reaches a maximum value of 4.8 at 278 K temperature and 100 kPa pressure [2.18].

Although inorganic zeolites and MOFs are known for sorption and separation, however report of MOFs or zeolites with channel-selective independent sorption and collection of hydrophilic and hydrophobic molecules are not available in the literature. The ionic salts, $Cs_2[Cr_3O-(OOCC_2H_5)_6(H_2O)_3]_2[\alpha-SiW_{12}O_{40}] \cdot 4H_2O$
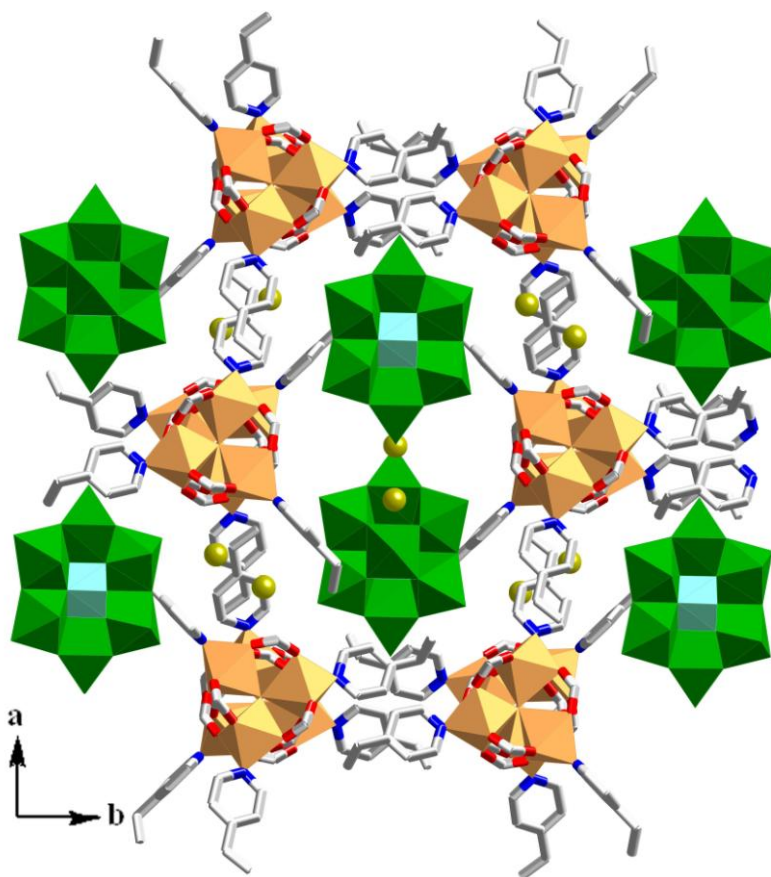
Figure 2.5: Crystal structure $K_2[Cr_3O(OOCH)_6$ (4-ethylpyridine)$_3]_2[\alpha-SiW_{12}O_{40}] \cdot 4CH_3OH$. The representation shows the arrangements of the constituent ions in the *ab*-plane. Green and orange polyhedra represent the WO_6 and CrO_5N units, respectively; golden spheres: potassium ions. Solvent molecules are removed for clarity (Figure reproduced from ref 2.18).

[Figure 2.6] prepared by crystallization of $[Cr_3O-(OOCC_2H_5)]^+$ cation, $[\alpha-SiW_{12}O_{40}]^{4-}$ anion and Cs^+, can adsorb dichloromethane and water in the hydrophilic and hydrophobic channels, respectively. The sorption property can be utilized for the collection of water (hydrophobic) and dichloromethane (hydrophobic) molecules from the mixture [2.19].

Hybridization of inorganic clusters with organic Cucurbit[*n*]uril [CB] macrocycles could produce multifunctional materials that can combine the key merits of both sources, for example, magnetic, redox, catalytic activity of POM, and recognition properties of CB. This new approach provides perspectives in the design of functional porous materials [Figure 2.7a]. This type of hybrid complex can show the host-guest chemistry of CBs, enhance the

versatile redox characteristic of POMs and provide a means to prepare reactive inclusion complexes that are otherwise hard to achieve [2.20].
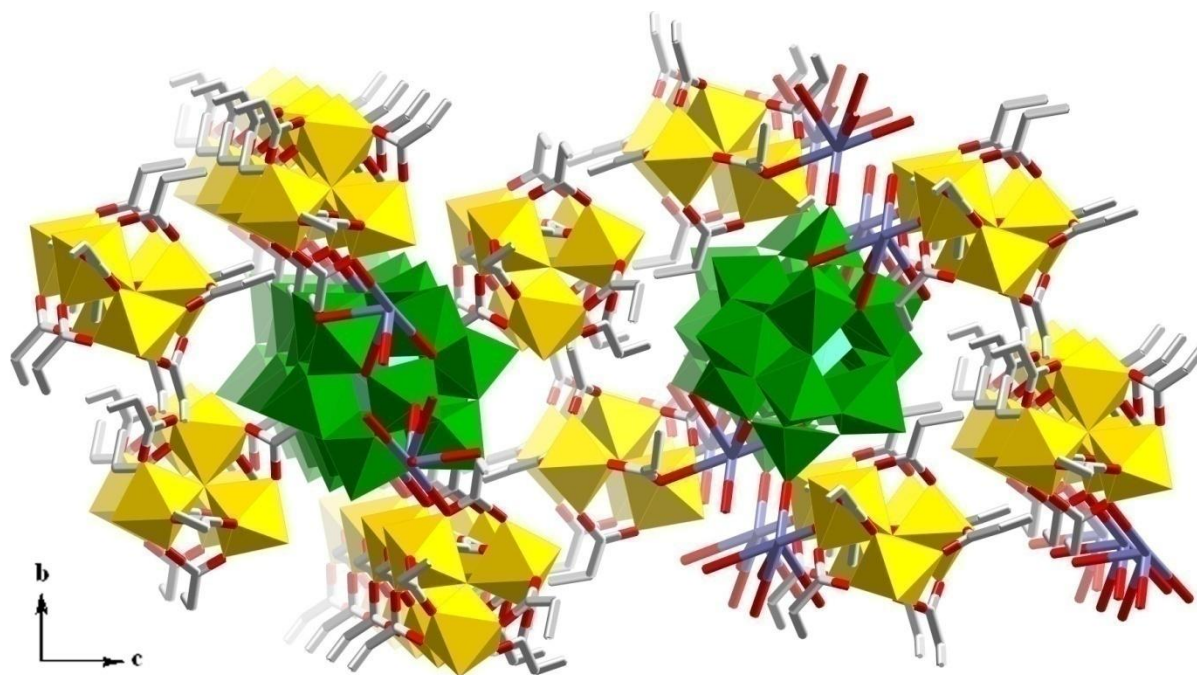
Figure 2.6: Crystal structure of $Cs_2[Cr_3O-(OOCC_2H_5)_6(H_2O)_3]_2[\alpha\text{-}SiW_{12}O_{40}]\cdot4H_2O$. Cyan, green, and yellow polyhedral showed the $[SiO_4]$, $[WO_6]$, and $[CrO_6]$ units. C, N, O are represented in grey, light blue and red colours respectively. Solvent molecules have been removed for clarity clarity (Figure reproduced from ref 2.19).

A series of ionic salts have been prepared by complexation of different Keggin anion keeping the macrocation $[Cr_3O(OOCH)_6\text{-}(H_2O)_3]^+$ same. This series of salts have been formulated as $Na_2[Cr_3O(OOCH)_6(H_2O)_3][\alpha\text{-}PW_{12}O_{40}]\cdot16H_2O$, $K_3[Cr_3O\text{-}(OOCH)_6(H_2O)_3][\alpha\text{-}SiW_{12}O_{40}]\cdot16H_2O$, $Rb_4[Cr_3O(OOCH)_6(H_2O)_3][\alpha\text{-}BW_{12}O_{40}]\cdot16H_2O$ and $Cs_5[Cr_3O(OOCH)_6\text{-}(H_2O)_3][\alpha\text{-}CoW_{12}O_{40}]\cdot5H_2O$. The calculated cell volumes per formula of evacuated salts decease in the order of $[\alpha\text{-}PW_{12}O_{40}]^{3-} > [\alpha\text{-}SiW_{12}O_{40}]^{4-} > [\alpha\text{-}BW_{12}O_{40}]^{5-} > [\alpha\text{-}CoW_{12}O_{40}]^{6-}$ composites respectively [Figure 2.7b]. This trend could be due to the charge associated with different Keggin anion. The evacuated salt of $[\alpha\text{-}PW_{12}O_{40}]^{3-}$ adsorbs $\leq$ C5 polar organic molecules such as 1-butanol, acetonitrile, and methyl propionate. The evacuated salt of $[\alpha\text{-}SiW_{12}O_{40}]^{4-}$ adsorbs ethanol, acetonitrile, and methyl formate. The evacuated salt of $[\alpha\text{-}BW_{12}O_{40}]^{5-}$ can adsorb water and methanol, whereas the evacuated salt of $[\alpha\text{-}CoW_{12}O_{40}]^{6-}$ can adsorb water only [2.21].

A group of researchers recently showed that protonated amines can not only act as counter-cations but also influence the final POM structure by limiting the reorganization rate of

different POM isomers in solution [2.22]. One of the main aspects of POM clusters is their solubility in various solvents, which puts POMs in a distinctive position as molecular metal oxides. Even when the counter ions of POM clusters are inorganic cations (such as Na^+, K^+, Cs^+, etc), POMs are still capable of being dissolved in polar organic solvents, which is very specific from the other metal-oxide materials. The clusters interact electrostatically with cationic groups when dissolved in solvent and this driving force allows associations between POMs and cations, charged molecules, metal complexes, polymers, as well as positively charged solid supports. POMs can also interact with proton donors such as ammonium analogues, proteins, etc by hydrogen bonding.
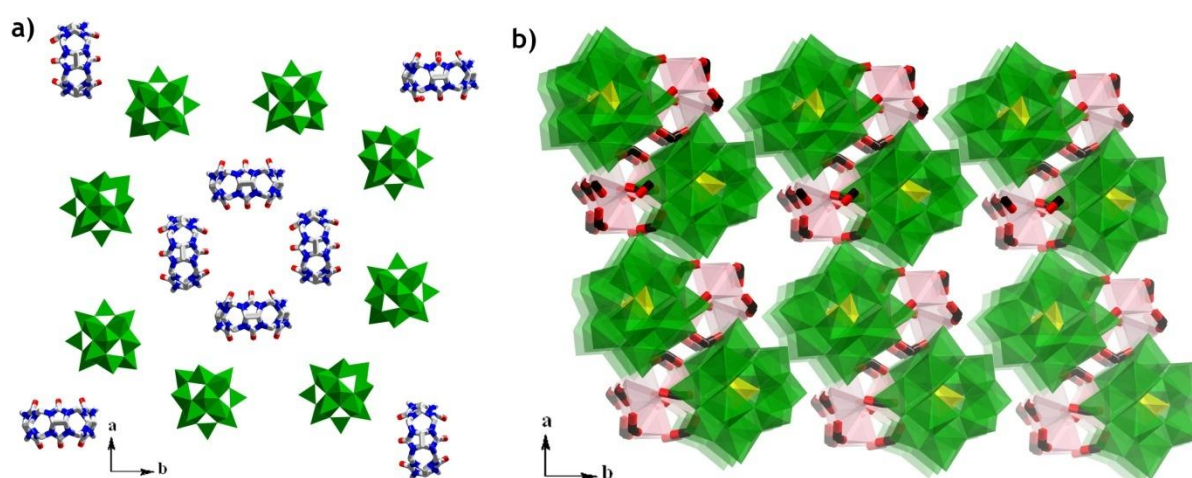
Figure 2.7: (a) Crystal structure of $[CB[6](H_2O \subset V^{IV}_{18}O_{42})]^{12-}$, the counter cation, K^+ has been removed for clarity. Green polyhedra represents vanadium centre. C, N, O have been represented in grey, blue and red colours respectively (Figure reproduced from ref 2.20). (b) Crystal structure of $Na_2[Cr_3O(OOCH)_6(H_2O)_3][\alpha-PW_{12}O_{40}]\cdot 16H_2O$. Green, yellow, and pink polyhedra represent WO_6, PO_4, CrO_6 units respectively. C, O have been represented in black and red colour respectively. Solvent molecules were removed for clarity (Figure reproduced from ref 2.21).

One of the most interesting aspects of POM chemistry lies with the fact that POM clusters in the crystal lattice can be considered as supramolecular synthons [2.23]. As a result, it is possible to engineer their assembly inside the polyoxometalate-based ionic crystals to create materials with desired properties [2.24]. However, despite increasingly active research, understanding of the self-assembly processes which govern the resulting polyoxometalate-based ionic crystal structure formation remains limited. Thus, there is a clear need to understand the crystallization aspects of POMs so that the key features of the mechanism of

the self-assembly of polyoxometalate clusters can be understood. The present work provides a perspective of the use of polyoxometalates: (i) in the rational syntheses of ionic crystals with porous tris(ethylenediamine)cobalt(III) cation, $[Co(en)_3]^{3+}$ under mild conditions; (ii) on the self-assembly of the discrete cationic components and sorption properties of the resulting supramolecular ionic crystals [2.24f].

Recently, researchers found that, $[Co(en)_3]Cl_3$, one of the most fundamental compound of coordination chemistry [2.25] can transform its ionic crystal structure to adopt various guest of different size and shape by weak physisorption [2.26]. Thus, an ionic crystal, unlike rigid metal organic frameworks (MOFs) [2.27], can be considered to possess extremely unrestricted transformability upon absorbing different gases. Although both POM based ionic crystals and $[Co(en)_3]Cl_3$ are well known for their absorption of organic solvents and H_2O, but POM clusters are greatly underutilized in terms of their capabilities of storing hydrogen or carbon-dioxide [2.28]. This made us interested in the rational synthesis of a series of polyoxometalate based hybrid materials with porous $[Co(en)_3]^{3+}$. These ionic solids are formulated as $[Co(en)_3Mo_8O_{26}(H_3O)(Cl)]·(DMF)_4·(H_2O)$ (***Co-Mo$_8$-DMF***), $[\alpha$-PW$_{12}$O$_{40}][Co(en)_3]·6DMF$ (***Co-W$_{12}$P-DMF***), $[\alpha$-PW$_{12}$O$_{40}][Co(en)_3]·6DEF$ (***Co-W$_{12}$P-DEF***), $[\alpha$-PMo$_{12}$O$_{40}][Co(en)_3]·5.5DMF$ (***Co-Mo$_{12}$P-DMF***), $[\alpha$-PMo$_{12}$O$_{40}][Co(en)_3]·6DEF$ (***Co-Mo$_{12}$P-DEF***), $[\alpha$-SiW$_{12}$O$_{40}][Co(en)_3]_{3/2}[Cl]_{1/2}·6DMF·3H_2O$ (***Co-W$_{12}$Si-DMF***), $[\alpha$-SiW$_{12}$O$_{40}][Co(en)_3]·6DEF$ (***Co-W$_{12}$Si-DEF***), $[\alpha$-PMo$_{12}$O$_{40}][Co(en)_2 (H_2O)_2]·DIOX$ (***Co-Mo$_{12}$P-DIOX***) (en = ethylenediamine, DMF = dimethyl formamide, DEF = diethyl
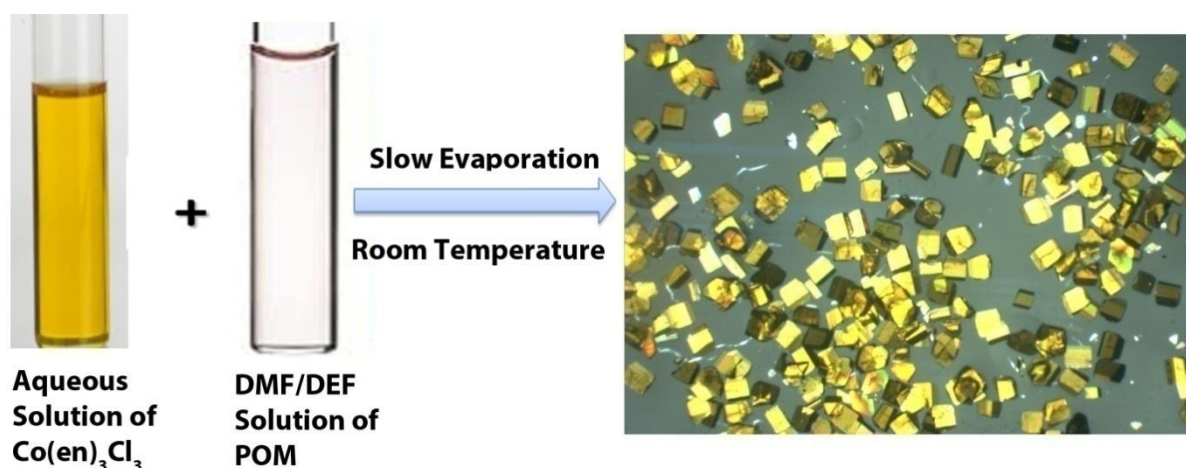
Figure 2.8: Room temperature crystallization of POM based ionic salts using aqueous solution of $[Co(en)_3]Cl_3$ salts and DEF/DMF solution of polyoxometalate.

formamide, DIOX = dioxane) [Figure 2.8]. These POM bassed ionic salts display interesting H-bonded structural features, selective hydrogen (H_2) and carbon-dioxide (CO_2) sorption over nitrogen (N_2). It is noteworthy that examples of POM based ionic salts, crystallized from non aqueous media is extremely rare as researchers prefer to crystallize it from H_2O [2.29]. These ionic solids have been determined by single crystal X-ray diffraction and further characterized by IR spectra, PXRD and TGA.

2.2.1 Synthesis of $[Co(en)_3]^{3+}$ and POM ionic composites

In a specific crystallization process many factors can affect the formation and crystal growth of products, such as the starting concentrations, pH values, temperature and nature of solvents. As the pH values and temperature are same in this study, we attempted to examine the other parameters more closely. Selection of the POM anions was an important factor for the complexation of the polyoxometalates with the $[Co(en)_3]^{3+}$ cation. Among a series of POM anions we found that β-octamolybdate (β-$Mo_8O_{26}^{4-}$) and α-Keggin (α-$PMo_{12}O_{40}^{3-}$, α-$PW_{12}O_{40}^{3-}$, α-$SiW_{12}O_{40}^{4-}$) yielded ionic complexes with good crystallinity. Ionic crystals reported in this work were obtained by the interactions between the $[Co(en)_3]^{3+}$ cations and POM anions [Figure 2.9]. We anticipated the formation of 1:1 ionic complex as the $3^-/4^-$ charged POM anions would be neutralized by the equimolar amount of the 3^+ charge of $[Co(en)_3]^{3+}$ cation. Two important aspects that we considered during the synthesis are: (i) the pH value of the reaction system should be carefully maintained so as to stabilize the structure and avoid early precipitation of microcrystalline powder; (ii) the usage of DMF and DEF as solvent for crystallization. Most of the POM based ionic crystals, reported so far, have been synthesized from water as researchers has avoided using high boiling solvents like DMF and DEF as a media for crystallization [2.30]. The complexation of $[Co(en)_3]^{3+}$ with POM anions was performed by mixing of aqueous solutions of $Co(en)_3Cl_3$ to a DMF/DEF solution of POM anion, which resulted in the crystallization of block/needle shaped crystals. It has been observed that in DEF media crystallization is faster (10 min-48 hours) than in DMF media (24 hours - 160 hours).

2.2.2 Crystal structures of $[Co(en)_3]^{3+}$ and POM ionic composites

Crystal Structure of Co-Mo$_8$-DMF $[Co(en)_3Mo_8O_{26}(H_3O)(Cl)]\cdot(DMF)_4\cdot(H_2O)$: The X-ray crystallographic study reveals that compound Co-Mo$_8$-DMF crystallizes in triclinic *P*-1 space group and consists of two β-$[Mo_8O_{26}]^{4-}$ anionic clusters [2.31], cationic $[Co(en)_3]^{3+}$

complexes, Cl^- anions, H_3O^+, free water and DMF molecules in the crystal lattice. The β-$[Mo_8O_{26}]^{4-}$ cluster can be described as a centro-symmetric assembly of octahedral molybdenum and oxygen atoms. The molybdenum atoms are not in the geometric centre of
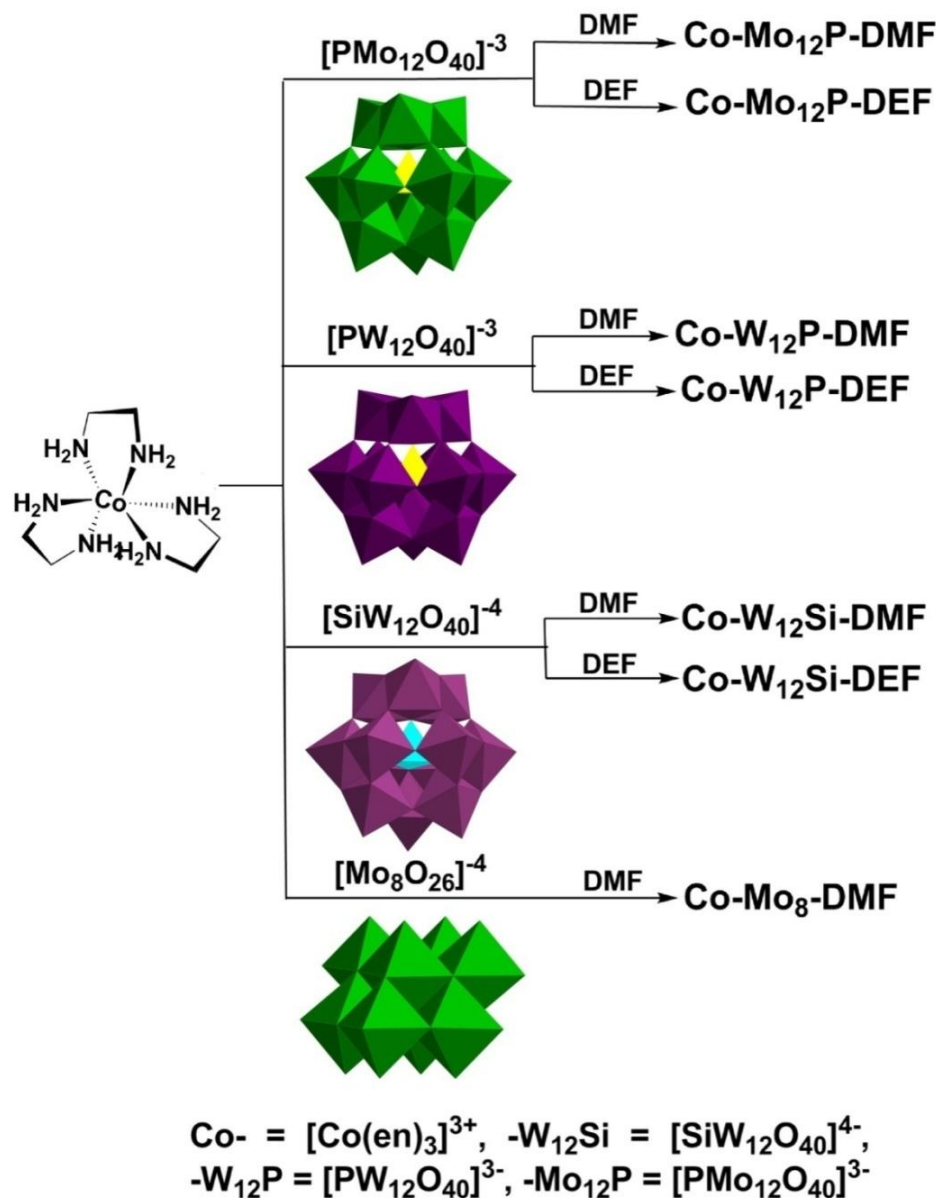
Figure 2.9: Synthesis and chemical composition of $[Co(en)_3]^{3+}$ cation and different keggin-type POM and β-octamolybdate based ionic solids discussed in this work. The series of salts have prepared from diethyl formamide (DEF)/dimethyl formamide (DMF).

the octahedral, but they are closer to the vertex occupied by the terminal oxygen atoms. The Mo–O bond distances ranges from 1.712(3) to 2.515(3) Å. Taking into account the polyanion with crystallographically imposed inversion symmetry, there is an equatorial plane

including Mo2, Mo6, Mo7 and Mo4, Mo5, Mo8 and their symmetry related ones in β-$[Mo_8O_{26}]^{4-}$ cluster I and II respectively. The structure contains three types of MoO_6 octahedra according to the position in the anion, each of which shows a particular distribution of the Mo–O distance. The first type of molybdenum is coordinated by two terminal O atoms, three μ_2-O atoms and one μ_5-O atom. The second type of molybdenum is coordinated by two terminal O atoms, one μ_2-O atom, two μ_3-O atoms and one μ_5-O atom. The central molybdenum is coordinated by one terminal O atom, one μ_2-O atom, two μ_3-O atoms and two μ_5-O atoms (Figure 2.10a). The average bond distances are 1.702 (4), 1.901 (3), 1.953
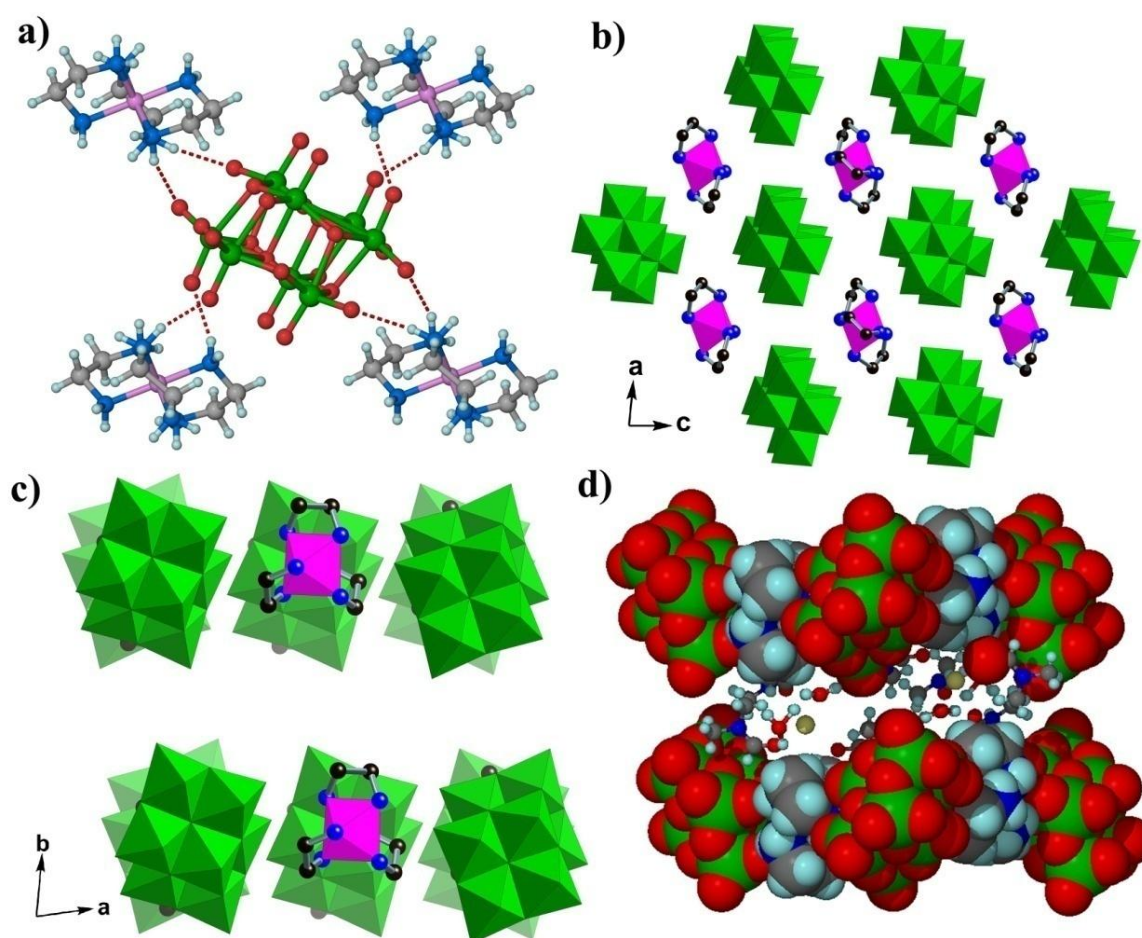
Figure 2.10: Crystal structure of Co-Mo8-DMF. (a) Hydrogen-bonding interactions between β-$[Mo_8O_{26}]^{4-}$ and $[Co(en)_3]^{3+}$. N-H···O hydrogen bonded interactions have been shown as red broken lines. (b) The two-dimensional structure of Co-Mo8-DMF consists of β-$[Mo_8O_{26}]^{4-}$ and $[Co(en)_3]^{3+}$ clusters. (c) 2D supramolecular layers formed by β-$[Mo_8O_{26}]^{4-}$ and $[Co(en)_3]^{3+}$ clusters stack on top of each other in AAAA fashion. (d) Space filling model of these 2D supramolecular layers. DMF, H_2O, and Cl^- molecules occupy the void space between the layers. Color code: Mo (green), N (blue), O (red), C (black), Co (magenta), H (light cyan), Cl (light green).

(4) and 2.357 (3) Å for Mo–O$_{terminal}$, Mo–O(μ_2), Mo–O(μ_3) and Mo–O(μ_5) respectively. The most interesting structural feature of Co-Mo$_8$-DMF is the two dimensional (2D) supramolecular H-bonded network comprising alternating [Co(en)$_3$]$^{3+}$ and β-[Mo$_8$O$_{26}$]$^{4-}$ clusters along *ac*-plane [Figure 2.10b]. [Co(en)$_3$]$^{3+}$ and β-[Mo$_8$O$_{26}$]$^{4-}$ clusters are connected to each other via strong N–H···O [D, 3.080(2) Å; *d*, 2.249(3) Å; θ, 149.7°] hydrogen bonds [2.32]. These 2-D supramolecular layers stack on top of each other in the AAAA fashion, the shortest distance between two layers being 5.432 (2) Å [Figure 2.10c]. Cl$^-$ anions, H$_3$O$^+$, free water and DMF molecules reside in the interlayer region [Figure 2.10d]. The Cl$^-$ anions forms a series of Cl···O-H [*d*, 2.323(3) and 2.405(4) Å] and Cl···O=C [2.335 (2) Å] interactions [2.33] and adopts a square pyramidal geometry.

Crystal structure of Co-Mo$_{12}$P-DEF [Co(en)$_3$PMo$_{12}$O$_{40}$](DEF) and Co-W$_{12}$P-DEF [Co(en)$_3$PW$_{12}$O$_{40}$](DEF) and Co-W$_{12}$Si-DEF [Co(en)$_3$SiW$_{12}$O$_{40}$](DEF): Co-Mo$_{12}$P-DEF and Co-W$_{12}$P-DEF crystallizes in orthorhombic $P2_12_12_1$ space group and consists of [PMo$_{12}$O$_{40}$]$^{3-}$ and [PW$_{12}$O$_{40}$]$^{3-}$ anionic α-Keggin clusters [2.34], cationic [Co(en)$_3$]$^{3+}$ complexes, and free DEF molecules in the iso-structural crystal lattice (*a* = 14.395(3); *b* =19.836(4); *c* = 28.009(5) Å; V= 7997.67 Å^3 *vs. a* = 14.538(3); *b* =19.929(4); *c* = 28.151(6) Å; V= 8156.13 Å^3). [PMo$_{12}$O$_{40}$]$^{3-}$ and [PW$_{12}$O$_{40}$]$^{3-}$anions exhibit the α-Keggin configurations which consists of one distorted [PO$_4$] tetrahedron, surrounded by four [M$_3$O$_9$] (M= Mo and W) sets. The [M$_3$O$_9$] sets are formed by three edge-sharing [MO$_6$] octahedra and are linked together through bridging oxygen atoms that are corner shared. Each [MO$_6$] octahedra is coordinated by one terminal O atom, four μ_2-O atoms and one μ_4-O atom. The central P atom is surrounded by four oxygen atoms which form a tetrahedral structure [Figure 2.11a]. The bond valence sum calculations confirm that all M (M= Mo and W) centers are in +VI oxidation state. Average M–O and P–O lengths in these complexes are 1.851(4) Å and 1.529(5) Å respectively. In the crystal structure, [PM$_{12}$O$_{40}$]$^{3-}$ (M= Mo/W) and [Co(en)$_3$]$^{3+}$ clusters arrange in a helical fashion along *c*-axis by forming strong N–H···O [3.080(2) Å; 2.249(3) Å; 149.7°] hydrogen bonds to each other. These parallel helices form a 2D corrugated layered structures comprising alternating [Co(en)$_3$]$^{3+}$ and [PM$_{12}$O$_{40}$]$^{3-}$ α-Keggin clusters along *bc*-plane [Figure 2.11b]. DEF molecules fill the void space between the [Co(en)$_3$]$^{3+}$ and [PM$_{12}$O$_{40}$]$^{3-}$ clusters. This type of iso-structurality is very rare in polyoxometalate based complexes considering the number of solvent molecules (24 DEF) present in the unit cell. Co-W$_{12}$Si-DEF (monoclinic, $P2_1/c$) also consists of [SiW$_{12}$O$_{40}$]$^{4-}$ α-Keggin anionic clusters, cationic [Co(en)$_3$]$^{3+}$ complexes and free DEF molecules in the

crystal lattice. $[SiW_{12}O_{40}]^{4-}$ consists of one distorted $[SiO_4]$ tetrahedron surrounded by four $[W_3O_9]$ sets which are formed by three edge-sharing $[WO_6]$ octahedra like $[PM_{12}O_{40}]^{3-}$and are linked together through bridging oxygen atoms that are corner shared. In one $[SiW_{12}O_{40}]^{4-}$ unit the central $[SiO_4]$ tetrahedron surrounded by four $[W_3O_9]$ sets, while in the second case it is disordered in such a way that Si atom is surrounded by a cube of eight half-occupied oxygen atoms. Co-W$_{12}$Si-DEF adopts a 2D sheet structure along crystallographic *ab*-plane comprising alternating $[SiW_{12}O_{40}]^{4-}$anionic clusters (with alternating cubic and tetrahedral SiO$_4$) and cationic $[Co(en)_3]^{3+}$ complexes via strong N–H$^{...}$O [3.049(3) Å; 2.772(2) Å, 141.9°] H-bonds [Figure 2.11c]. These 2D supramolecular layers stack on top of each other in the ABAB fashion, the shortest distance between two layers being 2.754(2) Å [Figure 2.11d].
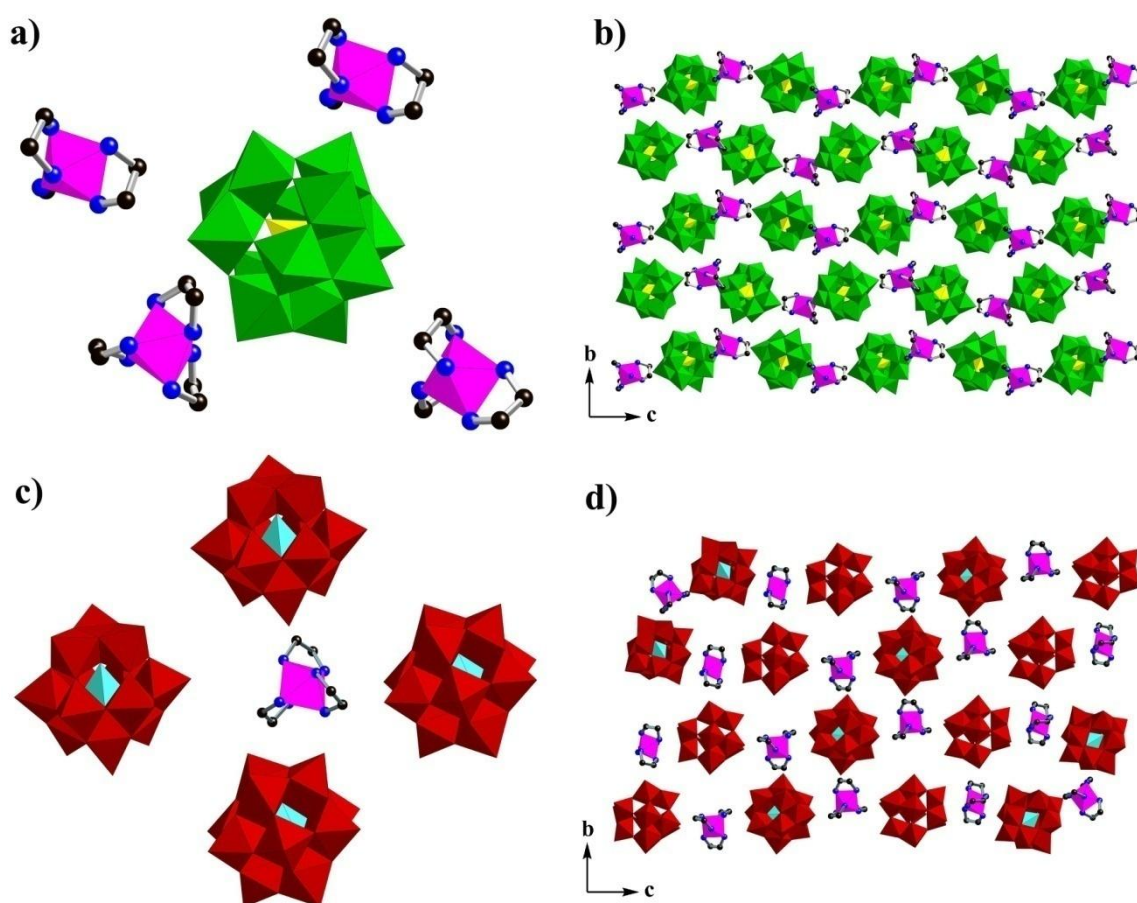
Figure 2.11: (a) One crystal structure unit of CoMo$_{12}$P-DEF consists of one Keggin unit which is surrounded by four tris-ethylenediamine complexes. (b) Packing arrangement of CoMo12P-DEF in *bc*-plane. (c) One Co-complex is surrounded by four keggin unit in CoW$_{12}$Si-DEF. (d) The two dimensional arrangement $[Co(en)_3]^{3+}$ and $[SiW_{12}O_{40}]^{4-}$ in *bc*-plane of CoW$_{12}$Si-DEF.

Crystal structure of Co-W$_{12}$P-DMF [Co(en)$_3$PW$_{12}$O$_{40}$]·(DMF)$_4$, Co-W$_{12}$Si-DMF [Co(en)$_3$SiW$_{12}$O$_{40}$(Cl)]·(DMF)$_4$.(H$_2$O) and (Co-Mo$_{12}$P-DMF)[Co(en)$_3$PMo$_{12}$O$_{40}$]·(DMF)$_{5.5}$: Co-W$_{12}$P-DMF (monoclinic, *P*2$_1$/*c*), Co-W$_{12}$Si-DMF (triclinic, *P*-1) and Co-Mo$_{12}$P-DMF (triclinic, *P*-1) crystallizes from DMF and contains free DMF molecules in the crystal lattice. Apart from common [Co(en)$_3$]$^{3+}$ cations, Co-W$_{12}$P-DMF, Co-Mo$_{12}$P-DMF and Co-W$_{12}$Si-DMF contains [SiW$_{12}$O$_{40}$]$^{4-}$ [Figure 2.12a], [PMo$_{12}$O$_{40}$]$^{3-}$ [Figure 2.12c] and type [PW$_{12}$O$_{40}$]$^{3-}$ [Figure 2.12e] of *α*-Keggin anionic clusters respectively. Co-W$_{12}$Si-DMF contains Cl$^-$ anions and free water molecules in the crystal lattice and adopts a 2D supramolecular H-bonded network comprising alternating [Co(en)$_3$]$^{3+}$, [SiW$_{12}$O$_{40}$]$^{4-}$ clusters and Cl$^-$ anions along the diagonal of the *bc*-plane [Figure 2.12b]. This H-bonded network could be described as an assembly of six [SiW$_{12}$O$_{40}$]$^{4-}$ clusters that encompasses four [Co(en)$_3$]$^{3+}$ clusters and two Cl$^-$ anions. Each [Co(en)$_3$]$^{3+}$ cluster is connected to the neighboring [SiW$_{12}$O$_{40}$]$^{4-}$ and Cl$^-$ anions via strong N–H···O [2.976(2) Å; 2.670(3) Å; 100.9°] and N–H···Cl$^-$ [3.199(2) Å; 2.137(3) Å; 152.2°] hydrogen bonds [2.32]. Central (PO$_4$) unit of the [PMo$_{12}$O$_{40}$]$^{3-}$ cluster of Co-Mo$_{12}$P-DMF is formed by a cube of eight half-occupied oxygen atoms. Average Mo–O and P–O lengths in these complexes are 1.781 (4) Å, and 1.502 (4) Å respectively. Co-Mo$_{12}$P-DMF adopts a 2D sheet structure along the diagonal of crystallographic *bc*-plane [Figure 12d] comprising alternating [PMo$_{12}$O$_{40}$]$^{4-}$ clusters and cationic [Co(en)$_3$]$^{3+}$ complexes via strong N–H···O [3.000(2) Å; 2.540(3) Å; 110.6°] H-bonds. These 2-D supramolecular layers stack on top of each other in the ABAB fashion, the shortest distance between two layers being 3.668 (2) Å. DMF molecules fill the void space between the [Co(en)$_3$]$^{3+}$ and [PMo$_{12}$O$_{40}$]$^{3-}$ clusters. Co-W$_{12}$P-DMF on the other hand adopts a 2D layer structure along crystallographic *bc*-plane comprising alternating [PW$_{12}$O$_{40}$]$^{4-}$ clusters and [Co(en)$_3$]$^{3+}$ complexes [Figure 8f]. This clusters form strong N–H···O [2.987(2) Å; 2.693(3) Å; 102.9°] H-bond and stack along crystallographic *a*-axis.

Crystal structure of Co-Mo$_{12}$P-DIOX [Co(en)$_2$(H$_2$O)$_2$PMo$_{12}$O$_{40}$](C$_4$H$_8$O$_2$): Co-Mo$_{12}$P-DIOX crystallizes in *C*2/*m* space group, and consists of free dioxane (C$_4$H$_8$O$_2$) molecules in the crystal lattice apart from [PMo$_{12}$O$_{40}$]$^{3-}$ anionic cluster and cationic [Co(en)$_2$(H$_2$O)$_2$]$^{3+}$ complexes. Central [PO$_4$] unit is formed by a cube of eight half-occupied oxygen atoms. Co-Mo$_{12}$P-DIOX forms a 2D supramolecular H-bonded network comprising alternating [Co(en)$_2$(H$_2$O)$_2$]$^{3+}$ and [PMo$_{12}$O$_{40}$]$^{3-}$ clusters along *ac*-plane. [Co(en)$_2$(H$_2$O)$_2$]$^{3+}$ and [PMo$_{12}$O$_{40}$]$^{3-}$ clusters are connected to each other via strong N–H···O [3.074(2) Å; 2.367(3) Å; 133.6°] hydrogen bonds. These 2D supramolecular layers stack on top of each other in the

offset fashion, the shortest distance between two layers being 4.518 (2) Å. Free dioxane molecules reside in the interlayer region.
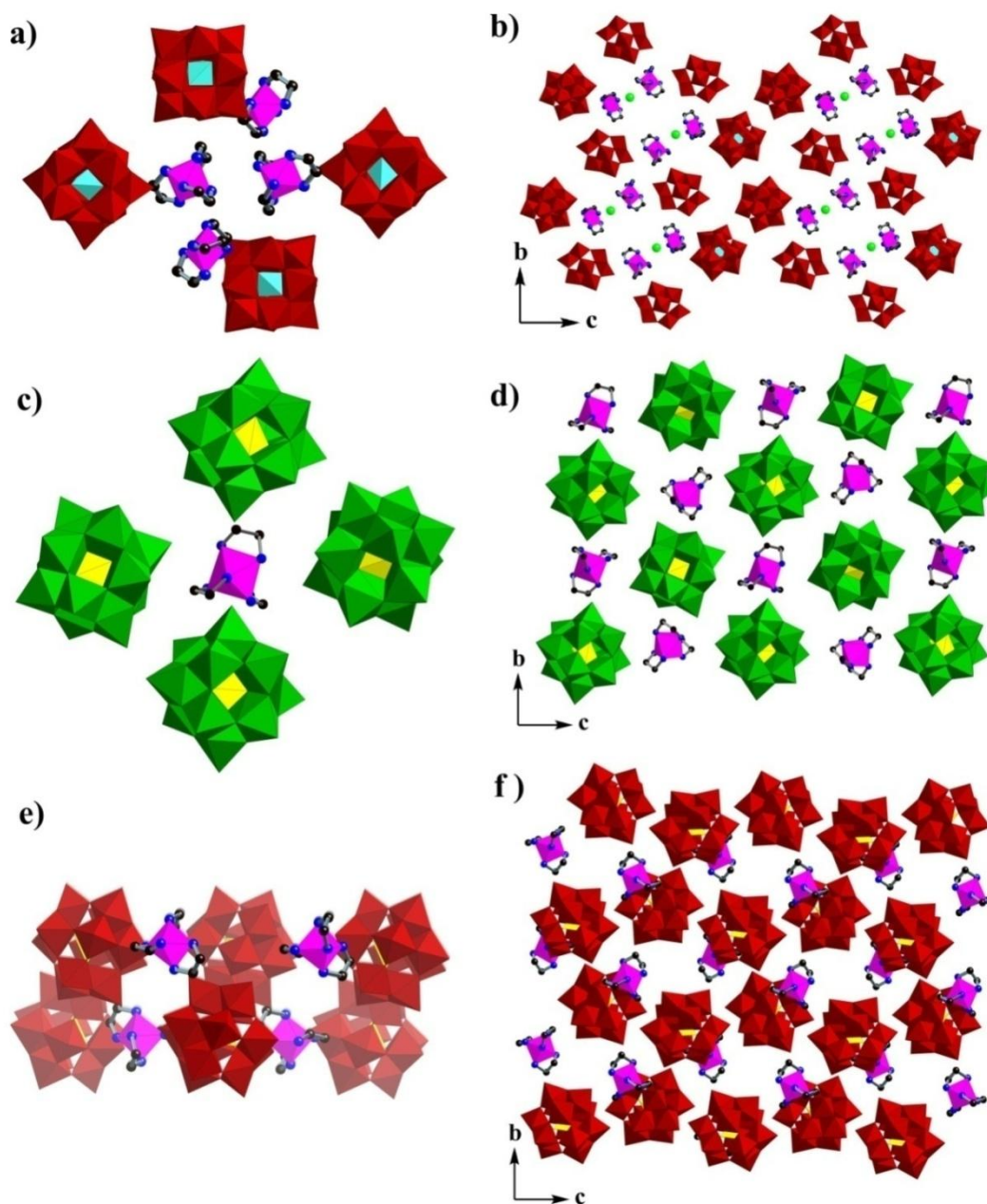
Figure 2.12: (a) Building unit of Co-W_{12}Si-DMF consist of four $[Co(en)_3]^{3+}$ complex and four Keggin units. (b) Two dimensional arrangement of Co-W_{12}Si-DMF, two Cl$^-$ and four $[Co(en)_3]^{3+}$ complexes are surrounded by six Keggin units. (c) Building unit of Co-Mo_{12}P-DMF. (d) Packing arrangement of Co-Mo_{12}P-DMF in *bc*-plane. (e) Alternate arrangement of $[Co(en)_3]^{3+}$ and Keggin in helical fashion in Co-W_{12}P-DMF. (f) Packing arrangement of Co-W_{12}P-DMF in *bc*-plane.

As mentioned previously, POMs as supramolecular synthons capable to dictate a particular crystal packing. However, it is extremely challenging to systematically design and synthesize

the supramolecular ionic crystals based on POMs, because many factors, such as initial reactants, concentrations, solvent of crystallization, pH value, reaction time and temperature could influence the formation of the resulting structure. The results here show that the nature of the solvent (DMF/DEF) influences the structures of these ionic crystals as it guides the orientation of the $[Co(en)_3]^{3+}$ and POM anions in the resulting crystal lattice. It is noteworthy that only a handful of POM based ionic crystals from non aqueous (DMF/DEF) media are reported [2.30]. We have also noticed that Co-Mo$_{12}$P-DEF and Co-W$_{12}$P-DEF crystallizes in chiral $P2_12_12_1$ space group although racemic $[dl$-Co(en)$_3]^{3+}$ has been used in synthesis of all the ionic crystals discussed in this chapter [2.35]. A possible explanation of this fact would be a selective crystallization of *d* or *l* isomer from the racemic mixture. Structural analysis reveals that of all Co(en)$_3$-POM ionic crystals majorly (66%) crystallize in chiral space group by selecting *d* or *l* isomer from the racemic mixture while crystallizing in DEF media. However, the same in the DMF media results in 100% centrosymmetric space group adoption as it fails to isolate the racemic $[dl$-Co(en)$_3]^{3+}$ cations. We have also noticed that all Co(en)$_3$-POM ionic crystals adopt a 2D sheet structure comprising alternating anionic POM clusters and cationic $[Co(en)_3]^{3+}$ complexes via strong N–H···OH-bonds. Interestingly in DEF media these layers stack on top of each other in the AAAA fashion whereas in DMF media they stack ABAB fashion.

2.2.3   Thermal properties and X-ray powder diffraction analysis of POM salts

In order to confirm the phase purity of the bulk materials powder X-ray diffraction (PXRD) experiments were carried out on those ionic complexes. Experimental and computer-simulated PXRD patterns of representative Co(en)$_3$-POM ionic crystals are shown in the Figure 2.13a-2.13d. All major peaks of experimental PXRD of Co(en)$_3$-POM ionic crystals matches quite well with the simulated PXRD, indicating their reasonable crystalline phase purity. To examine the architectural and thermal stability of Co(en)$_3$-POM ionic crystals reported in this work, we prepared them at the gram scale to allow detailed investigation of the aforementioned properties. Thermo gravimetric analysis (TGA) performed on as-synthesized Co(en)$_3$-POM ionic crystals [Figure 2.14a] revealed these compounds have high thermal stability. The TGA traces of compound CoMo$_{12}$P-DMF demonstrates a flat plateau till 150°C followed by a loss of 18 % weight (from 150 °C to 225 °C) due to removal of six DMF and one H$_2$O molecules from the lattice. For CoMo$_{12}$P-DEF this initial loss (20 % weight from 125 °C to 250 °C) indicates removal of six DEF molecules. For CoW$_{12}$P-DMF and CoW$_{12}$P-DEF initial loss of 10 % (70 to 250 °C) and 16.5% (100 to 250 °C) weight

indicates removal of six DMF, one water molecules and six DEF molecules respectively. Unlike the other Co(en)$_3$-POM ionic crystals, CoW$_{12}$Si-DMF and CoW$_{12}$Si-DEF losses its
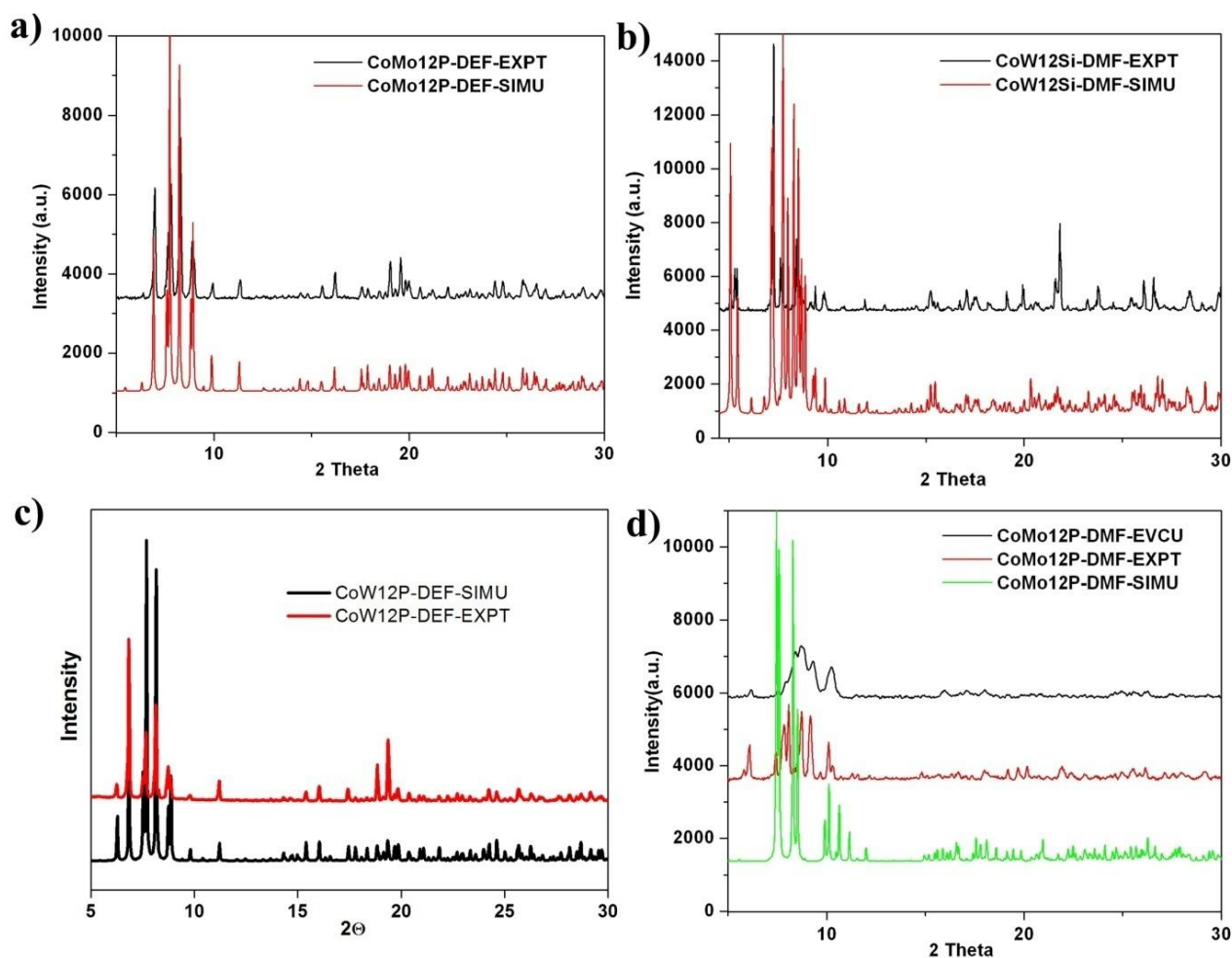
Figure 2.13: a) Comparison of the experimental PXRD pattern of as-synthesized CoMo$_{12}$P-DEF (top) with the simulated one from its single crystal structure (bottom). b) & c) Figures are the representation of same experiment for CoW$_{12}$Si-DMF and CoW$_{12}$P-DEF respectively. d) Simulated (bottom), experimental (middle) and evacuated sample (top) PXRD pattern of CoMo$_{12}$P-DMF.

solvent molecules in two steps. Initial weight loss of 7% (150 to 175 °C) is followed by a 7% (100 to 250 °C) weight loss indicates removal of six DMF and three water molecules for CoW$_{12}$Si-DMF. Similarly CoW$_{12}$Si-DEF loses its solvent in two steps. The first sharp solvent loss occurs at 125 °C with 7.5% decrease in weight. The rest solvent loss occurs in 240-280 °C range. For CoMo$_8$-DMF no strictly clean weight loss step occurred below 300 °C. A sharp weight loss at between 280-320 °C indicates decomposition of the host lattice for all Co(en)$_3$-POM ionic crystals reported in this work. PXRD has been carried out for CoMo$_{12}$P-DMF after removal of solvent by evacuation. The PXRD pattern shows significant similarity and

crystallinity [Figure 2.13d] with the experimental and simulated one, which shows the stability of the crystal lattice after solvent removal.

2.2.4 CO_2 and H_2 adsorption on Co(en)$_3$-POM based ionic crystals

Only very few ionic/molecular crystals have demonstrated permanent porosity since intermolecular coulombic/Van der Waals interactions are usually too weak for sustaining an open framework. Vapor adsorption properties of [Co(en)$_3$]Cl$_3$ and POM clusters have been well documented in order to understand the increase of cell volume with respect to different gas uptake [2.22]. But POM clusters are greatly underutilized on their capabilities of storing hydrogen and carbon-dioxide. We focused to examine the porosity of Co(en)$_3$-POM ionic crystals and prepared it at the gram scale to allow detailed investigation of the aforementioned properties. An important structural feature of these Co(en)$_3$-POM ionic crystals is that they possess voids which is less than 3.0 Å in diameter. To remove the guest species from the frameworks and prepare the evacuated forms of Co(en)$_3$-POM ionic crystals for gas-sorption analysis, the as-synthesized Co(en)$_3$-POM samples were immersed in dry CH$_2$Cl$_2$ at ambient temperature for 48 hours, and evacuated at ambient temperature for 5 hours, then at an elevated temperature (100 °C) for 2 hours. Co(en)$_3$-POM samples thus obtained were optimally evacuated, as evidenced by their well maintained PXRD patterns [Figure 2.9d] and the long plateau (25–300 °C) in their TGA traces.

All Co(en)$_3$-POM based ionic crystals were nonporous to nitrogen because void size (~ 3.0 Å) of salts were less than the kinetic diameter of nitrogen (3.6 Å); however, it was able to take up hydrogen (H$_2$) and carbon-dioxide (CO$_2$). All these Co(en)$_3$-POM based ionic crystals showed reversible hydrogen sorption behavior [Figure 2.14b]. The amount of hydrogen sorption varies, as the POM anion changes. CoMo$_{12}$P-DEF has the highest (0.9 wt%) H$_2$ uptake and CoW$_{12}$P-DEF has the lowest (0.4 wt%) uptake among the series when the adsorbate pressure approached 1 atm. Although the H$_2$ adsorptions are somewhat moderate, they are similar to the value of 0.7 wt% obtained for the highest capacity zeolite ZSM-5 and some of MOFs reported in the literature [2.36]. As shown in Figure 2.14c, the framework exhibits a unusual profile (similar to type-II) for CO$_2$ (kinetic diameters 3.4 Å) for Co-Mo$_{12}$P-DMF, Co-Mo$_{12}$P-DEF and Co-W$_{12}$Si-DEF at 298 K. Hysteretic sorption with CO$_2$ molecules suggests that the gases diffuse into aggregated [Co(en)$_3$]$^{3+}$cations and POM anions with some structural transformations, due to positional displacements of organic/inorganic moieties. Activated Co(en)$_3$-POM based ionic crystals exhibits very interesting selective adsorption of

H_2 over N_2. The gas uptake of $CoMo_{12}P$-DEF for H_2, and N_2 is 95.0 and 2.0 cm^3 g^{-1} and at $P/P_0 = 0.9$ respectively, underlying the potential of these ionic crystals for selective
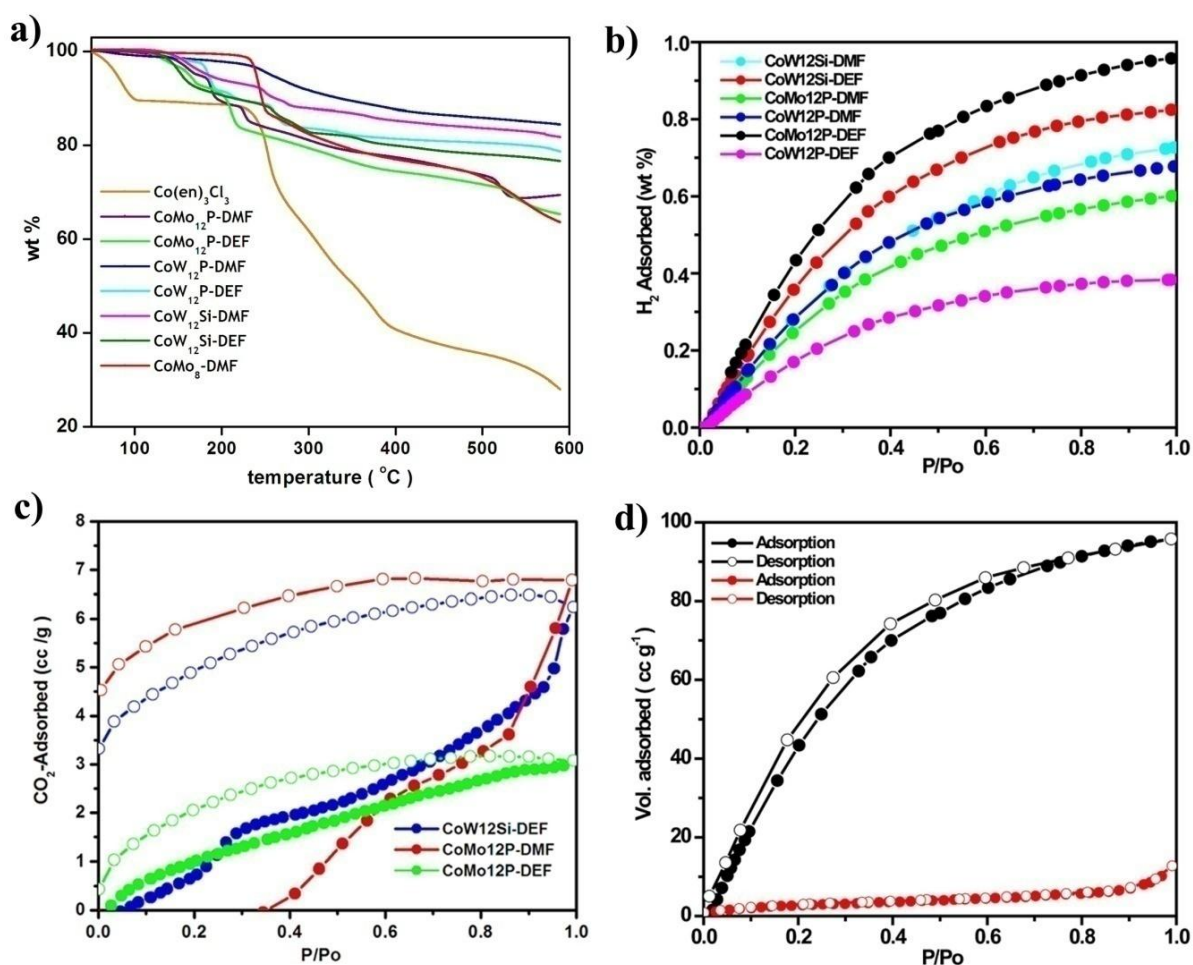
Figure 2.14: (a) Overlay of TGA traces of as-synthesized $Co(en)_3$-POM based ionic solids reported in this work indicating their thermal stability. The TGA trace of compound $Co(en)_3Cl_3$ has also been plotted as a reference. (b) Hydrogen absorption isotherms at 77 K of $Co(en)_3$-POM based ionic solids. Although absorption and desorption is completely reversible, only the absorption isotherm has been shown for clarity. (c) CO_2 absorption data of Co-W_{12}Si-DEF, Co-Mo_{12}P-DMF, and Co-Mo_{12}P-DEF at 298 K. The filled and open shapes represent adsorption and desorption, respectively. P/P_0, relative pressure at the saturation vapor pressure of the adsorbate gas. (d) Selective H_2 (black, circle) adsorption isotherms of Co-Mo_{12}P-DEF over N_2 (red, circle) at 77 K.

separation of H_2 over N_2 [Figure 2.14d]. Such preferential H_2 uptake over nitrogen might be attributed to size-exclusive effect in which the channels are accessible to hydrogen, but not to nitrogen because of their differential kinetic diameters of 2.8 and 3.64 Å respectively. To our knowledge this is the first report of selective hydrogen adsorption in POM based ionic

crystals and we believe such selective hydrogen storage capacity could be efficiently utilized for the H_2/N_2 separation.

2.3 Conclusion

POM based ionic crystals are mostly synthesized under hydrothermal condition and from H_2O media. In this work, we showed that it is possible to synthesize POM based ionic crystals by complexation of Keggin-type POMs with cationic $[Co(en)_3]^{3+}$ in DMF/DEF media that yielded eight crystalline ionic solids. The strong electrostatic interactions between the highly negatively charged POMs and the +ve-charged $[Co(en)_3]^{3+}$ as well as the N–H$^{..}$O hydrogen bonding resulted in the formation of the crystalline binary composites. The crystal structures of these ionic solids and their guest-free phases showed the sandwich type layered packing. Hydrogen and carbon dioxide sorption properties of these ionic solids were influenced by the types and charges of the polyoxometalates and their orientation in the crystal lattice. We believe that the successful synthesis of these eight new ionic solids and the discovery of their selective H_2 adsorption properties, as a result of the cooperative behavior between their cationic/anionic component species, will open-up new vista in the search for polyoxometalate based materials with useful absorptive properties. Further investigation of the magnetism and CO_2 sequestration mechanism of these types of ionic solids are ongoing.

2.4 Experimental Section

All reagents and solvents for synthesis and analysis were commercially available and used as received. The Fourier Transform Infrared *(FT-IR)* spectra (KBr pellet) were taken on a *PERKIN ELMER FT-IR SPECTRUM* (Nicolet) spectrometer. Powder X-ray diffraction (PXRD) patterns were recorded on a Phillips PNAlytical diffractometer for Cu Kα radiation (λ = 1.5406 Å), with a scan speed of 2° min^{-1} and a step size of 0.02° in 2θ. Thermo-gravimetric experiments (TGA) were carried out in the temperature range of 25–800 °C on a SDT Q600 TG-DTA analyzer under N_2 atmosphere at a heating rate of 10 °C min^{-1}. All low-pressure gas adsorption experiments (up to 1 bar) were performed on a *Quantachrome Quadrasorb* automatic volumetric instrument.

Synthesis of [Co(en)$_3$Mo$_8$O$_{26}$(H$_3$O)(Cl)]·(DMF)$_4$.(H$_2$O) (Co-Mo$_8$-DMF): Sodium molybdate dihydrate (5.8 g) was taken in a 100 mL beaker with 20 mL of DMF. The mixture was heated at 200 °C for 30 min. After 3 min of cooling, 3.3 mL of 12 M HCl was added to that solution. The filtrate was collected as a *β*-octamolybdate solution. To a 0.5 mL solution

of β-octamolybdate was added 2 mL of H_2O to make the solution dilute. A 0.025 M solution (0.5 mL) of tris(ethylenediamine)cobalt(III) chloride in water was added to that final solution. After two days, golden-yellow crystals formed. *FT-IR* (KBr 4000-450 cm^{-1}): 3267 (s, $\nu_{asym}NH_2$), 1646 (s, $\nu_{str}C=O$), 933 (s, $\nu_{asym}Mo=O$), 894 (s, $\nu_{asym}Mo-O_a$), 841 (s, $\nu_{asym}Mo-O_b$), 704 (s, $\nu_{asym}Mo-O_c$). E.A. Calcd: C, 12.18; H, 3.18; N, 7.83. Found: C, 12.09; H, 3.21; N, 7.85. [DMF/H_2O=1:5; Amount of water~85%].

Synthesis of [α-PW$_{12}$O$_{40}$][Co(en)$_3$]·6DMF (Co-W$_{12}$P-DMF): To 2 mL of a 0.05 M solution of sodium phosphotungstate hydrate (Na$_3$PW$_{12}$O$_{40}$·xH$_2$O) in DMF was added 9 mL of DMF and then 2.5 mL of a 0.05 M solution of tris(ethylenediamine)cobalt(III) chloride in water with gentle shaking. After 24 hours, golden-yellow crystals started forming. *FT-IR* (KBr 4000-450 cm^{-1}): 3240 (s, $\nu_{asym}NH_2$), 1650 (s, $\nu_{str}C=O$), 1055 (s, $\nu_{asym}P-O$), 952 (s, $\nu_{asym}W=O$), 884 (s, $\nu_{asym}W-O_c-W$), 814 (s, $\nu_{asym}W-O_e-W$). E.A. Calcd: C, 8.10; H, 1.85; N, 4.72. Found: C, 8.12; H, 1.85; N, 4.75. [DMF/H_2O=4:1; Amount of water~20%].

Synthesis of [α-PW$_{12}$O$_{40}$][Co(en)$_3$]$_3$·6DEF (Co-W$_{12}$P-DEF): Two milliliters of a 0.05 M solution of Na$_3$PW$_{12}$O$_{40}$·xH$_2$O in DEF was taken in a 30 mL culture tube. To that solution was added dropwise 1.5 mL of 0.05 M Co(en)$_3$Cl$_3$ in water. Within 10 min, golden-yellow crystals started forming. *FT-IR* (KBr 4000-450 cm^{-1}): 3263 (s, $\nu_{asym}NH_2$), 1643 (s, $\nu_{str}C=O$), 1079 (s, $\nu_{asym}P-O$), 977 (s, $\nu_{asym}W=O$), 896 (s, $\nu_{asym}W-Oc-W$), 820 (s, $\nu_{asym}W-Oe-W$). E. Al. Calcd: C, 10.34; H, 0.66; N, 4.67. Found: C, 10.35; H, 0.69; N, 4.66. [DEF/H_2O = 4:3; Amount of water ~42%].

Synthesis of [α-PMo$_{12}$O$_{40}$][Co(en)$_3$]·5.5DMF (Co-Mo$_{12}$P-DMF): To a solution of 2 mL of a 20 wt% solution of H$_3$PMo$_{12}$O$_{40}$ in ethanol was added dropwise 7 mL of DMF. Then 0.5 mL of 0.05 M [Co(en)$_3$]Cl$_3$ in H$_2$O was added dropwise. Green crystals form within 48 hours. *FT-IR* (KBr 4000-450 cm^{-1}): 3250 (s, $\nu_{asym}NH_2$), 1654 (s, $\nu_{str}C=O$), 1061 (s,$\nu_{asym}P-O$), 957 (s, ν_{asym} Mo=O), 878 (s, ν_{asym} Mo-Oc-Mo), 820 (s, ν_{asym} Mo-Oe-Mo). E.A. Calcd: C, 8.03; H, 1.66; N, 4.78. Found: C, 7.99; H, 1.70; N, 4.81. [DMF/EtOH/H_2O=14:4:1; Amount of water ~6%].

Synthesis of [α-PMo$_{12}$O$_{40}$][Co(en)$_3$]·6DEF (Co-Mo$_{12}$P-DEF): To 2 mL of a 20 wt% solution of H$_3$PMo$_{12}$O$_{40}$ in ethanol was added 1 mL of DEF. Then 0.5 mL of 0.05 M [Co(en)$_3$]Cl$_3$ in H$_2$O was added dropwise. Green crystals formed within 48 hours. *FT-IR* (KBr 4000-450 cm^{-1}): 3257 (s, $\nu_{asym}NH_2$), 1643 (s, $\nu_{str}C=O$), 1061 (s, $\nu_{asym}P-O$), 956 (s, $\nu_{asym}Mo=O$), 879 (s, ν_{asym} Mo-Oc-Mo), 804 (s, ν_{asym} Mo-Oe-Mo). E.A. Calcd: C, 16.19; H,

3.37; N, 7.29. Found: C, 16.22; H, 3.38; N, 7.23. [DEF/EtOH/H$_2$O=2:4:1; Amount of water ~14%].

Synthesis of [α-SiW$_{12}$O$_{40}$][Co(en)$_3$]$_{3/2}$[Cl]$_{1/2}$·6DMF·3H$_2$O (Co-W$_{12}$Si-DMF): To 2 mL of a 0.05 M solution of H$_4$SiW$_{12}$O$_{40}$·xH$_2$O in DMF was added dropwise 2 mL of a 0.05 M aqueous solution of [Co(en)$_3$]Cl$_3$ in water. Yellow crystals start growing after 7 days. *FT-IR* (KBr 4000- 450 cm^{-1}): 3252 (s, ν_{asym}NH$_2$), 1657 (s, ν_{str}C=O), 970 (s, ν_{asym}W=O), 921 (s, ν_{asym}Si-O), 882 (m, ν_{asym}W-Oc-W), 800 (s, ν_{asym}W-Oe-W). E.A. Calcd: C, 8.72; H, 2.10; N, 5.65. Found: C, 8.75; H, 2.05; N, 5.61. [DMF/H$_2$O=2:2; Amount of water ~50%].

Synthesis of [α-SiW$_{12}$O$_{40}$][Co(en)$_3$]$_3$·6DEF (Co-W$_{12}$Si-DEF). To a solution of 2 mL of 0.05 M H$_4$SiW$_{12}$O$_{40}$·xH$_2$O in DEF was added dropwise 3 mL of 0.05 M [Co(en)$_3$]Cl$_3$ in water. Yellow crystals form within 48 hours. *FT-IR* (KBr 4000-450 cm^{-1}): 3260 (s, ν_{asym}NH$_2$), 1644 (s, ν_{str}C=O), 969 (s, ν_{asym}W=O), 921 (s, ν_{asym} Si-O), 882 (m, ν_{asym} W-Oc-W), 795 (s, ν_{asym}W-Oe-W). E.A. Calcd: C, 10.59; H, 2.08; N, 4.79. Found: C, 10.61; H, 2.11; N, 4.80. [DEF/H$_2$O=2:3; Amount of water ~60%].

Synthesis of [α-PMo$_{12}$O$_{40}$][Co(en)$_2$(H$_2$O)$_2$]·DIOX (Co-Mo$_{12}$P-DIOX): 10 mL 1 M H$_3$PO$_4$ was added to mixture of 120 mL 1 M of Na$_2$MoO$_4$, 18 mL of 13 (M) HNO$_3$ and 100 mL of 1,4-dioxane. Yellow filtrate was collected after 2 hours. To the 3 mL of that filtrate, 1 mL 0.05 (M) solution of [Co(en)$_3$]Cl$_3$ in water was added drop wise in 30 mL culture tube. Green crystals form within 48 hours.

Single-Crystal X-ray Analysis: All single crystal data were collected on a Bruker SMART APEX three circle diffractometer equipped with a CCD area detector (Bruker Systems Inc., 1999a) [2.37] with Mo K$_\alpha$ radiation (λ= 0.71073 Å). Data were integrated using Bruker *SAINT* software [2.38]. Data were subsequently corrected for absorption by the program *SADABS* [2.39]. The space group determinations and tests for merohedral twinning were carried out using *XPREP* [2.40]. All structures were solved by direct methods and refined using the *SHELXTL 97* software suite [2.41]. The absorption coefficient (μ) range between 1 to 11 for all ionic crystals reported in this chapter. Since all the ionic crystals contain Mo/W there could be a possibility of high absorption of Mo Kα X-ray radiation. Data were collected at 293 (2) K for all Co(en)$_3$-POM ionic crystals except CoW$_{12}$P-DMF and CoMo$_{12}$P-DIOX where data collection took place at 100(2) K. All structures were examined using the *Adsym* subroutine of *PLATON* [2.42]. Crystallographic data (excluding structure factors) for the

structures reported in this chapter have been deposited with the CCDC as deposition No. CCDC 77722–777228. Copies of the data can be obtained, free of charge, on application to the CCDC, 12 Union Road, Cambridge CB2 lEZ UK (fax: + 44 (1223) 336 033; e-mail: deposit@ccdc.cam.ac.uk).

Magnetism and XPS measurements: DC magnetization vs. temperature curves were taken on all the samples for 1000 Oe external field in field cooled mode (FC) using a Physical Property Measurement System (PPMS) from Quantum Design Inc. San Diego, USA equipped with a 7 Tesla superconducting magnet. M-H loops were collected in a field sweep from -50 k Oe to 50 k Oe at a rate of 100 Oe/sec where data was collected at every second at the vibrating frequency of 40 Hz. These measurements were done using a vibrating sample magnetometer attachment of PPMS. Room temperature X-ray photoelectron spectroscopy (XPS) was used to confirm the oxidation state of the Co. For this purpose the high resolution XPS data was collected by using a VG Microtch, model number ESCA 3000 equipped with ion gun (EX-05) for cleaning the surface spectra. The binding energy resolution was 0.1 eV. Shirley algorithm was used for background correction and chemically distinct species were resolved using a nonlinear least square fitting procedure. The core level binding energies were aligned with the carbon binding energy of 285 eV.

Gas adsorption experiments: As-synthesized samples of all Co(en)$_3$-POM ionic crystals reported in this paper were immersed in dry dichloromethane at ambient temperature for 72 hours, evacuated at ambient temperature for 24 hours, then at an elevated temperature (85 °C) for 48 hours. Samples thus obtained were optimally evacuated.

2.5 References

2.1   (a) R. A. van Santen, G. J. Kramer, *Chem. Rev.* **1995**, *95*, 637. (b) A. Corma, *Chem. Rev.* **1995**, *95*, 559. (c) J. M. Thomas, *Angew. Chem.* **1999**, *111*, 3800. *Angew. Chem. Int. Ed.* **1999**, *38*, 3588. (d) A. P. Wight, M. E. Davis, *Chem. Rev.* **2002**, *102*, 3589.

2.2   (a) D. J. Tranchemontagne, Z. Ni, M. O'Keeffe, O. M. Yaghi, *Angew. Chem.* **2008**, *120*, 5214. *Angew. Chem. Int. Ed.* **2008**, *47*, 5136. (b) S. Kitagawa, R. Kitaura, S.-i. Noro, *Angew. Chem.* **2004**, *116*, 2388. *Angew. Chem. Int. Ed.* **2004**, *43*, 2334. (c) G. Ferey, *Chem. Soc. Rev.* **2008**, 37, 191. (d) L. J. Murray, M. Dinca , J. R. Long, *Chem. Soc. Rev.* **2009**, *38*, 1294. (e) Y. Inokuma, M. Kawano, M. Fujita, *Nat. Chem.* **2011**, *3*, 349.

2.3   (a) H. M. El-Kaderi, J. R. Hunt, J. L. Mendoza-Cortes, A. P. Cote, R. E. Taylor, M. O'Keeffe, O. M. Yaghi, *Science*, **2007**, *316*, 268. (b) A. P. Cote, A. I. Benin, N. W. Ockwig, M. O'Keeffe, A. J. Matzger, O. M. Yaghi, *Science*. **2005**, *310*, 1166.

2.4   (a) S. Noro, D. Tanaka, H. Sakamoto, S. Shimomura, S. Kitagawa, S. Takeda, K. Uemura, H. Kita, T. Akutagawa, T. Nakamura, *Chem. Mater*. **2009**, *21*, 3346. (b) Y. Ishii, Y. Takenaka, K. Konishi, *Angew. Chem.* **2004**, *116*, 2756. *Angew. Chem. Int. Ed.* **2004**, *43*, 2702. (c) H. Tagami, S. Uchida, N. Mizuno, *Angew. Chem.* **2009**, *121*, 6276. *Angew. Chem. Int. Ed*. **2009**, *48*, 6160. (d) S. Uchida, R. Kawamoto, H. Tagami, Y. Nakagawa, N. Mizuno, *J. Am. Chem. Soc.* **2008**, *130*, 12370. (e) S. Takamizawa, T. Akatsuka, T. Ueda, *Angew. Chem.* **2008**, *120*, 1713. *Angew. Chem. Int. Ed.* **2008**, *47*, 1689. (f) J.-B. Lin,W. Xue, J.-P. Zhang, X.-M. Chen, *Chem. Commun.* **2011**, *47*, 926.

2.5   (a) M. T. Pope, A. Muller, *Angew. Chem., Int. Ed. Engl*. **1991**, *30*, 34. (b) P. Gouzerh, A. Proust, *Chem. Rev.* **1998**, *98*, 77. (c) K. Binnemans, *Chem. Rev*. **2009**, *109*, 4283. (d) E. Coronadon, C. L. Gomez-Garcia, *Chem. Rev*. **1998**, *98*, 273. (e) D. E. Katsoulis, *Chem. Rev*. **1998**, *98*, 359. (f) Y. P. Jeannin, *Chem. Rev.* **1998**, *98*, 51. (g) A. Muller, S. Q. N. Shah, H. Bogge, M. Schmidtmann, *Nature*. **1999**, *397*, 48. (h) D.-L. Long, R. Tsunashima, L. Cronin, *Angew. Chem., Int. Ed*. **2010**, *49*, 1736.

2.6   A. Dolbecq, E. Dumas, C. R. Mayer, P. Mialane, *Chem. Rev.* **2010,** *110, 6009.*

2.7   (a) E. Coronado, S. Curreli, C. Gimenez-Saiz, C. J. Gomez-Garcia, A. Alberola, E. Canadell, *Inorg. Chem*. **2009**, *48*, 11314. (b) W. Bu, S. Uchida, N. Mizuno, *Angew. Chem., Int. Ed.* **2009**, *48*, 8281. (c) C. M. Granadeiro, R. A. S. Ferreira, P. C. R. Soares-Santos, L. D. Carlos, H. I. S. Nogueira, *Eur. J. Inorg. Chem.* **2009**, 5088. (d) T. Ito, H. Yashiro, T. Yamase, *Langmuir*. **2006**, *22,* 2806. (e) R. Cao, S. Liu, L. Xie, Y. Pan, J. Cao, Y. Ren, L. Xu, *Inorg. Chem*. **2007**, 46, 3541. (f) D. Honda, T. Ozeki, A. Yagasaki, *Inorg. Chem*. **2005**, *44*, 9616.

2.8   M. H. Rosnes, C. Yvon, D. –L. Long, L. Cronin, *Dalton Trans*. **2012**, *41*, 10071.

2.9   Y.-F. Song, N. McMillan, D.-L. Long, S. Kane, J. Malm, M. O. Riehle, C. P. Pradeep N. Gadegaard, L. Cronin. *J. Am. Chem. Soc.* **2009**, *131*, 1340.

2.10   A. Haimov, R. Neumann, *J. Am. Chem. Soc.* **2006**, *128*, 15697.

2.11   S. Uchida, N. Mizuno, *J. Am. Chem. Soc*. **2004**, *126*, 1602.

2.12   (a) F. –J. Ma, S. –X. Liu, C. –Y. Sun, D. –D. Liang, G. –J. Ren, F. Wei, Y. –G. Chen, Z. –M. Su, *J. Am. Chem. Soc.* **2011**, *133*, 4178.

2.13 (a) A. –X. Tian, J. Ying, J. Peng, J. –Q. Sha, H. –j. Pang, P.-P. Zhang, Y. Chen, M. Zhu, Z. –M. Su, *Cryst. Growth. Des.* **2008**, *8*, 3717. (b) Y. Zhu, P. Yin, F. Xiao, D. Li, E. Bitterlich, Z. Xiao, J. Zhang, J. Hao, T. Liu, Y. Wang, Y. Wei, *J. Am. Chem. Soc.* **2013**, *135*, 17155.

2.14 H. Li, S. Pang, S. Wu, X. Feng, K. Mullen, C. Bubeck, *J. Am. Chem. Soc.* **2011**, *133*, 9423.

2.15 S. Nlate, C. Jahier, *Eur. J. Inorg. Chem.* **2013**, 1606.

2.16 S. G. Mitchell, C. Streb, H. N. Miras, T. Boyd, D. –L. Long, L. Cronin, *Nature Chemistry*, **2010**, *2*, 308.

2.17 S. Uchida, R. Kawahara, Y. Ogasawara, N. Mizuno, *Dalton Trans.* **2013**, *42*, 16209.

2.18 R. Eguchi, S. Uchida, N. Mizuno, *Angew. Chem. Int. Ed.* **2012**, *51*, 1635.

2.19 C. Jiang, A. Lesbani, R. Kawamoto, S. Uchida, N. Mizuno, *J. Am. Chem. Soc.* **2006**, *128*, 14240.

2.20 X. Fang, P. Kogerler, L. Isaacs, S. Uchida, N. Mizuno, *J. Am. Chem. Soc.* **2009**, *131*, 432.

2.21 S. Uchida, R. Kawamoto, N. Mizuno, *Inorg. Chem.* **2006**, *45*, 5136.

2.22 S. –i. Noro, R. Tsunashima, Y. Kamiya, K. Uemura, H. Kita, L. Cronin, T. Akutagawa, T. Nakamura, *Angew. Chem. Int. Ed.* **2009**, *48*, 8703.

2.23 (a) G. R. Desiraju, *Angew. Chem. Int. Ed. Engl.* **1995**, *34*, 2311. (b) A. Nangia, G. R. Desiraju, *Top. Curr. Chem.* **1998**, *198*, 57. (c) A. Nangia, G. R. Desiraju, *Acta Crystallogr. A* **1998**, *54*, 934. (d) T. Gelbrich, M. B. Hursthouse. *CrystEngComm* **2005**, *53*, 324. (e) G. R. Desiraju. *Chem. Commun.* **1997**, 1475. (f) F. Vögtle, J. F. Stoddart, M. Shibasaki, *Stimulating Concepts in Chemistry*. Wiley-VCH: New York, **2000**, 293. (g) W.D.S. Motherwell, G. P. Shields, F. H. Allen, *Acta Crystallographica. B.* **1999**, *55*, 1044.

2.24 (a) L. Ouahab, *Chem. Mater.* **1997**, *9,* 1909. (b) X. Zhang, D. Wang, J. Dou, S. Yan, X. Yao, J. Jiang, *Inorg. Chem.* **2006**, *45*, 10629. (c) Y. Hou, L. Xu, M. J Cichon, S. Lense, K. I. Hardcastle, C. L. Hill, *Inorg. Chem.* **2010,** *49,* 4125. (d) G. Izzet, E. Ishow, J. Delaire, C. Afonso, J.-C. Tabet, A. Proust, *Inorg. Chem.* **2009**, *48*, 11865. (e) J. –H. Son, H. Choi, Y.-U. Kwon, *J. Am. Chem. Soc.* **2000,** *122,* 7432. (f) C. Dey, R. Das, P. Pachfule, P. Poddar, R. Banerjee. *Cryst. Growth Des.* **2011**, *11*, 139.

2.25 (a) A.G. Lappin, K. J. Haller, M. L. Robert, R. M. L. Warren, A. Tatehata, *Inorg. Chem.* **1993**, *3*, 4498. (b) J.T. Veal, D. J. Hodgson, *Inorg. Chem.* **1972**. *11,* 597. (c) R. Kuroda, *Inorg. Chem.* **1991***, 30,* 4955. (d) M. J. Gray, J. D. Jasper, A. P. Wilkinson,

Chem. Mater. **1997**, *9,* 976. (e) S. M. Stalder, A. P. Wilkinson, *Chem. Mater.* **1997,** *9,* 2168. (f) J. Yu, Y. Wang, Z. Shi, R. Xu. *Chem. Mater.* **2001,** *13,* 2972.

2.26 (a) S. Takamizawa, M. Kobbara, T. Akatsuka, R. Miyake, *New. J. Chem.* **2008**, *32,* 1782. (b) S. Takamizawa, T. Akatsuka, T. Ueda, *Angew. Chem. Int. Ed.* **2008**, *47,* 1689.

2.27 (a) R. Banerjee, A. Phan, B. Wang, C. Knobler, H. Furukawa, M. O'Keeffe, O. M. Yaghi, *Science* **2008**, *319*, 939. (b) O. M. Yaghi, M. O'Keeffe, N. W. Ockwig, H. K. Chae, M. Eddaoudi, J. Kim, *Nature*. **2003**, *423*, 705. (c) X.-C. Huang, Y.-Y. Lin, J.-P. Zhang, X.-M. Chen. *Angew. Chem., Int. Ed.* **2006**, *45*, 1557.

2.28 F. Ma, S. Liu, D. Liang, G. Ren, C. Zhang, F. Wei, Z. Su, *Eur. J. Inorg. Chem.* **2010**, 3756.

2.29 (a) M. M. Williamson, D.A. Bouchard, C. L. Hill, *Inorg. Chem.* **1987**, *26,* 1436. (b) C. P. Pradeep, D. -L. Long, C. Streb, L. Cronin, *J. Am. Chem. Soc.* **2008**, *130*, 14946. (c) Y. Ogasawara, S. Uchida, N. Mizuno. *J. Phys. Chem. C.* **2007**, *111,* 8218.

2.30 (a) C. Streb, R. Tsunashima, D. A. MacLaren, T. McGlone, T. Akutagawa, T. Nakamura, A. Scandurra, B. Pignataro, N. Gadegaard, L. Cronin. *Angew. Chem. Int. Ed.* **2009**, *48*, 6490. (b) Y.-F. Song, N. McMillan, D.-L. Long, J. Thiel, Y. Ding, H. Chen, N. Gadegaard, L. Cronin, *Chem. Eur. J.* **2008**, *14*, 2349. (c) X. Wang, Y. Guo, Y. Li, E.Wang, C. Hu, N. Hu, *Inorg. Chem.* **2003**, *42*, 4135.

2.31 (a) Z. Shi, X. Gu, J. Peng, Z. Xin, *Eur. J. Inorg. Chem.* **2005**, 3811. (b) Y.Q. Lan, S. L. Li, X. L. Wang, K. Z. Shao, D.Y. Du, H.Y. Zang, Z. M. Su, *Inorg. Chem.* **2008**, *47,* 8179. (c) C. D. Wu, C.-Z. Lu, X. Lin, H.-H. Zhuang, J.-S. Huang, *Inorg. Chem. Commun.* **2002**, 664.

2.32 (a) G. R. Desiraju, T. Steiner, *The Weak Hydrogen Bond in Structural Chemistry and Biology*; Oxford University Press: Oxford, 1999. (b) G. R. Desiraju, *Chem. Commun.* **2005**, 2995. (c) P. Metrangolo, H. Neukirch, T. Pilati, G. Resnati, *Acc. Chem. Res.* **2005**, *38*, 386. (d) K. Reichenbächer, H. I. Suss, J. Hulliger, *Chem. Soc. Rev.* **2005**, *34*, 22. (g) F. Zordan, L. Brammer, P Sherwood, *J. Am. Chem. Soc.* **2005**, *127*, 5979. (h) I. E. D. Vega, P.A. Gale, M. . Light, S. J. Loeb, *Chem. Commun.* **2005**, 4913. (k) A. Angeloni, P. C. Crawford, A. G. Orpen, T. J. Podesta, B. J. Shore, *Chem. Eur. J.* **2004**, *10*, 3783. (l) A. R. Choudhury, T. N. Guru Row, *Cryst. Growth Des.* **2004**, *4*, 47. (m) J.A. Van den Berg, K. R. Seddon, *Cryst. Growth Des.* **2003**, *3*, 643. (n) P. W. Baures, A. M. Beatty, M. Dhanasekaran, B. A. Helfrich, W. P Segarra, J. Desper, *J. Am. Chem. Soc.* **2002**, *124*, 11315.

2.33 (a) P. Metrangolo, G. Resnati, *Chem. Eur. J.* **2001**, *7*, 2511. (b) C.V. Ramana, S. Chatterjee, K. A. Durugkara, R. G. Gonnade, *CrystEngComm.* **2009**, *11,* 143. (c) A.C. Legon, *Angew.*

Chem. Int. Ed. Engl. **1999**, *38*, 2686. (d) S. C. Blackstock, J. P. Lorand, J. P Kochi, *J. Org. Chem.* **1987**, *52*, 1451.

2.34 (a) E. Coronado, S. Curreli, C. Gimenez-Saiz, C. J. Gomez-Garcıa, A. Alberola, E. Canadell, *Inorg. Chem.* **2009**, *48*, 11314. (b) W. Bu, S. Uchida, N. Mizuno, *Angew. Chem., Int. Ed.* **2009**, *48*, 8281. (c) C. M. Granadeiro, R. A. S. Ferreira, P. C. R. Soares-Santos, L. D. Carlos, H. I. S. Nogueira, *Eur. J. Inorg. Chem.* **2009**, 5088. (d) J.-X. Lin, J. Lu, H.-X. Yang, R. Cao, *Cryst. Growth Des*. **2010**, *10*, 1966. (e) A.-X. Tian, J. Ying, J. Peng, J. Q. Sha, H. J. Pang, P. P. Zhang, Y. Chen, M. Zhu, Z. M. Su, *Inorg. Chem.* **2009**, *48*, 100.

2.35 (a) S. M. Stalder, A. P. Wilkinson, *Chem. Mater.* **1997**, *9*, 2169. (b) Y. Wang, J. Yu, O. Pan, Y. Du, Y. Zou, R. Xu, *Inorg. Chem*, **2004**, *43*, 559. (c) Y. Wang, J. Yu, Y. Li, Z. Shi, R. Xu, *Chem. Eur. J.* **2003**, *9*, 5048; (d) H.-O. Stephan, M.G. Kanatzidis, *J. Am. Chem. Soc.* **1996**, *118,* 12226.

2.36 (a) J. Seo, H. Chun, *Eur. J. Inorg. Chem.* **2009**, 4946. (b) S. Ma, H.-C. Zhou, *Chem. Commun.* **2010**, *46*, 44. (c) P. Pachfule, C. Dey, T. Panda, R. Banerjee, *CrystEngComm*. **2010**, *12*, 1600. (d) P. Pachfule, T. Panda, C. Dey, R. Banerjee, *Cryst EngComm,* **2010**, *12*, 2381. (e) P. Pachfule, C. Dey, T. Panda, K.. Vanka, R Banerjee, *Cryst. Growth Des.* **2010**, *10*, 1351. (f) R. K.. Motkuri, J. Tian, P. K. Thallapally, C. A. Fernandez, S. J. Dalgarno, J. E. Warren, B. P. McGrail, J. L. Atwood, *Chem. Commun.* **2010**, *46*, 538. (g) C. A.. Fernandez, P. K.. Thallapally, R. K.. Motkuri, S. K.. Nune, J. C. Sumrak, J. Tian, J. Liu, *Cryst. Growth Des*. **2010**, *10*, 1037.

2.37 *SMART*, Version 5.05; Bruker AXS, Inc.: Madison, WI, **1998**.

2.38 *SAINT-Plus*, Version 7.03; BrukerAXS Inc.: Madison, Wisconsin, **2004**.

2.39 G. M. Sheldrick, *SADABS* (Version 2.03) and *TWINABS* (Version 1.02); University of Gottingen; Germany, **2002**.

2.40 G. M. Sheldrick, *SHELXS'97*; University of Gottingen: Germany, **1997**.

2.41 G. M. Sheldrick, *SHELXTL '97*; University of Gottingen: Germany, **1997**.

2.42 A. L. Spek, *PLATON*, A Multipurpose Crystallographic Tool; Utrecht University: Utrecht, The Netherlands, **2005**.

Note:

The results of this chapter have already been published in *Crystal Growth & Design*. 2011, 11, 139-146. with the title: "Structural and Selective Gas Adsorption Studies of Polyoxometalate and Tris(ethylenediamine) Cobalt(III) Based Ionic Crystals". This publication was the result of a collaboration between the group of Dr. Rahul Banerjee and his students Chandan Dey and Pradip Pachfule from the Physical/Materials Chemistry Division at CSIR-National Chemical Laboratory in Pune, India and the group of Dr. Pankaj Poddar with his student Raja Das from the Physical/Materials Chemistry Division at CSIR-National Chemical Laboratory in Pune, India. Pradip Pachfule was involved in adsorption study of the salt materials.

Synthesis and Morphological Study of Polyoxometalate (POM) Based Hybrid Materials

3.1 Introduction

Morphology of materials plays a crucial role in determining their property [3.1]. The change in morphology not only considers the deformation in shape and size of the particle but also involves changing of surface area and distribution of active sites on surface [3.2]. The properties of particular materials can be modified or tuned by changing the morphology to make them suitable for various applications [3.3]. Morphology of particle has considered
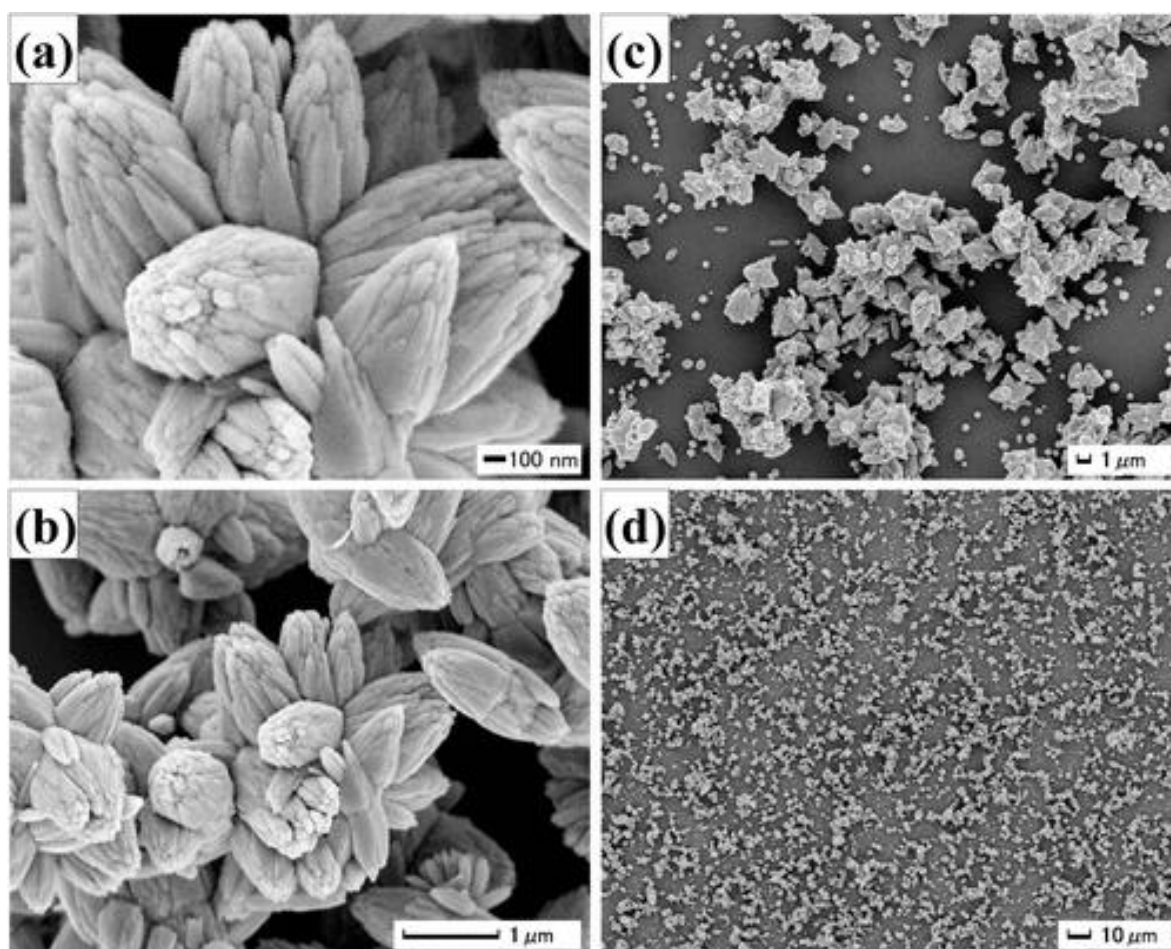

Figure 3.1: SEM images of ZnO multi-needle structure taken at different zoomed view (Figure taken from ref 3.3b with permission).

playing crucial role for electrode performance. Spherical particles, for example are accounted to have better performance than random particles. Different morphologies of LiFePO$_4$ particles (platelets and flowerlike balls) were obtained by post-synthetic treatment of hydrothermal products with supercritical carbon dioxide (scCO$_2$) [3.4]. The morphology of ZnO particles was modified to enhance electrical conductivity, specific surface area, and mechanical strength to make them suitable for solar cells and sensors applications. Typical ZnO particles are generally grown at low supersaturation degree and have shown edged hexagonal faces and elongated parallel along the crystallographic *c*-axis. ZnO particles grow as hexagonal cylinder shape by slow crystal growth because crystal structure of ZnO has hexagonal packing. The controlled synthesis of ZnO in aqueous solution generates multi-needle shape particles [Figure 3.1]. Multi-needle particles possess high specific surface area compared to hexagonal cylinder particles [3.3b]. Gels are broadly used as the separation medium for biomolecules such as proteins and DNA in electrophoretic applications. The internal morphology of novel gel materials has been

Figure 3.2: Optical images of K$_4$[α-SiW$_{12}$O$_{40}$] showing the tubular morphology of crystals (Figure taken from ref 3.7 with permission).

modified in last few decades to make then suitable for wide range of applications such as separation of biomolecules, drug delivery, electro kinetic pumping, sensor applications, etc [3.5]. It is also familiar that the electronic and optical properties of nanoparticles and nanoclusters largely depend on the symmetry of structural geometry, morphology and surface bonding of the system [3.6].

3.2 Morphological studies in polyoxometalate (POM) based hybrid materials

Morphology of polyoxometalate based hybrid materials is important for their catalytic applications. In the recent years several studies have been carried out to investigate the morphology of POM based hybrid materials and their applications. Since the discovery of carbon nanotubes, lots of attention has been paid to design organic and inorganic microtubular structures. Inorganic microtubular structures have potential application in

photovoltaic and electronic transport. A tubular POM, formulated as $K_4[\alpha\text{-SiW}_{12}O_{40}]$ [Figure 3.2] was prepared by acidification of aqueous solution of tungstosilicate $K_8[\alpha\text{-SiW}_{11}O_{39}]$ using H_3PO_4 or HCl, followed by heating and crystallization [3.7]. A novel dumbbell shaped POM–organic hybrid was prepared by covalently binding of polyhedral oligomeric silsesquioxane (POSS) to the POM cluster. Characterization of the supramolecular structures reveals a nano-structural packing order forming *via* a synergetic self-assembly. The self-assembled supramolecular hybrid shows lamellar morphology with a 4.9 nm periodicity [3.8].

A new hybrid POM complex with two azo groups chemically connect on both sides of an Anderson-type cluster was prepared. The charge of the complex was balanced by two quaternary ammoniumionized *β*-cyclodextrins (CDs). Two host CD units {grafted with pyridine (Py) group} and two guest Azo units assembled in a complex to provide a opportunity for the formation of a self-crosslinked supramolecular arrangement. The morphological study of CD-Azo-POM was carried out using scanning electron microscopy (SEM). The *cis*-form of CD-Azo-POM after UV light irradiation reveals irregular nanofiber structures, which are almost similar to the morphology of *β*-CD-Py itself with very little influence from Azo-POM. Aging the sample in dark promotes gradual formation of *trans*-form, which encourages the formation of right-handed twisted assemblies with lamellar structures (size of *ca.* 10 mm) [Figure 3.3] [3.9].
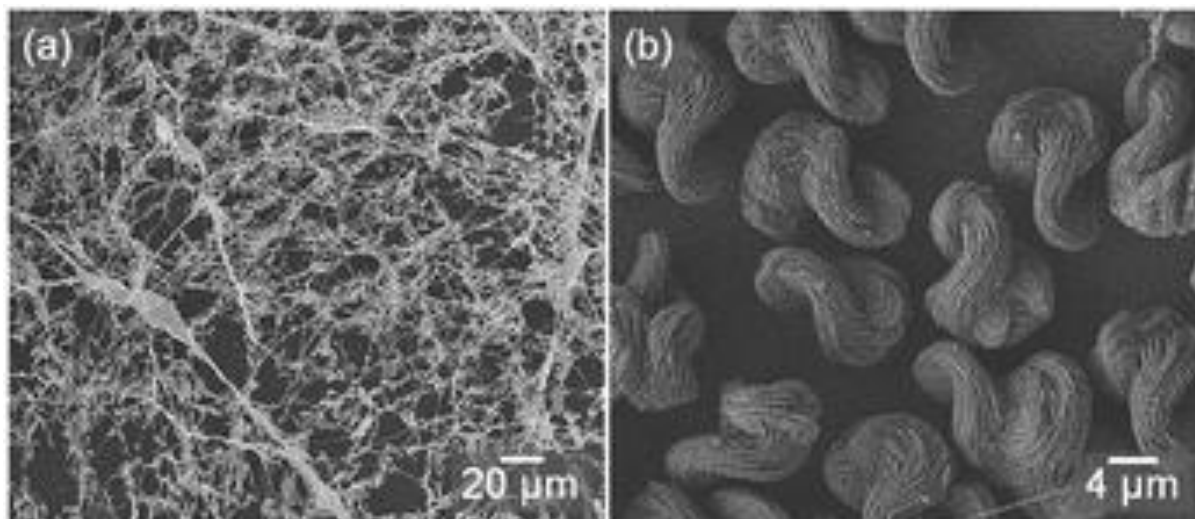
Figure 3.3: SEM images of CD-Azo-POM hybrid structure after (a) initial UV light irradiation for 2 hours and (b) aging the sample in the dark for 7 days (Figure taken from ref 3.9 with permission).

A hybrid nanofibers of polyaniline/polyoxometalate was reported recently. The composite

was prepared by interfacial polymerization consisting of phosphomolybdic acid anion, $[PMo_{12}O_{40}]^{3-}$ in polyaniline matrix. The polyaniline/POM hybrid possessed unique 1D nanofibrous morphology [Figure 3.4] and was used as a cathode material for lithium ion batteries to achieve improved electrochemical properties [3.10].

The SEM images of $[TMGHA]_{2.4}H_{0.6}PW$

(TMGHA: N''-(3-amino-2-hydroxypropyl)-N,N,N',N'-tetramethylguanidinium) illustrate irregular fluffy coral-shaped morphology with micrometer size hollow structure [Figure 3.5
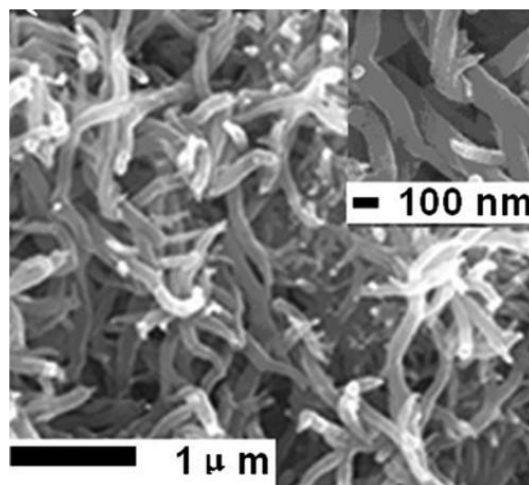
Figure 3.4: SEM image of hybrid nanofibers consisting of polyaniline and polyoxometalate (Figure taken from ref 3.10 with permission).

a-b]. This irregular morphology can be considered as a reflection of the interconnected ionic-liquid (IL)-POM secondary structure.
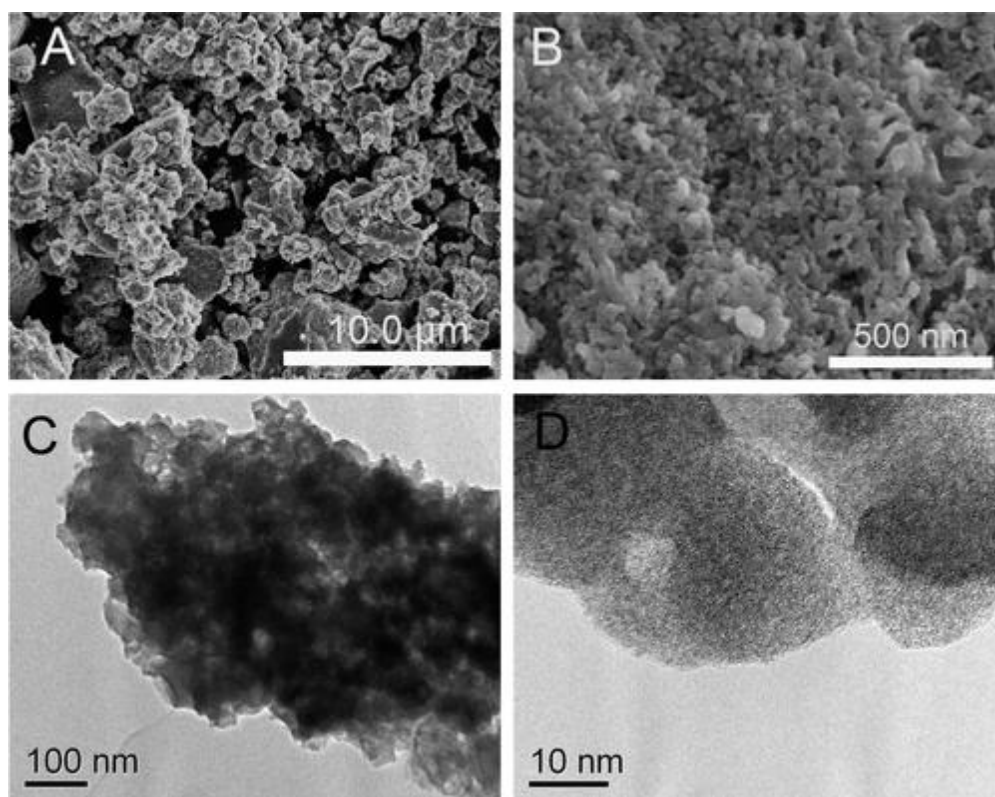
Figure 3.5: SEM images (A, B) and TEM images (C, D) of $[TMGHA]_{2.6}H_{0.4}PW$ (Figure taken from ref 3.11 with permission).

The TEM images of [TMGHA]$_{2.4}$H$_{0.6}$PW reveal the existence of arbitrary mesopores among the intertwine particles and micropores among IL-cations and POM-anions [Figure 3.5 c,d]. The use of analogous ILs such as imidazolium cation [MimHA]$^+$ and pyridinium cation [PyHA]$^+$ resulted in different morphologies in the hybrid structures [3.11].
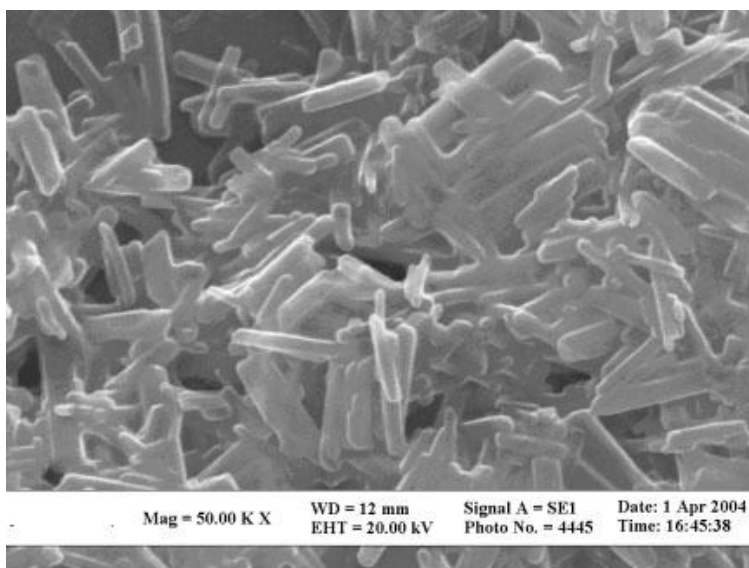
Figure 3.6: SEM image of an as-synthesised sample (HTyr)$_4$Si-W$_{12}$O$_{40}$·5H$_2$O) (Figure taken from ref 3.12 with permission).

A convenient room temperature solid state synthesis method for preparation of nanomaterials has been reported previously. A nanotubular morphology [Figure 3.6] was perceived using amino acid and POMs. Three novel tyrosine (Tyr) polyoxometalate nanotubes, (HTyr)$_3$PMo$_{12}$O$_{40}$·3H$_2$O, (HTyr)$_3$PW$_{12}$O$_{40}$·3H$_2$O, and (HTyr)$_4$SiW$_{12}$O$_{40}$·5H$_2$O were successfully prepared via one-step solid-state reaction at room temperature [3.12].

A cesium hydrogen silicododecatungstate Cs$_{3.0}$H$_{0.3}$ [SiW$_{12}$O$_{40}$]$_{0.83}$·3.0H$_2$O with a cubic cell was prepared and was utilized for selective water sorption and cation-exchange. The compound consisted of highly crystalline particles with flat rhombic bipyramidal morphology [Figure 3.7] [3.13].
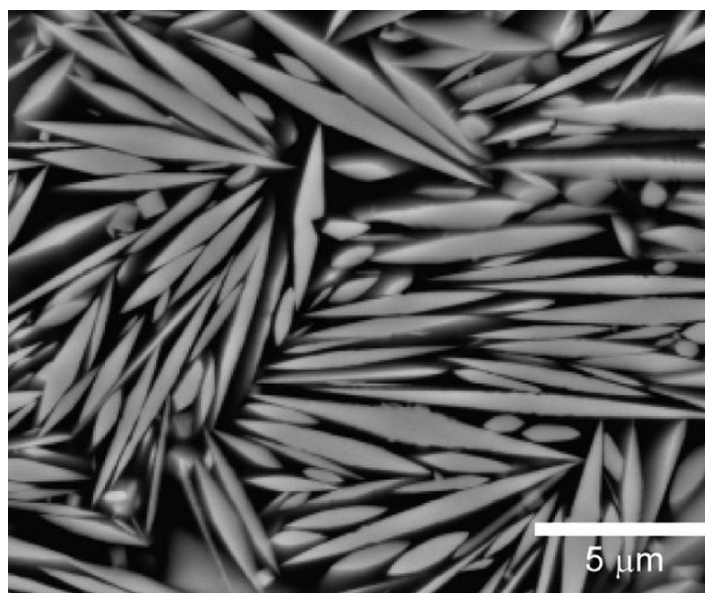
Figure 3.7: SEM image of Cs$_{3.0}$H$_{0.3}$ [SiW$_{12}$O$_{40}$]$_{0.83}$·3.0 H$_2$O with rhombic bipyramidal morphology (Figure taken from ref 3.13 with permission).

A luminescent lanthanide based POM, $[Eu(H_2O)_2SiW_{11}O_{39}]^{5-}$ was encapsulated with dimethyl dioctadecylammonium (DODA) to form a supramolecular surfactant-encapsulated cluster (SEC), $(DODA)_4H\text{-}[Eu(H_2O)_2SiW_{11}O_{39}]$. The SEC aggregates in chloroform as vesicle and forms honeycomb structures when casted onto solid support [Figure 3.8] [3.14].
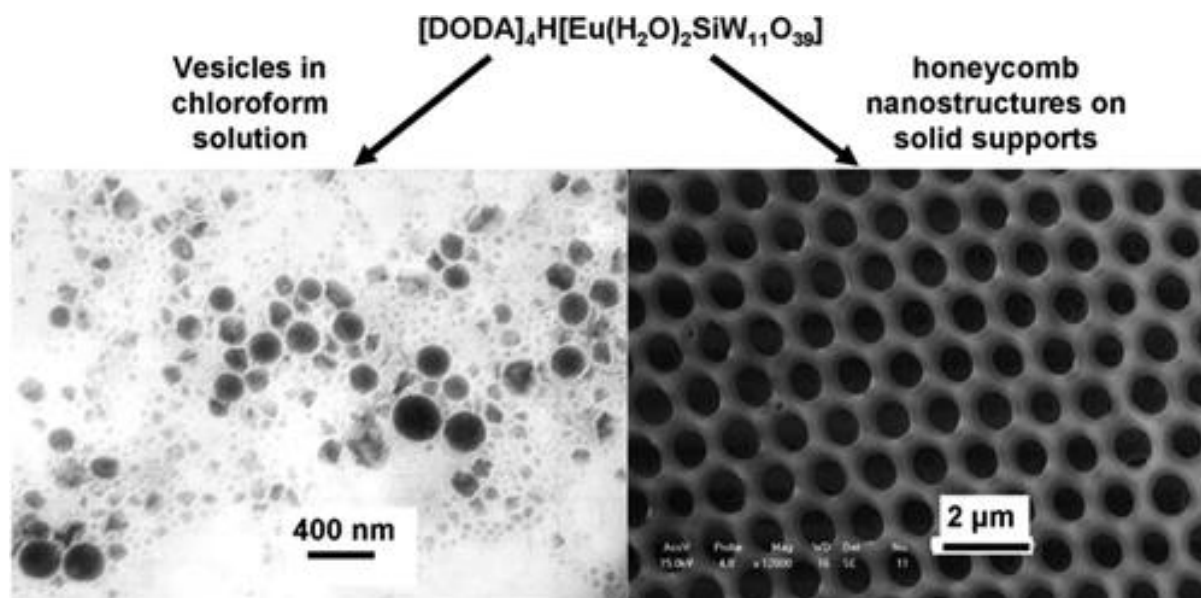
Figure 3.8: SEM images of POM and DODA base vesicles and honeycomb structures (Figure taken from ref 3.14 with permission).

An asymmetrical hybrid composed of an Anderson-type molybdenum−POM ($MnMo_6O_{18}$) encapsulated by two alkyl chains was designed and the charge of the complex was balanced by three TBA^+ (tetrabutylammonium) cation to prepared POM-containing hybrid amphiphiles (PCHAs) [Figure 3.9]. The three TBA^+ cations were replaced by H^+ ions to prepare a series of hybrid material. The interesting structural aspect is the distribution dark and bright domains on the monolayer, specifying the coexistence of two phases with dissimilar packing densities [3.15].
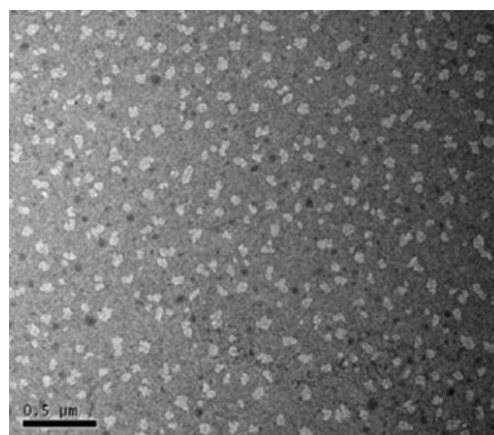
Figure 3.9: TEM image of POM-containing hybrid amphiphiles (Figure taken from ref 3.15 with permission).

A series of POM based amphiphilic catalysts were synthesized *via* self-assembly of the vanadium containing Keggin-type POM $H_4PMo_{11}VO_{40}$ with cationic surfactants of different carbon-chain lengths. Among the composites $(ODA)_4PMo_{11}VO_{40}$ [ODA: octadecylmethylammonium] shows flowerlike

morphology in the SEM images [Figure 3.10 a-c]. TEM of the same reveals that the assembly is consisted of the amphiphilic building blocks organized in lamellar manner[Figure 3.10d] [3.16]. In this chapter we will discuss the preparation of a vanadium based coordination polymer which shows simultaneous occurrence of two morphologies (flower and needle) in hydrothermal condition.
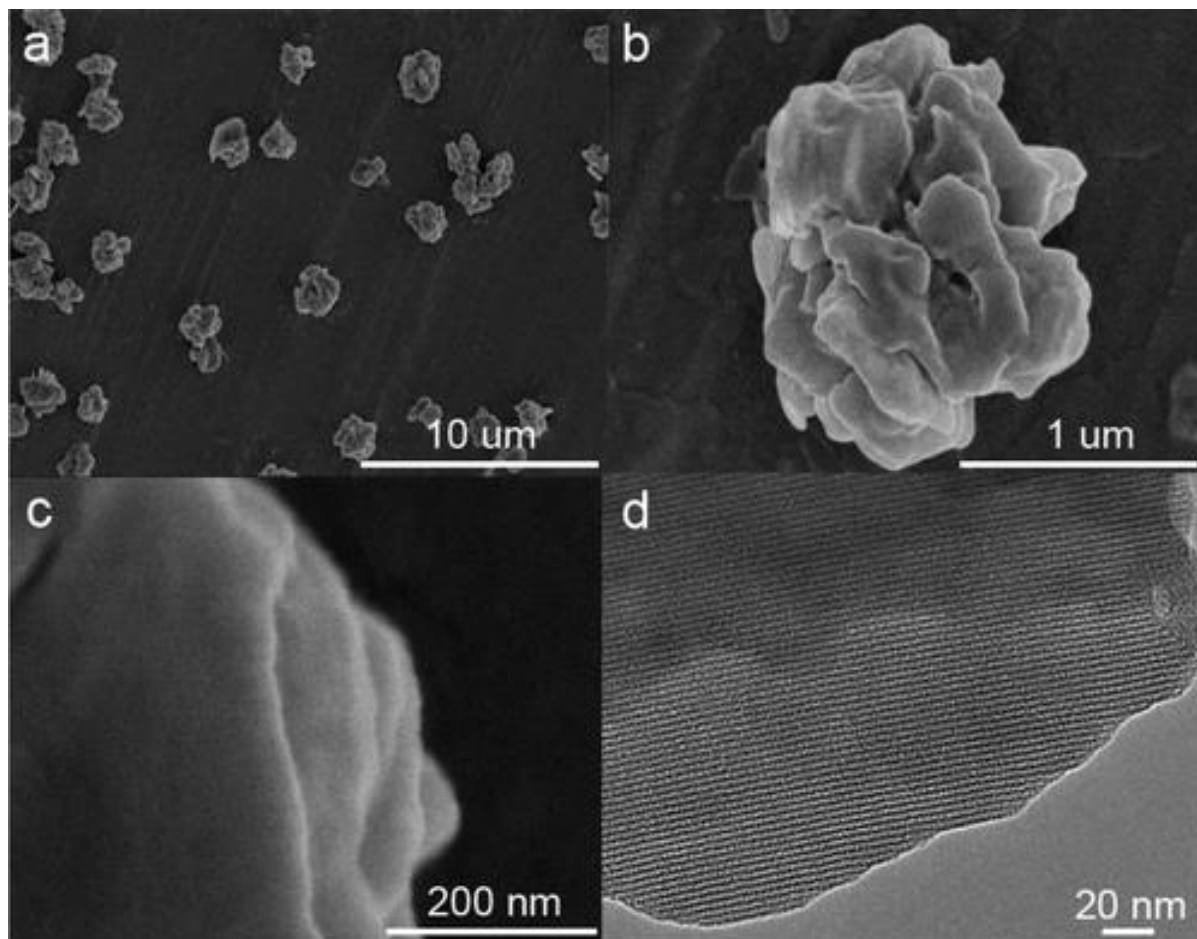
Figure 3.10: (a-c) SEM images of $(ODA)_4PMo_{11}VO_{40}$ with different zoomed view. (d) TEM image $(ODA)_4PMo_{11}VO_{40}$ (Figure taken from ref 3.16 with permission).

3.3 Hydrothermal synthesis of POM based coordination polymer

The design and synthesis of POM based inorganic–organic hybrid architecture have gathered extensive interest due to their potential applications in the fields of catalysis, adsorption, separation, conductivity (electrical/proton), magnetic, sensing, optical materials, etc. A large number of hybrid POMs built with Keggin or Dawson cluster units and transition metal complexes have been prepared during the past few decades. Amines (aliphatic and aromatic) are the most commonly used organic component to build the cationic component of transition metal substituted polyoxometalate (TM-POM) hybrids. It is sometimes challenging to

prepare TM-POM hybrid through conventional method, due to the immiscibility of metal oxide ingredient, transition metal complexes and organic ligand in the same solvent or solvent mixture at an ambient condition. The hydrothermal reaction condition (high temperature and pressure) makes it feasible to put all the component of the reaction in same phase.
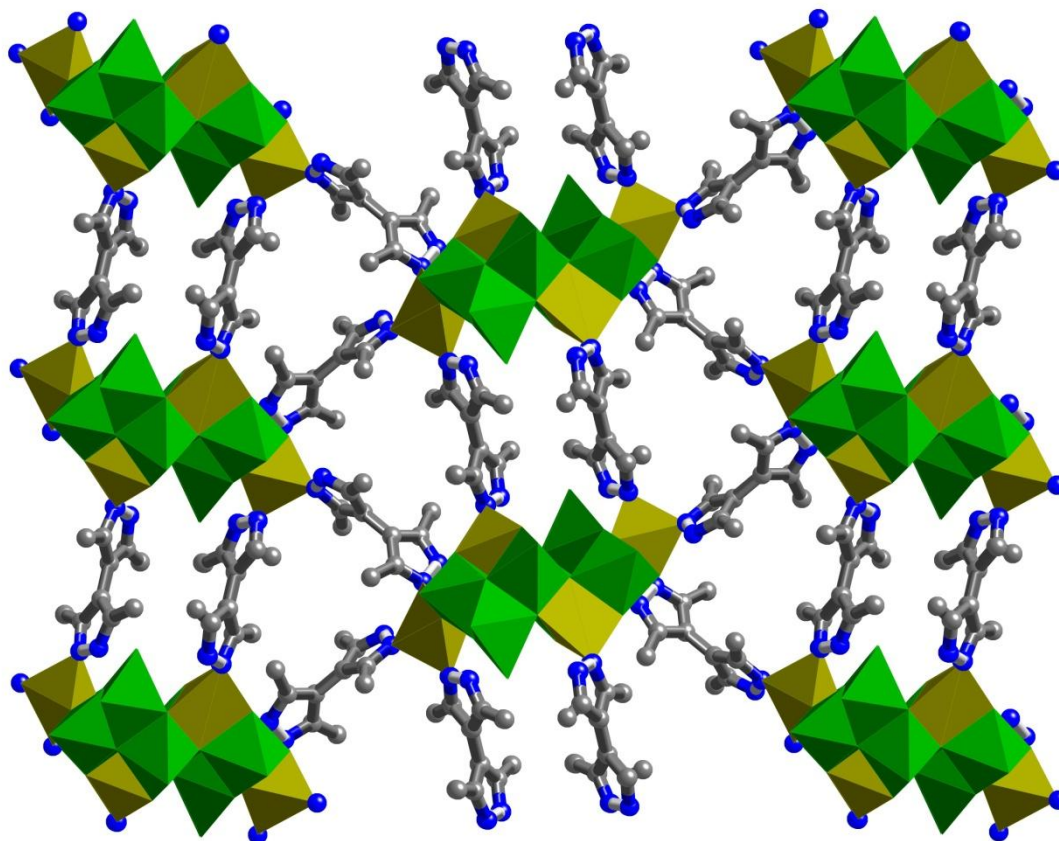
Figure 3.11: 3,3′,5,5′-tetramethyl-4,4′-bipyrazole (4,4'-bpz) connected to $Cu_2Mo_6O_{22}$ cluster to form three dimensional architecture**.** Colour code: Mo: green polyhedra, Cu: yellow polyhedra, N: blue ball, C: grey ball (Figure reproduced from ref. No. 32f).

3.3.1 Purpose of designing POM connected coordination polymer

Research on network structures especially metal organic frameworks (MOFs) has picked up immense attention due to their versatile application in gas storage, sequestration, catalysis, drug delivery etc [3.17]. Recently researchers attempted to introduce POMs inside the MOFs [3.18]. POM incorporated MOFs not only introduce functionality inside the structure, but also enhance the thermal stability of the network [3.19]. Owing to these facts researchers became interested to design and synthesize new MOFs composed of transition-metal complexes (TMCs) as well as polyoxometalates (POMs) to produce TMC-linked POMs [3.20].

Polyoxovanadates (POVs) are an important class of polyoxometalates which has a unique oxidation states of the vanadium and to the best of our knowledge, this work is the first report of TMC connected V_4O_{16} cubane based MOF architecture.

3.3.2 Preparation of V_4O_{16} connected coordination polymer

As a part of ongoing investigations of different synthetic approaches, hydrothermal method became most efficient method for the synthesis of MOFs [3.21]. One-pot synthesis of this type, where four/five inhomogeneous phases were used as precursor, are able to adopt different coordination geometries like tetrahedral, square-pyramidal and octahedral. As vanadium can form POMs with IV and V oxidation states [3.22], POVs could be used in catalysis [3.23]. The catalytic reactions of POVs are influenced by the facile change in oxidation state [3.24]. However, successful design and synthesis of desirable MOFs with existing POVs are still challenging [3.25]. In this chapter, we report the synthesis and structural study of a 2D transition-metal complexes (TMC) linked V_4O_{16} cubane [3.26] based MOF structure formulated as *$Cu_2(phen)_2(V_4O_8)(PO_4)_4$* [$Cu_2V_4O_{16}$-2D]. Although there have been reports of V_4O_{16} cubane and V_4O_{12} boat type POVs based structure in the literature [3.27], but this V_4O_{16} cubane structure, what we have reported in this chapter is very rare. The extended structure or supramolecular assembly with abundant POVs such as decavanadate is reported, but the extended structure with small POVs such as the V_4O_{16} unit will enrich the probability of synthesizing different types of POV hybrid based materials with the desired architectures and properties [3.28]. The $Cu_2V_4O_{16}$-2D MOF was synthesized in hydrothermal condition by heating the mixture of Na_3VO_4 (0.49 mmol), $Cu(NO_3)_2 \cdot 3H_2O$ (0.13 mmol), 1,10-Phenanthroline (0.08 mmol) and 0.5 mL conc. H_3PO_4 in 5mL water (pH $\cong$ 2.10–2.40) at 150 °C for 96 hours and characterized by single crystal X-ray diffraction, powder X-ray diffraction (PXRD), thermal gravimetric analysis (TGA), IR-spectroscopy, scanning electron microscopy (SEM) and elemental analysis (EA).

3.3.3   Crystal structure of V_4O_{16} based coordination polymer

$Cu_2V_4O_{16}$-2D crystallizes in triclinic (*P*-1 space group) crystal system. The asymmetric unit contains four distorted VO_6 octahedra, two distorted $Cu(phen)(O)_3$ square pyramidal unit and four phosphate groups. In each VO_6 octahedra V−O$_{Bridging}$, V−O$_{Phosphate}$ and V−O$_{Terminal}$ bond distances are 1.865(3), 1.896(3) and 1.593(3) Å respectively. The $Cu(phen)(O)_3$ square pyramidal unit consists of two equatorial Cu-O bonds [1.896(3) Å and 1.948(3) Å] and one

axial Cu-O bond [2.390(3) Å]. The average Cu-N bond distances in $Cu(phen)(O)_3$ unit lies
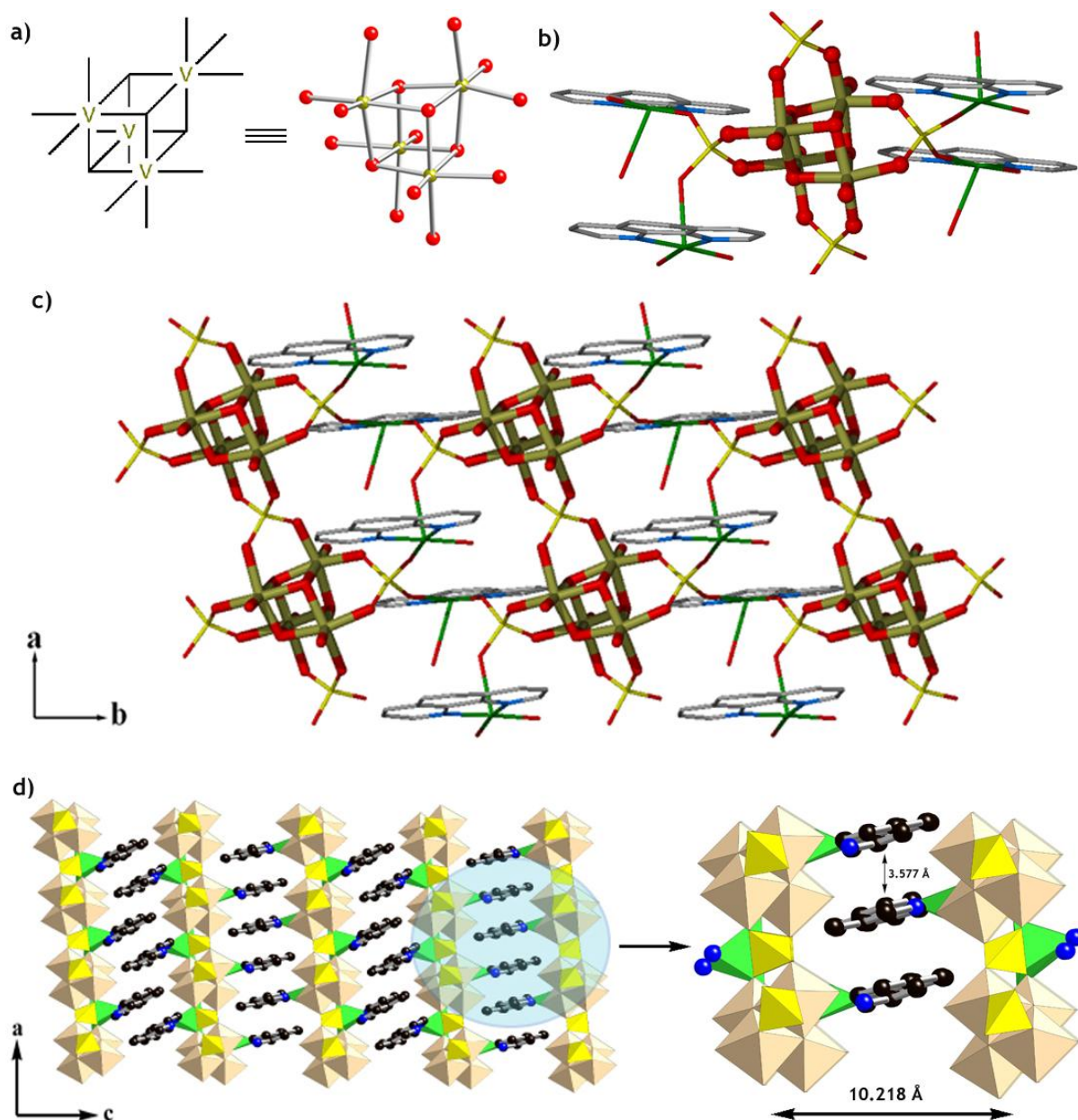
Figure 3.12: (a) Schematic and ball−stick models of the V_4O_{16} unit. (b) One V_4O_{16} cubane connected to four phosphates and four Cu(II) square-pyramid units. (c) 2-D arrangement of $Cu_2V_4O_{16}$-2D, where one V_4-cubane is connected to the next V_4-cubane via one phsophate group through the *a*-axis and via two phosphates and two Cu(II) units through the *b*-axis. (d) Interdigitation of 2-D sheets of $Cu_2V_4O_{16}$-2D via the phenanthroline ring in the *ac*-plane. [Color code: C: black, Cu: green, O: red, N: blue, P: yellow, V: dark yellow.]

between 1.997(3)–2.017(3) Å. Four such VO_6 octahedra are packed together to form one V_4O_8 cubane unit. Each VO_6 octahedra is edge shared, four μ_3–oxygen atoms connect four octahedra together to form a cubane like architecture [Figure 12a]. Inside the cubane the V−

O–V and O–V–O bond angles varies from 78° to 102°, creating the structural distortion from perfect cubane. Each V_4O_8 cubane is connected to four different $Cu(phen)(O)_3$ square pyramidal unit [Figure 2.12b]. One V_4O_8 cubane is connected to two V_4O_8 cubane via PO_4 group through crystallographic *c*-axis, the same V_4O_8 cubane is connected to two other V_4O_8 cubane via two PO_4–Cu–PO_4 units through crystallographic *b*-axis. A square pyramidal Cu(II) is connected to each V_4O_8 unit via axial Cu–O bond. These 'V–O–P–O–V' connectivity in *c*-axis and 'V–O–P–O–Cu–O–P–O–V' connectivity in *b*-axis creates a 2D sheet like architecture that propagates along *bc*-plane [Figure 2.12c]. These 2D sheets are interdigitated *via* phenanthroline rings which are coordinated with coppers. The closest distance between two interdigitated phenanthroline rings is 3.577 Å and the closest distance between two vanadium layers is 10.218 Å [Figure 2.12d]. The difference of $Cu_2V_4O_{16}$-2D structure from earlier phosphate connected V_4O_8 cubane structure, $(C_{10}H_{10}N_2)\{(VO_2)_4(PO_4)_2\}$ (where $C_{10}H_{10}N_2$ = 4,4′-bipyridinium cation) is that, in the reported structure cubanes were connected *via* PO_4 group in both the direction and there was no Cu(II) atoms in the structure to form a TMC-POM based MOF [3.27a]. Whereas, in $Cu_2V_4O_{16}$-2D, through *c*-axis connectivity was *via* PO_4 and through *b*-axis V_4O_{16} cubanes are connected *via* PO_4–Cu–PO_4 units and the resulting structure is a TMC-POM based MOF.

3.3.4   Characterization of V_4O_{16} based coordination polymer

The scanning electron microscopy (SEM) data, collected for as-synthesized $Cu_2V_4O_{16}$-2D reveals an unusual morphological difference of the bulk material. The major portion of the compound consists of needle shaped crystal (150-200 μm in length and 2-6 μm width), one of the best of which was used for X-ray crystal data collection. We surprisingly found few flower like morphology along with the needle like crystal in the SEM images, which are composed of several fine plates [Figure 2.13a-2.13d]. The PXRD data (there is no significant difference in experimental PXRD as compared to simulated one [Figure 2.14a] and IR-spectra [Figure 2.14b] support the presence of only one phase which was identified by crystal structure. Therefore the flower type of morphology could be an intermediate stage of crystallization which is en route towards needle like crystal form of the same MOF [2.29]. It is noteworthy that this type of morphological difference of the solid phase in extended metal-organic hybrid material is rare and has not been perceived in POV based MOFs literature. All major peaks of experimental PXRD of $Cu_2V_4O_{16}$-2D matches well with simulated PXRD, indicating their reasonable crystalline phase purity. The strong bands at 916 (band 4) and 965
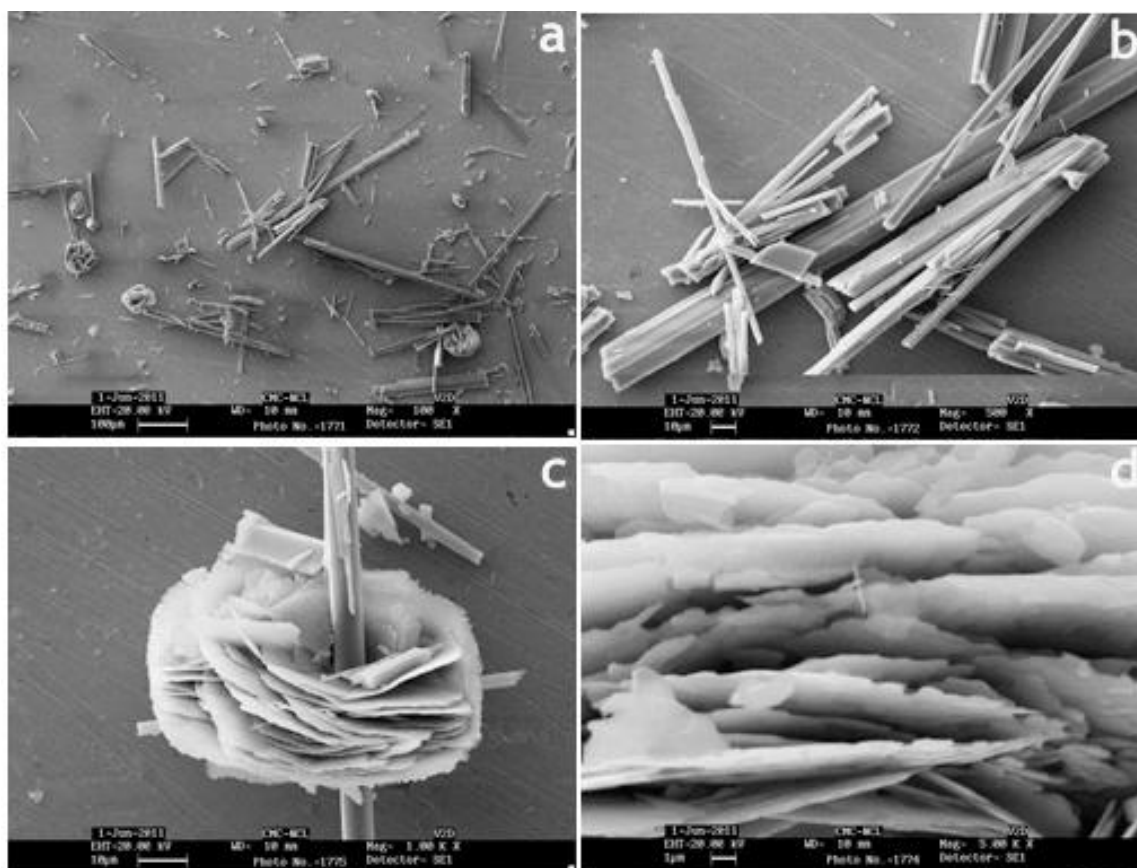
Figure 3.13: (a) SEM image of the bulk material showing both flower- and needle-like morphologies. b) SEM image of $Cu_2V_4O_{16}$-2D showing the crystalline edge of the needle-like crystals. (c) Flower-like morphological phase of $Cu_2V_4O_{16}$-2D which is present in the bulk product along with the needle-like crystal; one flower-like morphology grown around the needle-like crystal. (d) Zoomed view of one flower-like morphology showing the aggregation of flakes.

cm^{-1} (band 5) in the IR spectrum are due to the typical stretching vibrational mode of terminal V=O double bonds. The bands at 1036 cm^{-1} (band 6) are assigned to the PO_4 anti-symmetric stretching vibrational modes and the band at 839 cm^{-1} (band 3) could be attributed to the related PO_4 symmetric stretching modes. The peaks at 643 (band 1) and 718 (band 2) cm^{-1} region are also associated with V–O–V stretching vibrational modes, and several intense bands between 1200 and 1650 cm^{-1} arise from the presence of copper coordinated phenanthroline rings inside the structure. Thermal gravimetric analysis (TGA) was performed on as-synthesized $Cu_2V_4O_{16}$-2D in order to understand the thermal stability of the MOF with respect to temperature. The decomposition point at around 325 °C indicates the high thermal stability of the MOF [Figure 2.14b]. Gas adsorption in POM based hybrid materials is rare [3.30]. We have shown in our earlier work that POM based ionic salt could be used as H_2 and

CO_2 storage materials [3.31]. As-synthesized sample of $Cu_2V_4O_{16}$-2D was immersed in dry chloroform at ambient temperature for 72 hours, evacuated at ambient temperature for 24 hours, then at an elevated temperature (85 °C) for 48 hours. Sample thus obtained was optimally evacuated, as evidenced by their well-maintained PXRD patterns and the long plateau (ambient temperature to 300 °C) in their TGA traces. The H_2 adsorption isotherm
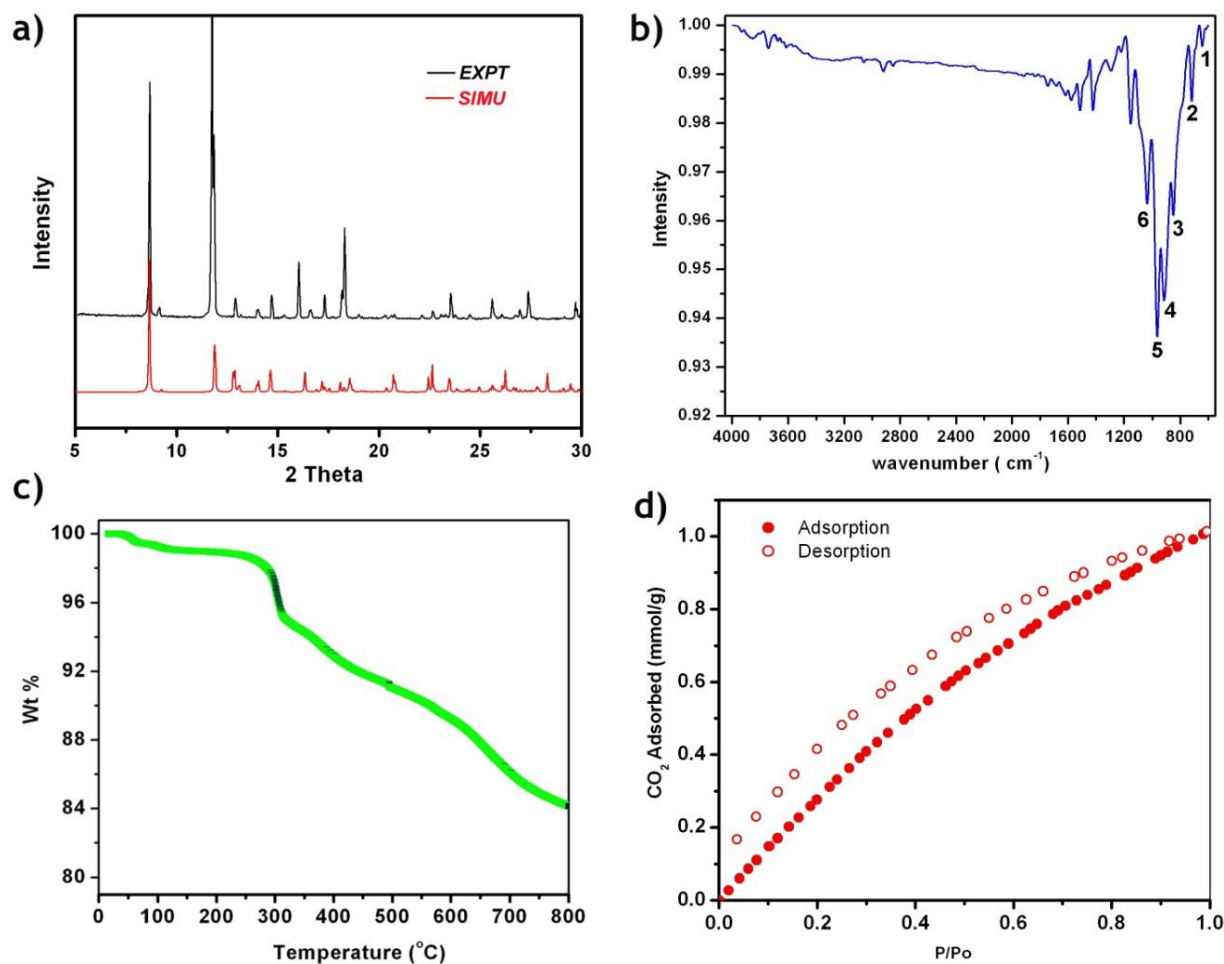
Figure 3.14: (a) Comparison of the experimental PXRD pattern of as-synthesized $Cu_2V_4O_{16}$-2D (top) with the simulated one from its single crystal structure (bottom). (b) IR-spectroscopy of $Cu_2V_4O_{16}$-2D. (c) The image shows the thermal gravimetric analysis curve for $Cu_2V_4O_{16}$-2D. The coordination polymer is stable thermally stable upto 300 °C. Beyond that temperature it gradually decomposes. (d) CO_2 adsorption−desorption isotherm for $Cu_2V_4O_{16}$-2D at 298 K below 1.0 bar. [Filled circles are for adsorption, and empty circles are for desorption].

exhibits type-II sorption behavior. At 760 Torr and 77 K, $Cu_2V_4O_{16}$-2D adsorbs 0.37 wt% H_2. The framework of $Cu_2V_4O_{16}$-2D exhibits a typical type-II profile for CO_2 (3.3 Å) adsorption. $Cu_2V_4O_{16}$-2D adsorbs 1.01 mmol/g of CO_2 at 298 K and 1 bar pressure [Figure 2.15d].

3.4 Conclusion

We have successfully synthesized a two dimensional Cu(II) connected and rarely observed vanadium cubane based MOF. To the best of our knowledge, this is the first example of a transitional metal connected V_4O_{16} cubane based metal organic architecture. The SEM image of the bulk material shows two types of morphologies: needle-like crystals (major) and flower type aggregation (minor). However, IR spectroscopy, PXRD, and EA data of the bulk material show the presence of only one phase. As a result, one could incur that the flower type of morphology could be an intermediate stage of crystallization which is en route toward the needle-like crystal. We also studied H_2 and CO_2 adsorption on $Cu_2V_4O_{16}$-2D, which is a rare effort in POM chemistry.

3.5 Experimental Section

All reagents and solvents for synthesis and analysis were commercially available and used as received. The Fourier Transform *(FT)-IR* spectra (KBr pellet) were taken on a *PERKIN ELMER FT-IR SPECTRUM* (Nicolet) spectrometer. Powder X-ray diffraction (PXRD) patterns were recorded on a Phillips PNAlytical diffractometer for Cu Kα radiation (λ = 1.5406 Å), with a scan speed of $2°$ min^{-1} and a step size of $0.02°$ in 2θ. Thermo-gravimetric experiments (TGA) were carried out in the temperature range of 25–800 °C on a SDT Q600 TG-DTA analyzer under N_2 atmosphere at a heating rate of 10 °C min^{-1}. All low-pressure gas adsorption experiments (up to 1 bar) were performed on a *Quantachrome Quadrasorb* automatic volumetric instrument.

Synthesis of {Cu₂(phen₂)}{(V₄O₈)(PO₄)₄} [Cu₂V₄O₁₆-2D]: The compound was synthesized in hydrothermal condition at 150 °C for 96 hours using the mixture of Sodium (Meta) Vanadate (0.49 mmol), $Cu(NO_3)_2 \cdot 3H_2O$ (0.13 mmol), 1,10-Phenanthroline (0.08 mmol), 0.5 mL conc. H_3PO_4 and 5 mL water. *FT-IR* : (KBr 4000-450cm^{-1}): 2919(w), 2851(w), 1744(w), 1617(w), 1576(w), 1513(w), 1420(w), 1219(m), 1036(s), 965(s), 916(s), 849(s), 718(m), 643(w). E.A. Calcd, C= 25.26, H=1.75, N= 4.91; Found (%) C= 24.89, H= 1.85, N= 4.63.

Single-Crystal structure analysis: The single crystal data was collected on a Bruker SMART APEX three circle diffractometer equipped with a CCD area detector (Bruker Systems Inc., 1999a) [3.32] with Mo K$_\alpha$ radiation (λ= 0.71073 Å). Data were integrated using Bruker *SAINT* software [3.33]. Data were subsequently corrected for absorption by the program *SADABS* [3.34]. The space group determinations and tests for merohedral twinning

were carried out using *XPREP* [3.35]. The structure was solved by direct methods and refined using the *SHELXTL 97* software suite [3.36]. The structure was examined using the *Adsym* subroutine of *PLATON* [3.37]. Crystallographic data (excluding structure factors) for the structure reported in this chapter have been deposited with the CCDC as deposition No.837584. Copies of the data can be obtained, free of charge, on application to the CCDC, 12 Union Road, Cambridge CB2 lEZ UK (fax: + 44 (1223) 336 033; e-mail: deposit@ccdc.cam.ac.uk).

Gas adsorption experiments: As-synthesized sample of coordination polymer was immersed in dry dichloromethane at ambient temperature for 72 hours, evacuated at ambient temperature for 24 hours, then at an elevated temperature (85 °C) for 48 hours. Samples thus obtained were optimally evacuated.

3.6 References

3.1   a) T. Kasuga, M. Hiramatsu, A. Hoson, T. Sekino, K. Niihara, *Adv. Mater.* **1999**, *11*, 1307. (b) Y. Oaki, H. Imai, *J. Am. Chem. Soc.* **2004**, *126*, 9271.

3.2   R. C. Schroden, C. F. Blanford, B. J. Melde, B. J. S. Johnson, A. Stein, *Chem. Mater.* **2001,** *13,* 1074.

3.3   (a) P. M. Tessier, Orlin D. Velev, A. T. Kalambur, J. F. Rabolt, A. M. Lenhoff, E. W. Kaler, *J. Am. Chem. Soc.* **2000**, *122,* 9554. (b) Y. Masuda, K. Kato, *Cryst. Growth & Des.* **2008**, *8*, 7378.

3.4   M. Xie, X. Zhang, J. Laakso, H. Wang, E. Levanen, *Cryst. Growth Des.* **2012**, *12*, 2166.

3.5   J. J. Simhadri, H. A. Stretz, M. Oyanader, P. E. Arce, *Ind. Eng. Chem. Res.* **2010**, *49,* 11866.

3.6   C. Noguez, A. Sanchez-Castillo, F. Hidalgo, *J. Phys. Chem. Lett*. **2011**, *2*, 1038.

3.7   Z. Xin, J. Peng, T. Wang, B. Xue, Y. Kong, L. Li, E. Wang, *Inorg. Chem.* **2006**, *45*, 8856.

3.8   T. Okada, K. Miyamoto, T. Sakai, S. Mishima. *ACS Catal.* **2014**, *4*, 73.

3.9   L. Yue, H. Ai, Y. Yang, W. Lu, L. Wu, *Chem. Commun.* **2013**, *49*, 9770.

3.10   H. Yang, T. Song, L. Liu, A. Devadoss, F. Xia, H. Han, H. Park, W. Sigmund, K. Kwon, U. Paik, *J. Phys. Chem. C.* **2013**, *117*, 17376.

3.11   G. Chen, Y. Zhou, Z. Long, X. Wang, J. Li, J. Wang, *ACS Appl. Mater. Interfaces* **2014**, *6*, 4438.

3.12   R. –Y. Wang, D. –Z. Jia, L. Zhang, L. Liu, Z. –P. Guo, B. –Q. Li, J. –X. Wang, *Adv. Funct. Mater.* **2006**, *16*, 687.

3.13   Y. Ogasawara, S. Uchida, T. Maruichi, R. Ishikawa, N. Shibata, Y. Ikuhara, N. Mizuno, *Chem. Mater.* **2013**, *25*, 905.

3.14   W. Bu, H. Li , H. Sun, S. Yin, L. Wu, *J. Am. Chem. Soc.* **2005**, *127*, 8016.

3.15   X. –L. Wang, Y. –L. Wang, W. –K. Miao, M. –B. Hu, J. Tang, W. Yu, Z. –Y. Hou, P. Zheng, W. Wang, *Langmuir.* **2013**, *29*, 6537.

3.16   L. Jing, J. Shi, F. Zhang, Y. Zhong, W. ZhuInd, *Ind. Eng. Chem. Res.* **2013**, *52,* 10095.

3.17   (a) B. Moulton, M. J. Zaworotko, *Chem. Rev.* **2001**, *101*, 1629. (b) M. Eddaoudi, D. B. Moler, H. Li, B. Chen, T. M. Reineke, M. O'Keeffe, O. M. Yaghi, *Acc. Chem. Res.* **2001**, *34*, 319. (c) O. M. Yaghi, *Nat. Mater.* **2007**, *6*, 92. (d) I. G. Georgiev, L. R. MacGillivray. *Chem. Soc. Rev.* **2007**, *36*, 1239. (e) A. Corma, H. Garcia, F. X. L. Xamena. *Chem. Rev.* **2010**, *110*, 4606. (f) S. L. James, *Chem. Soc. Rev.* **2003**, *32*, 276. (g) O. M. Yaghi, H. Li, C. Davis, D. Richardson, T. L. Groy. *Acc. Chem. Res.* **1998**, *31*, 474. (h) C. Janiak. *Angew. Chem., Int. Ed. Engl.* **1997**, *36*, 1431. (i) A. J. Blake, N. R. Champness, P. Hubberstey, W.-S. Li, M. A. Withersby, M. Schroder. *Coord. Chem. Rev.* **1999**, 183. (j) B. Kesanli, Y. Cui, M. Smith, E. Bittner, B. Bockrath, W. Lin, *Angew. Chem., Int. Ed.* **2005**, *44*, 72.

3.18   (a) X.-L. Wang, C. Qin, E.-B. Wang, Z.-M. Su, *Chem. Commun.* **2007**, 4245. (b) S.-T. Zheng, G.-Y. Yang, *Dalton Trans.* **2010**, *39*, 700. (c) X. Wang, H. Hu, G. Liu, H. Lin, A. Tian, *Chem. Commun.* **2010**, 46, 6485. (d) C.-Y. Sun, S.-X. Liu, D.-D. Liang, K.-Z. Shao, Y. - H. Ren, Z.-M. Su. *J. Am. Chem. Soc.* **2009**, *131*, 1883.

3.19   (a) M. Fournier, C. Feumi-Jantou, C. Rabia, G. Herve S. Launay, *J. Mater. Chem.* **1992**, *2*, 971. (b) P. G. Rickert, M. R. Antonio, M. A. Firestone, K.-A. Kubatko, T. Szreder, J. F. Wishart, M. L. Dietz, *J. Phys. Chem. B*. **2007**, *111*, 4685. (c) D. Mustafa, E. Breynaert, S. R. Bajpe, J. A. Martens, C. E. A. Kirschhock, *Chem. Commun.* **2011**, *47*, 8037.

3.20   (a) Y.-Z. Zheng, M. Evangelisti, R. E. P. Winpenny, *Angew. Chem., Int. Ed.* **2011**, *50*, 3692. (b) C.-D. Zhang, S.-X. Liu, C.-Y. Sun, F.-J. Ma, Z.-M. Su, *Cryst. Growth Des.* **2009**, *9*, 3655. (c) X.-L. Wang, Y.-G. Li, Y. Lu, H. Fu, Z.-M. Su, E.-B. Wang, *Cryst. Growth Des.* **2010**, *10*, 4227. (d) D. Dutta, A. D. Jana, M. Debnath, A. Bhaumik, J. Marek, M. Ali, *Dalton Trans.* **2010**, *39*, 11551. (e) H. An, Y. Li, E. Wang, D. Xiao,

C. Sun, L. Xu, *Inorg. Chem.* **2005**, 44, 6062. (f) Y. –M. Xie, R. –M. Yu, X. –Y. Wu, F. Wang, J. Zhang, C. –Z. Lu. *Cryst. Growth Des.* **2011**, *11*, 4739.

3.21 (a) Y. Qiu, H. Deng, J. Mou, S. Yang, M. Zeller, S. R. Batten, H. Wue, J. Li, *Chem. Commun*. **2009**, 5415. (b) K. E. Knope, C. L. Cahill, *Inorg. Chem.* **2007**, 46, 6607.

3.22 (a) C. Streb, R. Tsunashima, D. A. MacLaren, T. McGlone, T. Akutagawa, T. Nakamura, A. Scandurra, B. Pignataro, N. Gadegaard, L. Cronin, *Angew. Chem., Int. Ed.* **2009**, *48*, 6490. (b) W. Hu, X.-b. Zhang, Y.-l. Cheng, Y.-m. Wua, L.-m. Wang, *Chem. Commun.* **2011**, *47*, 5250. (c) W. Yang, C. Lu, Q. Zhang, S. Chen, X. Zhan, J. Liu, *Inorg. Chem. 2007*, 42, 7309. (d) N. V. Izarova, N. Vankova, A. Banerjee, G. B. Jameson, T. Heine, F. Schinle, O. Hampe, U. Kortz, *Angew. Chem., Int. Ed.* **2010**, *49*, 1.

3.23 (a) Y. Hu, F. Luo, F. Dong, *Chem. Commun.* **2011**, *47*, 761. (b) J. W. Han, C. L. Hill, *J. Am. Chem. Soc.* **2007**, *129*, 15094. (c) F. Hillerns, F. Olbrich, U. Behrens, D. Rehder. *Angew. Chem., Int. Ed. Engl*. **1991**, *30*, 148.

3.24 (a) C. D. Abernethy, F. Bottomley, R. W. Day, A. Decken, D. A. Summers, R. C. Thompson, *Organometallics.* **1999**, *18*, 870. (b) T. Chirayil, P. Y. Zavalij, M. S. Whittingham. *J. Mater. Chem*. **1997**, 7, 2193. (c) T. Arumuganathan, S. K. Das, *Inorg. Chem.* **2009**, *48*, 496. (d) Y. Hu, F. Luo, F. Dong, *Chem. Commun.* **2011**, *47*, 761.

3.25 (a) A. Muller, H. Reuter, S. Dillinger, *Angew. Chem., Int. Ed. Engl.* **1995**, *34*, 2328. (b) W. Yang, C. Lu, Q. Zhang, S. Chen, X. Zhan, J. Liu, *Inorg. Chem.* **2003**, *42*, 7309.

3.26 (a) S. U. Son, J. A. Reingold, S. B. Kim, G. B. Carpenter, D. A. Sweigart, *Angew. Chem., Int. Ed.* **2005**, *44*, 7710. (b) S. Diewald, Y. Lan, R. Clerac, A.-K. Powell, C. Z. Feldmann, *Z. Anorg. Allg. Chem.* **2008**, *634*, 1880. (c) A. Mukherjee, R. Raghunathan, M. K. Saha, M. Nethaji, S. Ramasesha, A. R. Chakravarty, *Chem.-Eur. J.* **2005**, *11*, 3087. (d) T. J. Boyle, T. M. Alam, K. P. Peters, M. A. Rodriguez. *Inorg. Chem.* **2001**, *40*, 6281. (e) F. Bottomley, D. E. Paez, P. S. White, *J. Am. Chem. Soc.* **1981**, *103*, 5581.

3.27 (a) F. -N. Shi, F. A. A. Paz, J. Rocha, J. Klinowski, T. Trindade, *Eur. J. Inorg. Chem.* **2004**, 3031. (b) Y. Zhang, P. J. Zapf, L. M. Meyer, R. C. Haushalter, J. Zubieta, *Inorg. Chem.* **1997**, *36*, 2159. (c) Z.-H. Yi, X.-B. Cui, X. Zhang, J.-H. Yu, J. Lu, J.-Q. Xu, G.-D. Yang, T.-G. Wang, H.-H. Yu, W.-J. Duan, *Dalton Trans.* **2007**, 2115. (d) Y. Zhang, R. C. Haushalter, C. Abraham, *Inorg. Chem.* **1996**, *35*, 4950. (e) F. Jiang, O. P. Anderson, S. M. Miller, J. Chen, M. Mahroof-Tahir, C. C. Debbie, *Inorg. Chem.*

1998, *37*, 5439. (f) I. Cavaco, J. C. Pessoa, M. T. Duarte, P. M. Matias, R. T. Henniques. *PoIyhedron* **1993**, *12*, 1231.

3.28 (a) E. Coronado, J. R. Galan-Mascaros, C. Gimenez-Saiz, C. J. Gomez- Garcia, E. Martinez-Ferrero, M. Almeida, E. B. Lopes. *Adv. Mater.* **2004**, *16*, 324. (b) L. Chen, F. Jiang, Z. Lin, Y. Zhou, C. Yue, M. Hong, *J. Am. Chem. Soc.* **2005**, *127*, 8588. (c) C. Streb, R. Tsunashima, D. A. MacLaren, T. McGlone, T. Akutagawa, T. Nakamura, A. Scandurra, B. Pignataro, N. Gadegaard, L. Cronin. *Angew. Chem., Int. Ed*. **2009**, *48*, 6490.

3.29 (a) A. Nisar, Y. Lu, X. Wang, *Chem. Mater.* **2010**, *22*, 3511. (b) K. Okamoto, S. Uchida, T. Ito, N. Mizuno, *J. Am. Chem. Soc.* **2007**, *129*, 7378. (c) P. Mothe-Esteves, M. M. Pereira, J. Arichi, B. Louis. *Cryst. Growth Des.* **2010**, *10*, 371. (d) Y. Yan, H. Wang, B. Li, G. Hou, Z. Yin, L. Wu, V. W. W. Yam, *Angew. Chem., Int. Ed.* **2010**, *49*, 9233.

3.30 S.-I. Noro, R. Tsunashima, Y. Kamiya, K.. Uemura, H. Kita, L. Cronin, T. Akutagawa, T. Nakamura, *Angew. Chem., Int. Ed.* **2009**, *48*, 8703.

3.31 C. Dey, R. Das, P. Pachfule, P. Poddar, R. Banerjee, *Cryst. Growth Des.* **2011**, *11*, 139.

3.32 *SMART*, Version 5.05; Bruker AXS, Inc.: Madison, WI, **1998**.

3.33 *SAINT-Plus*, Version 7.03; BrukerAXS Inc.: Madison, Wisconsin, **2004**.

3.34 G. M. Sheldrick, *SADABS* (Version 2.03) and *TWINABS* (Version 1.02); University of Gottingen; Germany, **2002**.

3.35 G. M. Sheldrick, *SHELXS'97*; University of Gottingen: Germany, **1997**.

3.36 G. M. Sheldrick, *SHELXTL '97*; University of Gottingen: Germany, **1997**.

3.37 A. L. Spek, *PLATON*, A Multipurpose Crystallographic Tool; Utrecht University: Utrecht, The Netherlands, **2005**.

Note:

The results of this chapter have already been published in *Crystal Growth & Design*. **2012**, 12, 12-17. with the title: 'Solid Phase Morphological Diversity of a Rare Vanadium Cubane (V_4O_{16}) Based Metal Organic Framework'. This publication was the result of a collaboration between the group of Dr. Rahul Banerjee and his students Chandan Dey from the Physical/Materials Chemistry Division at CSIR-National Chemical Laboratory in Pune, India and the group of Dr. Pankaj Poddar with his student Raja Das from the Physical/Materials Chemistry Division at CSIR-National Chemical Laboratory in Pune, India.

Synthesis and Proton Conductivity Measurement of Polyoxometalate (POM) Based Composites

4.1 Introduction

Proton conductivity [4.1] in solid state has caught much attention due to its potential application in fuel cells, batteries and chemical sensors. Proton conducting material plays a crucial role in fuel cell [4.2], a promising energy conversion means for automobiles and portable electronic devices. A fuel cell is a tool that transforms the chemical energy of a fuel into electrical energy through chemical reaction. The fuel cell requires a separator between two electrodes which will be good conductor of proton at moderate temperature. Nafion is used as proton conductor in fuel cell application and shows excellent activity at low temperatures (< 80 °C) under humidified condition [4.3]. But limitation of these polymeric materials is their poor proton conductivity at higher temperatures. On the other hand $MgCrO_4$-TiO_2, ZrO_2-MgO, $Ba_{0.5}Sr_{0.5}TiO_3$, TiO_2-$K_2Ti_6O_{13}$, $HZr_2P_3O_{12}$, etc oxides [4.4] are also known for their proton conducting property under humidified conditions at comparatively elevated temperatures. Nanocomposite membranes consist of hydrophilic inorganic nanoparticles and polyelectrolyte collected considerable attention due to their proton conducting nature at high temperature [4.5]. Organic sulfonic and phosphonic acid functionalized mesoporous silica and zeolites are also rectified for proton conduction [4.6].

4.2 POM based ionic salts for proton conduction

Recently synthesis of organic-inorganic hybrid solid materials with tunable porosity is of more interest due to their applications in catalysis, sorption, ion exchange and conductivity. Polyoxometalate (POM) [4.7] composites of transition metal (Mo, W, V etc) oxide are thermally stable and hydrophilic in nature. Although, POMs have desired functionality to be a good proton conducting material, but so far report on POM based proton conducting materials are very few [4.8]. Designing a POM based three dimensional hybrid materials with porous hydrophilic channel is still challenging. Five different types of POM based composites have been studied for proton conduction till date. They can be classified as (i) POM incorporated inside perfluorinated sulfonic acid polymer, (ii) POM immobilized in

silica material via sol-gel method, (iii) POM casted in inert polymer matrix, (iv) POM directly attached to polymer through functionalization, (v) POM based metal organic material, were tested for proton conductivity [4.9]. These aforementioned facts encourage us to design phosphate decorated POM based hybrid materials for proton conduction. In this work we have tried to synthesize POM anion and organic cation based ionic hybrid composites system for proton conduction. To design such materials, we have selected $[NiMo_{12}O_{30}(PO_4)_8]^{n-}$ POM anion [4.10] and ethylene-diamine/ 4,4′-bipyridine/ 4,4′-dimehyl-2,2′-bipyridine, which eventually gets protonated in the reaction medium to form POM anion and organic cation based ionic composite [Figure 4.1].

Green: NiO$_6$ Cyan: PO$_4$ Yellow: MoO$_6$ Black: C   Blue: N
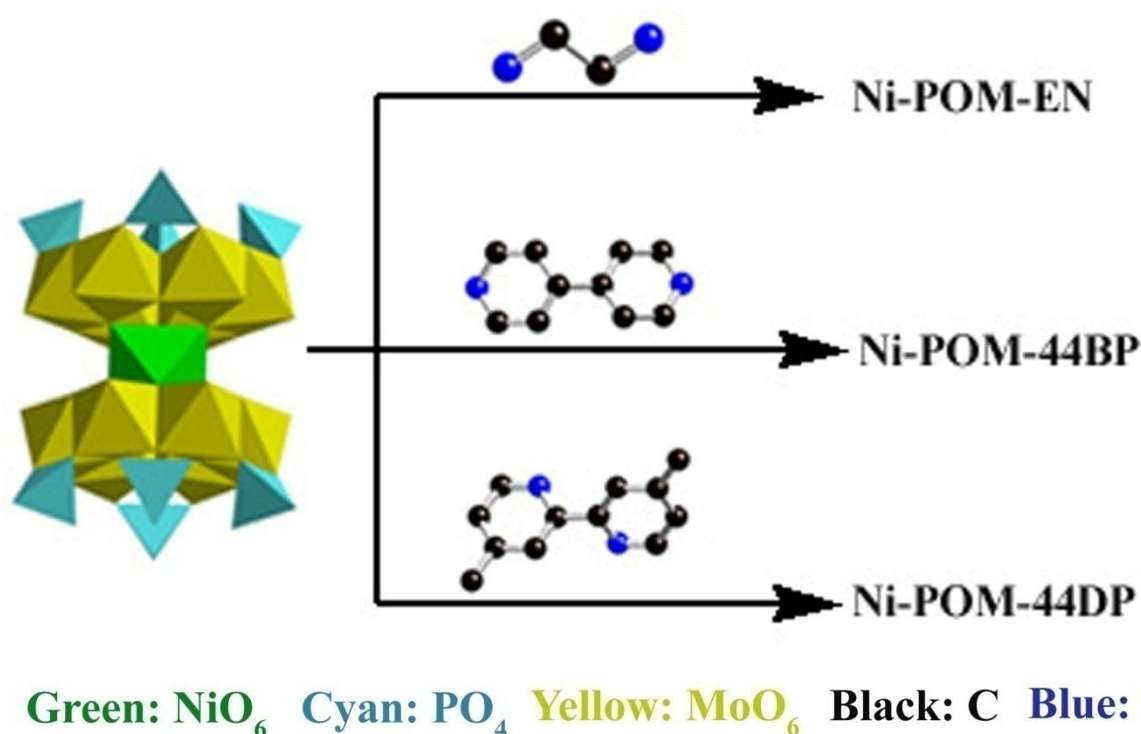
Figure 4.1: Polyhedral model of $[NiMo_{12}O_{30}(PO_4)_8]^{n-}$ POM anion. In the reaction medium ethylene diamine, 4,4′- bipyridine, and 4,4′-dimethyl 2,2′- bipyridine form protonated organic cations to crystallize ionic composites Ni-POM-EN, Ni-POM-44BP, Ni-POM-44DP respectively.

4.2.1 Hydrothermal synthesis of POM based ionic salts

The development of metal oxide chemistry is reliant on the production of new architecture possessing unique structures and properties, although the production of such compounds by routine design remains elusive till date. Different synthetic methods, like hydrothermal synthesis, solvothermal synthesis, ionothermal synthesis, microwave synthesis, etc. have

already been used to synthesize polyoxometalate based material. But hydrothermal synthesis is proven to be most efficient method used so far. The $[NiMo_{12}O_{30}(PO_4)_8]^{n-}$ POM can be consider as dimer of $Mo_6O_{15}(PO_4)_4$ connected via metal or metal ions (where, metal = Ni, Co, Cr, etc). This POM contains eight of phosphate functionality per unit, which could be the potential candidates for catalysis in its intra-crystalline regions. The most of the POMs of this type are classified as reduced molybdenum cluster because few of the molybdenum in the clusters are in (+V) oxidation state whereas rest are in regular (+VI) oxidation state. According to earlier report, to synthesize such compound metallic molybdenum (0) was used with molybdenum (VI) precursor in the reaction medium. The synthesis report of these type of clusters without using molybdenum (0) as precursor is very rare. But for our synthesis we have used only molybdenum (VI) compound as a starting material. Few reports of synthesis of these type clusters are present in the literature, where obtained products are not the reduced molybdenum POM. We have used hydrothermal method to synthesize all the compounds (150 °C for 96 hours). The reaction conditions almost remain same for all the synthesis reported in the work, except the change in the organic moiety for individual ionic composites.

4.2.2 Crystal structure of POM based ionic salts

Crystal structure of Ni-POM-EN: The asymmetric unit of Ni-POM-EN crystal structure (Triclinic, space group: *P*-1) contains half of $[NiMo_{12}O_{30}(PO_4)_8]^{n-}$ POM unit, two and half dication of ethylene diamine and four water molecules [Figure 4.2a]. The charges of the materials are balanced by protonation of water, ethylene diamine and phosphates attached to POM, we could able to locate most the protons crystallographically. In the system two of ethylene diamine molecules are in *anti* form and one is in *gauche* form. The $[NiMo_{12}O_{30}(PO_4)_8]^{n-}$ anion can be described as a dimer of two $Mo_6O_{15}(PO_4)_4$ hexanuclear rings, connected via one Ni(II) octahedra. Each monomeric ring, $Mo_6O_{15}(PO_4)_4$ consists of six edge shared MoO_6 polyhedra unit. Inside the ring the distance between two opposite Mo atom is around 6.081 Å. The periphery of the ring is decorated by three tetrahedral phosphates [average P-O distance ranges from 1.523-1.558 Å] groups at an alternate position in-between two MoO_6 units. One more phosphate group is exposed from the centre of the ring connecting three $[MoO_6]_2$ units in a ring. In the cluster the average Mo-O bond distance lies in-between 1.665-2.084 Å and the average Ni-O bond distance is 2.145 Å. The POMs are arranged in crystallographic *ac*-plane to from a two dimensional layers arrangement. The layers are stacked on top of each other through crystallographic *b*-axis [Figure 4.2b]. In-

between two layers of POMs, the free solvent molecules and ethylene diamine molecules are floating. These layers may act as proton conducting pathway inside the structure [Figure 4.2c]. The ethylene diamine and water molecules are hydrogen bonded to oxygen of POM units. The average hydrogen bonding distances between protonated ethylene diamine molecules and POM units are in the range of 2.638–3.053 Å. Whereas the average hydrogen bonding distance among water molecules and POM units are in the range of 2.288–2.900 Å.
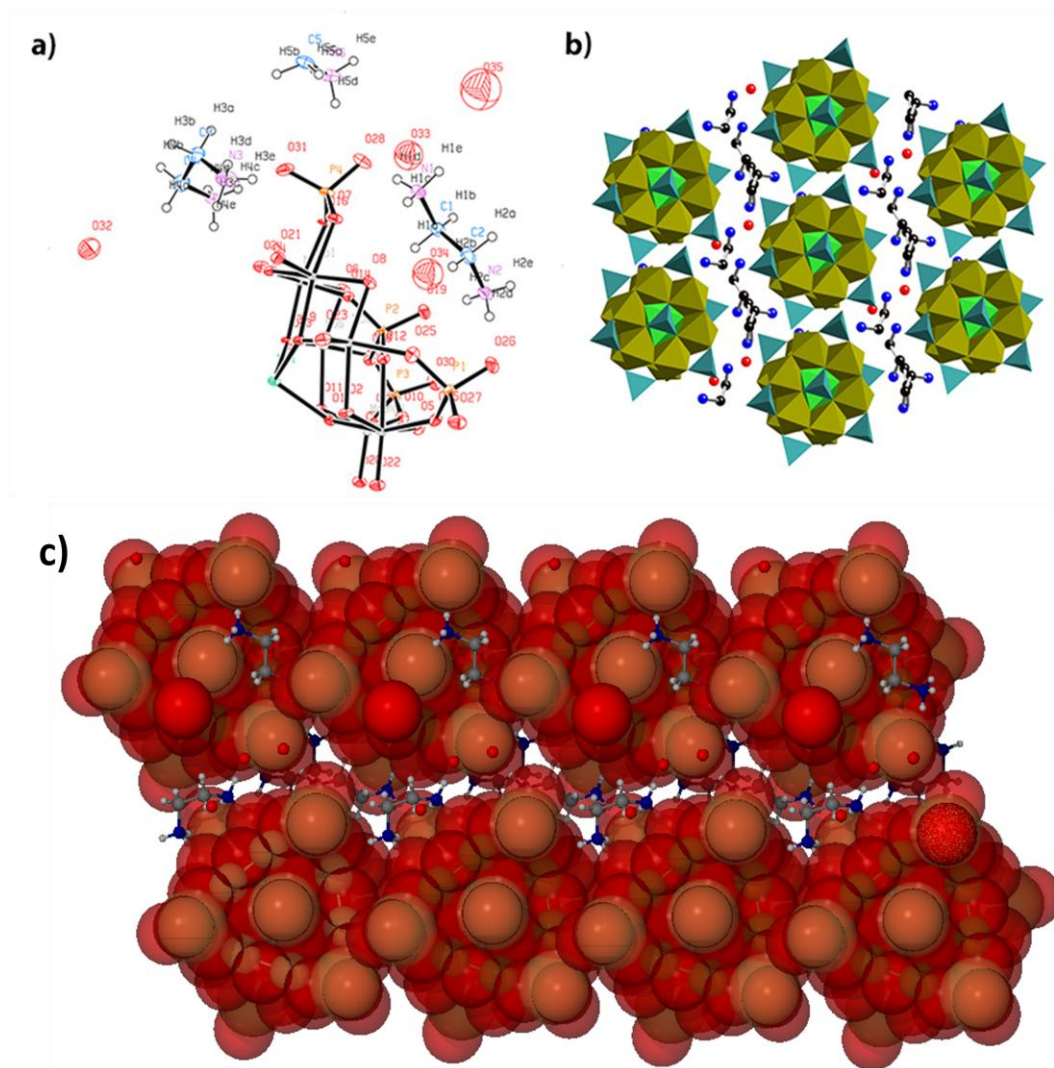
Figure 4.2: (a) Asymmetric unit of Ni-POM-EN contains half of $[NiMo_{12}O_{30}(PO_4)_8]^{n-}$ POM unit, two and half dication of ethylene diamine and four water molecules. (b) The POMs are arranged in crystallographic *ac*-plane to from a two dimensional layers. (c) In-between layers protonated ethylene diamine and water molecules are floating. (POMs have been represented as space-fill model and solvent molecules are represented as ball-stick model, red: O, blue: N, grey: C, white: H).

Crystal structure of Ni-POM-44BP: The Ni-POM-44BP crystallizes in monoclinic crystal system (Space group: $P2_1/c$). The asymmetry unit consists of two half of $[NiMo_{12}O_{30}(PO_4)_8]^{n-}$ POM anion, one 4,4′-bipyridine molecule and eight water molecules [Figure 4.3a]. The water molecules are protonated to balance the charge. The 4,4′-bipyridine molecules and POM anions are alternatively arranged in the crystallographic *ac*-plane to form two dimensional sheets [Figure 4.3b]. These sheets are stack on top of each other to through crystallographic *b*-axis with inter layer distance of ~3.601 Å.   In-between two parallel sheets protonated water molecules are floating. The water molecules are hydrogen bonded with other water molecules and POM cluster (closest hydrogen bonding distance: 2.317 Å), which help to hold the three dimensional arrangement.
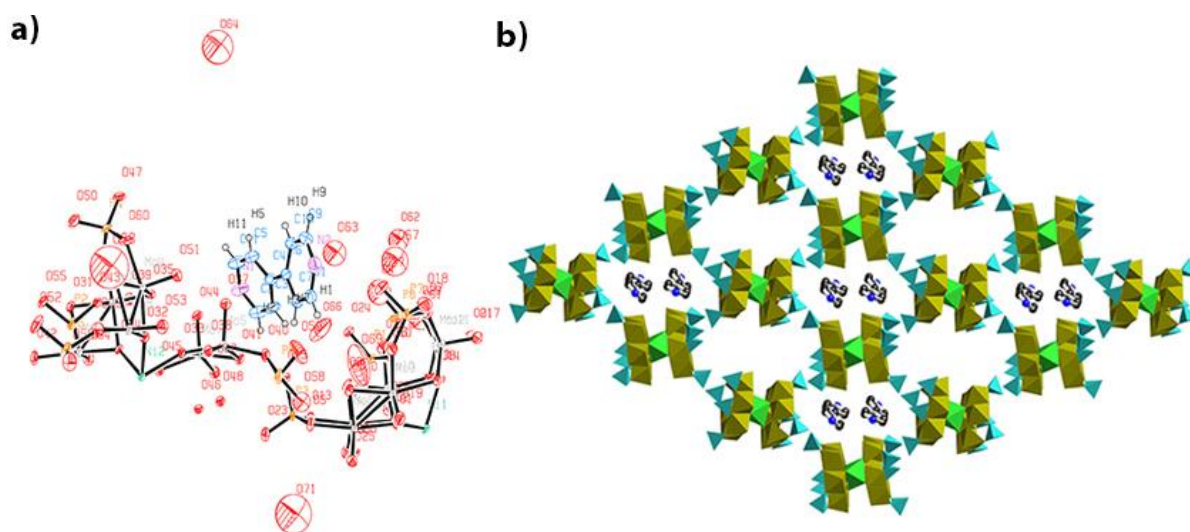
Figure 4.3: (a) ORTEP diagram showing the asymmetric unit of Ni-POM-44BP, consist of two half of $[NiMo_{12}O_{30}(PO_4)_8]^{n-}$ POM anion, one 4,4′-bipyridine molecule and eight water molecules. (b) 4,4′-bipyridine molecules and POM anions are alternatively arranged in the crystallographic *ac*-plane. Protonated water molecules are removed for clarity. green polyhedra: NiO_6, yellow polyhedra: MoO_6, cyan tetrahedra: PO_4, black ball: C, blue ball: N.

Crystal structure of Ni-POM-44DP: The asymmetric unit of Ni-POM-44DP crystal structure (Triclinic, Space group: *P*-1) contains half of $[NiMo_{12}O_{30}(PO_4)_8]^{n-}$ POM unit, one 4,4′-dimethyl-2,2′-pyridyl and seven water molecules [Figure 4.4a]. Each POM unit is surrounded by six 4,4′-dimethyl-2,2′-pyridyl molecules. The 'N' atoms from each 4,4′-dimethyl-2,2′-pyridyl molecule are hydrogen bonded to 'O' atoms of POM ['N–O' distance: 2.609(6) Å and 2.690(7) Å respectively]. This unit repeats in the crystallographic *ac*-plane to form two dimensional sheets.   These sheets are stacked on top of each other through crystallographic *b*-axis with an inter layer distance of ~3.664 Å. In a sheet the distance

between two closest POMs is 13.743 Å along crystallographic *b*-axis, whereas the distance is 12.891 Å along crystallographic *a*-axis [Figure 4.4b].
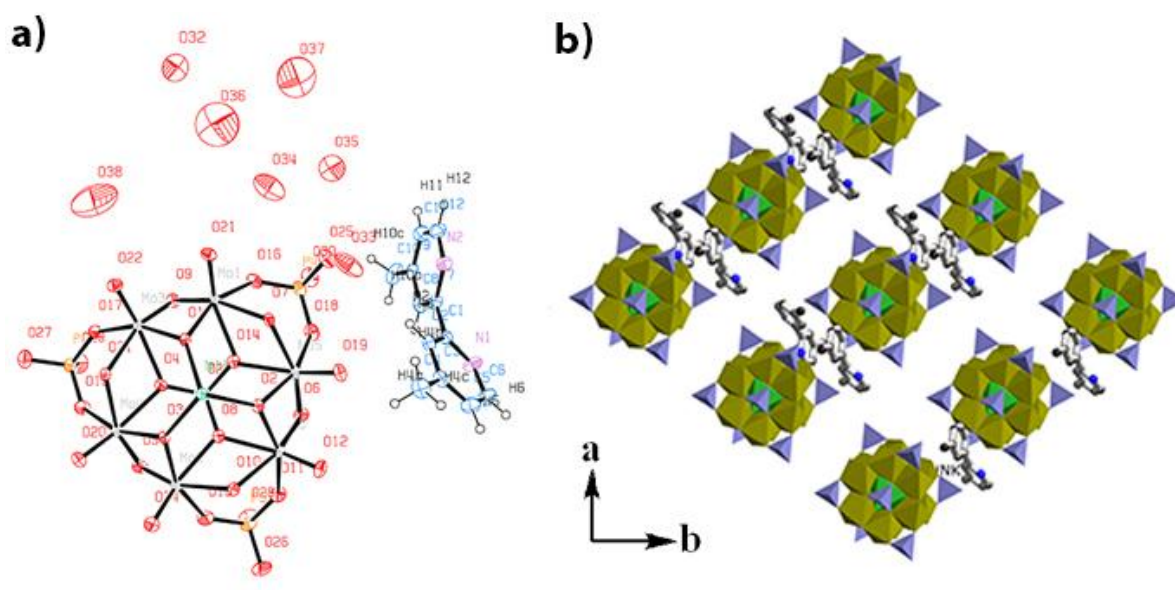
Figure 4.4: (a) Asymmetric unit of Ni-POM-44DP. (b) Packing diagram of Ni-POM-44DP in *ab*-plane. Water molecules have been removed for clarity. green polyhedra: NiO_6, yellow polyhedra: MoO_6, cyan tetrahedra: PO_4, black ball: C, blue ball: N.

4.2.3 Characterization of Ni-POM-EN salt

The Scanning Electron Microscopy (SEM) data were collected for as-synthesized *Ni-POM-EN* which showcased rectangular shaped morphology of the bulk material. The crystals are having ~25 μm length and ~5 μm width in average [Figure 4.5a]. The PXRD pattern of as-synthesized compound matches quite well with the simulated pattern which proves the bulk phase purity of *Ni-POM-EN* [Figure 4.5b]. The thermal stability of *Ni-POM-EN* was examined from thermo gravimetric analysis (TGA) data, collected in the temperature range of 30–900 °C. The compound is stable upto 350 °C, beyond this temperature it starts decomposing. The ~3 % weight lose around 100 °C is due to removal of non-coordinated water molecules from the structure [Figure 4.5c]. The *Ni-POM-EN* demonstrates characteristic IR frequencies for $[NiMo_{12}O_{30}(PO_4)_8]^{n-}$ POM units at $1117(\nu_{asym}P\text{-}O_a)$, $998(\nu_{asym}P\text{-}O_b)$, $897(\nu_{asym}Mo\text{=}O)$, $819 (\nu_{asym}Mo\text{-}O_a)$, $725(\nu_{asym}Mo\text{-}O_b)$ and $668(\nu_{asym}Mo\text{-}O_c)$ cm^{-1} [Figure 4.5d]. We also have collected PRXD of *Ni-POM-EN* after proton conductivity measurement. The PXRD pattern of the sample obtained after proton conductivity measurement shows a different crystalline phase, whereas heating (at 60 °C) causes the

regeneration of parent phase. Heating of the sample at 180 $^\circ$C (*Ni-POM-EN-180*) generates a completely new phase. The IR spectroscopic analysis of sample, *Ni-POM-EN-180* shows shift from 897 to 945 cm^{-1} and 989 to 1005 cm^{-1}. The shift could be due to the removal of hydrogen bonded water molecules from the structure. We could not able to make *Ni-POM-44BP* and *Ni-POM-44DP* in bulk as a pure form due to simultaneous formation of different phases. But analysis of *Ni-POM-44BP* and *Ni-POM-44DP* crystal structures suggest that both the compounds in their pure phase could be used as proton conducting materials.
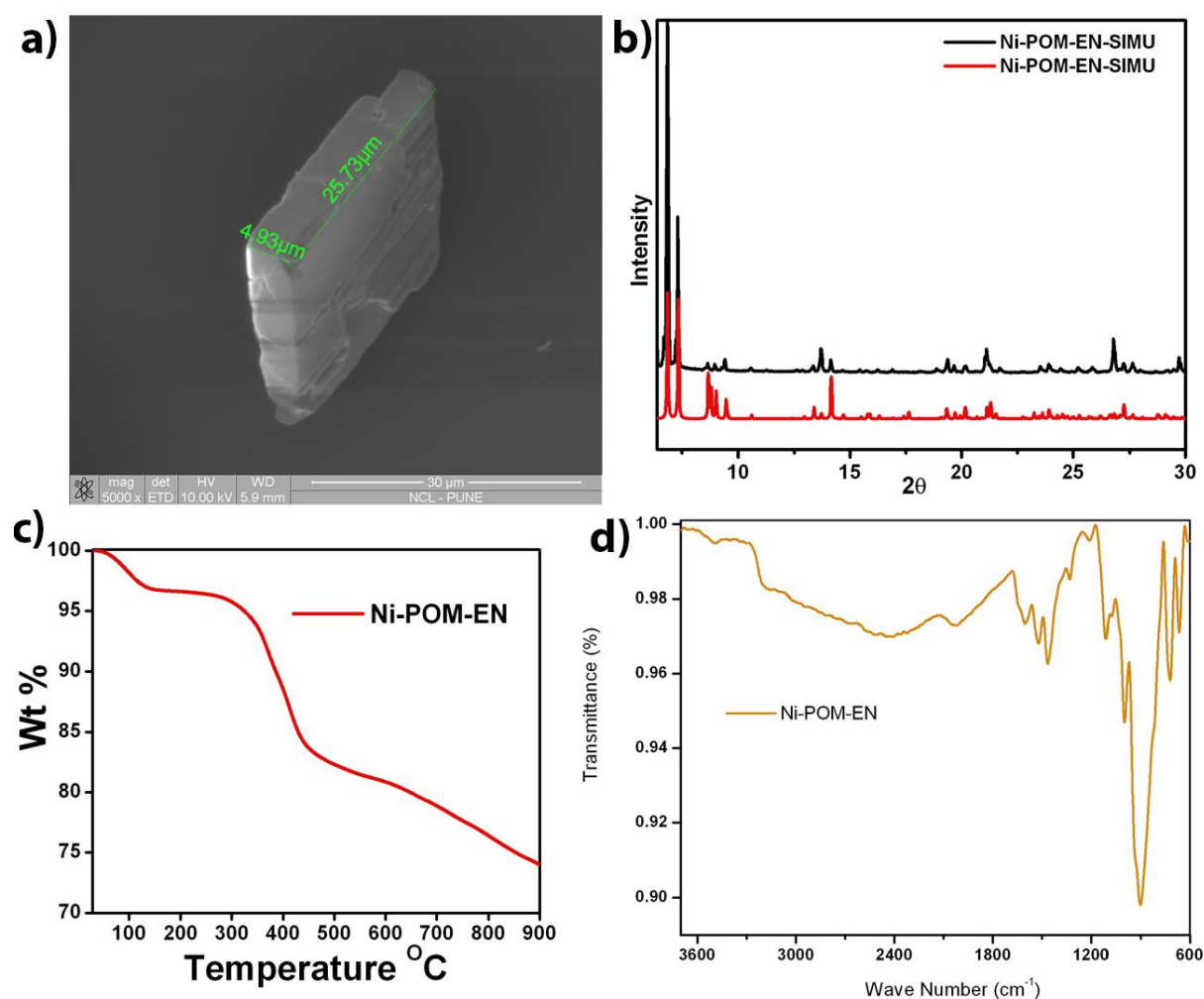
Figure 4.5: (a) SEM image of Ni-POM-EN crystal, zoomed view shows the crystalline edge and plane. (b) Simulated and experimental PXRD patter of Ni-POM-EN, showing the phase purity of the bulk product when compared with simulated one. (c) Inset image shows the thermo gravimetric analysis plot for Ni-POM-EN. (d) IR spectroscopic analysis for as synthesized Ni-POM-EN.

4.2.4 Proton conductivity measurement of Ni-POM-EN

Polyoxometalate based composite materials have drawn current research attention on proton conductivity for fuel cell application due to their high thermal stability. $CsHSO_4$ and $H_3PW_{12}O_{40} \cdot 6H_2O$ composite prepared by mechanical milling have shown proton conductivity 3.3×10^{-3} Scm^{-1} at 100 °C [4.11]. Proton conducting gel, prepared by encapsulating heteropolyacids within Poly(methyl methacrylate) matrix showed proton conductivity wide in range of temperature, -60 °C to 90 °C (5×10^{-4} Scm^{-1} and 8×10^{-4} Scm^{-1} respectively) [4.12]. POM embedded glass composite membrane prepared by sol-gel method exhibit proton conductivity to 1.01×10^{-1} Scm^{-1} under 85% relative humidity (RH) at 85 °C
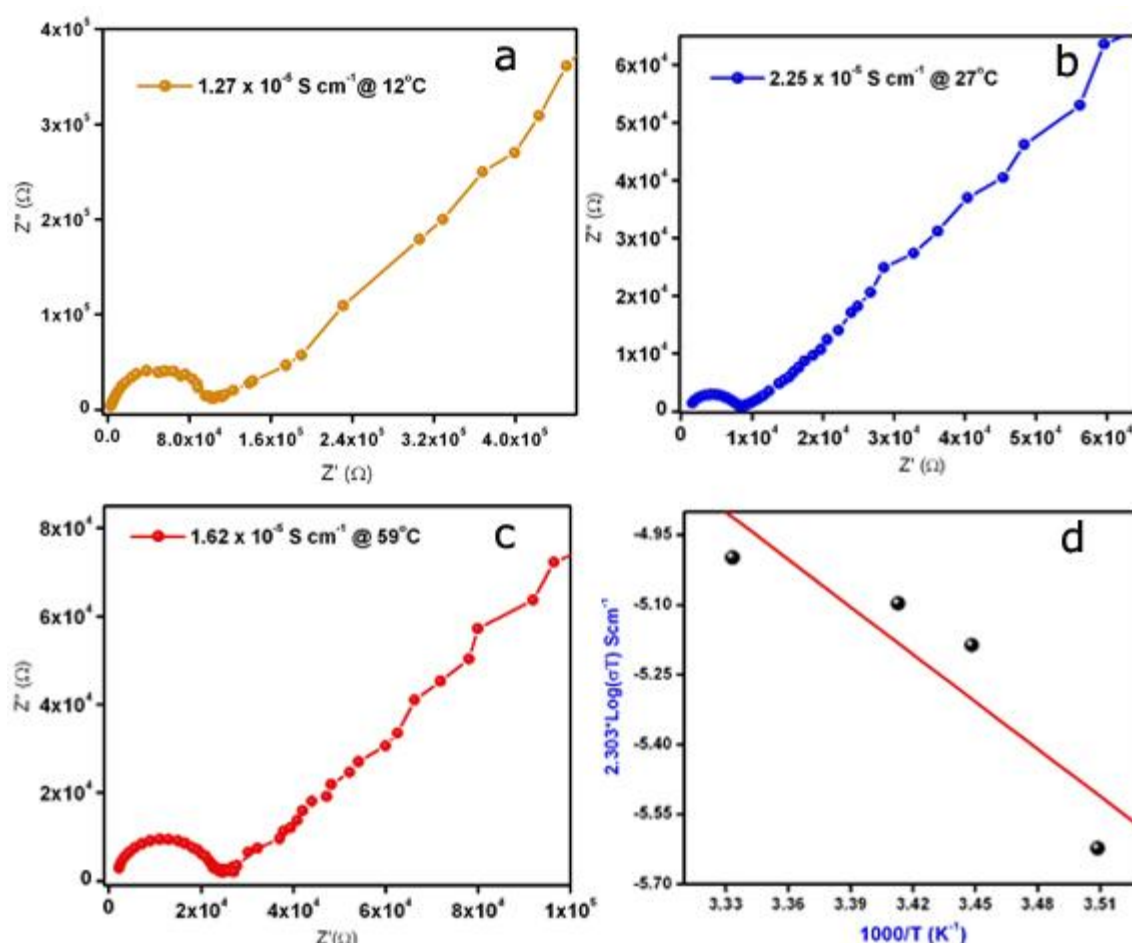
Figure 4.6: (a) Nyquist plot for Ni-POM-EN at 12 °C with 98 % relative humidity (RH) showing characteristic proton conducting behaviour. (b) Nyquist plot for Ni-POM-EN at 27 °C with 98 % RH. (c) Nyquist plot for Ni-POM-EN at 59 °C with 98 % RH. (d) Arrhenius plot of proton conductivity for Ni-POM-EN with respect to temperature.

[4.13]. In this work for the first time we have studied proton conductivity on POM based ionic composite. We have measured impedance spectra for *Ni-POM-EN* at room temperature, low temperature and high temperature. The conductivity was calculated from impendence data using $\sigma = L/(S \times R)$ equation, where R is the resistance, L is the thickness, and S is the area of the sample plate. The conductivity value recorded at room temperature (27 °C) and 98% relative humidity (RH) is 2.25×10^{-5} Scm^{-1} [Figure 4.6b], which is highest for *Ni-POM-EN* in the temperature range of 12 °C to 59 °C. We have observed relatively low proton conductivity value at high temperature as well as low temperature compare to room temperature value. The proton conductivity value recorded at 12, 17, 20, 39 and 59 °C (with 98 % RH) are found to be 1.27×10^{-5}, 1.93×10^{-5}, 2.09×10^{-5}, 1.69×10^{-5} Scm^{-1} respectively. The activation energy for the process was calculated using Arrhenius equation [Figure 4.6d]. The value (0.29 eV) suggests the involvement of Grotthuss mechanistic pathway during proton conduction.

4.3 Synthesis of proton conducting coordination polymer

Metal organic framework (MOFs) or coordination polymers (CPs) have gained intensive attention due to their structural integrity in three dimensions [4.14]. Very recently researchers took interest in MOFs for proton conductivity as these porous materials can have one dimensional porous channels which hold inbuilt or loaded guest molecules (mostly water) as proton conducting materials [4.15]. But major limits of MOFs for proton conduction are their poor thermal and water stability. POMs, being thermally more stable and anionic in nature, can be a component to prepare coordination polymers which will overcome the limitation of MOFs for proton conduction. Keeping this idea in mind, we have tried to prepare CPs using different types of POMs. This type of POM based coordination polymers are advantageous for proton conduction not only due to the presence of water channel inside the structures but also for the presence of coordinate water and oxide (O^{2-}) inside the frameworks. These coordinated moieties are thermally and chemically very stable inside the frameworks which result in a proton conducting pathway within the materials. During designing such materials we have chosen Strandberg POMs which have peripheral oxide (O^{2-}) and phosphate (PO_4^{3-}) as coordinating sites to link with heterometals. After designing the CP, it was tested for proton conductivity and guest dependent reversible phase transformability.

4.3.1 Strandberg type POM based coordination polymer for proton conduction

Herein, we have synthesized Strandberg-type POM and Cu(II) based Metal organic framework (MOF) [4.16], namely *[Mo$_5$P$_2$O$_{23}$][Cu(phen)(H$_2$O)]$_3$.4H$_2$O* (Cu$_3$Mo$_5$P$_2$) which contains one dimensional H-bonded parallel water channels inside the structure. Cu$_3$Mo$_5$P$_2$ shows rare reversible phase transformation [4.17] (with distinct color change) upon removal of water molecules from the framework. However, the most important feature of Cu$_3$Mo$_5$P$_2$ we report herein is its proton conducting nature due to the presence of these water channels inside the structure. To the best of our knowledge this is the first report of proton conductivity on POM based coordination polymer. Blue needle like crystals of Cu$_3$Mo$_5$P**$_2$** was synthesized in hydrothermal condition using the mixture phosphomolybdic acid hydrate (0.2 g), CuCl$_2$.2H$_2$O (0.032 g), conc. H$_3$PO$_4$ (0.5 mL), 1, 10-phenanthroline (0.023 g) and 18 mL water (pH=2.83) at 170 °C for 96 hours.

4.3.2 Crystal structure of coordination polymer (Cu$_3$Mo$_5$P$_2$)

Cu$_3$Mo$_5$P$_2$ crystallizes in monoclinic crystal system (Space group *P*2$_1$/*c*). The asymmetric unit of Cu$_3$Mo$_5$P$_2$ contains one [Mo$_5$P$_2$O$_{23}$]$^{6-}$ cluster [Figure 4.7a], three Cu(II) atoms, three phenanthroline, three coordinated and five non-coordinated water molecules [Figure 4.7b]. The [Mo$_5$P$_2$O$_{23}$]$^{6-}$ cluster is covalently connected to six copper units (three from each side). The geometry of the [Mo$_5$P$_2$O$_{23}$]$^{6-}$ cluster can be described as a ring of five distorted MoO$_6$ octahedra with two PO$_4$ tetrahedral units capped from each side. Each phosphate subunit shares three oxygen atoms with the molybdate ring. Two among the three Cu(II) atoms adopt square pyramidal arrangement and third one is distorted octahedral in nature. Each Cu(II) atom is connected to two nitrogen atoms of one phenanthroline moiety. One [Mo$_5$P$_2$O$_{23}$]$^{6-}$ POM unit is connected to next POM unit via one octahedral and one square pyramidal copper units to form a one dimensional chain through crystallographic *a*-axis. These one dimensional chains are interdigitated to each other via phenanthroline rings to form the three dimensional network. The closest distance between two interdigitated phenanthroline rings is 3.79 Å [Figure 4.7c]. The five non-coordinated water molecules in the asymmetric unit are interconnected to each other as well as with Cu(II)-coordinated hydroxyl and oxygen atoms of POM *via* H-bonding. The average H···A and D···A distance inside the channel lies in the range of 1.90–2.59 Å and 2.741(12)–3.43(5) Å respectively [Figure 4.7d]. While refining the crystal structure, we found that oxygen atoms coordinated to Cu(II) could be refined well as hydroxyl (OH$^-$) anion rather than water. As a result balancing of the change of overall

framework requires protonation of water molecules per hydroxyl anion. However, we are unable to locate the protons crystallographically.

4.3.3 Thermo gravimetric analysis

Thermo gravimetric analysis (TGA) was performed on as-synthesized $Cu_3Mo_5P_2$ to study the thermal stability. The initial weight loss in the temperature range of 20-100 °C is due to the
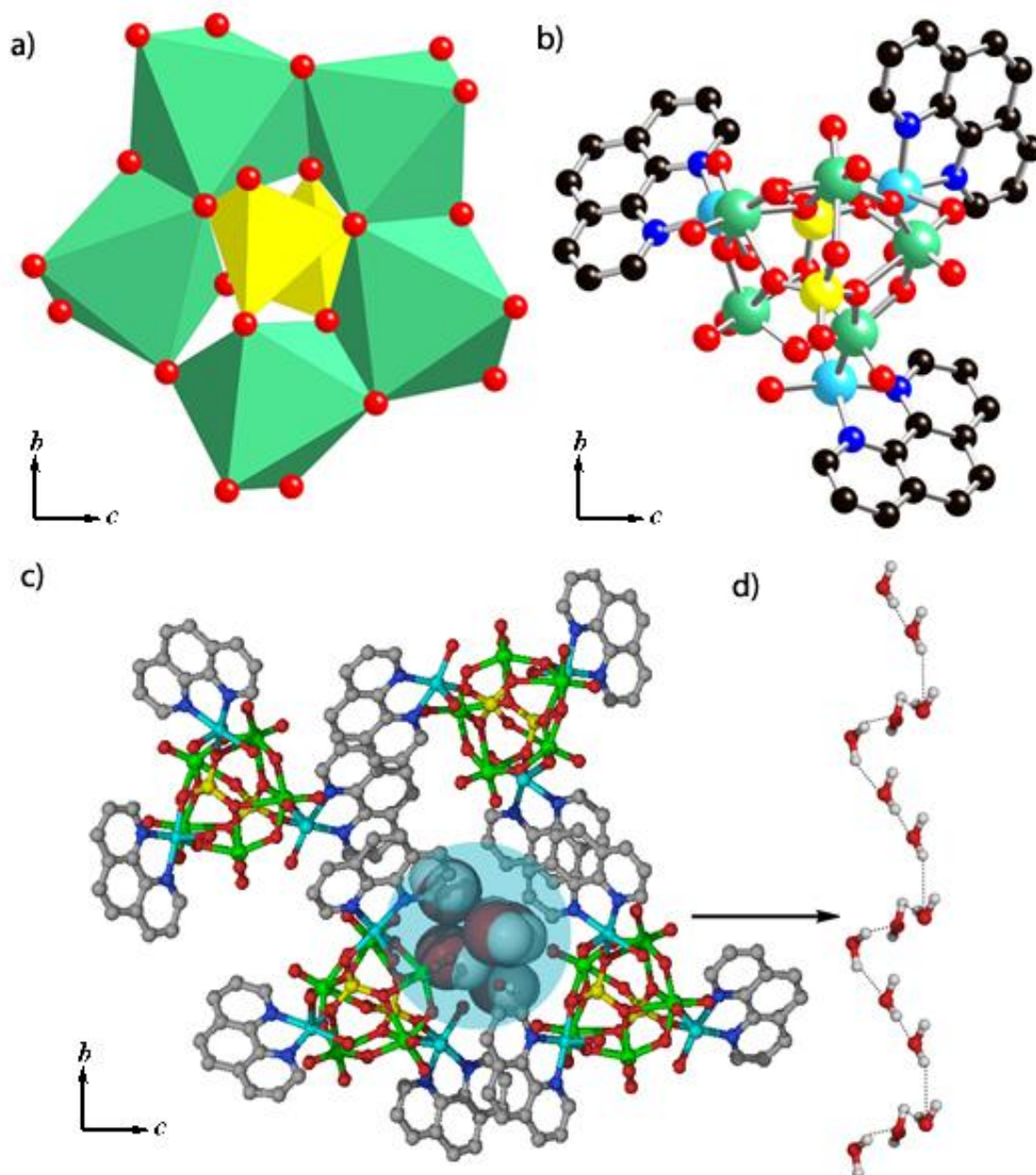
Figure 4.7: (a) Polyhedral representation of Strandberg type polyoxometalate discussed in this chapter. (b) One polyoxometalate unit is connected to three Cu(II)-phen complex. (c) Interdigitation of phenanthroline rings of four $Cu_3Mo_5P_2$ one dimensional chain surrounds one 1D channel of waters. (d) One H-bonded 1D channel of water has been highlighted. [Color Code: green:Mo, yellow:P, red:O, blue:Cu, deep blue:N, black/grey:C white:H]

removal of adsorbed moisture. $Cu_3Mo_5P_2$ loses all lattice water molecules (~ 4% weight loss) around 160 °C. The solvent free framework is stable upto 600 °C and after 650 °C it starts decomposing [Figure 4.8a]. The compound have shown characteristic IR stretching frequency at 3463(br), 3051(w), 1623(s), 1513(m), 1422(w), 1150(m), 1098(w), 1037(m), 910(s), 871(s), 845(m), 721(s), 664s) and 563(w) cm^{-1} [Figure 4.8b]. In order to confirm the phase purity of the bulk materials, PXRD experiments were carried out on the bulk sample of $Cu_3Mo_5P_2$. The PXRD of experimental and computer-simulated patterns are shown in Figure 4.10. All major peaks of experimental powder X-ray pattern (PXRD) matches quite well that of simulated PXRDs, indicating their reasonable crystalline phase purity.
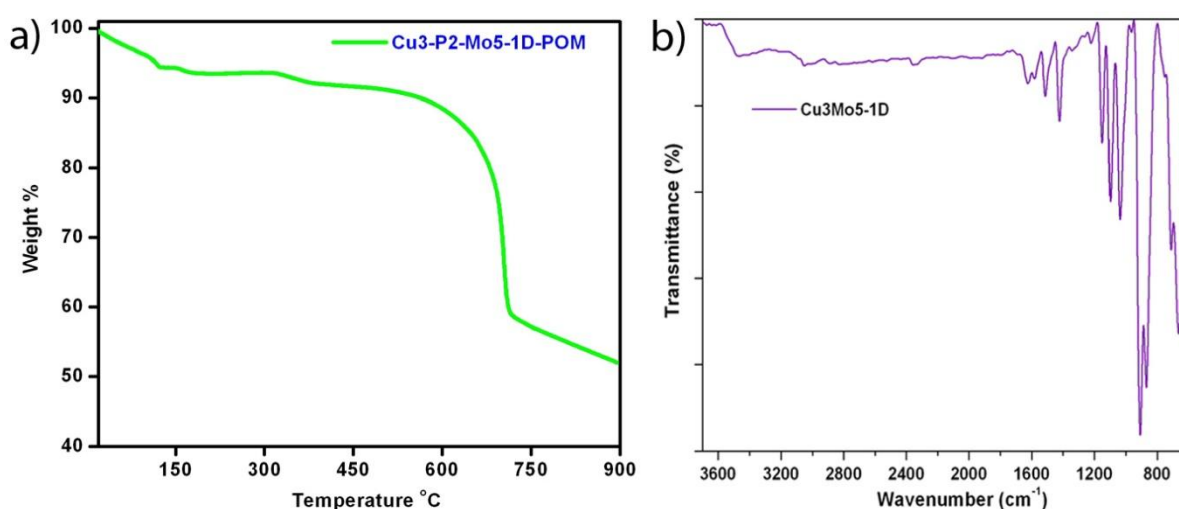
Figure 4.8: (a) Thermo gravimetric analysis for coordination polymer ($Cu_3Mo_5P_2$). (b) IR Spectroscopy of as-synthesized $Cu_3Mo_5P_2$. Characteristic *FTIR* bands at 3463 (br), 1623(br), 1513, and 1422 cm^{-1} confirmed the presence of 1,10-phenanthroline and water, and bands at 947, 910, 871, 712, 664, and 563 cm^{-1} are characteristic of phosphomolybdate anion.

4.3.4 Guest dependent reversible phase transformation

From TGA data it is evident that the guest water molecules could be removed from the crystal structure at ~150 °C [Figure 4.8a]. To study the structural change due to evacuation of guest molecules (water) we have collected the *in situ* Variable Temperature Powder X-ray Diffraction (VTPXRD) data. The change in VTPXRD data beyond 150 °C indicates a crystalline phase change in the solid state [Figure 4.10a]. As TGA plot shows that the compound loses all its solvent molecules near 150 °C, this could be the possible reason for crystalline phase transformation with distinct color change beyond 150 °C. The SEM images of as-synthesized $Cu_3Mo_5P_2$ depict the edges of micro-crystal [Figure 4.9a and Figure 4.9b]

whereas, in the SEM image of thermally treated compound the crystalline edges disappear [Figure 4.9c and Figure 4.9d]. When the evacuated $Cu_3Mo_5P_2$ was retreated with water, the
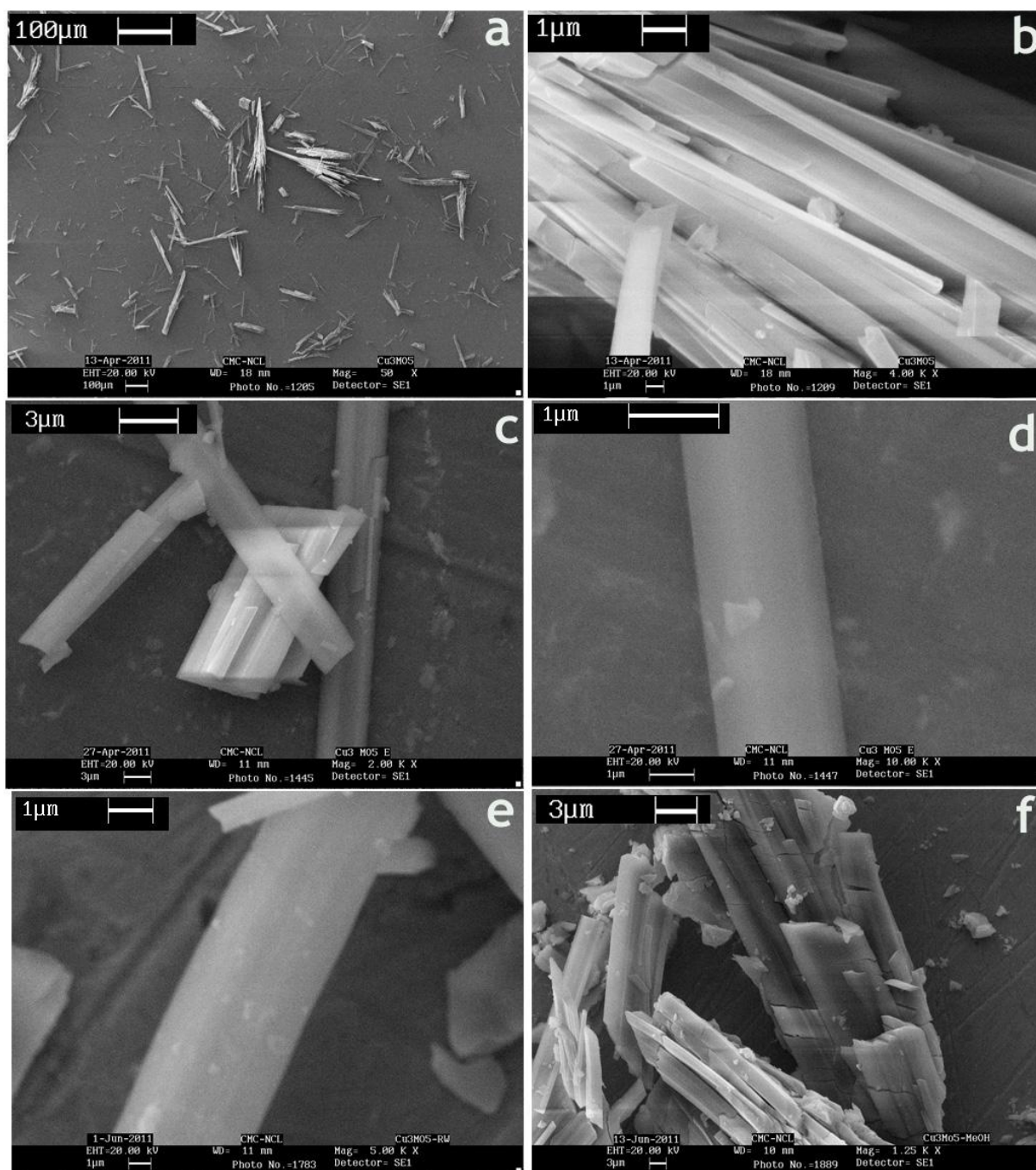
Figure 4.9: (a) SEM image of as-synthesied $Cu_3Mo_5P_2$ showing bulk morphology. (b) SEM image of as-synthesied $Cu_3Mo_5P_2$ showing crystalline edge. (c) SEM image of evacuated $Cu_3Mo_5P_2$. (d) SEM image of evacuated $Cu_3Mo_5P_2$ where the crystalline edges are not prominent. (e) SEM image of resolvated $Cu_3Mo_5P_2$. (f) SEM image of $Cu_3Mo_5P_2$ after methanol treatment.
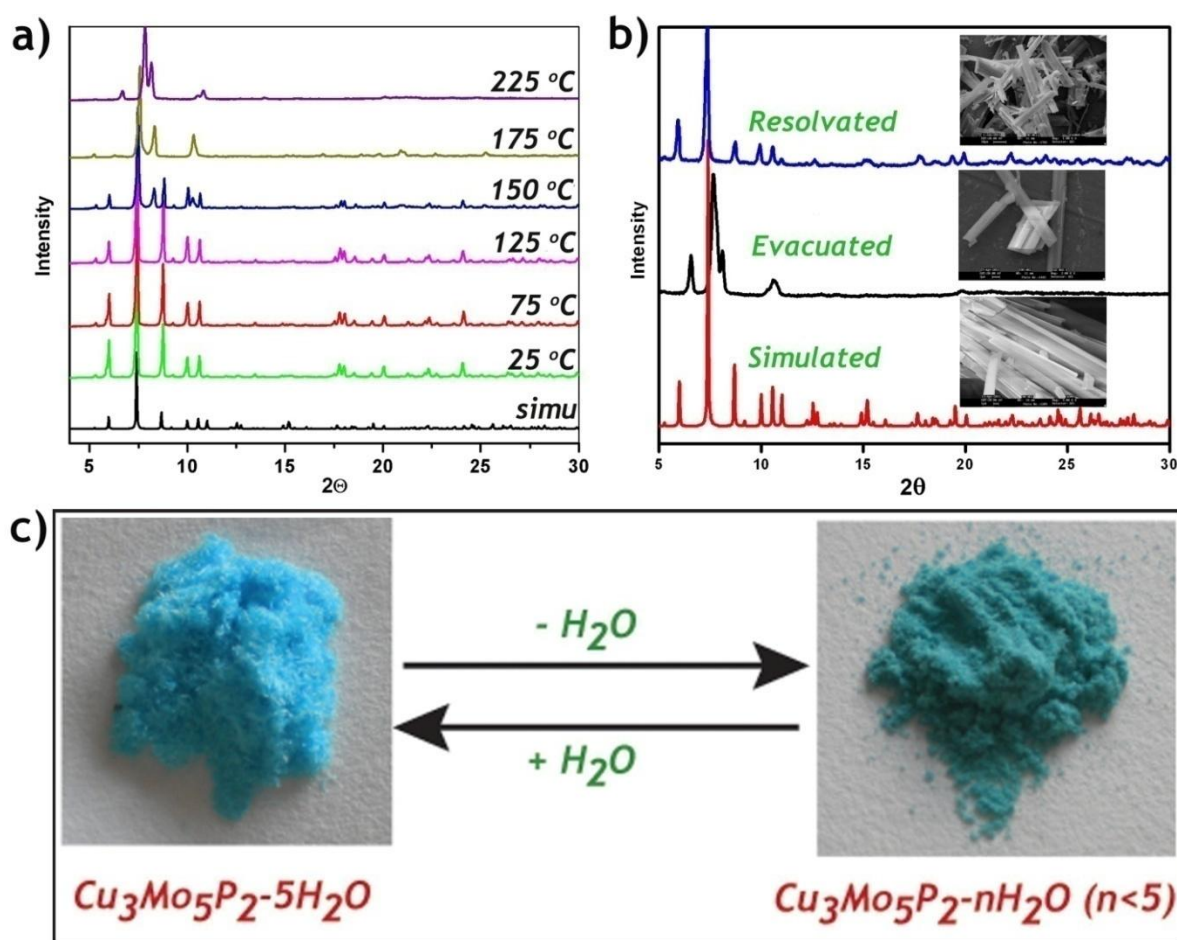
Figure 4.10: (a) Variable Temperature Powder X-ray Diffraction for $Cu_3Mo_5P_2$. (b) PXRD pattern of simulated, evacuated and resolvated $Cu_3Mo_5P_2$ with their SEM images showing morphological changes. (c) Solvent dependent reversible phase change with distinct change in color.

compound regains its original phase as well as the color, which was also confirmed by PXRD [Figure 4.10b and Figure 4.10c]. This type of structural change upon removal of lattice water molecule is rare in POM based hybrid materials. As the large position of $Cu_3Mo_5P_2$ framework is hydrogen bonded one would anticipate a structural reorientation upon removal of lattice water molecule.

4.3.5 Solvent exchange experiment

When $Cu_3Mo_5P_2$ (~50 mg) was treated separately with different dry organic solvents (~ 2 mL of ethanol, methanol, dimethylformamide, acetonitrile, dichloromethane, chloroform and acetone) to study the structural change due to solvent exchange. It is surprising that $Cu_3Mo_5P_2$ showed distinct color change in presence of methanol, while for the other solvents

the color remains unchanged [Figure 4.11]. However, the PXRD data of all the aforementioned solvents (including methanol) treated sample showed the identical phase of as-synthesized $Cu_3Mo_5P_2$.. We were unable to draw any conclusion for color change from the *FTIR* data of the solvent treated $Cu_3Mo_5P_2$. The same experiment was carried out with methanol vapor; but it took longer time (~48 hour) as compare to direct methanol treatment (< 1 min) to show the color change.
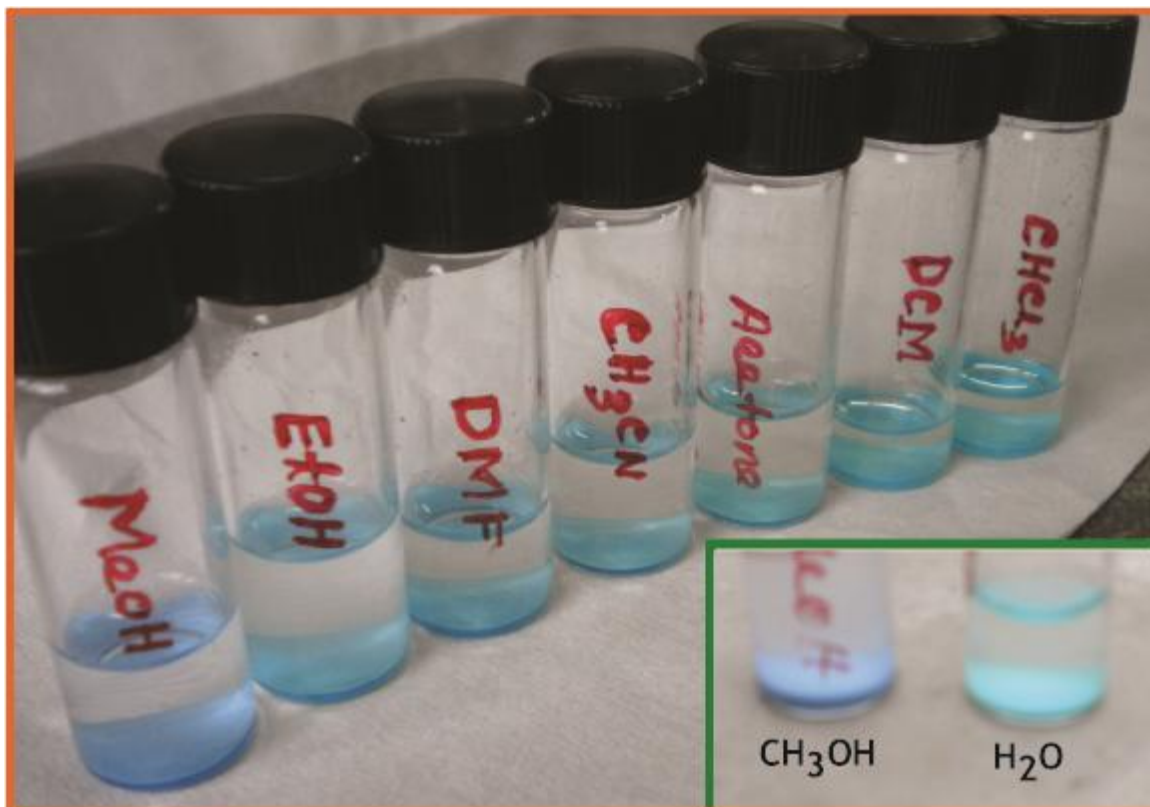
Figure 4.11: When the $Cu_3Mo_5P_2$ was treated with different organic solvent like acetone, dimethyl formamide, chloroform, dichloromethane, acetonitrile, ethanol, methanol etc, it shows distinct color change with methanol. Inset picture shows the significant difference in color of $Cu_3Mo_5P_2$ in methanol and H_2O.

4.3.6 H_2O vapor, H_2 and CO_2 gas adsorption study

The water vapor adsorption was carried out on the evacuated $Cu_3Mo_5P_2$. The evacuated $Cu_3Mo_5P_2$ [at 150 ^oC for 48 hour] shows the strong affinity towards water vapor due to absence of free lattice water which was present in the original structure. $Cu_3Mo_5P_2$ takes 120 mL/g of water vapor at STP [Figure 4.12a]. The de-solvation and re-solvation of $Cu_3Mo_5P_2$ involves reversible phase change, which was confirmed by PXRD as well as distinct color change [Figure 4.10b and Figure 4.10c]. The H_2 and CO_2 adsorption studies were performed

on evacuated $Cu_3Mo_5P_2$. At 760 Torr and 77 K, $Cu_3Mo_5P_2$ adsorbs 1.4 wt% H_2. The framework of $Cu_3Mo_5P_2$ exhibits a typical Type-I profile for CO_2 (kinetic diameter: 3.4 Å) adsorption. $Cu_3Mo_5P_2$ adsorbs 0.95 mmol/g of CO_2 at 298 K temperature and 1 bar pressure. Hysteretic sorption with CO_2 molecules suggests strong interaction with the pore surfaces.

4.3.7 Proton conductivity in POM based coordination polymer

Proton conducting materials are important due to its application in electrochemical device fabrication, fuel cells and most importantly to understand the complex biological ion channels [4.18]. Researchers have tried to design hybrid materials [4.19] like metal phosphate, oxalate, metal oxides, and recently MOFs as a replacement of the polymer based electrolyte membranes. However, only a handful of MOFs are reported in literature with proton conducting behavior, as most of them have been synthesized in high boiling solvent instead of H_2O [4.20]. Also, most of the MOFs are moisture sensitive, including some well known MOF like MOF-5 and MOF-177. Researchers tried to design proton conducting MOFs where, either lattice backbone [4.21a], addition of guest molecules like imidazole [3.21a], and 1,2,4-triazole [4.21e] in anhydrous medium, or already present water chains [3.21d] inside the framework promotes proton conduction. Kitagawa *et al.* and others have extensively studied the proton conductivity in various MOFs and complexes where coordinated water or guest molecules play a vital role in proton conduction [4.22].

In the crystal structure of $Cu_3Mo_5P_2$, we observed continuous water channel immobilized by hydrogen bonding with the oxygen molecule of polyoxomolybdate cluster and coordinated water molecules linked with Cu(II). These acidic water molecules assembled through hydrogen bonding with each other, which made this material an attractive candidate for proton conduction. In order to measure the proton conductivity, pellets with the thickness of 0.4 mm were prepared from as-synthesized sample and subjected to humidification overnight for partial removal of grain boundary. The proton conductivity of $Cu_3Mo_5P_2$ was measured as 2.2×10^{-5} Scm^{-1} at 301K with 98% humidity [Figure 4.12b], which is comparable with zinc phosphonate MOF (1.3×10^{-5} Scm^{-1}) reported by Shimizu *et al.* [4.19b], but lower than ferrous oxalate dihydrate [4.22b] and cucurbit[6]uril [4.23]. The variable temperature proton conductivity revealed the activation energy value of 0.232 eV [4.24], which is quite low compared to most well known proton conducting MOFs, and comparable to that of nafion (0.22 eV). To account for the role of humidity in proton conduction, humidity dependant proton conductivity measurement has been carried out, which clearly shows decrease in

proton conductivity value of 1.2×10^{-5} and 1.0×10^{-5} Scm^{-1} at 75% and 60% relative humidity, respectively. We also measured the high temperature proton conductivity of Cu$_3$Mo$_5$P$_2$, which shows loss of proton conducting behavior beyond 42 °C. The probable reason of this could be the rupture of H-bonded water channel inside the framework. However, on cooling this material regain its normal proton conducting property, indicating the role of water dynamics to control the proton conduction pathways.
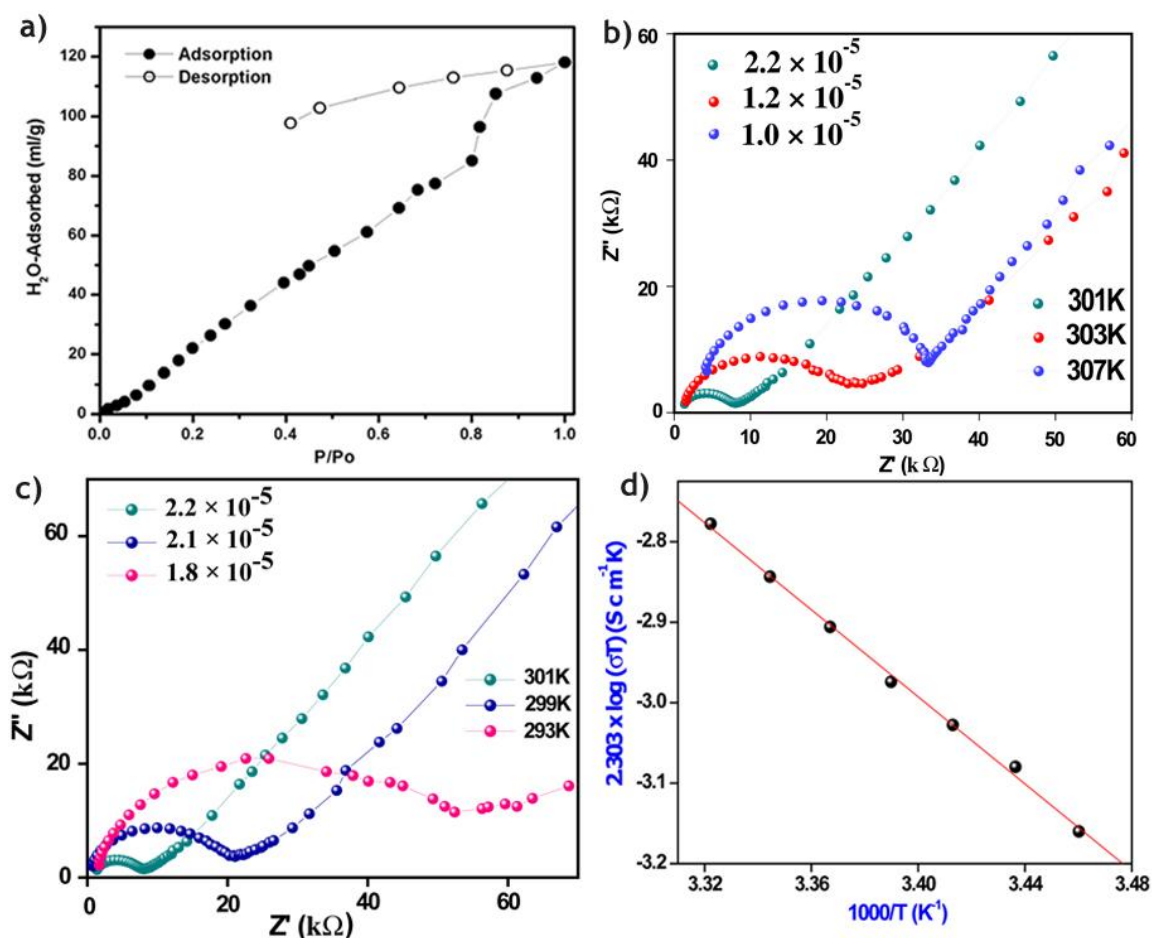
Figure 4.12: (a) Water vapor adsorption desorption isotherm for Cu$_3$Mo$_5$P$_2$ at STP (Standard Temperature and Pressure). (b) Nyquist plot for Cu$_3$Mo$_5$P$_2$ at elevated temperature range showing decrease in proton conductivity. (c) Nyquist plot for Cu$_3$Mo$_5$P$_2$ at lower temperature range showing decrease in proton conductivity. (d) Arrhenius plot of proton conductivity of Cu$_3$Mo$_5$P$_2$ with 98% RH condition. Least square fitting is shown as a straight line.

4.4 Conclusion

We have synthesized a series of organic cation and polyoxometalate based hybrid ionic salts. The Ni-POM-EN salt of this series has been studied for proton conductivity at humidified condition. The one-pot synthetic method used for the synthesis of salts could further be used

to design new polyoxometalate based ionic architecture for sorption, conductivity, magnetism, etc. The presence of phosphate functionality of this particular polyoxometalate could facile catalytic activity in the intra-crystalline region. We have also synthesized a Strandberg-type POM and Cu(II) based coordination polymer, $Cu_3Mo_5P_2$. This material adopts a three dimensional H-bonded architecture with parallel water chain propagating along crystallographic *c*-axis. $Cu_3Mo_5P_2$ shows reversible structural transformation upon removal of these lattice water molecules. $Cu_3Mo_5P_2$ shows proton conductivity at solid state due to this parallel water chain in the network. Although a lot of research on POM based hybrid materials are reported, this is the first report of proton conductivity in POM-based coordination polymers. We believe that successful proton conductivity of this POM based hybrid material will provide a roadmap and motivate researchers to engage in detailed investigation in this area.

4.5 Experimental Section

All reagents and solvents for synthesis and analysis were commercially available and used as received. The Fourier transform (FT) IR spectra (KBr pellet) were taken on a *PERKIN ELMER FT-IR SPECTRUM* (Nicolet) spectrometer. Powder X-ray diffraction (PXRD) patterns were recorded on a Phillips PNAlytical diffractometer for Cu Kα radiation ($\lambda =$ 1.5406 Å), with a scan speed of 2° min^{-1} and a step size of 0.02° in 2θ. Thermo-gravimetric experiments (TGA) were carried out in the temperature range of 25–900 °C on a SDT Q600 TG-DTA analyzer under N_2 atmosphere at a heating rate of 10 °C min^{-1}. Proton conductivity data were measured by a quasi-two-probe method, with a Solartron 1287 electrochemical interface and a frequency response analyzer.

Synthesis of Ni-POM-EN: The brown crystals of Ni-POM-EN was obtained by heating the mixture of 20% wt solution of phosphomolybdic acid in ethanol (1mL), ethylene diamine (0.6 mL), 85% H_3PO_4 (0.5 mL), $NiCl_2·6H_2O$ (0.21mmol) and H_2O (8mL) at 150 °C for 96 hours in hydrothermal condition. *FT-IR:* (KBr 4000-450 cm^{-1}): 2354(w), 2320(w), 2014(b), 1606(w), 1519(w), 1469(w), 1107(w), 999(m), 894(s), 818(s), 780(m), 716(s), 667(s), 606(s).

Synthesis of Ni-POM-44BP: The yellow block shaped crystals of Ni-POM-44BP were synthesized by heating the mixture of 20% wt solution of phosphomolybdic acid in ethanol (1mL), 4,4′-bipyridyl (0.16 mmol), 85% H_3PO_4 (0.5 mL), $NiCl_2·6H_2O$ (0.21mmol) and H_2O (8 mL) at 150 °C for 96 hours in hydrothermal condition.

Synthesis of Ni-POM-44DP: The red block shaped crystals of Ni-POM-44BP were synthesized by heating the mixture of 20% wt solution of phosphomolybdic acid in ethanol (1mL), 4,4′-dimethyl-2,2′-pyridyl (0.14 mmol), 85% H_3PO_4 (0.5 mL), $NiCl_2·6H_2O$ (0.21mmol) and H_2O (8 mL) at 150 °C for 96 hours in hydrothermal condition.

Synthesis of $[Mo_5P_2O_{23}][Cu(phen)(H_2O)]_3·5H_2O$ ($Cu_3Mo_5P_2$): A mixture phosphomolybdic acid hydrate (0.2 g), $CuCl_2.2H_2O$ (0.032g), conc. H_3PO_4 (0.5 mL), 1, 10-Phenanthroline (0.023g) and 18 mL water was stirred for 30 minutes. The pH of the reaction medium was maintained to 2.83 by using 2M NaOH solution. Then the reaction mixture was put to 25mL hydrothermal container and kept at 160 °C for 120 hours. Blue tiny needle like crystals were obtained after cooling to room temperature for 24 hours. Few best crystals were washed with water for single crystal data collection.

X-ray Crystallography: Data were collected on a Bruker SMART APEX [4.25] three circle diffractometer equipped with a CCD area detector and operated at 1500 W power (50 kV, 30 mA) to generate Mo Kα radiation (λ = 0.71073 Å). The incident X-ray beam was focused and monochromated using Bruker Excalibur Gobel mirror optics. The Crystal of the ionic composites reported in this work, were mounted on nylon CryoLoops (Hampton Research) with Paratone-N (Hampton Research). The structures were solved by direct methods and refined using the *SHELXTL 97* [4.26] software suite. Atoms were located from iterative examination of difference F-maps following least-squares refinements of the earlier models. Hydrogen atoms were placed in calculated positions and included as riding atoms with isotropic displacement parameters 1.2-1.5 times Ueq of the attached Carbon atoms. All the data reported in this chapter were collected at 293(2) K. The structures were examined using the Addsym subroutine of *PLATON* [4.27] to ensure that no additional symmetry could be applied to the models. All ellipsoids in ORTEP diagrams are displayed at the 50% probability level unless noted otherwise. Crystallographic data (excluding structure factors) for $Cu_3Mo_5P_2$ are reported in this chapter have been deposited with the CCDC as deposition No. CCDC 839380 Copies of the data can be obtained, free of charge, on application to the CCDC, 12 Union Road, Cambridge CB2 lEZ, U.K. [fax: þ 44 (1223) 336 033; e-mail: deposit@ccdc.cam.ac.uk].

4.6 References

4.1   (a) K. -D. Kreuer, *Chem. Mater.* **1996**, *8,* 610. (b) H. Wang, X. Xu, N. M. Johnson, N. K. R. Dandala, H.-F. Ji, *Angew. Chem. Int. Ed.* **2011**, *50*, 12538.

4.2   (a)Y. -J. Wang, D. P. Wilkinson, J. Zhang, *Chem. Rev.* **2011**, *111*, 762. (b) K. -D. Kreuer, S. J. Paddison, E. Spohr, M. Schuster, *Chem. Rev.* **2004**, *104*, 4637.

4.3   K. A. Mauritz, R. B. Moore, *Chem. Rev.* **2004**, *104*, 4535.

4.4   (a) T. Uma, M. Nogami, *Chem. Mater.* **2007**, *19,* 3604. (b) S. Fengf, M. Greenblatt *Chem. Mater.* **1993**, *5*, 1277. (c) Y. Yamazaki, R. Hernandez-Sanchez, S. M. Haile, Chem. Mater. **2009**, *21*, 2755. (d) J. C. McKeen, Y. S. Yan, M. E. Davis, *Chem. Mater.* **2008**, *20,* 5122. (e) F. M. Vichi, M. I. Tejedor-Tejedor, M. A. Anderson, *Chem. Mater.* **2000**, *12,* 1762. (f) J. F. Shin, K. Joubel, D. C. Apperley, P. R. Slater, *Dalton Trans.* **2012**, *41*, 261. (g) M. Nogami, R. Nagao, C. Wong, T. Kasuga, T. Hayakawa, *J. Phys. Chem. B*. **1999**, *103,* 9468.

4.5   (a) J. J. Smith, I. Zharov, *Chem. Mater.* **2009**, *21,* 2013. (b) X. Wei, M. Z. Yates, *Chem. Mater.* **2012**, *24*, 1738.

4.6   (a) J. C. McKeen, Y. S. Yan, M. E. Davis, *Chem. Mater.* **2008**, *20,* 3791. (b) J. M. Taylor, R. K. Mah, I. L. Moudrakovski, C. I. Ratcliffe, R. Vaidhyanathan, G. K. H. Shimizu, *J. Am. Chem. Soc.* **2010**, *132*, 14055. (c) J. C. McKeen, Yushan S. Yan, M. E. Davis, *Chem. Mater.* **2008**, *20,* 5122.

4.7   (a) D. -L. Long, R. Tsunashima, L. Cronin, *Angew. Chem. Int. Ed.* **2010**, *49*, 1736. (b) R. Neumann, M. Dahan, *Nature.* **1997**, *388*, 353. (c) N. Mizuno, M. Misono, *Chem. Rev.* **1998**, *98*, 199. (d) C. P. Pradeep, D. -L. Long, C. Streb, L. Cronin, *J. Am. Chem. Soc.* **2008**, *130*, 14946.

4.8   (a) Y. Daiko, S. Hayashi, A. Matsuda*, Chem. Mater*. **2010***, 22*, 3418. (b) T. Uma, M. Nogami, *Chem. Mater.* **2007**, *19,* 3604. (c) X. Tong, X. Wu, Q. Wu, W. Zhu, F. Cao, W. Yan, *Dalton Trans.* **2012**, *41*, 9893. (d) K. Checkiewicz, G. Zukowska, W. Wieczorek, *Chem. Mater.* **2001,** *13,* 379. (e) T. Uma, M. Nogami, *Chem. Mater.* **2007**, *19*, 3604. (f) C. Dey, T. Kundu, R. Banerjee, *Chem. Commun.* **2012**, *48*, 266.

4.9   S. Sachdeva, J. A. Turner, J. L. Horan, A. M. Herring, *Struct. Bond.* **2011**, *141*, 11.

4.10   (a) C. Streb, D. –L. Long, L. Cronin, *Chem. Commun.* **2007**, 471. (b) A. Leclaire, C. Biot, H. Rebbah, M. M. Borela, B. Raveaua, *J. Mater. Chem.* **1998**, 8, 439. (c) L. A. Mundit, R, C. Haushalter, *Inorg. Chem.* **1992**, *31*, 3050. (d) W. -J. Chang, Y.-C. Jiang, S.-L. Wang, K. -H. Lii, *Inorg. Chem.* **2006**, 45, 6586. (e) Y.-S. Zhou, L. –J. Zhang, H. –K. Fun, J. –L. Zuo, I. A. Razak, S. Chantrapromma, X. –Z. You, *New J.*

Chem. **2001**, *25*, 1342. (f) A. Guesdon, M. M. Borel, A. Leclaire, B. Raveau, *Chem. Eur. J.* **1997**, *3*, 1797.

4.11   Y. Daiko, S. Hayashi, A. Matsuda, *Chem. Mater.* **2010**, *22*, 3418.

4.12   K. Cheü ckiewicz, G. Zú ukowska, W. Wieczorek. *Chem. Mater.* **2001**, *13,* 379.

4.13   M. Yamada, D. Li, I. Honma, H. Zhou, *J. Am. Chem. Soc.* **2005**, *127*, 13092.

4.14   (a) B. Zheng, J. Bai, J. Duan, L. Wojtas, M.J. Zaworotko, *J. Am. Chem. Soc.* **2011**, *133*, 748. (b) D. J. Tranchemontagne, J. L. Mendoza-Cortes, M. O'Keeffe, O. M. Yaghi, *Chem. Soc. Rev.* **2009**, *38,* 1257. (c) B. Chen, S. Xiang, G. Qian, *Acc. Chem. Res.,* **2010**, *43,* 1115. (d) M. Plabst, L. B. McCusker, T. Bein, *J. Am. Chem. Soc.* **2009**, *131*, 18112. (e) D. B. Cordes, C .V. K. Sharma, R. D. Rogers. *Crys. Growth & Des.* **2007**, *7*, 1943.

4.15   (a) H.-L. Jiang, Y. Tatsu, Z.-H. Lu, Q. Xu, *J. Am. Chem. Soc.* **2010**, *132*, 5586. (b) P. Jutzi, A. Mix, B. Neumann, B. Rummel, W. W. Schoeller, H.-G. Stammler, A. B. Rozhenko, *J. Am. Chem. Soc.* **2009**, *131*, 12137. (c) K. S. Mali, D. Wu, X. Feng, K. Mullen, M. Van der Auweraer, S. De Feyter, *J. Am. Chem. Soc.* **2011**, *133*, 5856. (d) N. Yanai, W. Kaneko, K. Yoneda, M. Ohba, S. Kitagawa, *J. Am. Chem. Soc.* **2007**, *129*, 3496.

4.16   C. Dey, T. Kundu, R. Banerjee. *Chem. Commun*. **2012**, *48*, 266.

4.17   (a) H. -L. Jiang, Y. Tatsu, Z.-H. Lu , Q. Xu, *J. Am. Chem. Soc.* **2010**, *132*, 5586. (b) P. Jutzi, A. Mix, B. Neumann, B. Rummel, W. W. Schoeller, H.-G. Stammler, A. B. Rozhenko, *J. Am. Chem. Soc.* **2009**, *131*, 12137. (c) K. S. Mali, D. Wu, X. Feng, K. Mullen, M. Van der Auweraer, S. De Feyter, *J. Am. Chem. Soc.* **2011**, *133*, 5856. (d) N. Yanai, W. Kaneko, K. Yoneda, M. Ohba, S. Kitagawa, *J. Am. Chem. Soc.* **2007**, *129*, 3496.

4.18   (a) B. C. Wood, N. Marzari, *Phys. Rev. B,* **2007**, *76*, 134301. (b) K. D. Kreuer, S. J. Paddison, E. Spohr, M. Schuster, *Chem. Rev*. **2004**, *104*, 4637. (c) M. A. Hickner, H. Ghassemi, Y. S. Kim, B. R. Einsla, J. E. McGrath, *Chem. Rev*. **2004**, *104*, 4587. (d) A. Akutu-Sato, H. Akutsu, S. S. Turner, P. Day, M. R. Probert, J. A. K. Howard, T. Akutagawa, S. Takeda, T. Nakamura, T. Mori, *Angew. Chem., Int. Ed.,* **2005**, *44*, 292. (e) B. C. Steele, A. Heinzel, *Nature.* **2001**, *414*, 345. (f) L. M. Saiz, L. Klein, *Acc. Chem. Res.* **2002**, *35*, 482. (g) A. Sapronova, V. S. Bystrov, M. E. Green, *Front. Biosci.* **2003**, *8*, 1356. (h) *Proton Conductors: Solids, Membranes and Gels— Materials and Devices. Series: Chemistry of Solid State Materials (No. 2),* ed. P.

Colomban, Cambridge University Press, **1992**. (i) Z. Zhou, S. Li, Y. Zhang, M. Liu, *J. Am. Chem. Soc*. **2005**, *127*, 10824.

4.19   (a) G. K. H. Shimizu, R. Vaidhyanathan, J. M. Taylor, *Chem. Soc. Rev*. **2009**, *38*, 1430. (b) J. M. Taylor, R. K. Mah, I. L. Moudrakovski, C. I. Ratcliffe, R. Vaidhyanathan, G. K. H. Shimizu, *J. Am. Chem. Soc*. **2010**, *132*, 14055. (c) K. D. Kreuer, *Annu. Rev. Mater. Res*. **2003**, *33*, 333. (d) M. F. H. Schuster, W. H. Meyer, *Annu. Rev. Mater. Res*. **2003**, *33*, 233. (e) M. F. H. Schuster, W. H. Meyer, M. Schuster, K. D. Kreuer, *Chem. Mater*. **2004**, *16*, 329. (f) K. A. Maruitz, R. B. Moore, *Chem. Rev*. **2004**, *104*, 4535. (g) M. Casciola, G. Alberti, M. Sganappa, R. Narducci, *J. Power Sources*, **2006**, *162*, 141. (h) S. Hasegawa, S. Horike, R. Matsuda, S. Furukawa, K. Mochizuki, Y. Kinoshita, S. Kitagawa, *J. Am. Chem. Soc*. **2007**, *129*, 2607. (i) R. Matsuda, R. Kitaura, S. Kitagawa, Y. Kubota, R. V. Belosludov, T. C. Kobayashi, H. Sakamoto, T. Chiba, M. Takata, Y. Kawazoe, *Nature.* **2005**, *436*, 238.

4.20   (a) J. Y. Lee, J. M. Roberts, O. K. Farha, A. A. Sarjeant, K. A. Scheidt, J. T. Hupp, *Inorg. Chem.,* **2009**, *48*, 9971. (b) J. R. Li, Y. Tao, Q. Yu, X. H. Bu, H. Sakamoto, S. Kitagawa, *Chem. Eur. J.* **2008**, *14*, 2771. (c) J. L. C. Roswell, O. M. Yaghi, *J. Am. Chem. Soc.* **2006**, *128*, 1304. (d) H. Furukawa, N. Ko, Y. B. Go, N. Aratani, S. B. Choi, E. Choi, A. O. Yazaydin, R. Q. Snurr, M. O'Keeffe, J. Kim, O. M. Yaghi, *Science,* **2010**, *239,* 424. (e) H. Deng, C. J. Doonan, H. Furukawa, R. B. Ferreira, J. Towne, C. B. Knobler, B. Wang, O. M. Yaghi, *Science.* **2010**, *327*, 846.

4.21   (a) S. Bureekaew, S. Horike, M. Higuchi, M. Mizuno, T. Kawamura, D. Tanaka, N. Yanai, S. Kitagawa, *Nat. Mater.* **2009**, *8,* 831. (b) S. Li, Z. Zhou, Y. Zhang, M. Liu, *Chem. Mater*. **2005**, *17*, 5884. (c) Y. Nagao, *Synth. Metals,* **2005**, *154*, 892. (d) Y. Nagao, M. Fujishima, R. Ikeda, S. Kanda, H. Kitagawa, *Synth. Metals,* **2003**, *133*, 43. (e) J. A. Hurd, R. Vaidhyanathan, V. Thangadurai, C. I. Ratcliffe, I. M. Moudra-kovski, G. K. H. Shimizu, *Nat. Chem*. **2009**, *1*, 705.

4.22   (a) M. Sadakiyo, T. Yamada, H. Kitagawa, *J. Am. Chem. Soc*. **2009**, *131*, 9906. (b) T. Yamada, M. Sadakiyo, H. Kitagawa, *J. Am. Chem. Soc*. **2009**, *131*, 3144. (c) A. Shigematsu, T. Yamada, H. Kitagawa, *J. Am. Chem. Soc*. **2011**, *133*, 2144. (d) S. Morikawa, T. Yamada, H. Kitagawa, *Chem. Letters,* **2009**, *38*, 654.

4.23   M. Yoon, K. Suh, H. Kim, Y. Kim, N. Selvapalam, K. Kim, *Angew. Chem. Int. Ed.,* **2011**, *50*, 7870.

4.24 N. G. Hainovsky, Y. T. Pavlukhin, E. F. Hairetdinov, *Solid State Ionics,* **1986**, *20*, 249.

4.25 *SMART*, Version 5.05; Bruker AXS, Inc.: Madison, WI, **1998**.

4.26 G. M. Sheldrick, *SHELXS'97*; University of Gottingen: Germany, **1997**.

4.27 A. L. Spek, *PLATON*, A Multipurpose Crystallographic Tool; Utrecht University: Utrecht, The Netherlands, **2005**.

Note:

The results of this chapter have already been published in *Chem. Commun.* **2012***, 48,* 266–268. with the title: "Reversible phase transformation in proton conducting Strandberg-type POM based metal organic material". This publication was the result of the group of Dr. Rahul Banerjee and his students Chandan Dey and Tanay Kundu from the Physical/Materials Chemistry Division at CSIR-National Chemical Laboratory in Pune, India. Tanay Kundu was involved in proton conductivity measurement of the materials.

Incorporation of Metal Oxide Sites in Metal Organic Frameworks (MOFs)

5.1 Introduction

Metal organic frameworks (MOFs) are formed by the linkage of organic ligands to metal atoms to built extended structures. MOFs are well known for last two decades due to absorption property in their porous network [5.1]. MOFs are advantageous over other porous materials due to systematic arrangement of pores in the network and their ability to change pore size by changing the metal ions or ligands. Although MOFs have shown some activity on catalysis [5.2], magnetism [5.3], ion exchange [5.4] etc, but major activity of MOFs are still limited in the area of absorption. The aim of this chapter is to provide an insight towards incorporation of functionality inside MOFs by introducing polyoxometalates (POMs) [5.5] in the network. POMs have the potential to link metal ions via its peripheral oxygen to form network structures [5.6]. POM incorporated networks not only introduce functionality inside the structure, but also enhance their thermal stability [5.7]. Recent investigation on POM based covalently linked transition-metal complex frameworks has received considerable attention. There are three ways to introduce POMs inside extended network; (i) building up of MOFs keeping the POMs inside the pores of MOFs [Figure 5.1a] [5.8], (ii) coordination of oxygen atom of polyoxometalate to hetero metal ions to form extended structure [Figure 5.1b] [5.9], (iii) replacing the oxygen atom of POMs via organic ligands to join them in one, two or three dimensional fashion (1-D, 2-D or 3-D) [Figure 5.1c] [5.10].

The design of active, selective, environmentally benevolent, and recyclable heterogeneous catalysts is expected to have a major importance for industrial applications. POMs have received increasing attention because of their numerous advantageous properties. The POMs with strong Bronsted acidity show promising potential as solid-acid catalysts for many acid catalyzed organic transformations and industrial applications, such as the hydration of alkenes, esterification, and alkylation [5.11].
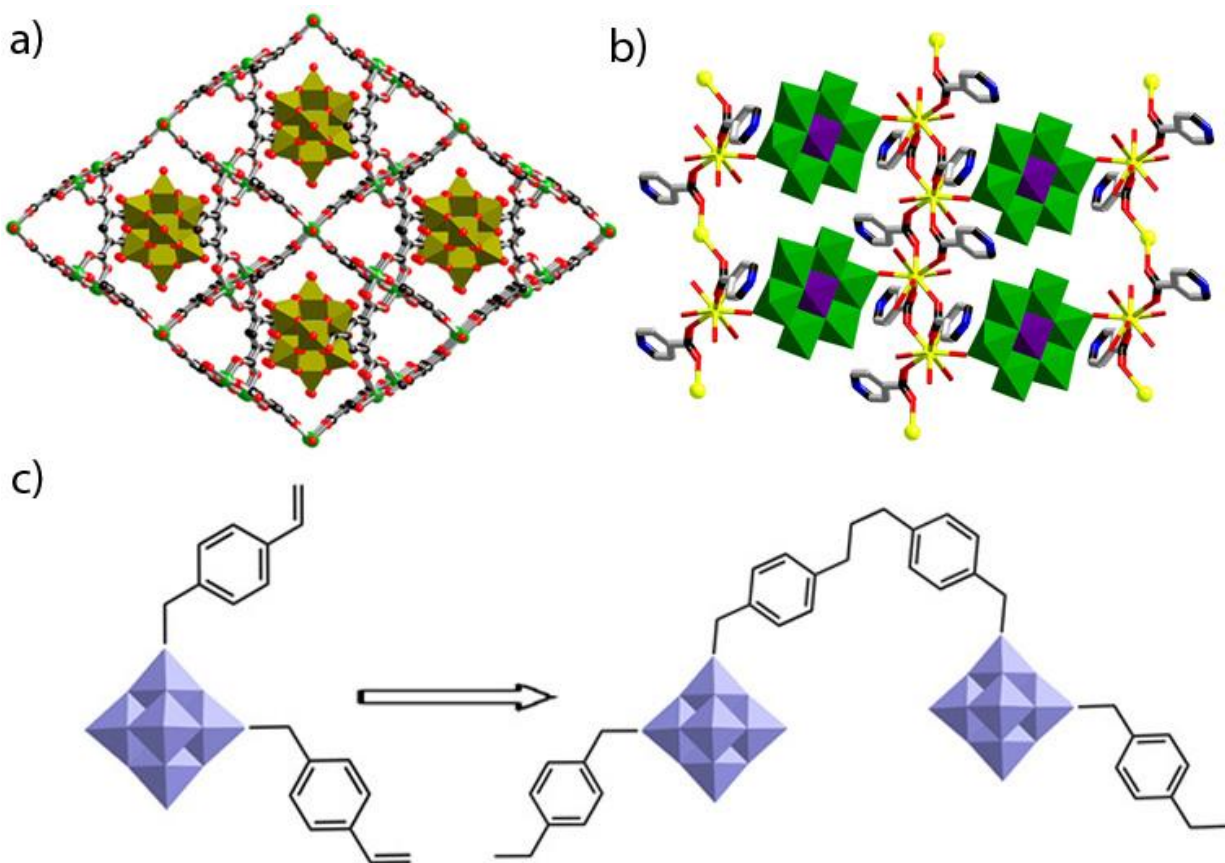
Figure 5.1: (a) POM incorporated MOF structure, sites showing the particular cavity where Keggin type POMs are sitting (Figure reproduced form ref 5.8 with permission). (b) Dawson type POMs are covalently linked to each other in 3-D via Ag$^+$ ion and the oxide ions of the POMs (Figure reproduced form ref 5.9a with permission). (c) Polymerization of functionalized Lindqvist structure to Polyoxometalate hybrid (Figure reproduced form ref 5.10).

Zeolitic imidazolate frameworks (ZIFs) are one subclass of metal organic frameworks (MOFs) [5.12] having crystalline porous architecture with tetrahedral metal ions [Zn(II), Co(II), Cd(II), etc.] bridged by imidazolate and imidazolate derivatives [5.13]. ZIFs offer flexible as well as porous structures with excellent thermal and chemical stability and tunable pore size, which make them useful for gas sorption, separation, catalysis, magnetism, and sensing applications [5.14]. More than a hundred ZIFs have been reported in literature, categorized within 15-20 topologies like SOD, RHO, GME, MER, etc. However, one would assume that incorporation of flexible structural units inside ZIFs not only increase the possibility of adaptation of new topology but also enhances chemical diversity within the structures. Tetrahedral metal oxide

units (MO_4, M=Mo, W, etc) are suitable candidates to fit inside ZIF architectures as they replicate the tetrahedral SiO_4/AlO_4 units of inorganic zeolites due to their similarity in shape and size. However, the fabrication of ZIFs with metal oxide units (MO_4) is challenging, due to the not-so-straightforward reactions which increase the possibility of unwanted side product formation. Zhang and coworkers have recently shown that it is possible to incorporate MoO_4/WO_4 tetrahedral units within ZIFs [5.15a]. They have shown that tetrahedral MoO_4/WO_4 units substitute the tetrahedral $Zn(Im)_4/ZnN_4$ units inside ZIFs and incorporate catalytically active sites [5.15]. This interesting new class of porous frameworks could be considered as intermediate between Zeolites and ZIFs.

5.2 Synthesis of metal oxide incorporated zeolitic imidazolate frameworks (ZIFs)

Two isostructural hybrid ZIFs (HZIFs) were synthesized using $Zn(NO_3)_2 \cdot 6H_2O$, 2-methyl imidazole (2-MIm) and H_2MO_4, where Zn(II) centers are connected *via* 2-MIm and $[MO_4]^{2-}$ units [5.15a]. The hybrid structures were proven to be thermally more stable compared to zinc imidazolate based ZIFs. At the same time, due to the presence of MoO_4/WO_4 tetrahedral units within the frameworks, these HZIFs were found to be catalytically active. However, as mentioned earlier, the synthesis of such compounds is extremely challenging, since it involves more number of reactants than necessary for the synthesis of regular ZIFs, which creates the possibility of forming numerous side products. As a result, only two metal oxide based hybrid ZIFs have been reported in the literature, although more than hundred metal imidazolate based ZIFs have been reported. Herein, we report the synthesis of a new hybrid structure of this class, $[(MoO_4)\{Zn(2\text{-NIm})\}_2] \cdot 2DMF$, namely MOZIF-1, where Zn(II) metal centers are coordinated to 2-nitro imidazolates (2-NIm) and the MoO_4 tetrahedral unit. In this work, we report our attempt to fine-tune the synthetic conditions by varying the concentration of reagents, temperature, and the duration of the reaction, in order to isolate pure MOZIF-1. When we performed the reaction without $Na_3[PMo_{12}O_{40}]$ (the source for MoO_4^{2-}), Zn-ZIF-65 (SOD) crystals were obtained from the reaction mixture. But while increasing the concentration of $Na_3[PMo_{12}O_{40}]$, MOZIF-1 crystals started growing and only at a concentration higher than 0.006 mmol/mL of $Na_3[PMo_{12}O_{40}]$ and a precise reaction time of 24-32 hours, MOZIF-1 was isolated in the pure phase [Figure 5.2].
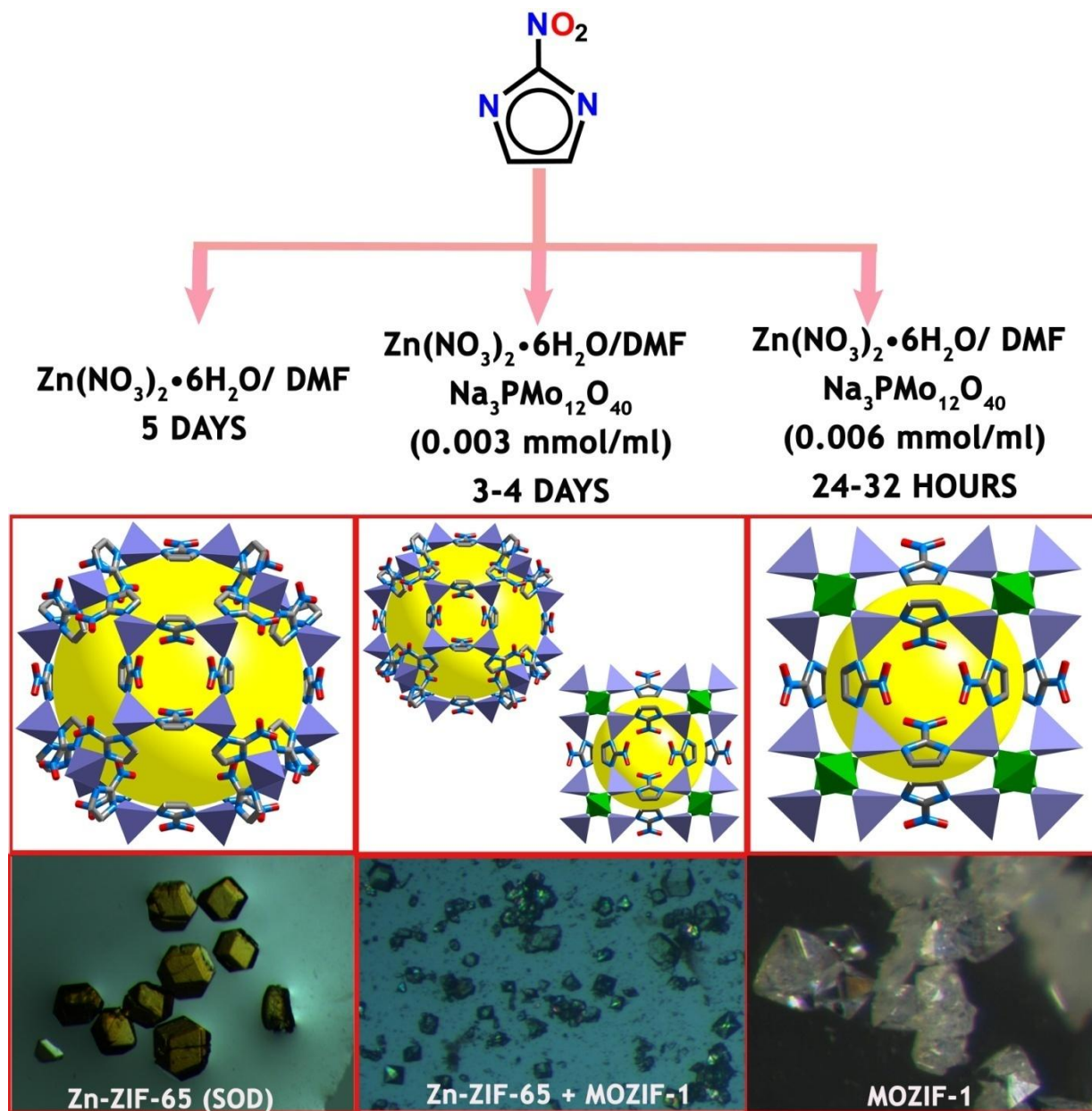
Figure 5.2: Schematic representation of the preparation of Zn–ZIF-65(SOD), MOZIF-1, in the pure phase and the mixed phase under different solvothermal conditions.

We have studied the role of $Na_3[PMo_{12}O_{40}]$ in the formation of the pure MOZIF-1 phase. A mixture of Zn-ZIF-65 and MOZIF-1 phase was obtained at lower concentration [<0.015 mmol] of $Na_3[PMo_{12}O_{40}]$. The usage of polyoxometalate (POM), $Na_3[PMo_{12}O_{40}]$, as a reactant generates the simultaneous possibility of formation of different metal oxide phases. In few batches $[(CH_3)_2NH_2]_3[PMo_{12}O_{40}]$ ionic crystals [5.16] were found along with Zn-ZIF-65 and
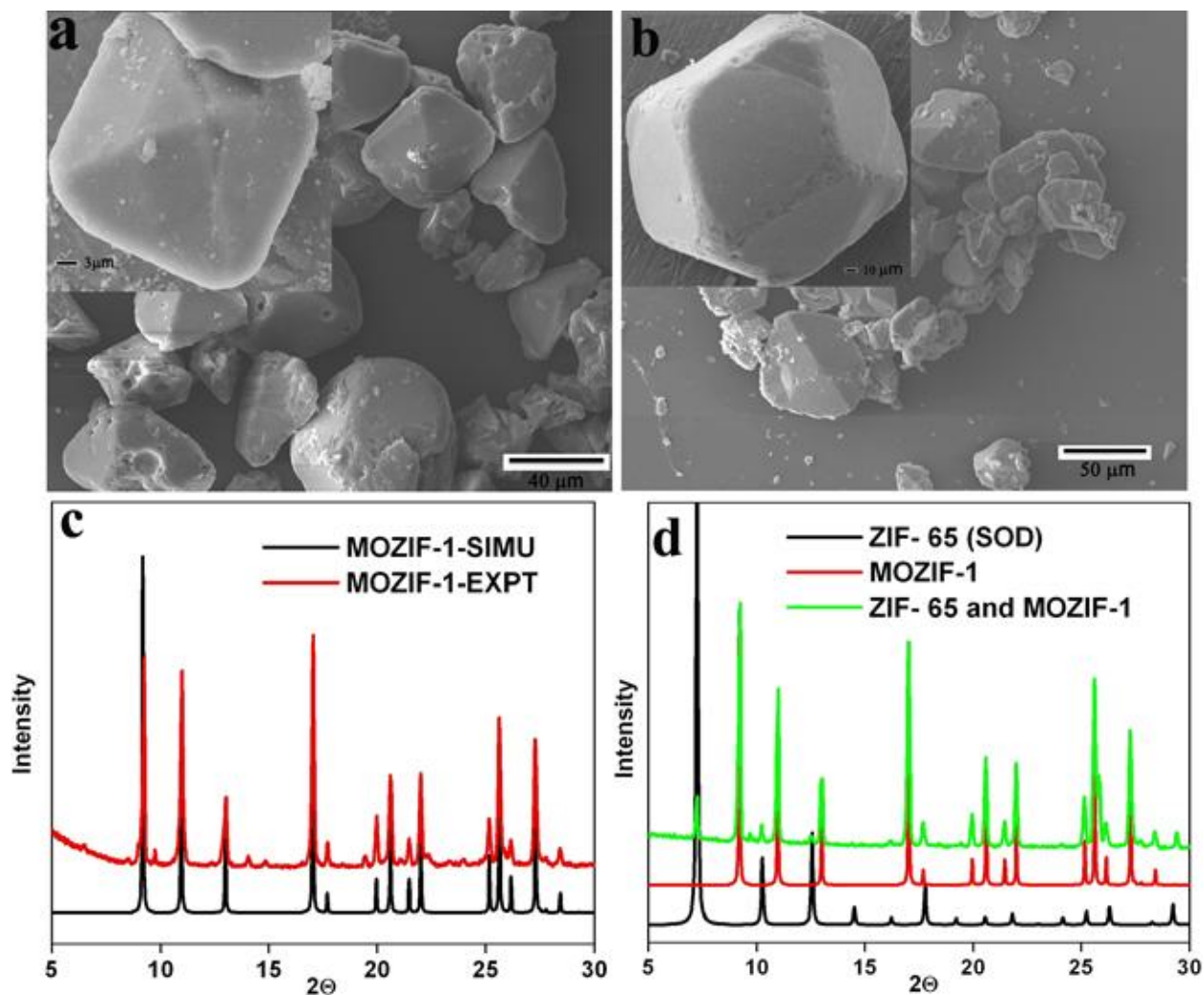
Figure 5.3: (a) SEM image of the pure MOZIF-1 phase. (b) SEM image of MOZIF-1 and Zn–ZIF-65 (SOD) mixed phase. (c) Comparison of the experiment and simulated PXRD pattern of pure MOZIF-1. (d) Comparison of the mixed phase with simulated PXRD patterns of MOZIF-1 and Zn–ZIF-65 (SOD).

MOZIF-1 crystals. Octahedral colourless crystals of MOZIF-1 were isolated at higher concentration [0.04g, (0.02 mmol)] of $Na_3[PMo_{12}O_{40}]$ [Figure 5.3a]. The duration of the reaction also plays a crucial role in product conversion. Although a lower concentration of $Na_3[PMo_{12}O_{40}]$ produces a mixture of Zn-ZIF-65 and MOZIF-1(3-4 days), the shorter reaction time (2 days) decreases the possibility of Zn-ZIF-65 formation [Figure 5.2]. A reaction timing of 24-32 hours has been observed as the optimum time for isolating pure MOZIF-1 crystals without any side products at the aforementioned conditions. MOZIF-1 and Zn-ZIF-65 phases are easily

distinguishable from their morphological differences. MOZIF-1 crystals are nearly octahedral in shape, whereas Zn-ZIF-65 crystals are cuboctahedron in shape [Figure 5.3]. This morphological difference was also observed in Scanning Electron Microscopic (SEM) images [Figure 5.3b] and was confirmed by Powder X-ray diffraction (PXRD) analysis. Experimental PXRD patterns of the bulk sample obtained from the reaction mixture of $Zn(NO_3)_2·6H_2O$, 2-NIm and

$Na_3[PMo_{12}O_{40}]$ (high concentration, 2 days) shows a good match with the simulated patterns obtained from the MOZIF-1 single crystal structure, confirming the phase purity of the bulk material [Figure 5.3c]. When the same experiment was carried out with the products obtained from lower concentration (<0.006 mmol/mL) of $Na_3[PMo_{12}O_{40}]$, a second impure phase (Zn-ZIF-65- SOD) was found along with the MOZIF-1, which was confirmed by PXRD and SEM images [Figure 5.3c & 5.3d].
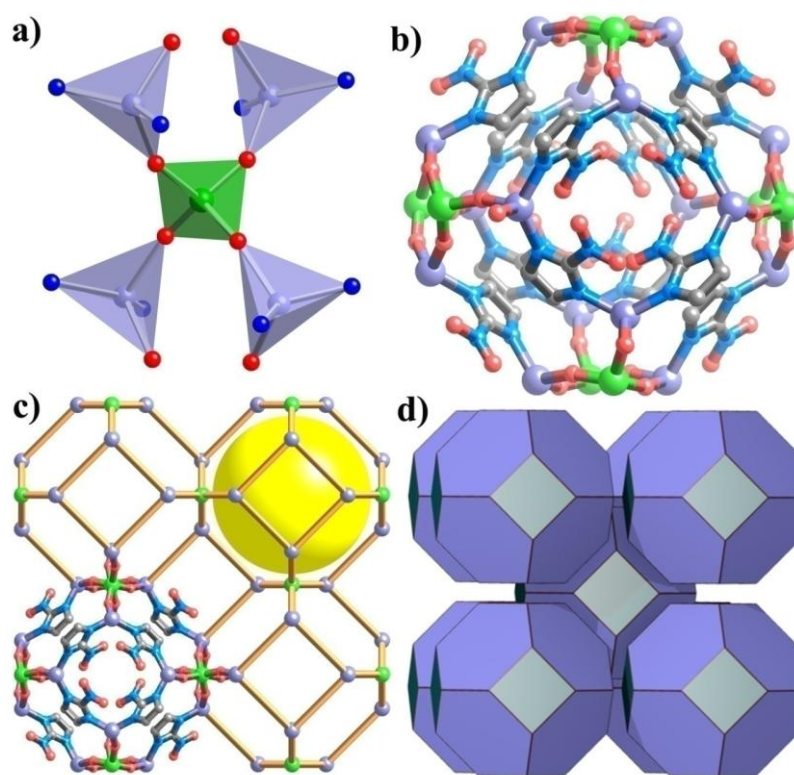
Figure 5.4: (a) Structural building unit, one MoO_4 tetrahedral unit is connected to four $Zn(O)_2(N)_2$ tetrahedral units. (b) Ball-stick model of one cage of MOZIF-1, showing 'Zn-2NIm' and 'Zn-MoO_4' connectivity. (c) Metal to metal connectivity in MOZIF-1, one unit shows Zn-(2NIm)-Zn connectivity and another unit shows the available space in each cavity. (d) SOD topological model of MOZIF-1, green: Mo, light blue: Zn, dark blue: N, grey: C, red: O.

5.3 Crystal structure of MOZIF-1

MOZIF-1 crystallizes in a tetragonal crystal system (Space group: *I-42m*). In the crystal structure, both Zn(II) and Mo(VI) centers are tetrahedrally coordinated. In MOZIF-1 Mo1 atom

possesses $\bar{4}$ symmetry, whereas, Zn1 lies on twofold axis, and C1, N1 lie on a mirror plane. All the four tetrahedral sites of Mo(VI) are occupied by oxygen atoms (O^{2-}), whereas two sites of Zn(II) are occupied by nitrogen atoms from 2-NIm and two other sites are occupied by oxygen atoms (O^{2-}) [Figure 5.4a]. MOZIF-1 can be considered as a 4-connected zeolitic type structure where alternate corners of the squares are occupied by Mo(VI) and Zn(II) centers connected by μ_2-O atoms with a 155° 'Zn–μ_2O–Mo' angle. Inside the MOZIF-1 framework, there exists another type of four membered ring consisting of 2NIm and Zn(II) with a 140.9° 'Zn–2NIm–Zn' angle [Figure 5.4b]. The inner diameter of the pore inside MOZIF-1 is *ca.* 10.5 Å. However, the pore apertures are almost blocked by the nitro groups of 2-NIm ligands, exposed towards the pore window [Figure 5.4c]. In MOZIF-1, two types of four-member rings are present. One four-member ring consists of 'Zn–(2-NIm)–Zn' connectivity and another four member ring consists of 'Zn–(MoO_4)–Zn' connectivity. The six member rings of MOZIF-1 or ZIF-1Mo/ ZIF-1W are always built form 'Zn–[2-(M/N)Im]–Zn–(Mo)O_4' units [Figure 5.5]. MOZIF-1 possesses same zeolitic sodalite (SOD) topology like ZIF-1Mo and HZIF-1W [Figure 5.4d].

5.4 Thermo gravimetric analysis

TGA analysis data suggests that MOZIF-1 is thermally more stable compared to Zn-ZIF-65 (SOD), although both have been prepared under the same reaction conditions. Zn-ZIF-65 (SOD) decomposes sharply at 350 °C, whereas MOZIF-1decomoses gradually at the temperature range of 350–500 °C [Figure 5.6a]. The incorporation of the metal oxide part (MoO_4 tetrahedral unit) into the ZIF matrix could be one probable reason for this higher thermal stability of MOZIF-1. MOZIF-1 is stable in water for 5-6 hours, which was confirmed by PXRD. IR Spectroscopy (*FT-IR*, 4000-450 cm^{-1}) of as-synthesized MOZIF-1 shows characteristic stretching frequency at 3789(w), 3571(br), 1667(m), 1496(s), 1358(s), 1167(m), 1112(m), 900(s), 866(s), 825(s), 647(m) cm^{-1} [Figure 5.6b].

5.5 Gas adsorption study

We have carried out gas adsorption studies on as-synthesized MOZIF-1after exchanging with low boiling solvent followed by evacuation at 100 °C for 24 hours. Although MOZIF-1 has a large (30.5%) solvent accessible void, it does not show significant porosity since all the pore
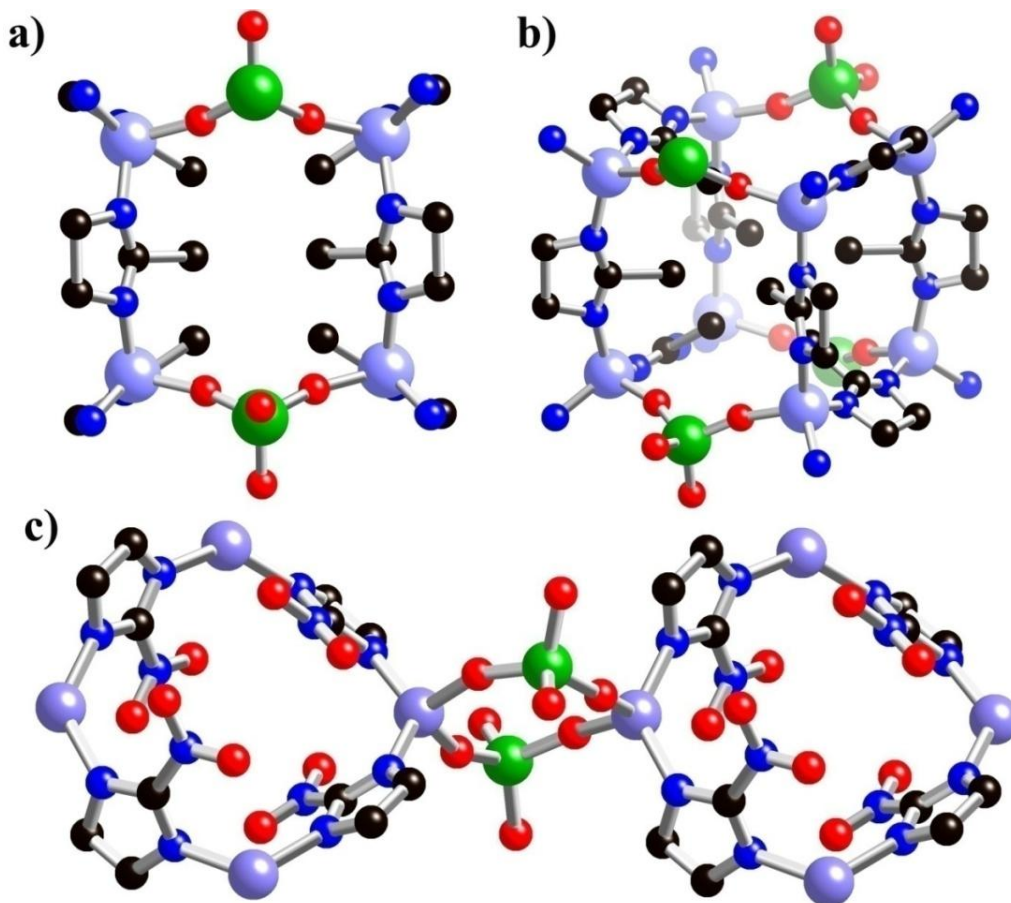
Figure 5.5: (a) & (b) In ZIF-1Mo and ZIF-1W structures 'Zn−(2-MIm)−Zn' units form 4-connected rings, whereas 'MO$_4$−Zn−(2-MIm)−Zn−MO$_4$' (M=Mo, W) units form six metal centre rings and both the rings are edge shared. (c) In MOZIF-1 'Zn−(2-NIm)−Zn' and 'Zn−MO$_4$−Zn' both forms four metal centre rings. [The 'Zn-Zn' distance in 'Zn-MoO$_4$-Zn' unit is 5.147Å and 'Zn-Mo-Zn' angle is 91.52°, whereas in Zn-ZIF-65(SOD) the 'Zn-Zn' distance is 6.124 Å and 'Zn-2NIm-Zn' angle is 145.14°] Both the hybrid zeolitic imidazolate framework (ZIF-1Mo and HZIF-1W) reported by Zhang and coworker are isostructural and crystallize in cubic space group *Im$\overline{3}$m* [*a=b=c*=23.4345(2) Å, α=β=γ=90°]. In both structures, there is only one type of four member ring consisting of 'Zn−(2-MIm)−Zn' units. But in MOZIF-1, two type of four member rings are present, one four member ring consists of 'Zn−(2-NIm)−Zn' connectivity and another four member ring consists of 'Zn−(MoO$_4$)−Zn' connectivity. The six member rings of the reported structures (HZIFs) and new structure (MOZIF-1) are always built form 'Zn−[2-(M/N)Im]−Zn−(Mo/W)O$_4$' units. MOZIF-1 possesses same zeolitic sodalite (SOD) topology like ZIF-1Mo and HZIF-1W.

apertures are blocked by the nitro groups of imidazole rings. The BET surface area of MOZIF-1was calculated from the N_2 adsorption isotherm as 35 m^2g^{-1}.
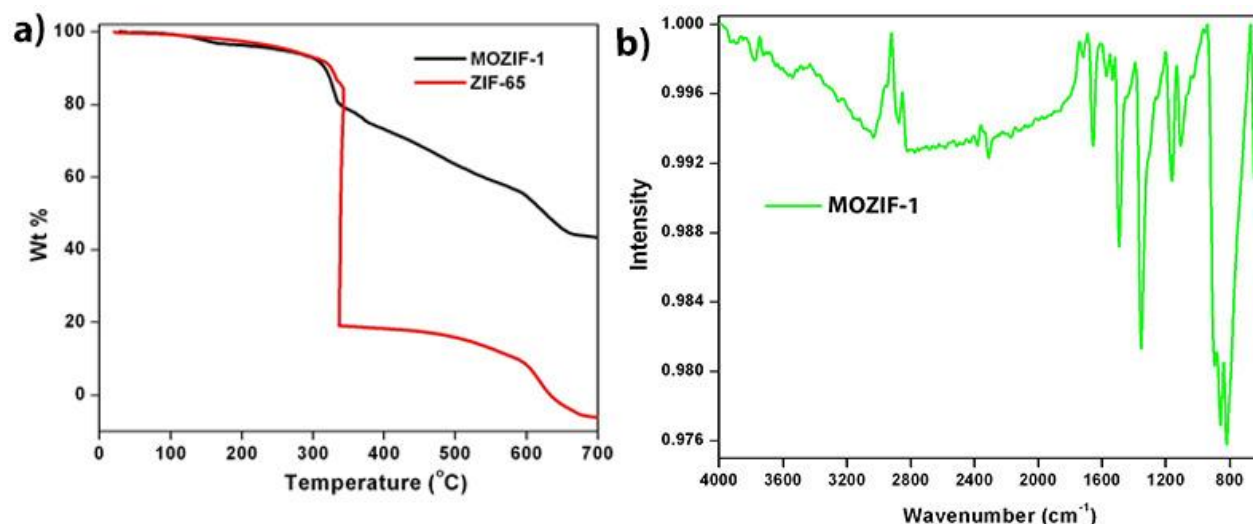

Figure 5.6 (a) Thermo Gravimetric Analysis (TGA) data suggest that MOZIF-1 is thermally more stable compare to Zn-ZIF-65 (SOD) although both have been prepared under the same reaction conditions. Zn-ZIF-65 (SOD) decomposes sharply at ~350 °C, whereas MOZIF-1decomoses gradually at temperature range of 350−500 °C. (b) IR Spectroscopy of as-synthesized MOZIF-1 (*FT-IR*, 4000-450 cm^{-1}).

5.6 Dye degradation study

POMs are known to catalytically activate hydrogen peroxide, which is eco-friendly and inexpensive oxidant for oxidation of hydrocarbons selectively [5.17]. POM/H_2O_2 systems can be used as environmental detoxification agent. POMs have been used as catalyst to thermally bleach of the dyes pollutant by hydrogen peroxide in basic aqueous solutions at the dark condition [5.18]. The major disadvantage of POM based system is their homogeneity in aqueous medium which decreases the recyclability of the materials [5.19]. To overcome this problem, few attempts have been made to immobilize POMs on solid supports, such as zeolite, silica, and TiO_2 [5.19, 5.20]. A group of researcher recently prepared POMs supported on zeolite [5.19b], which considerably increased the photo-degradation of 1,2-dichlorobenzene by O_2 under UV irradiation. The resin supported POM can efficiently activate H_2O_2 for the removal of dye pollutant under visible light [5.21]. Another way to make POM catalyst heterogeneous is to crystallize them with macro cations [5.22]. These salts can easily form rigid micro/mesoporous

solid materials and can be used as efficient catalysts for oxidation of organic compounds. $Cs_3PW_{12}O_{40}$ is an example of efficient heterogeneous photo-catalyst of this class for degradation of organic pollutants by O_2 under UV (Ultraviolet) irradiation [5.19, 5.23]. The photodegradation of dye pollutants by H_2O_2 [5.24] or O_2 [5.25] in water by visible light is an efficient way to utilize solar energy for environment friendly purpose. Various types of dye pollutants can be photodegraded effectively in the TiO_2 dispersions under visible irradiation, which is initiated by electron injection from the photoexcited dyes to the conduction band of TiO_2 [5.26].
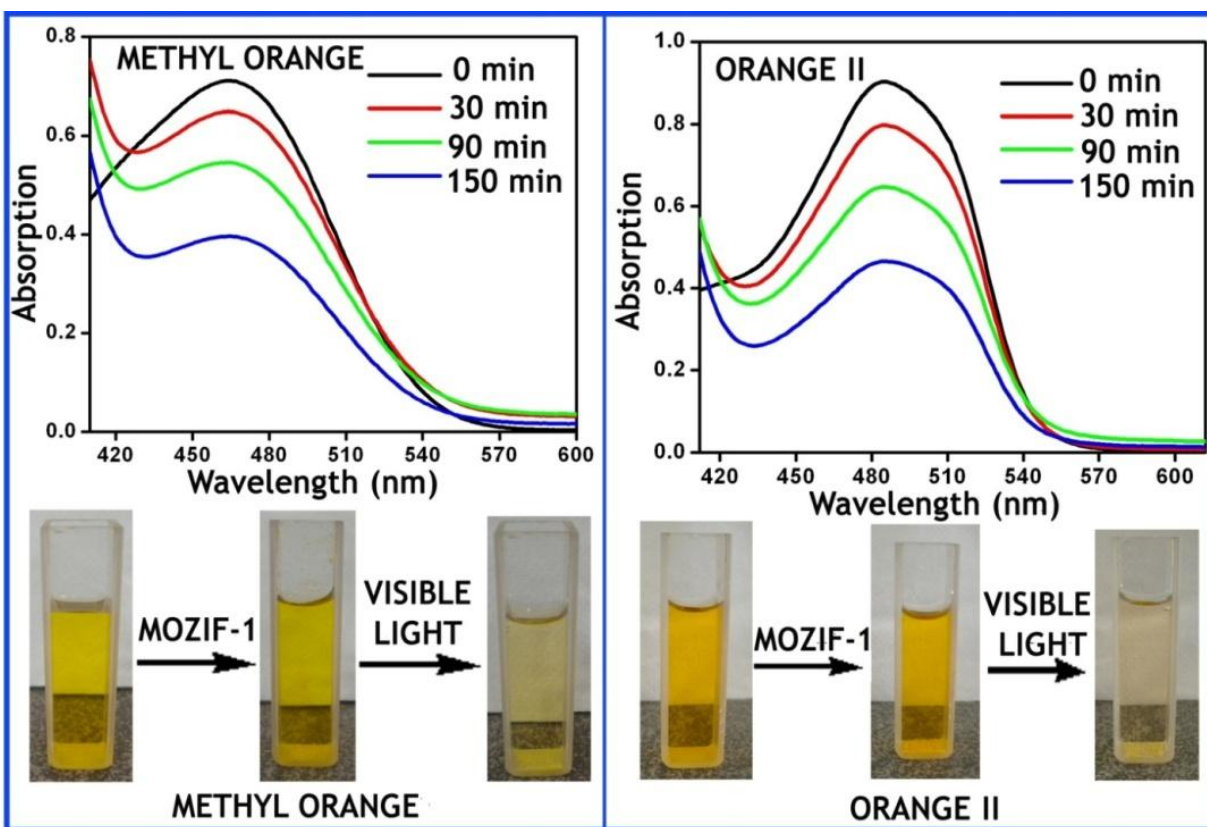
Figure 5.7: Photocatalytic degradation of methyl orange and orange II dye in the presence of MOZIF-1 under visible light.

Methyl orange (MO) is widely considered as a representative of dye pollutant in waste water [5.27]. The purpose of photocatalytic degradation of organic dyes is to decompose them into small nonpolluting organic molecules such as organic acids, CO_2, etc. POMs and POM based MOFs are well known materials for decades due to their catalytic activity [5.28]. MOZIF-1 contains the active MoO_4 tetrahedral site of POM, which makes it suitable for photocatalysis.

Bearing this idea in mind, we have carried out dye degradation [5.29] experiments with MOZIF-1 in water [Figure 5.7].

A 3×10^{-5} (M) methyl orange stock solution in water was prepared. In each 15 mL of methyl orange solution batch, 7 mg of MOZIF-1 was added under visible light source and different batches were taken out at an interval of 30 minutes with gradual decrease in color intensity indicating the degradation of dye which was also confirmed by UV-visible spectra. The stability of the compound after catalytic cycle was confirmed by PXRD analysis. The same experiment has been carried out with Orange II dye with discoloration of orange color solution [Figure 5.7].

5.7 Conclusion

In summary, we have successfully synthesized a new metal oxide based hybrid ZIF, MOZIF-1 using $Zn(NO_3)_2$, 2-NIm and $Na_3[PMo_{12}O_{40}]$ under solvothermal conditions. In almost the same condition, pure Zn-ZIF-65 (SOD) crystals have been isolated when the reaction was carried out without $Na_3[PMo_{12}O_{40}]$. With the increasing concentration of $Na_3[PMo_{12}O_{40}]$, the purity of MOZIF-1 phase was found to increase and the amount of ZIF-65 phase was found to decrease. At higher concentrations of $Na_3[PMo_{12}O_{40}]$ and shorter reaction times, we were able to isolate the pure MOZIF-1 phase. Due to the presence of catalytically active tetrahedral MoO_4 unit, the compound shows degradation of organic dyes. We are trying to utilize this strategy to prepare topologically new metal oxide based hybrid ZIFs using different imidazolate derivatives.

5.8 Experiment Section

Synthesis of [(MoO₄){Zn(Im-NO₂)}₂]·2DMF (MOZIF-1): MOZIF-1 was synthesized in solvothermal condition using the mixture of $Zn(NO_3)_2·6H_2O$ (0.03 g, 0.1 mmol), 2-nitro imidazole (0.01 g, 0.09 mmol) and sodium phosphomolybdate hydrate (0.04 g, 0.02 mmol) in 3mL DMF for 2 d. With lower concentration 0.01 g (0.005 mmol), 0.02 g (0.01 mmol), 0.03 g (0.015 mmol) of sodium phosphomolybdate hydrate mixture of products were isolated. In few of the cases ZIF-65-SOD crystals were observed in the mixture along with the MOZIF-1 crystals. But with 0.04 g, (0.02 mmol) or higher concentration of sodium phosphomolybdate hydrate we also found pure octahedral colorless crystals. When the same reaction was carried out without sodium phosphomolybdate ZIF-65-SOD crystals were isolated as pure phase. *FT-IR* **:** (KBr

$4000\text{-}450 cm^{-1}$): 3789(w), 3571br), 1667(m), 1496(s), 1358(s), 1167(m), 1112(m), 900(s), 866(s), 825(s), 647(m). Elemental Analysis**:** Found (%) C= 21.80, H= 2.81, N= 16.87; Calc. (%) C= 21.79, H= 2.72, N= 16.95.

Single crystal structure analysis: Data was collected on a Bruker SMART APEX three circle diffractometer equipped with a CCD area detector and operated at 1500 W power (50 kV, 30 mA) to generate Mo Kα radiation (λ = 0.71073 Å). The incident X-ray beam was focused and monochromated using graphite monochromator. The crystal reported in this chapter was mounted on nylon CryoLoops (Hampton Research) with Paraton-N (Hampton Research). Initial scans of each specimen were performed to obtain preliminary unit cell parameters and to assess the mosaicity (breadth of spots between frames) of the crystal to select the required frame width for data collection. *Bruker SMART* [5.30a] software was used suite to carry out overlapping φ and ω scans at detector (2θ) settings (2θ = 28). Following data collection, reflections were sampled from all regions of the Ewald sphere to redetermine unit cell parameters for data integration and to check for rotational twinning using *CELL_NOW* [5.30b]. Following exhaustive review of collected frames the resolution of the dataset was judged. Data were integrated using Bruker SAINT [5.30c] software with a narrow frame algorithm and a 0.400 fractional lower limit of average intensity. Data were subsequently corrected for absorption by the program SADABS [5.30d]. The space group determination and tests for merohedral twinning were carried out using *XPREP* [5.30c]. The structure was solved by direct methods and refined using the *SHELXTL 97* [5.30e] software suite. Atoms were located from iterative examination of difference F-maps following least squares refinements of the earlier models. Final models were refined anisotropically (if the number of data permitted) until full convergence was achieved. The structure was examined using the *Adsym* subroutine of *PLATON* [5.30f,g] to assure that no additional symmetry could be applied to the models. Electron density within the cavity has not been assigned as any guest molecules other than scattered carbon, oxygen and nitrogen atoms. *SQUEEZE* on *PLATON* [5.30f] has been applied to take out highly disordered solvent molecules (DMF) floating inside the cage. All ellipsoids in ORTEP diagrams are displayed at the 30% probability level unless noted otherwise. Crystallographic data (excluding structure factors) for the structure reported in this chapter has been deposited with the CCDC as deposition No. CCDC 934758. Copies of the data can be obtained, free of charge, on application to the CCDC, 12

Union Road, Cambridge CB2 lEZ, U.K. [fax: þ 44 (1223) 336 033; e-mail: deposit@ccdc.cam.ac.uk].

5.9 References

5.1   (a) A. -C. Sudik, A. -P. Cote, A. G. Wong-Foy, M. O'Keeffe, O. M. Yaghi, *Angew. Chem., Int.* Ed. **2006**, *45,* 2528. (b) A. Kondo, H. Noguchi, H. Kajiro, L. Carlucci, P. Mercandelli, D. -M. Proserpio, M. Respiration, *J. Phys. Chem. B.* **2006**, *110,* 25565. (c) M. Hong, *Cryst. Growth Des*. **2007**, *7,* 10. (d) C. Janiak, *Dalton Trans.* **2003**, *14,* 2781. (e) C. N. R. Rao, A. K. Cheetham, A. Thirumurugan, *J. Phys.:Condens. Matter* **2008**, *20,* 083202. (f) R. Robson, *Dalton Trans.* **2008**, 5113.

5.2   (a) C. D. Wu, A. Hu, L. Zhang, W. B. Lin, *J. Am. Chem. Soc.* **2005**, *127,* 8940. (b) W. B. Lin, *J. Solid State Chem.* **2005**, *178,* 2486. (c) M. Fujita, Y. J. Kwon, S. Washizu, K. Ogura, *J. Am. Chem. Soc*. **1994**, *116*, 1151. (d) J. S. Seo, D. Whang, H. Lee, S. I. Jun, J. Oh, Y. J. Jeon, K. Kim, *Nature*. **2000**, *404*, 982. (e) O. Ohmori, M. Fujita, *Chem. Commun*. **2004**, *10,* 1586. (f) W. Lin, *MRS Bull.* **2007**, *32,* 544.

5.3   (a) R. -D. Poulsen, A. Bentien, M. Chevalier, B. -B. Iversen, *J. Am. Chem. Soc.* **2005**, *127,* 9156. (b) S. -K. Ghosh, J. Ribas, M. -S. Fallah, P. -K. Bharadwaj, *Inorg. Chem.* **2005**, *44,* 3856. (c) S. -C. Xiang, X. -T. Wu, J. -J. Zhang, R. -B. Fu, S. -M. Hu, X. -D. Zhang, *J. Am. Chem. Soc*. **2005**, *127,* 16352. (d) F. Luo, D. -X. Hu, L. Xue, Y. -X. Che, J. -M. Zheng, *Cryst. Growth Des.* **2007**, *7,* 851.

5.4   (a) O. M. Yaghi, H. Li, *J. Am. Chem. Soc.* **1996**, *118,* 295. (b) T. K.. Maji, R. Matsuda, S. Kitagawa, *Nat. Mater.* **2007**, *6*, 142. (c) K. S. Min, M. P. Suh, *J. Am. Chem. Soc.* **2000**, *122,* 6834.

5.5   (a) P. Gouzerh, A. Proust, *Chem. Rev.* **1998**, *98*, 77. (b) K. Binnemans, *Chem. Rev.* **2009**, *109*, 4283. (c) D. –L. Long, R. Tsunashima, L. Cronin, *Angew. Chem., Int. Ed.* **2010**, *49,* 1736. (d) E. Coronado, C. L. Gomez-Garcia, *Chem. Rev*. **1998**, *98*, 273. (e) D. E. Katsoulis, *Chem. Rev*. **1998**, *98*, 359. (f) Y. P. Jeannin, *Chem. Rev.* **1998**, *98*, 51. (g) A. Muller, S. Q. N. Shah, H. Bogge, M. Schmidtmann, *Nature*. **1999,** *397*, 48. (h) A. Muller, E. Beckmann, H. Bogge, M. Schmidtmann, A. Dress, *Angew. Chem., Int. Ed*. **2002**, *41*, 1162.

5.6   (a) Y.-Z. Zheng, M. Evangelisti, R. E. P. Winpenny *Angew. Chem. Int. Ed.* **2011**, *50*, 3692.   (b) J. Gao, J. Yan, S. G. Mitchell, H. N. Miras, A. G. Boulay, D.-L. Long, L. Cronin, *Chem. Sci.* **2011**, *2*, 1502.

5.7   (a) M. Fournier, C. Feumi-Jantou, C. Rabia, G. Herve, S. Launay *J. Mater. Chem.* **1992**, *2*, 971.   (b) D. Mustafa, E. Breynaert, S. R. Bajpe, J. A. Martens, C. E. A. Kirschhock, *Chem. Commun.* **2011**, *47*, 8037

5.8   C. −Y. Sun, S. −X. Liu, D. D. Liang, K. −Z. Shao, Y. −H. Ren, Z. −M. Su, *J. Am. Chem. Soc*. **2009**, *131*, 1883.

5.9   (a) H. An, Y. Li, D. Xiao, E. Wang, C. Sun, *Cryst. Growth Des.* **2006**, *6,* 1107. (b) H. An, Y. Li, E. Wang, D. Xiao, C. Sun, L. Xu, *Inorg. Chem.* **2005**, *44,* 6062.

5.10 (a) Y. -F. Song, N. McMillan, D. −L. Long, S. Kane, J. Malm, M. O. Riehle, C. P. Pradeep, N. Gadegaard, L. Cronin, *J. Am. Chem. Soc.* **2009,** *131,* 1340. (b) W. Qi, L.; Wu, *Polym. Int.* **2009**, *58,* 1217.

5.11 (a) M. Misono, *Catal. Rev. Sci. Eng.* **1987**, *29*, 269. (b) M. Misono, *Catal. Rev. Sci. Eng.* **1988**, *30*, 339. (c) I. V. Kozhevnikov, *Chem. Rev.* **1998**, *98*, 171.

5.12 (a) F. Wang, Y. -B. Shu, X. Bu, J. Zhang, *Chem. Eur. J.* **2012**, *18*, 11876. (b) D. Zacher, R. Schmid, C. Woll, R. A. Fischer, *Angew. Chem. Int. Ed.* **2011**, *50,* 176. (c) A. W. Thornton, K. M. Nairn, J. M. Hill, A. J. Hill, M. R. Hill, *J. Am. Chem. Soc.* **2009**, *131*, 10662. (d) T. Panda, P. Pachfule, Y. Chen, J. Jiang, R. Banerjee, *Chem.Commun*., **2011**, *47*, 2011. (e) Y. -Q. Tian, S. -Y. Yao, D. Gu, K. -H. Cui, D. -W. Guo, G. Zhang, Z. -X. Chen, D. -Y. Zhao, *Chem. Eur. J.* **2010**, *16*, 1137.

5.13 (a) R. Banerjee, A. Phan, B. Wang, C. Knobler, H. Furukawa, M. O'Keeffe, O. M. Yaghi, *Science,* **2008**, *319*, 939. (b) H. Yang, X.-W. He, F.Wang, Y. Kang, J. Zhang, *J. Mater. Chem.* **2012**, *22*, 21849.

5.14 (a) R. Banerjee, H. Furukawa, D. Britt, C. Knobler, M. O'Keeffe, O. M. Yaghi, *J. Am. Chem. Soc.* **2009**, *131*, 3875. (b) B. P. Biswal, T. Panda, R. Banerjee, *Chem.Commun*. **2012**, *48*, 11868.

5.15 (a) F. Wang, Z. −S. Liu, H. Yang, Y. −Xi Tan, J. Zhang, *Angew. Chem. Int. Ed.* **2011**, *50*, 450. (b) A. Corma, H. Garcia, F. X. L. i Xamena, *Chem. Rev.* **2010**, *110*, 4606.

5.16 (a) M. I. Khan, A. Muller, S. Dillinger, H. Bogge, Q. Chen, J. Zubieta, *Angew. Chem. Int. Ed. Engl.* **1993**, *32*, 1780. (b) S. Uchida, N. Mizuno, *J. Am. Chem. Soc.* **2004**, *126*, 1602.

5.17 R. Noyori, M. Aoki, K. Sato, *Chem. Commun.* **2003**, 1977.

5.18 D. M. Gould, W. P. Griffith, M. Spiro, *J. Mol. Catal. A: Chem.* **2001**, *175*, 289.

5.19 (a) D. A. Friesen, L. Morello, J. V. Headley, C. H. Langford, *J. Photochem. Photobiol. A: Chem.* **2000**, *133*, 213. (b) R. R. Ozer, J. L. Ferry, *J. Phys. Chem. B.* **2002**, *106*, 4336.

5.20 (a) B. Yue, Y. Zhou, J. Y. Xu, Z. Z. Wu, X. A. Zhang, Y. F. Zou, S. L. Jin, *Environ. Sci. Technol.* **2002**, *36*, 1325. (b) Y. H. Guo, Y. H. Wang, C. W. Hu, Y. H. Wang, E. B. Wang, Y. C. Zhou, S. H. Feng, *Chem. Mater.* **2000**, *12*, 3501. (c) P. Lei, C. Chen, J. Yang, W. Ma, J. Zhao, L. Zang, *Environ. Sci. Technol.* **2005**, *39*, 8466.

5.21 P. Lei, C. Chen, J. Yang, W. Ma, J. Zhao, L. Zang, *Environ. Sci. Technol.* **2005**, *39*, 8466.

5.22 (a) T. Ito, K. Inumaru, M. Misono, *J. Phys. Chem. B.* **1997**, *101*, 9958. (b) J. Haber, K. Pamin, L. Matachowski, B. Napruszewska, J. Poltowicz, *J. Catal.* **2002**, *207*, 296. (c) J. Haber, K. Pamin, L. Matachowski, B. Napruszewska, J. Poltowicz, *J. Catal.* **2002**, *207*, 296.

5.23 D. Friesen, J. Headley, C. Langford, *Environ. Sci. Technol.* **1999**, *33*, 3193.

5.24 (a) X. Tao, W. H. Ma, T. Y. Zhang, J. C. Zhao, *Angew. Chem., Int. Ed.* **2001**, *40*, 3014. (b) F. Chen, J. J.He, J. C. Zhao, J. C. Yu, *New J. Chem.* **2002**, *26*, 336.

5.25 (a) R. Asahi, T. Morikawa, T. Ohwaki, K.. Aoki, Y. Taga, *Science.* **2001**, *293*, 269. (b) S. Sakthivel, H. Kisch, *Angew. Chem., Int. Ed.* **2003**, *42*, 4908. (c) W. Zhao, W. Ma, C. Chen, J. Zhao, Z. Shuai, *J. Am. Chem. Soc.* **2004**, *126*, 4782. (d) G. Liu, T. Wu, J. Zhao, H. Hidaka, N. Serpone, *Environ. Sci. Technol.* **1999**, *33*, 2081.

5.26 (a) M. Vautier, C. Guillard, J. Herrmann, *J. Catal*. **2001**, *201*, 46. (b) C. Bauer, P. Jacques, A. Kalt, *J. Photochem. Photobiol., A: Chem.* **2001**, *140*, 87. (c) E. Stathatos, T. Petrova, P. Lianos, *Langmuir* **2001**, *17*, 5025.

5.27 M. L. Marin, L. Santos-Juanes, A. Arques, A. M. Amat, M. A. Miranda, *Chem. Rev.* **2012**, *112*, 1710.

5.28 (a) D. −L. Long, R.Tsunashima, L. Cronin, *Angew. Chem. Int. Ed.* **2010**, *49*, 1736. (b) A. Muller, S. Q. N. Shah, H. Bogge, M. Schmidtmann, *Nature.* **1999**, *397*, 48. (c) N. V. Izarova, M. T. Pope, U. Kortz, *Angew. Chem. Int. Ed.* **2012**, *51*, 9492. (d) A. Haimov, R. Neumann, *J. Am. Chem. Soc.* 2006, **128**, 15697. (e) C. Dey, T. Kundu, R. Banerjee, *Chem. Commun***. 2012**, *48*, 266. (f) C. Dey, R. Das, B. K. Saha, P. Poddar, R. Banerjee,

Chem. Commun. **2011**, *47*, 11008. (g) C. Dey, R. Das, P. Poddar, R. Banerjee, *Crys. Growth & Des.* **2012**, *12*, 12.

5.29 (a) C. L. Hill, D. A. Bouchard, *J. Am. Chem.* Soc. **1985**, *107*, 5148. (b) B. Liu, J. Yang, G. -C. Yang, J. -F. Ma, *Inorg. Chem.* **2013**, *52*, 84. (c) P. Lei, C. Chen, J. Yang, W. Ma, J. Zhao, L. Zang, *Environ. Sci. Technol.* **2005**, *39*, 8466.

5.30 (a) Bruker (**2005**). *APEX2*. Version 5.053. Bruker AXS Inc., Madison,Wisconsin, USA. (b) G. M. Sheldrick, (**2004**). *CELL_NOW*. University of Göttingen, Germany. Steiner, Th. (**1998**). *Acta Cryst*. B54, 456. (c) Bruker (**2004**). *SAINT-Plus* (Version 7.03). Bruker AXS Inc., Madison, Wisconsin, USA. (d) G. M. Sheldrick, (2002). *SADABS* (Version 2.03) and *TWINABS* (Version 1.02).University of Göttingen, Germany. (e) G. M. Sheldrick, (**1997**). *SHELXS '97* and *SHELXL '97*. University of Göttingen, Germany. (f) A. L. Spek (**2005**) PLATON, *A Multipurpose Crystallographic Tool*, Utrecht. University, Utrecht, The Netherlands. (g) WINGX

POM Catalyzed in situ Ligand Synthesis to Prepare Coordination Polymer

6.1 Introduction

Combination of multiple reagents in a vessel for the easy access of the products in single step reduce the time of the reaction and avoid the difficulties of separating the products in each steps of reaction. It sometime minimizes the difficulties of using hazardous chemicals, like azide, cyano etc. *In situ* ligand synthesis [6.1] not only provides a synthetic root for organic ligands which are not readily accessible but also represents a potential new direction for construction of novel inorganic–organic hybrid network construction through crystal
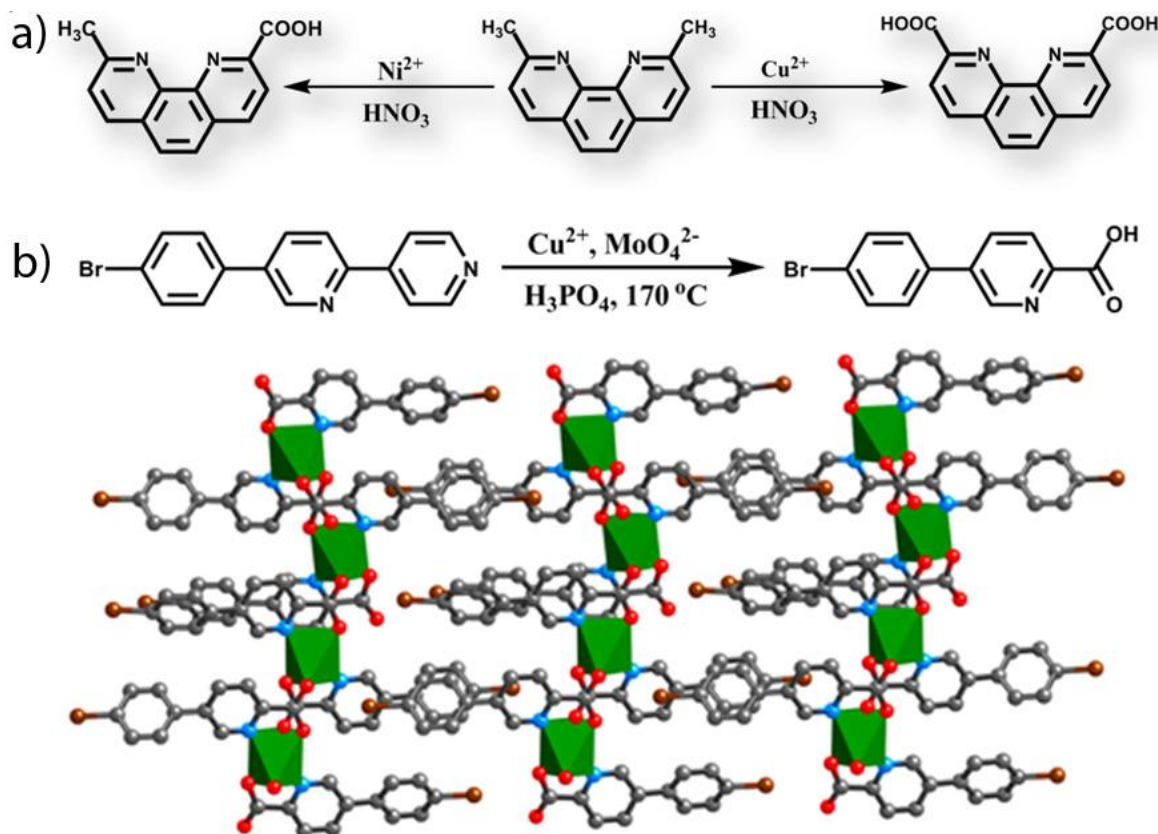

Figure 6.1: (a) Scheme of in situ oxidation, Ni^{2+}/Cu^{2+} in presence of HNO_3 gives mono and di-methyl oxidized carboxylic acid. (b) Cu^{2+}, MoO_4^{2-}, H_3PO_4 system oxidized hetero cyclic ring to carboxylic acid which form one dimensional coordination polymer in the reaction medium.

engineering [6.2]. Current studies prove that hydrothermal synthesis under high pressure and moderate temperature (~ 150 °C) is an effective method for *in situ* ligand generation. Various methods like hydrolysis of -CN and -COOR groups, reduction of -COO-, hydroxylation, C-C bond formation by reductive or oxidative coupling, and cleavage and formation of disulfide bonds, etc were used while *in situ* ligand formation [6.3].

Coordination polymers (CPs) being a new class of hybrid network solids, have potential applications in separation, storage and controlled drug delivery. One-pot synthesis of CPs using mixture of ligand and metal salt is routine process but preparation of ligand from ligand precursor during formation of CPs is still challenging. Recently click chemistry process was utilized with various metal ions such as Zn(II), Cd(II), Cu(I)/Cu(II), and Ag(I) in the construction of CPs [6.4]. The example of *in situ* oxidation during formation of CP is very rare. *In situ* selective oxidation of one or two methyl groups of neocuproine in presence Ni(NO$_3$)$_2$ or Cu(NO$_3$)$_2$ and HNO$_3$ were reported in literature [Figure 6.1a] [6.5]. One 1-D CP was synthesized in hydrothermal reaction of Cu(NO$_3$)$_2$, Na$_2$MoO$_4$, H$_3$PO$_4$ and 5-(4-bromophenyl)-2-(pyridin-4-yl) pyridine. During the course of reaction 5-(4-bromophenyl)-2-(pyridin-4-yl) pyridine was oxidized to 5-(4-bromophenyl) picolinic acid which leads to formation of the CP with Cu^{2+} ion [Figure 6.1b] [6.6].
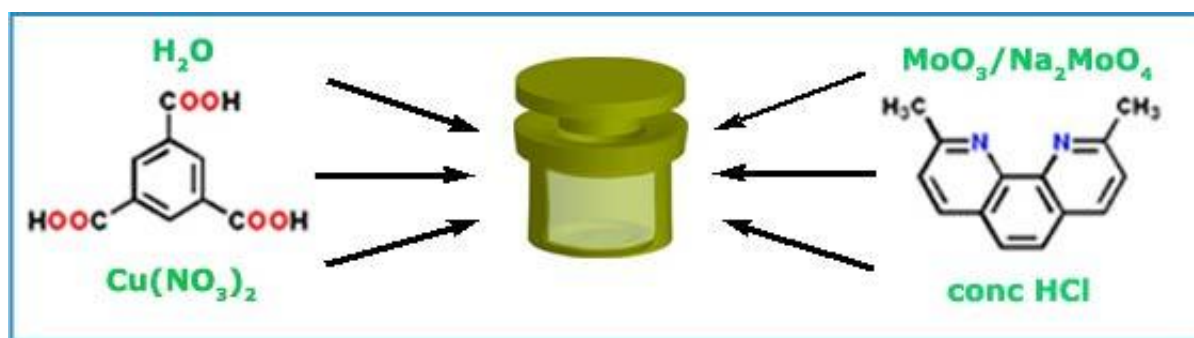

Figure 6.2: Schematic representation of one pot synthesis of ligand and coordition polymer.

6.2 Preparation of ionic salts and coordination polymers

In this work, we have used oxidation of neocuproine to form coordination complex as well as coordination polymer in presence Cu^{2+} and HCl using Na$_2$MoO$_4$/MoO$_3$ as catalyst [Figure 6.2]. Depending upon the reaction condition we got different extent of oxidation of methyl groups of neocuproine, moreover at high temperature and pressure we could able to obtain decarboxylated products as well. In some cases we could able to isolate the polyoxometalates

(POMs) with the oxidation products, which indicate POMs as an active form of catalyst for the oxidation reaction. All these hybrid structures were isolated using almost same ingredient but mild variation in concentrations, pH and temperature of the reaction medium. When we used 1,3,5 benzene tricarboxylic acid (BTC) as co-ligand in the reaction medium, we could able to isolate two CPs, where individual Cu(II) complex of oxidized neocuproine are connected via BTC to form extended network [Figure 6.3].
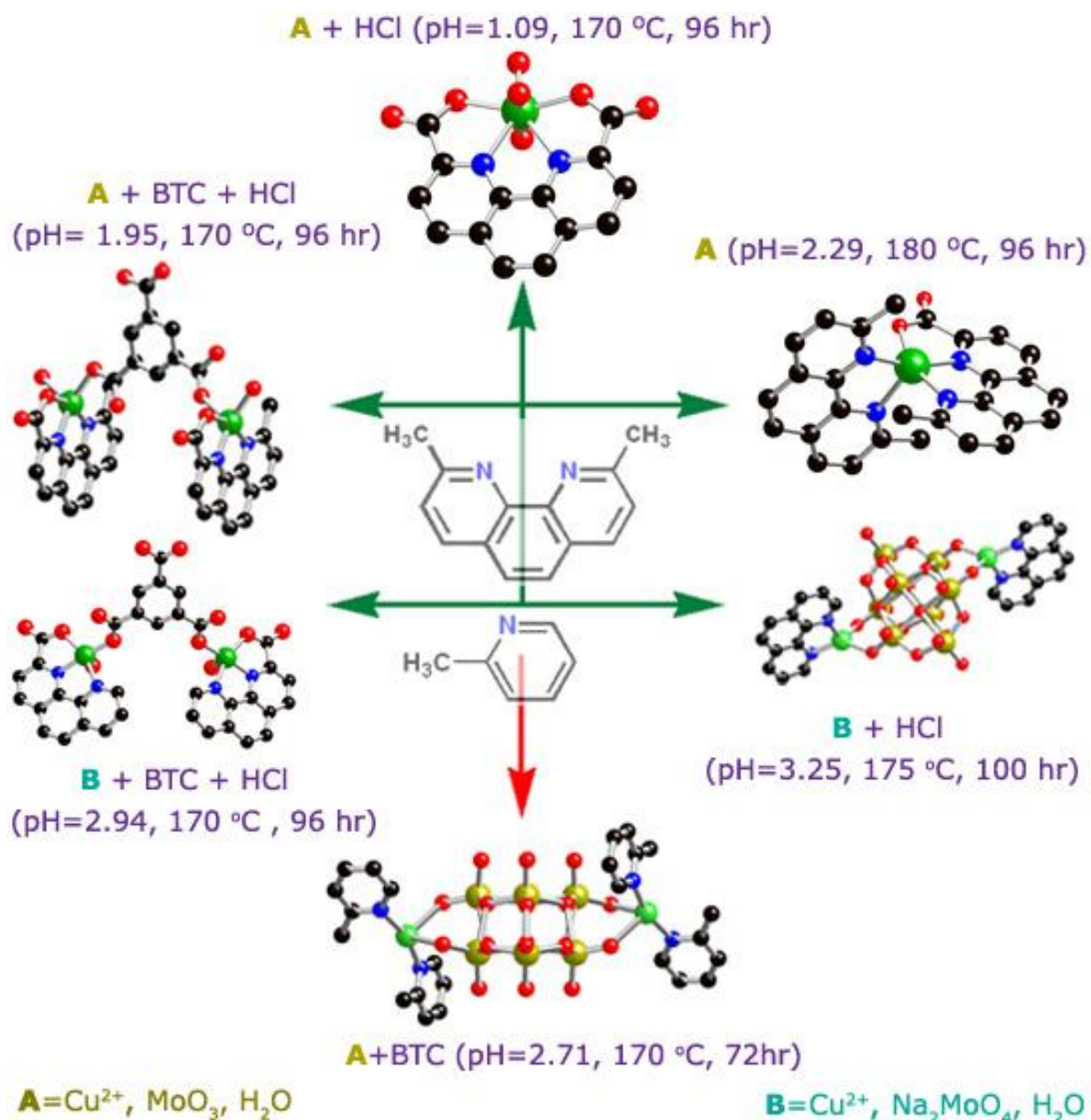

Figure 6.3: Schematic view of *in situ* ligand formation and subsequent synthesis of coordination polymers. Reaction condition for preparation of six organic-inorganic hybrid materials. Color code: Black: C, Blue: N, Red: O, Green: Cu, Yellow: Mo; H atoms are omitted for clarity.

6.3 Crystal structure of ionic composites and coordination polymers

Crystal structure of Mo6-Cu-COPHEN: The crystal structure of Mo_6-Cu-COPHEN {[Cu(neocuproine)-{Phen(Me)(COOH)}] [Mo_6O_{19}]·2H_2O, space group: $P2_1/c$} consists of one Cu(2-carboxy-9-methylphenanthroline) (neocuproine) complex (25% oxidation, 0% decarboxylation), one Lindqvist [Mo_6O_{19}]$^{2-}$ cluster [6.7], and three non-coordinated H_2O molecules [Figure 6.4a]. One of the three H_2O molecules is protonated to balance the charge, but we were unable to locate the proton crystallographically. In Mo6-Cu-COPHEN, the Cu(II) center is pentacoordinated to two nitrogen atoms from one neocuproine ring and one oxygen atom and two nitrogen atoms from 2-carboxy-9-methylphenanthroline. The Cu complex, the [Mo_6O_{19}]$^{2-}$ cluster, and three H_2O molecules are hydrogen bonded [6.8] to form a 3D supramolecular architecture [Figure 6.4c].
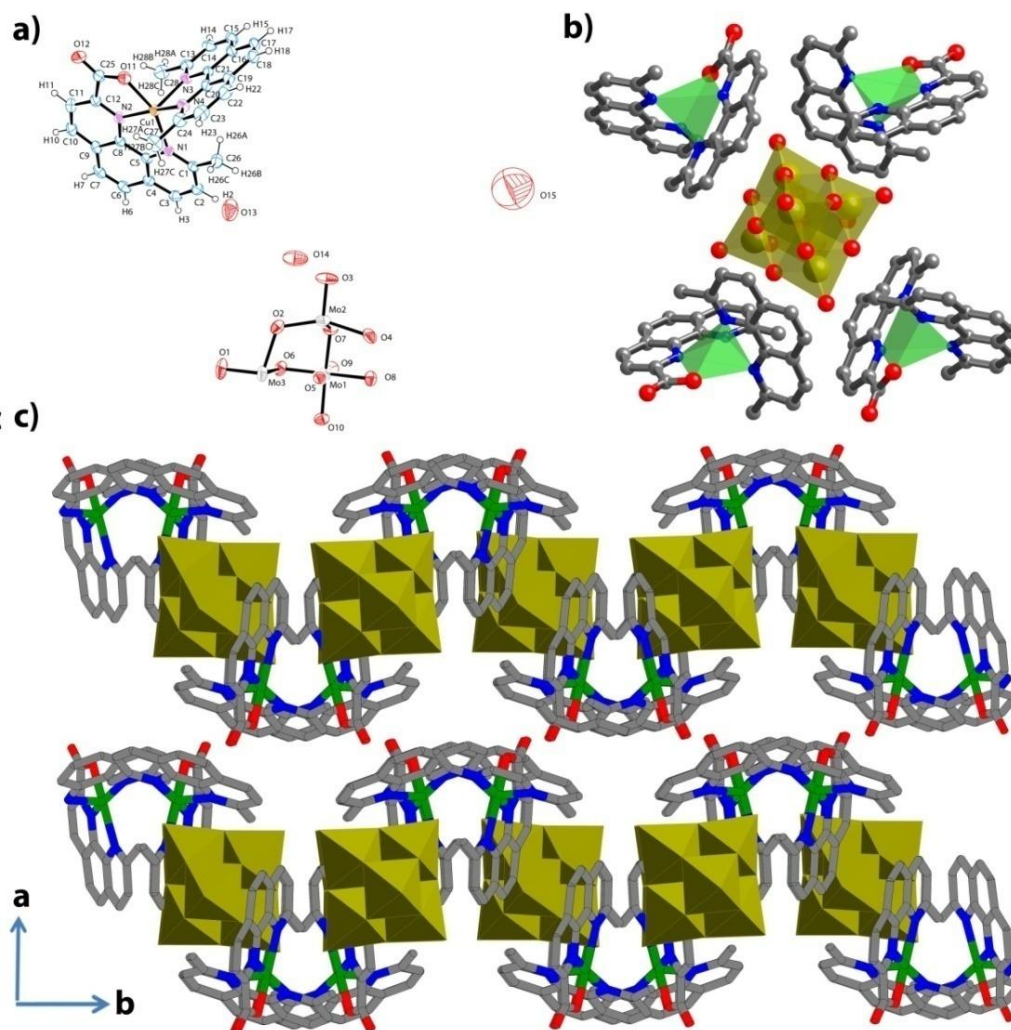

Figure 6.4: (a) ORTEP diagram of Mo6-Cu-COPHEN. (b) building units of Mo6-Cu-COPHEN. (c) Packing diagram for Mo6-Cu-COPHEN composite.

Crystal structure of Cu-NEO-BTC: The asymmetric unit of Cu-NEO-BTC [Cu{Phen(Me)(COOH)}-(BTC), space group: *P*2$_1$/*c*] contains one 2-carboxy-9-methylphenanthroline (50% oxidation, 0% decarboxylation) and BTC is coordinated to the Cu(II) center. The Cu(II) center in Cu-NEO-BTC adopts a distorted octahedral geometry that is occupied by two nitrogen atoms and one oxygen atom of 2-carboxy-9-methyl phenanthroline and three oxygen atoms from BTC. Two of the three carboxylates (-COO$^-$) of BTC act as connectors between two Cu(II) centers to form a 1D chain, whereas the third – COOH group remains free [Figure 6.5]. Hydrogen bonding of this type helps to hold the 3D supramolecular structure together (O···O distance is 2.615 Å).
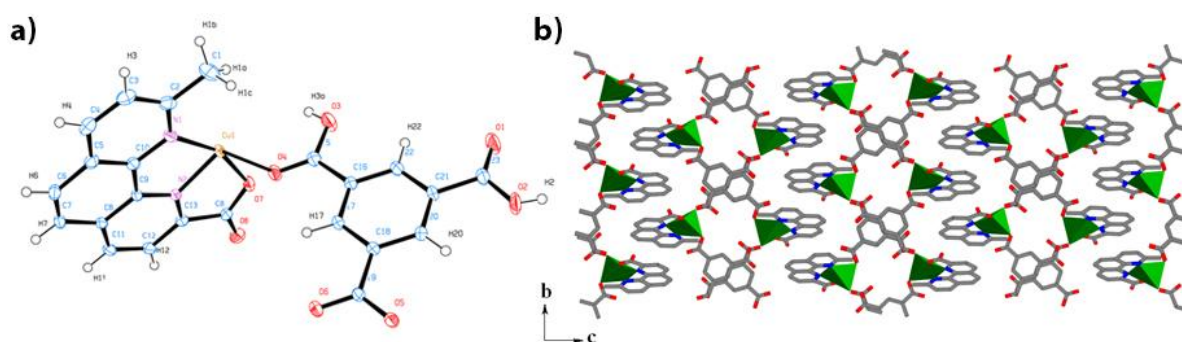

Figure 6.5: (a) ORTEP diagram of Cu-NEO-BTC. (b) One dimensional coordination polymer of Cu-NEO-BTC are assembled via supra-molecular (π-π interaction) interaction.

Crystal structure of Cu-COPHEN: In the crystal structure of Cu-COPHEN [Cu{Phen(COOH)$_2$}-(H$_2$O)$_3$·H$_2$O, space group: *C*2/*c*], we found that the Cu(II) centers are in a pentagonal–bipyramidal environment. The Cu(II) ions are chelated with 2,9-dicarboxyphenanthroline [Phen(COOH)$_2$] (100% oxidation, 0% decarboxylation) and the H$_2$O molecules [Figure 6.6]. The 3D supramolecular arrangement of the Cu(II) complexes and the isolated water molecules in Cu-COPHEN are governed by three different types of hydrogen-bonding interactions [O$_{7carboxy}$–O$_{3coord.water}$: 2.684(4) Å, O$_{3coord.water}$–O$_{8freewater}$: 2.630(6) Å, and O$_{8free water}$–O$_{2carboxy}$: 2.820(5) Å].

Crystal structure of Cu-LAD: In the crystal structure of Cu-LAD [Cu$_2$(Phen-COOH)$_2$(BTC)·3H$_2$O, space group: *Pnma*], the Cu(II) atoms are equatorially connected to two nitrogen atoms and one oxygen atom of 2-carboxyphenanthroline (Phen-COOH; 100% oxidation, 50% decarboxylation) and one oxygen atom from the carboxylate groups of BTC [Figure 6.7a]. The other oxygen atoms of the carboxylate groups of BTC are axially coordinated to other Cu(II) atoms. This unit repeats along the crystallographic *a*-axis to form
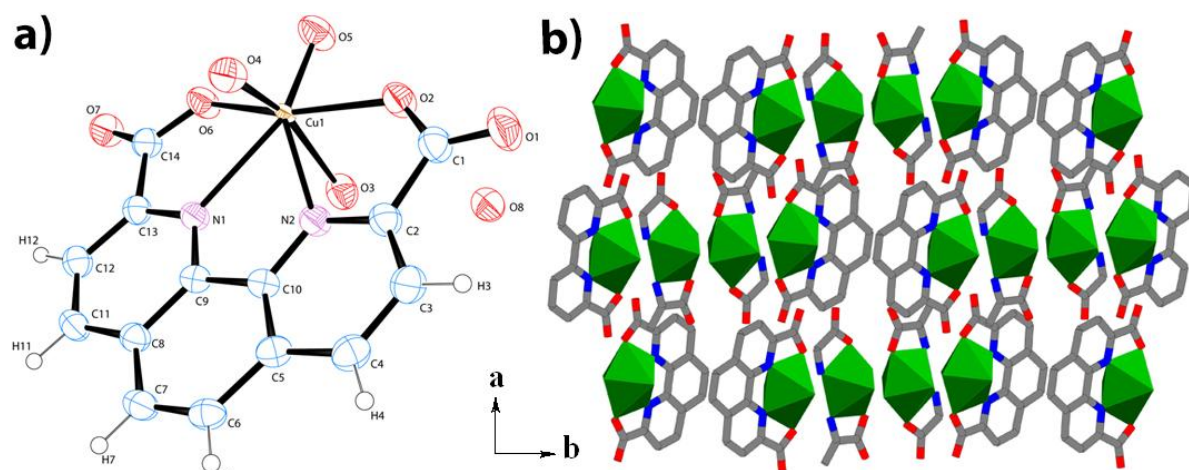
Figure 6.6: (a) ORTEP diagram of Cu-COPHEN. (b) Packing structure of diagram of Cu COPHEN.
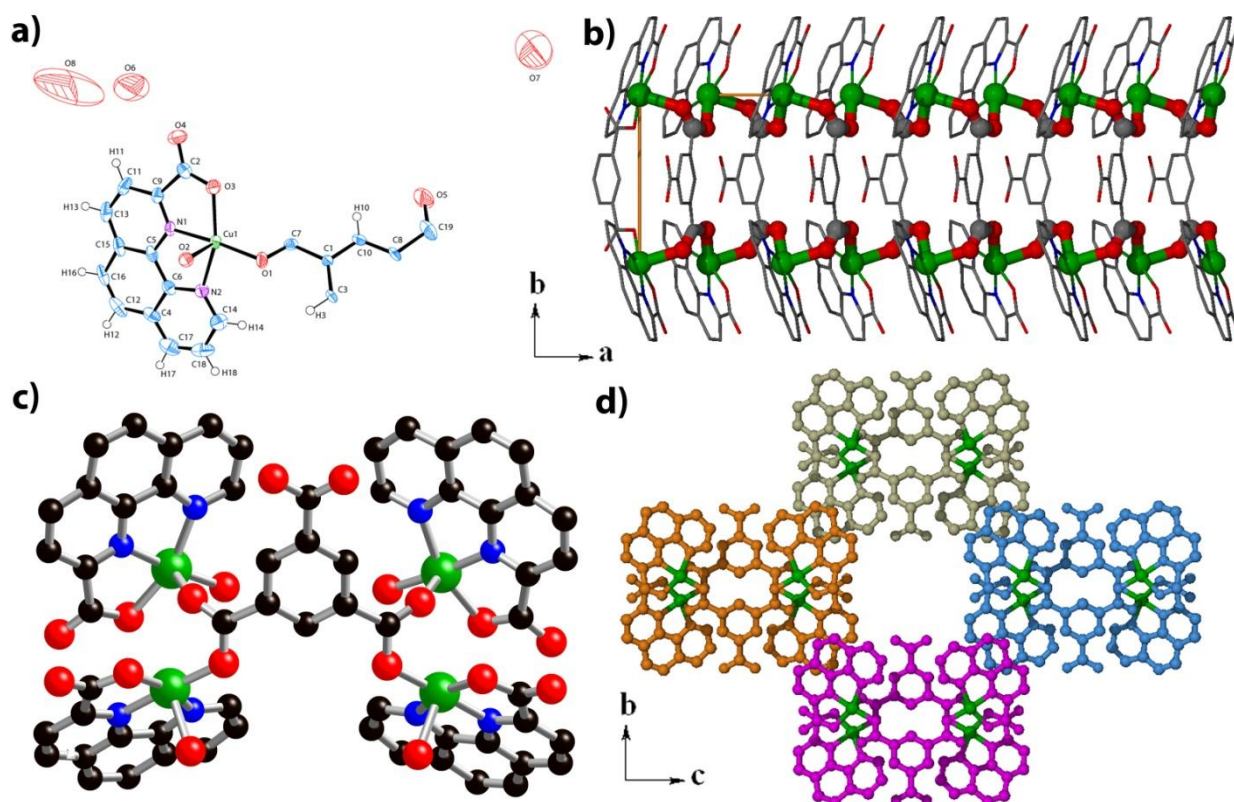
Figure 6.7: (a) ORTEP diagram of Cu-LAD. (b) One isolated fragment of Cu-LAD showing the intra-chain and inter-chain Cu-Cu distance. (c) Complexation of 2–carboxy phenanthroline with Cu(II) and intra-chain and inter-chain connectivity of BTC. (d) Interdigitation of four such fragments via phenanthroline rings creates one dimensional channel, [Colour Code; black: C, green: Cu, red: O, blue: N, yellow: H].

a 1D zigzag $\cdots\mu_2$-OCO$^-$Cu(II)$-\mu_2$-OCO$^-\cdots$ chain. Two carboxylate groups of BTC connect two such chains to form a 1D ladder-like structure, in which the benzene rings act as spacers

between the two chains [Figure 6.7b], Cu–Cu interchain distance of 8.39 Å. Interdigitation of four of these isolated ladders in the *bc*-plane through π–π interactions between the closest aromatic rings (~3.53 Å) of phenanthroline create a 1D channel through the crystallographic *a*-axis. The channels are occupied by hydrogen bonded water molecules (O···O distance is 2.740 Å). The Cu-LAD structure shows a solvent-dependent irreversible phase change upon evacuation, which was confirmed by powder X-ray diffraction (PXRD) patterns [Figure 6.16a].

Crystal structure of Mo8-Cu4-PHEN: Crystals of Mo8-Cu4-PHEN [{Cu(Phen)$_2$}$_2${Mo$_8$O$_{26}$[Cu-(Phen)$_2$]$_2$}·H$_2$O, space group: *C*2/*c*] were isolated with 100% oxidation of the methyl groups followed by 100% decarboxylation of the –COOH functionalities. The higher pH of the reaction medium could be the reason for the facile oxidation of the Me groups and the decarboxylation of the –COOH functionalities. The crystal structure consists of two Cu(phenanthroline)$_2$ tetrahedral complexes, two Cu(phenanthroline)(O)$_2$ tetrahedral units connected to the [Mo$_8$O$_{26}$]$^{4-}$ cluster, and one free H$_2$O molecule. The phenanthroline rings of the Cu(II) complexes are stacked through π–π interactions between the closest aromatic rings (~3.803 Å). The building units are arranged in a parallel fashion in the *ac*-plane to from a 2D sheet; these sheets are stacked on top of each other through the crystallographic *b*-axis to form a 3D architecture [Figure 6.8].
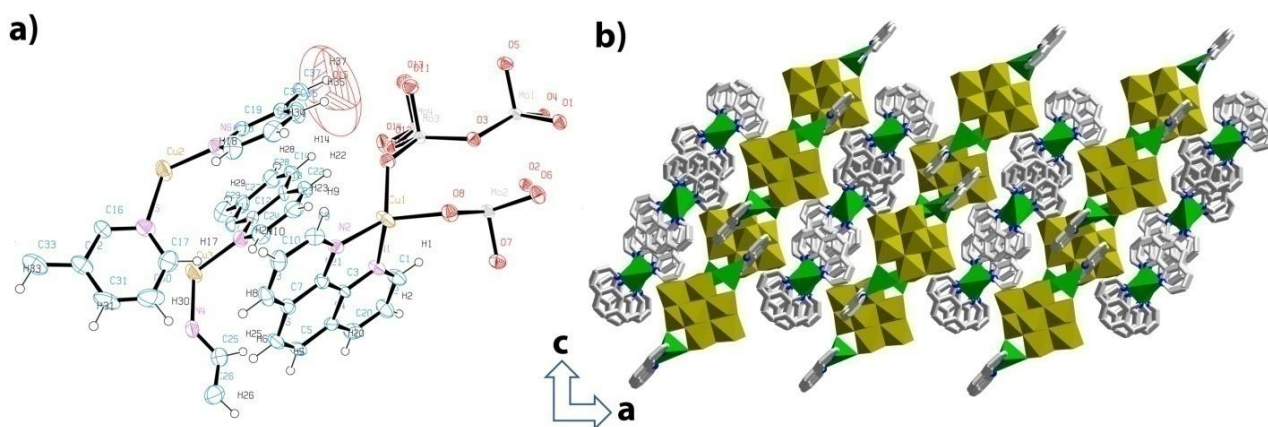
Figure 6.8: (a) ORTEP diagram for Mo$_8$-Cu$_4$-Phen. (b) Packing diagram of Mo$_8$-Cu$_4$-Phen. The image shows the arrangement POM and Cu-complex in crystallographic *ac*-plane. Colour code. Golden: Mo, Green: Cu, Grey: C.

Crystal structure of Mo8-Cu2-5(2PIC): Mo8-Cu2-5(2PIC) [Mo$_8$O$_{26}${Cu(2-picoline)$_2$}$_2$]·2-picoline, space group: *P*2$_1$/*n*] crystallizes in a monoclinic crystal system. The crystal structure of Mo8-Cu2-5(2PIC) consists of two Cu(2-picoline)$_2$ tetrahedral units connected to a

$[Mo_8O_{26}]^{4-}$ cluster and one free 2-picoline. The aromatic rings of two 2-picoline groups in the complex are perpendicular to each other to avoid steric crowding. The two copper centers are connected to the two opposite faces of each $[Mo_8O_{26}]^{4-}$ unit to form a symmetric structure. The $[\{Cu(2\text{-picoline})_2\}_2\}(Mo_8O_{26})]$ units in the *bc*-plane form a 2D architecture [Figure 6.9].
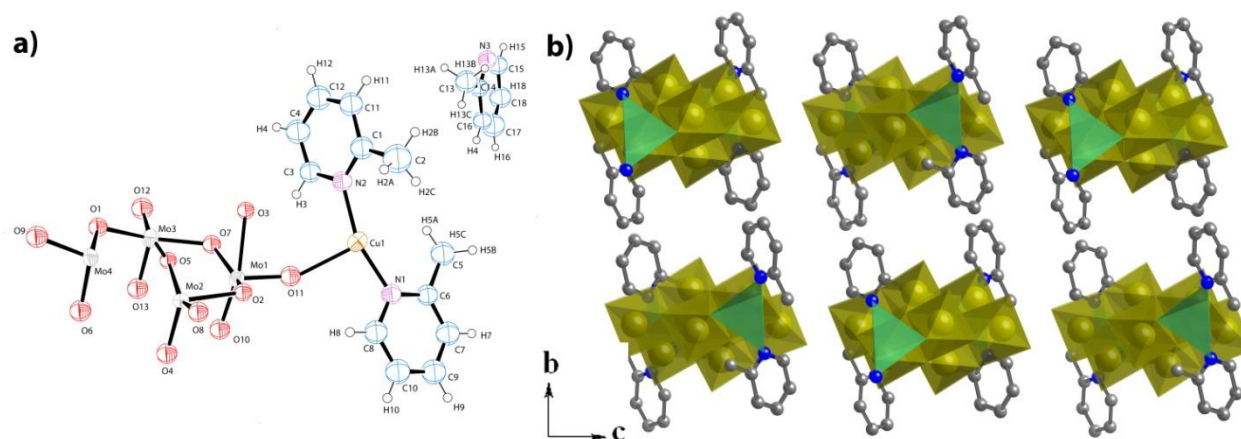

Figure 6.9: (a) ORTEP diagram for Mo8-Cu2-5(2PIC). (b) Packing diagram of Mo8-Cu2-5(2PIC).

6.4 Mechanistic view of the in situ oxidation and CP formation

After analyzing all of the products obtained under the different reaction conditions, we proposed a mechanism for the formation of the CPs through the *in situ* oxidation method [Figure 6.10]. The complexion of Cu(II) with neocuproine is the initial step of the reaction. Although we were unable to isolate a Cu(neocuproine) complex during the course of the reaction, but there are reports of Cu(neocuproine) complexes [6.9]. The oxidation of neocuproine of the Cu(II) complex to 2-carboxy-9-methylphenanthroline, Phen(COOH)$_2$ or Phen in the presence of a catalyst [6.10] (MoO$_3$/Na$_2$MoO$_4$) could be considered as the second and crucial step of the process. We were able to isolate a POM during this process, which supports this speculation. We tried to apply the same oxidation strategy on different Me substituted heterocyclic rings by replacing neocuproine with 2- and 3-picoline, but we did not observe any oxidation product in either case. The Cu–N bond in the Cu(PIC)$_2$(O)$_2$ cluster can rotate freely. The incorrect position (i.e. free rotation) of the Me groups with respect to the Cu(II) atoms could possibly be the reason why 2- and 3-picoline did not undergo oxidation to the desired products. The proper position (i.e. restricted rotation) of the Me groups of neocuproine make the oxidation process facile, because neocuproine is coordinated to Cu(II) with two nitrogen atoms.
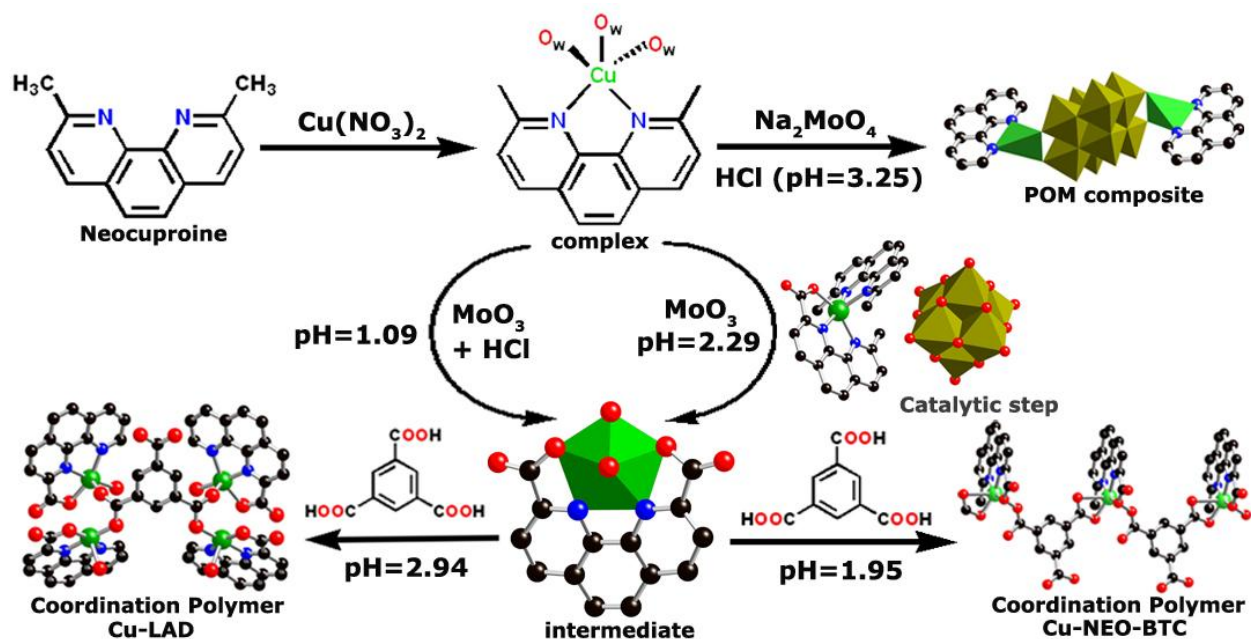
Figure 6.10: Mechanistic view of formation of coordination polymer via metal ligand complexation followed by in situ oxidation of ligand. STEP-I: Formation of Cu(II)-neocuproine complex, STEP-II: Oxidation of methyl groups of neocuproine in presence of POM catalyst, STEP-III: Decarboxylation of one of the carboxylic acid followed by formation of 1D coordination polymer with benzene tri-carboxylic acid.

Many researchers have attempted different synthetic methods for the preparation of ligands during the formation of CPs, but the synthesis of ligands *in situ* to make CPs is unusual and challenging. Although there are a few other general reports, so far only two approaches have been explored to prepare CPs through the in situ oxidation of methyl groups on heterocyclic rings [6.7]. In this work, we used Na_2MoO_4/MoO_3 as a catalyst in presence of Cu^{2+} and HCl to oxidize neocuproine. Upon changing the pH of the solution and the concentration of the catalyst in the reaction, we observed different extents of oxidation of the Me groups of neocuproine. However, under extreme conditions, only decarboxylated products were obtained. After analyzing all of the reaction conditions, we can conclude that higher pH values facilitate both the oxidation and the decarboxylation processes, as in case of Mo8-Cu4-PHEN at pH 3.25, where 100% oxidation followed by 100% decarboxylation occurred. At lower pH values, only oxidation is facile, as in case of Cu-COPHEN at pH 1.09, where 100% oxidation occurred without any decarboxylation. Facile decarboxylation at higher pH values could be attributed to the easy deprotonation of the –COOH group of oxidized neocuproine. The concentration of Cu^{2+} does not affect the extent of oxidation or decarboxylation, but with an increasing concentration of Mo, we observed higher extents of

decarboxylation [Figure 6.11]. In the literature, the formation of Keggin-type POMs as the active forms of catalysts have been speculated. However, in our study we were able to isolate and detect the $[Mo_6O_{19}]^{2-}$ POM in Mo6-Cu-COPHEN and the $[Mo_8O_{26}]^{4-}$ POM in Mo8-Cu4-PHEN and Mo8-Cu2-5(2PIC), which shows that the POM is the active catalyst for the in situ formation of the ligands. Upon using BTC as a coligand, one of the coordination sites of Cu(II) was replaced by the carboxylate group of BTC to form two 1D CPs, Cu-NEO-BTC and Cu-LAD, which were isolated at pH 1.95 and 2.95, respectively. Due to the simultaneous formation of these different phases, we were unable to isolate pure single phases as bulk products, except in the cases of Mo8-Cu2-5(2PIC) and Cu-LAD [Figure 6.16a & 6.16b].
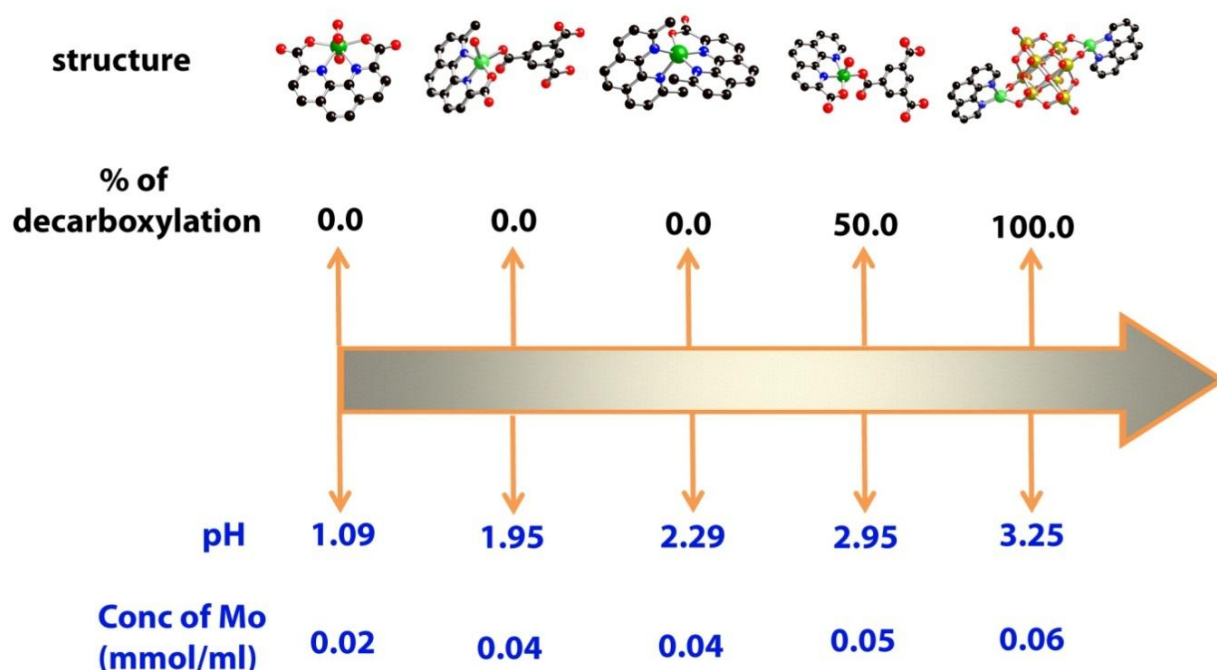

Figure 6.11: Schematic view of effect of pH and concentration of Mo(IV) on extent of decarboxylation of oxidized neocuproine. Decarboxylated products were isolated at higher pH of the reaction medium. With increasing pH there is increase in extend of oxidation and at pH=3.25, 100% decarboxylated product is obtained.

6.5 Gas adsorption studies of coordination polymers

To understand the porous nature of the Cu-LAD and Cu-NEO-BTC CPs, we carried out H_2 and CO_2 adsorption studies on evacuated sample. Before evacuation, both compounds were exchanged with a low-boiling solvent. The Langmuir and BET (Brunauer, Emmett and Teller) surface areas of Cu-LAD were calculated from N_2 adsorption isotherm as 31 and 16 m^2g^{-1}, respectively. Cu-LAD adsorbs 42 mLg^{-1} of H_2 gas at 760 Torr and 77 K and 0.95

mmolg^{-1} of CO_2 at 298 K and 1 bar pressure, whereas Cu-NEO-BTC adsorbs 5 mLg^{-1} of H_2 gas and 0.22 mmolg^{-1} of CO_2 under the same conditions. The water vapour uptake for Cu-LAD and Cu-NEO-BTC at 293 K and 1 bar pressure are 52 and 14 mLg^{-1}, respectively [Figure 6.12].
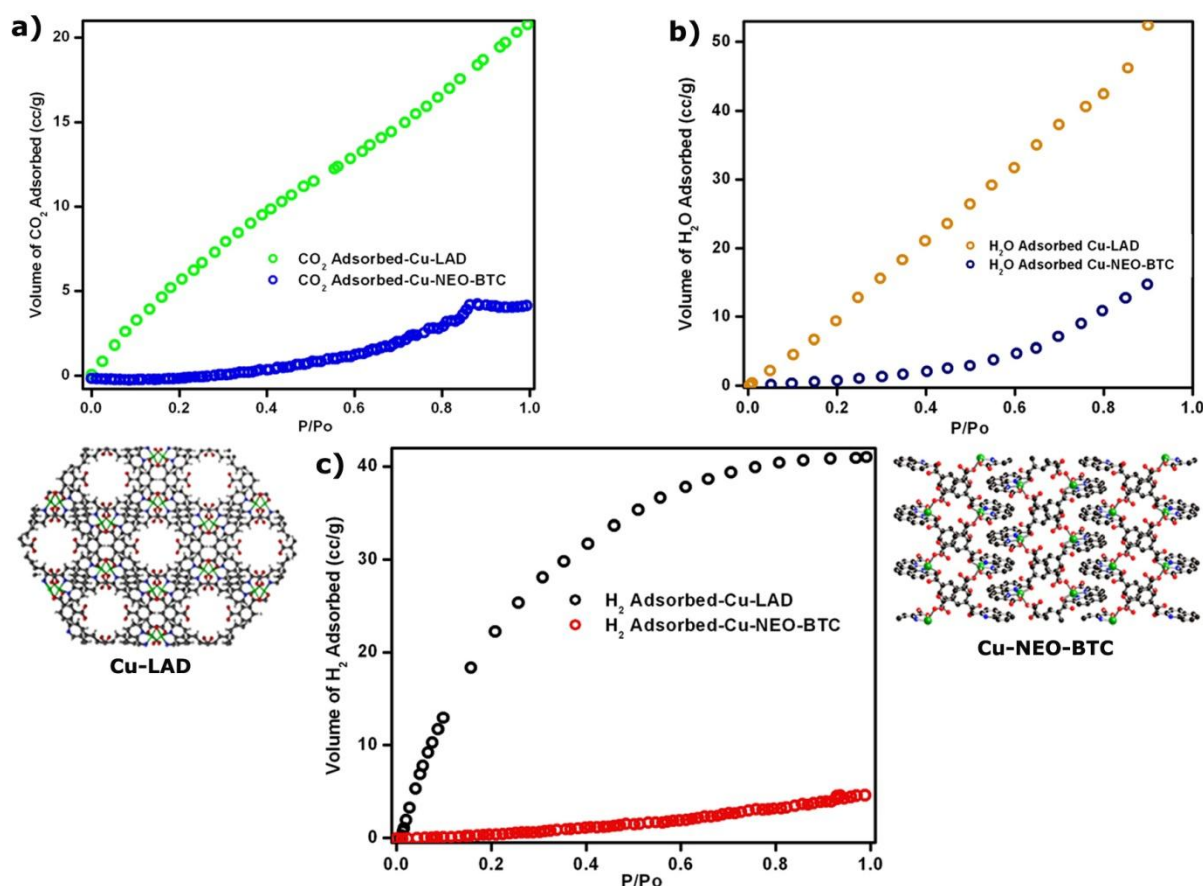

Figure 6.12: (a) The CO_2 adsorption isotherm for Cu-LAD and Cu-NEO-BTC at 298 K and 1 bar pressure. (b) The H_2O vapor adsorption isotherm for Cu-LAD and Cu-NEO-BTC at 298 K and 1 bar pressure. (c) The H_2 adsorption isotherm for Cu-LAD and Cu-NEO-BTC at 760 Torr & 77K. Left hand side picture shows porous nature of Cu-LAD and right hand side picture shows non porous nature of Cu-Neo-BTC. Only adsorption is plotted and desorption has been removed for clarity.

6.6 Magnetic study of Cu-LAD

We anticipated that down to a certain temperature, Cu-LAD should exhibit 1D magnetic character [similar to Single Chain Magnets (SCMs)] since the intra-chain magnetic coupling of Cu(II) ions via the carboxylate linkage is stronger due to a shorter distance (3.99 Å) than the inter-chain coupling via the BTC ligand (8.39 Å). The temperature dependence of magnetic susceptibility (χ) and χT for Cu-LAD is shown in Figure 6.13a. The χT value for

two Cu(II) of Cu-LAD at 300K is 1.08 emu Kmol^{-1} Oe^{-1}. Upon cooling, the χT (ZFC) value remains almost constant down to ~120 K, followed by a gradual decrease until 40 K. Below

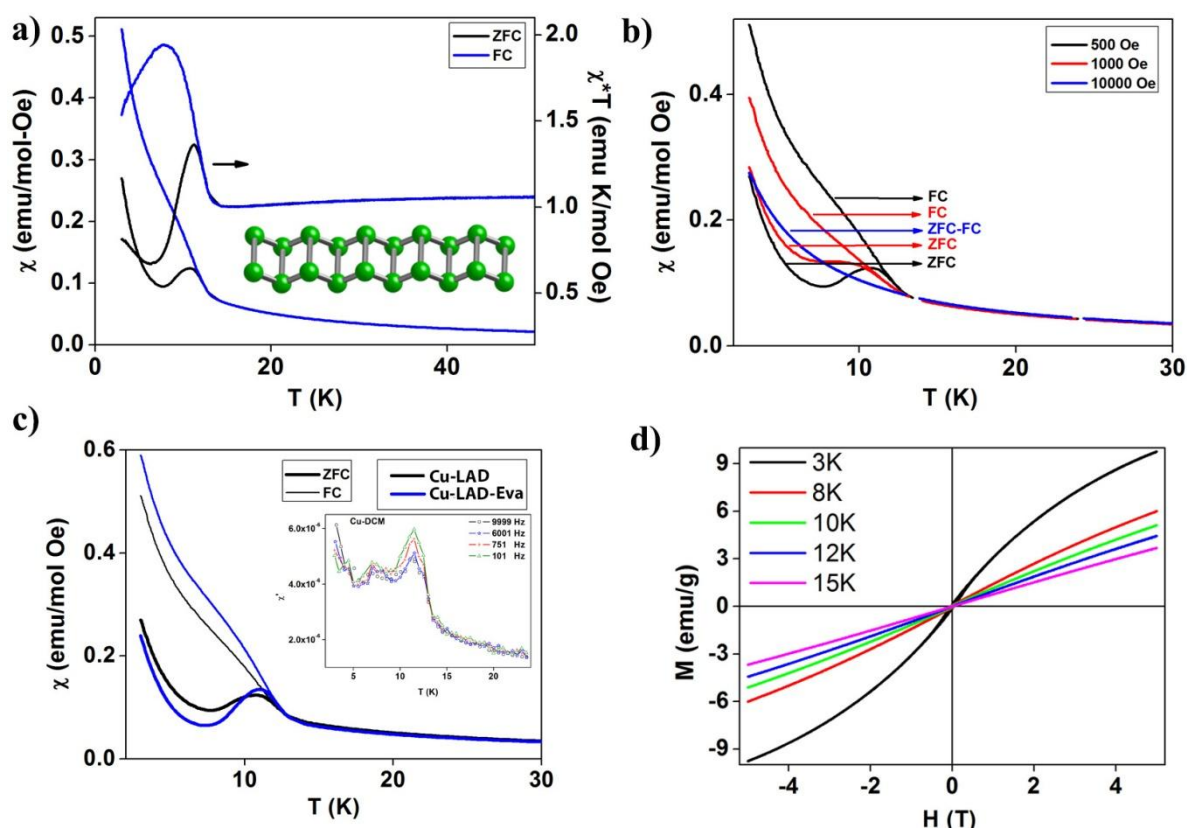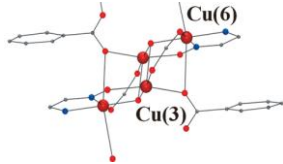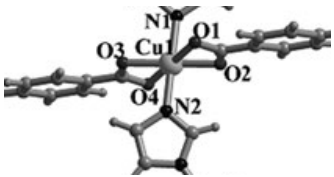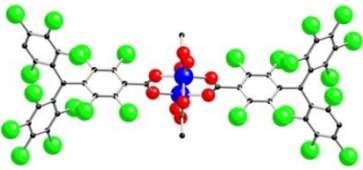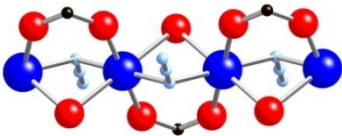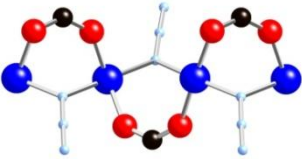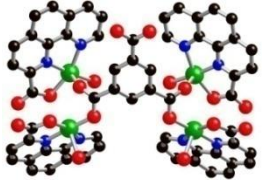**Figure 6.13:** (a) The temperature dependence of the magnetic susceptibility χ (left axis), the χT (right axis) for Cu-LAD, inset image shows the finite length of a isolated Cu-LAD. (b) The temperature dependence of the magnetic susceptibility χ for Cu-LAD at different applied fields. (c) The temperature dependence of the magnetic susceptibility χ (thick:ZFC & thin:FC) for Cu-LAD (black), Cu-LAD-Eva (blue), inset temperature dependance of real part ac susceptibility for Cu-LAD. (d) MH loops taken at temperatures 3, 8, 10, 12 and 15 K for Cu-LAD. Below 12 K the magnetization starts showing non linear behavior due to the onset of ferromagnetic coupling. At 3 K the magnetization shows strong non-linearity however the magnetization does not saturate up to 5 T for all the measured temperatures.

40 K, the χT (ZFC) value falls at an increased rate down to 15 K, then again increases with a peak at the 12K value, below which it falls rapidly until 8K and then again rises until temperature of 3K. The rapid increase of χT (ZFC) below 14 K shows the signature of the onset of ferromagnetic exchange interactions between the closest Cu(II) atoms within a chain, [Cu(II)–Cu(II) distance 3.99 Å]. The peak at 12K indicates the occurrence of an antiferromagnetic transition due to the inter-chain magnetic interaction. The rise below 8K indicates the second order phase transition to a totally magnetically ordered state. The reason

for this ferromagnetic behaviour is due to the parallel and stacked orientation of two '−μ_2-OCO–Cu(II)–μ_2-OCO–'chains in Cu-LAD [with a Cu–Cu distance of 8.39 Å]. To investigate the nature of the 3D magnetic ordering in Cu-LAD and to probe the field dependence of the magnetic susceptibility, we measured χ (in both ZFC and FC method) at different applied fields [Figure 6.13b]. Up to an applied field of 1000 Oe, the ZFC-FC curves show strong bifurcation, and show the onset of a ferromagnetic transition at around 14 K and an inflection point at around 8 K. This bifurcation disappears at a field of 10 kOe as a sufficiently higher field can overcome both intra and inter-chain magnetic interactions.

At this field the Zeeman energy will be higher than the uniaxial anisotropy energy, therefore an increasing number of spins will orient in the field direction with decreasing temperature. There is no report in the literature where a ZFC curve shows an upright behaviour below 8 K after showing a peak such as we have observed at 12 K due to long range antiferromagnetic ordering. There are only a handful of examples where the SCM type of interaction (intra-chain ordering) is followed by the modified-SCM type of behaviour when inter-chain magnetic coupling decreases uniaxial anisotropy [6.11]. The *ac* susceptibility measurements also showed these peaks but without any frequency shift, thereby ruling out spin-type behaviour [Figure 6.13c, Inset]. Probably, this is the first example of a Cu(II) based double chain magnetic framework where such types of competing magnetic interactions and their temperature and field dependencies are observed. So far only two Cu(II) based MOFs are reported where antiferromagnetic and ferromagnetic interactions have been observed [6.12]. One of them being [Cu(F-pymo)$_2$(H$_2$O)1.25]$_n$ where both antiferromagnetic (a broad hump) and weak ferromagnetic (spin canting) interactions were observed at 60 K and 17 K respectively [6.12a]. Whereas in another Cu(II) based MOF [Cu$_3$(PTMTC)$_2$ (py)$_6$(CH$_3$CH$_2$OH)$_2$ (H$_2$O)], [py: pyridine] long range antiferromagnetic ordering was observed below 2 K. To check the uniaxial magnetic ordering and the effect of the perturbation exerted by the guest (water) molecules in Cu-LAD, we compared the χ-T and M-H measurements on as synthesized, evacuated and re-solvated samples [Figure 6.13c]. As mentioned previously the PXRD study showed that the evacuated and re-solvated Cu-LAD crystal structure is different from the as-synthesized Cu-LAD [Figure 6.14a]. However, the magnetic study of as-synthesized, evacuated and re-solvated Cu-LAD shows that the magnetic behaviour of these three phases remains largely unchanged with little difference at low temperatures. This indicates that the removal of the guest molecule does not affect the

Table 5.1: Structural and magnetic aspects of Cu-carboxylate based MOF

S.N	Formula (figure are reproduced from CIF)	Structure	Interaction	χT at 300 K	Ref No.
1	$[Cu_4(OH)_2\{(py)C(CN)NO\}_2(O_2CPh)_4]_{2n}$ ·$n[Cu_4(OH)_2\{(py)C(CN)NO\}_2(O_2CPh)_4]$	Chain	Anti-ferromagnetic	0.08 emu K mol^{-1}	12d
2	$\{[Cu(4\text{-imidazole-1-yl-benzoate})_2]\}_n$	2D-Structure	No interaction	0.39 emu K mol^{-1}	12e
3	$Cu_2(PTMMC)_2(O_2CH_3)_2(H_2O)_2$ PTMMC=Perchlorinated monocarboxylic triphenylmethyl radical	Complex	Anti-ferromagnetic	0.225 emu K mol^{-1}	12f
4	$Cu(L)(N_3)(H_2O)_{0.5}]_n$ L=Isonicotinate N-oxide	Chain	ferromagnetic	0.64 emu K mol^{-1}	12g
5	$Cu(L)(N_3)(H_2O)_{0.5}]_n$ L=Nicotinate N-oxide	Chain	ferromagnetic	0.57 emu K mol^{-1}	12g
6	Cu-LAD	Ladder	ferromagnetic	0.54 emu K mol^{-1}	This work

122

overall intra and inter-chain magnetic coupling. Moreover, these results also present an indication of the absence of any magnetic interaction (dipolar or exchange) outside these isolated double chain magnets in 3D and the magnetic behaviour seen by us in this study purely reflects individual Cu-LAD behaviour. Additionally, the major peaks at 722 cm^{-1}, 846 cm^{-1}, 916 cm^{-1}, 1365 cm^{-1}, 1435 cm^{-1}, 1566 cm^{-1}, and 1622 cm^{-1} in the IR spectra were similar for as-synthesized, evacuated and re-solvated samples [Figure 6.14b], indicating the retention of the basic skeleton (double chain) even though the H-bonded structure collapses after evacuation of the guest water molecules. The SEM and TEM (Transmission electron microscopy) images of as-synthesised and evacuated Cu-LAD show the morphological change after evacuation [Figure 6.15]. This observation is also in agreement with our earlier
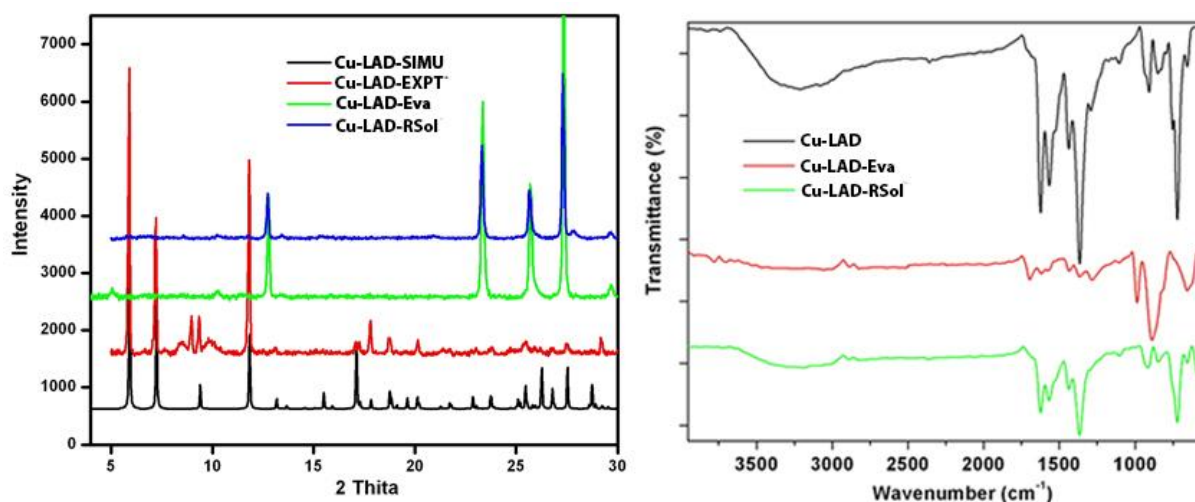
Figure 6.14: (a) Comparison of the PXRD patterns of as-synthesized Cu-LAD (Cu-LAD-EXPT), evacuated Cu-LAD (Cu-LAD-Eva) and re-solvated Cu-LAD (Cu-LAD-RSol) with respected to simulated PXRD pattern (Cu-LAD-RSol) obtained from single crystal X-ray data. The evacuated sample is crystalline but the structure of different. (b) Comparison of the IR Spectra of as-synthesized sample (Cu-LAD), evacuated sample (Cu-LAD-Eva) and re-solvated sample (Cu-LAD-RSol).

conclusion that the magnetic behaviour observed in Cu-LAD originates only from the double chain. It is noteworthy that in most MOF based molecular magnets the entrapped guest molecules in the pores have low boiling points and tend to evaporate on approaching room temperature, thereby limiting its application [6.13].

6.7 Investigation of microstructure and morphology of Cu-LAD and Cu-LAD-evacuated

Selected Area Electron Diffraction (SAED) pattern of the Cu-LAD and Cu-LAD-Eva shows the crystallinity of the samples. These gives further proof that the Cu-LAD-Eva remains crystalline after evacuation even though there is change in crystalline structure. The TEM
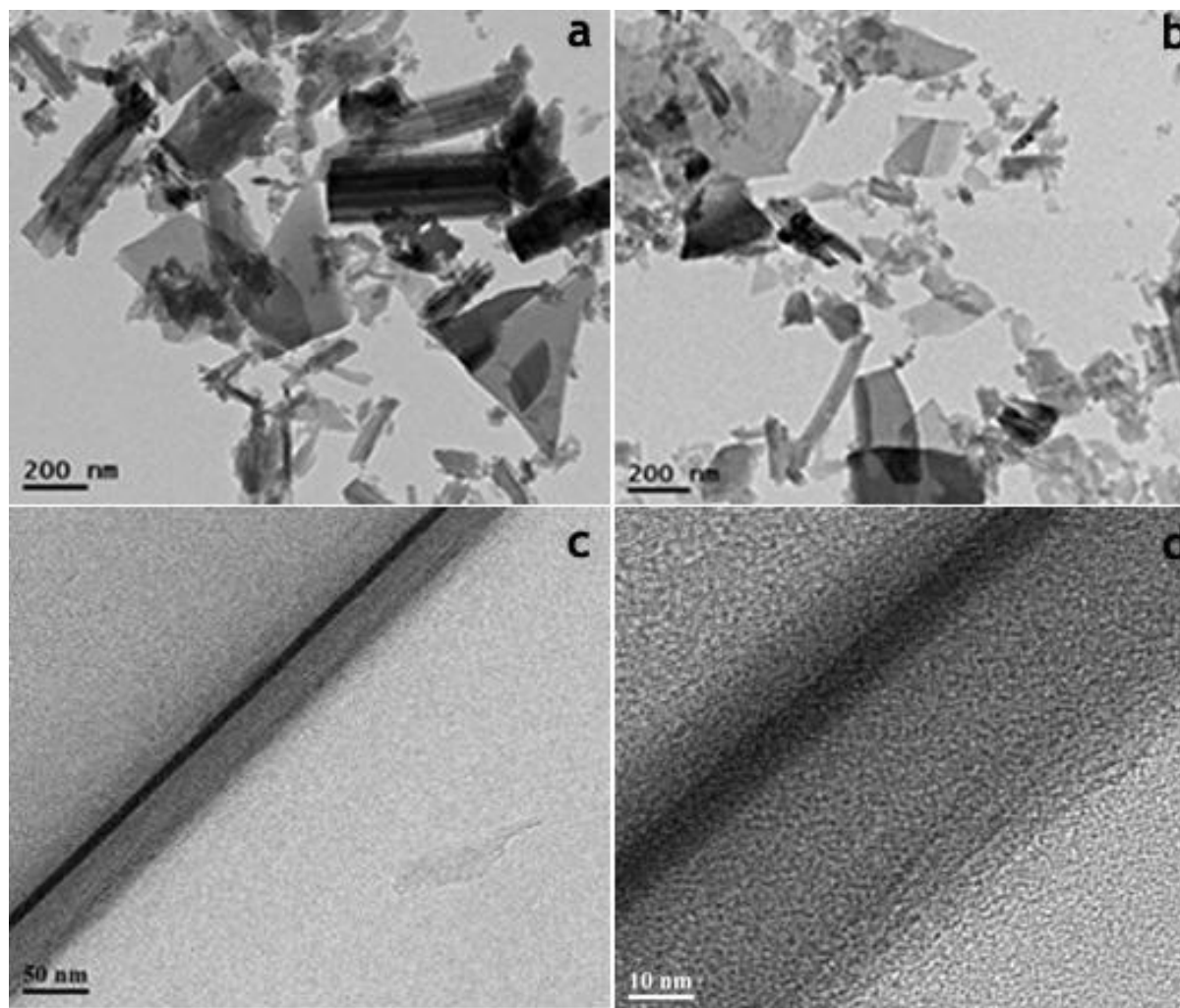
Figure 6.15: (a) TEM image of as-synthesized compound showing the crystalline form of Cu-LAD before evacuation. (b) TEM image of nanocrystalline phase of Cu-LAD after evacuation. c) TEM image showing edges of nanocrystal of evacuated Cu-LAD d) Zoomed nanocrystal of evacuated Cu-LAD.

image has shown in Figure 6.15, we observed the rod like structure for both Cu-LAD and Cu-LAD-Eva. In Cu-LAD each rod like structure is made up of several small diameter rods which bundles together to form the microcrystalline Cu-LAD rods. The Cu-LAD evacuated samples images show that after evacuation these bundles of rods are separated and forms

individual rods nanocrystalline rods. The sizes of individual rods are from 30 to 40 nm in diameter and several hundred nanometer in length.

6.8 Magnetic property of as-synthesized, evacuated and re-solvated Cu-LAD

We anticipated that in contrast to SCMs, the interplay of competing *intra* and *inter* chain magnetic interactions within a DCM (double chain megnet) framework might present more complex, interesting, tunable behavior at low temperature. Indeed, we observed a unique and interesting magnetic behavior where below the paramagnetic region Cu-LAD behaves quite similar to conventional SCMs down to certain temperature.

To investigate the nature of magnetic interaction in Cu-LAD and to probe the field dependence of the magnetic susceptibility, we measured ZFC and FC χ at different applied fields. It is observed that the peak position in ZFC does not change appreciably beyond an applied field of 1000 Oe but the peak shows significant broadening along with the strong bifurcation of ZFC-FC curves, showing irreversibility of ZFC and FC magnetization curves. The bifurcation temperature becomes weaker with increasing field strength. At 10 kOe field, the complete disappearance of bifurcation of ZFC-FC curves and disappearance of the onset of ferromagnetic transition around 14 K and inflection point around 8 K (which is seen for 500, 1000 Oe data) indicates that a sufficiently higher field (1T) can overcome both *intra* and *inter* chain magnetic interactions as at this field the Zeeman energy will be higher than uniaxial anisotropy energy therefore increasing number of spins will orient in the field direction with decreasing temperature. Below 15 K, the FC magnetization curve shows a gradual increase and changes its slope further at 8 K and shows no saturation effect till the lowest measured temperature. Similar to FC curve, the ZFC magnetization also shows upright behavior, till it reaches a maximum at 12 K, then decreases beyond 8 K which is followed by an increase till 3 K. The maxima at 12 K in the ZFC-χ is signature of long-range antiferromagnetic ordering induced by π-π interaction of two parallel '$\cdots-\mu_2$-OCO$-$Cu(II)$-\mu_2$-OCO$-\cdots$'chains within a double chain [6.14]. This type of ZFC-FC divergence has been observed in few cases and one such example being [Ni(μ-N$_3$)(bmdt)(N$_3$)]$_n$(DMF)$_n$, where ZFC-χ reaches a peak at 14 K and diverges out from FC-χ at 16 K but the ZFC-χ does not show any upright behavior at low temperature [6.15].

To further investigate the *intra-* and *inter*-chain magnetic interactions in various temperature regions, we performed isothermal magnetization experiment at different temperatures around

which magnetic transition was observed in magnetic susceptibility study. At 12 K the magnetization starts showing non linear behavior due to the onset of ferromagnetic coupling. On the other hand at 15 K the magnetization shows complete linear behavior. At 3 K the magnetization shows strong non-linearity[Figure however the magnetization does not saturate up to 5 T for all the measured temperatures. The value of coercive field (H_C) at 12 K is 60 Oe which increases up to 422 Oe at 8 K, then again decreases to 296 Oe at 3 K which is consistent with the features shown by χ-T curves. The decrease in the coercivity below 8 K suggests the reduction in the uniaxial effective anisotropy. The higher value of H_C at 8 K shows the enhanced ferromagnetic ordering around the transition temperature which was also observed in temperature dependent magnetization as high μ_{eff} value. The remnant magnetization (H_r) decreases continuously.

6.9 Conclusion

In conclusion, we have successfully developed a synthesis strategy to prepare ligands through the POM-catalyzed in situ oxidation of the precursor during the synthesis of CPs. In our study, we tried to determine the effects of pH, temperature of the reaction medium, and concentration of the reagents on the extent of the catalytic oxidation and decarboxylation of the Me groups of neocuproine. Upon introduction of BTC to the reaction medium, we were able to isolate coordination polymers. Further mechanistic studies with different Me-substituted heterocyclic rings suggest the requirement of the proper orientation (confinement) and proximity of the Me group to the Cu(II) center for oxidation. This strategy was utilized further to design new double chain magnetic framework (Cu-LAD). These types of magnetic frameworks are rare in literature and especially with Cu(II) this is the first report. Moreover the synthesis was predesigned and performed *in situ* which decreased the number of steps. Cu-LAD is the first example of a Cu(II) based DCM framework where we demonstrated a modified-SCM type of behaviour with rich interplay between *intra* and *inter* chain Cu(II) spins at low temperatures resulting competing ferromagnetic and antiferromagnetic interactions. Additionally, it is remarkable that inherent magnetic behaviour of Cu-LAD remains intact even after the framework collapses indicating absence of magnetic interaction outside these isolated double chains. This robust magnetic nature of Cu-LAD type materials may be useful in magnetic device related applications.

6.10 Experiment Section

Materials and general methods: All reagents were commercially available and used as received. Powder X-ray diffraction (PXRD) patterns were recorded on a Phillips PANlytical diffractometer for Cu Kα radiation (λ = 1.5406 Å), with a scan speed of 2° min^{-1} and a step size of 0.02° in 2θ. Thermogravimetric (TGA) experiments were carried out in the temperature range of 25–700 °C on a SDT Q600 TG-DTA analyzer under N_2 atmosphere at a heating rate of 10 °C min^{-1}. All low pressure gas adsorption experiments (up to 1 bar) were performed on a Quantachrome Quadrasorb automatic volumetric instrument. All the magnetic measurements were done using a Physical Property Measurement System (PPMS) from Quantum Design Inc. San Diego, USA equipped with a 7 Tesla superconducting magnet and a vibrating sample magnetometer. The magnetic signal from the sample holder was negligible to affect our data accuracy. These measurements were carried out on polycrystalline samples. DC magnetization vs. T curves were taken at 500 Oe field in field cooled (FC) and zero field cooled (ZFC) modes with heating/cooling rate of 2 K per minute. Magnetizations vs. field loops were taken in a field sweep from -50 kOe to +50 kOe at a rate of 75 Oe/sec. We used the FEI (model Tecnai F30) high resolution transmission electron microscope (HRTEM) equipped with field emission source operating at 300 KV voltage to image the drop coated dilute solution of Cu-LAD and Cu-LAD evacuated in ethanol on carbon-coated copper TEM grid.

Preparation of [Cu(Neo){Phen(Me)(COOH)}][Mo$_6$O$_{19}$]·2H$_2$O *[Mo6-Cu-COPHEN]* : A mixture of 0.1 g Cu(NO$_3$)$_2$·3H$_2$O (0.4mmol), 0.2 g MoO$_3$ (0.35mmol), 0.1 g (0.48mmol) neocuproine and 10 mL water was stirred for 20 min (pH=2.29), then kept in a Teflon lined autoclave at 180°C for 4 days. *Element Analysis:* Found (%) C= 33.31, H= 2.23, N= 5.49; Calc. (%) C= 33.70, H= 2.10, N= 5.62.

Preparation of Cu{Phen(Me)(COOH)}(BTC) *[Cu-NEO-BTC]*: A mixture of 0.1 g of Cu(NO$_3$)$_2$·3H$_2$O, 0.2 g (0.35mmol) MoO$_3$, 0.05 g(0.24mmol) neocuproine, 0.35 g (1.67mmol) 1,3,5 benzene tri-carboxylic acid and 10mL water were stirred for 15 min. The pH of the reaction was carefully maintained at 1.95. The mixture was transferred to 25 Teflon lined autoclave and kept at 170°C for 4 days. *Element Analysis:* Found (%) C= 53.91, H= 2.97, N= 5.77; Calc. (%) C= 54.12, H= 2.75, N= 5.49.

Preparation of Cu{Phen-(COOH)$_2$}(H$_2$O)$_3$·H$_2$O *[Cu-COPHEN]* : A mixture of 0.05 g (0.2mmol) Cu(NO$_3$)$_2$·3H$_2$O, 0.2 g (0.35mmol) MoO$_3$, 0.05 g (0.24mmol) neocuproine in10

mL water were stirred for 10 min. The pH of the solution was adjusted to 1.09 using 0.05 mL conc. HCl and finally the solution was kept in 25mL Teflon lined autoclave at 180 °C for 4 days. ***Element Analysis:*** Found (%) C= 42.51, H= 1.69, N= 7.23; Calc. (%) C= 42.67, H= 1.52, N= 7.11

Synthesis of Cu$_2$(Phen-COOH)$_2$(BTC).3H$_2$O *[Cu-LAD]* : Cu$_2$(Phen-COOH)$_2$(BTC)·3H$_2$O was prepared using mixture of Cu(NO$_3$)$_2$.xH$_2$O (1 mmol), neocuproine (0.4 mmol), Na$_2$MoO$_4$ (2 mmol) and 1,3,5-BTC (0.9 mmol) in 18mL deionized water in hydrothermal condition at 170°C for 4 days. We tried the reaction in the pH range of 1.45 to 3.25. However, we could able to isolate the product in 2.90-3.05 pH range. The quality of the crystal suitable for X-ray diffraction was obtained when pH was equal to 2.95. ***Element Analysis:*** Found (%) C= 48.20, H= 2.81, N= 6.70; Calc. (%) C= 48.80, H= 2.67, N= 6.50.

Preparation of [{Cu(Phen)$_2$}$_2${Mo$_8$O$_{26}${Cu(Phen)$_2$}$_2$}·H$_2$O] *[Mo8-Cu4-PHEN]*: A mixture of Cu(NO$_3$)$_2$·xH$_2$O (0.1875gram, 1mmol), neocuproine (0.083gram, 0.4mmol) and Na$_2$MoO$_4$ (0.43gram, 2mmol) was stirred for half an hour in 15 mL water. The pH of the solution was adjusted to 3.25 by using conc. HCl. The mixture was kept in 25mL Teflon lined autoclave at 175 °C for 100 hours. ***Element Analysis:*** Found (%) C= 33.82, H= 2.05, N=6.71; Calc. (%) C= 34.08, H= 1.89, N= 6.63.
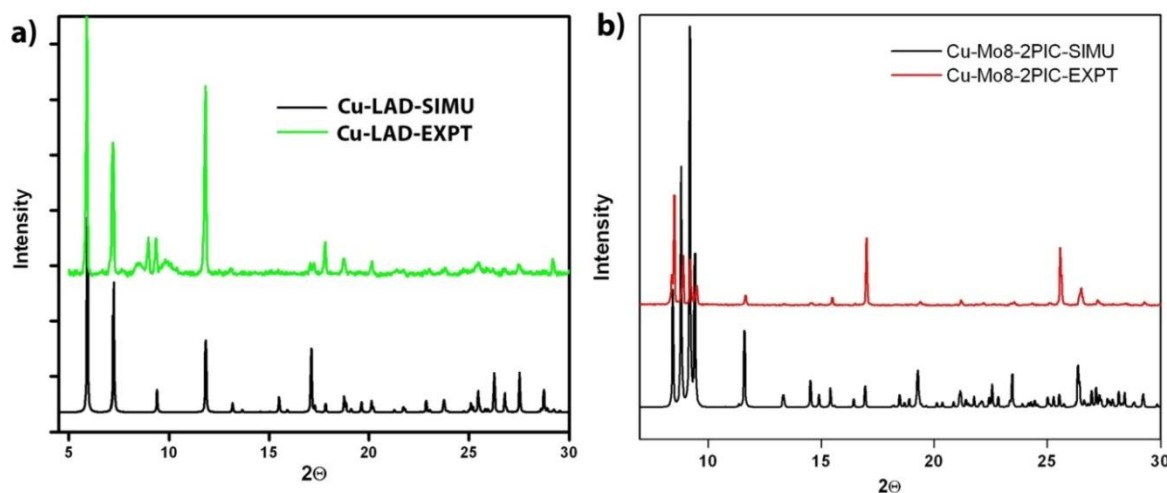
Figure 6.16: Comparison of experimental and simulated PXRD pattern of Cu-LAD and Cu-Mo8-2PIC. The match shows the bulk purity of the compound with single crystalline phase.

Preparation of [Mo$_8$O$_{26}${Cu(2-PIC)$_2$}$_2$·2-PIC] *[Mo8-Cu2-5(2PIC)]*: A mixture of Cu(NO$_3$)$_2$·3H$_2$O (0.1 gram, 0.4mmol), MoO$_3$(0.2gram, 0.35mmol), 1,3,5 benzene tri-carboxylic acid (0.35gram) and 1.5 mL 2-methyl pyridine was stirred in 10 mL of water

(pH=2.71). The mixture was kept in hydrothermal condition at 170 °C for 72 hours. ***Element Analysis:*** Found (%) C= 33.82, H= 2.05, N=6.71; Calc. (%) C= 34.08, H= 1.89, N= 6.63.

**Single crystal X-ray diffraction data collection, structure solution and refinement procedures:** Single crystal data were collected on Bruker SMART APEX three circle diffractometer equipped with a CCD area detector and operated at 1500 W power (50 kV, 30 mA) to generate Mo K_α radiation (λ=0.71073 Å). The incident X-ray beam was focused and monochromated using Bruker Excalibur Gobel mirror optics. The Crystals reported in the chapter was mounted on nylon CryoLoop (Hampton Research) with Paraton-N (Hampton Research). Initial scans of each specimen were performed to obtain preliminary unit cell parameters and to assess the mosaicity (breadth of spots between frames) of the crystal to select the required frame width for data collection. In every case frame widths of 0.5° were judged to be appropriate and full hemispheres of data were collected using the *Bruker SMART* [a] software suite. Following data collection, reflections were sampled from all regions of the Ewald sphere to redetermine unit cell parameters for data integration and to check for rotational twinning using *CELL_NOW*. In no data collection was evidence for crystal decay encountered. Following exhaustive review of the collected frames the resolution of the dataset was judged. Data were integrated using Bruker *SAINT* software with a narrow frame algorithm and a 0.400 fractional lower limit of average intensity. Data were subsequently corrected for absorption by the program *SADABS*. The space group determinations and tests for merohedral twinning were carried out using *XPREP*. In these cases, the highest possible space group was chosen.

Structures were solved by direct methods and refined using the *SHELXTL* 97 software suite. Atoms were located from iterative examination of difference F-maps following least squares refinements of the earlier models. Final model was refined anisotropically (if the number of data permitted) until full convergence was achieved. Hydrogen atoms were placed in calculated positions (C-H = 0.93 Å) and included as riding atoms with isotropic displacement parameters 1.2-1.5 times U_{eq} of the attached C atoms. In some cases modeling of electron density within the voids of the frameworks did not lead to identification of recognizable solvent molecules in these structures, probably due to the highly disordered contents of the large pores in the frameworks. Highly porous crystals that contain solvent-filled pores often yield raw data where observed strong (high intensity) scattering becomes limited to ~1.0 Å at best, with higher resolution data present at low intensity. A common strategy for improving

X-ray data, increasing the exposure time of the crystal to X-rays, did not improve the quality of the high angle data in these cases, as the intensity from low angle data saturated the detector and minimal improvement in the high angle data was achieved. Additionally, diffuse scattering from the highly disordered solvent within the void spaces of the framework and from the capillary to mount the crystal contributes to the background and the 'washing out' of the weaker data. The only optimal crystals suitable for analysis were generally small and weakly diffracting. Unfortunately, larger crystals, which would usually improve the quality of the data, presented a lowered degree of crystallinity and attempts to optimize the crystal growing conditions for large high-quality specimens have not yet been fruitful. Single Crystal X-ray Diffraction data for Cu-LAD was collected at 293(2) K. The foremost errors in all the models are thought to lie in the assignment of guest electron density. Structures were examined using the *ADDSYM* subroutine of *PLATON* to assure that no additional symmetry could be applied to the models. All ellipsoids in ORTEP diagrams are displayed at the 50% probability level unless noted otherwise.

N$_2$, H$_2$, and CO$_2$ adsorption measurements: Hydrogen adsorption-desorption experiments were conducted at 77K using Quantachrome Quadrasorb automatic volumetric instrument. Ultrapure H$_2$ (99.95%) was purified further by using calcium aluminosilicate adsorbents to remove trace amounts of water and other impurities before introduction into the system. For measurements at 77 K, a standard low-temperature liquid nitrogen Dewar vessel was used. CO$_2$ adsorption-desorption measurements were done at room temperature (298 K). To check the porosity of Cu-1D MOF, it was exchanged with anhydrous dichloromethane in 3 hours interval for 2 days. Before gas adsorption measurements, the sample was activated at 30 °C (for 12 h) under ultrahigh vacuum (10^{-8} mbar) overnight. About 75 mg of samples were loaded for gas adsorption, and the weight of each sample was recorded before and after out gassing to confirm complete removal of all guest molecules.

6.11 References

6.1　　(a) A. Moulin, M. Bibian, A. L. Blayo, S. E. Habnouni, J. Martinez, J. A. Fehrentz, *Chem. Rev.* **2010**, *110*, 1809. (b) J. Climent, A. Corma, S. Iborra, *Chem. Rev.* **2011**, *111*, 1072.

6.2　　(a) G. R. Desiraju, *Crystal Engineering: The Design of Organic Solids*; Elsevier: New York, **1989**. (b) J. -M. Lehn, *Supramolecular Chemistry: Concepts and Perspectives*; VCH Publishers: New York, **1995**. (c) T. J. Marks, M. A. Ratner,

Angew. Chem. Int. Ed. **1995**, *34*, 155. (d) G. R. Desiraju, *Acc. Chem. Res.* **2002***, 35*, 565.

6.3   (a) W. Lin, Z. Wang, L. Ma, *J. Am. Chem. Soc.* **1999***, 121*, 11249. (b) O. R. Evans, W. Lin, *Chem. Mater.* **2001***, 13*, 3009. (c) J. Tao, Y. Zhang, M. -L. Tong, X. -M. Chen, T. Yuen, C. L. Lin, X. Huang, J. Li, *Chem. Commun.* **2002**, 1342. (d) X.-M. Zhang, M.-L. Tong, X.-M. Chen, *Angew. Chem. Int. Ed.* **2002***, 41,* 1029.

6.4   H. Zhao, Z.-R. Qu, H.-Y. Ye, R.-G. Xiong, *Chem. Soc. Rev.* **2008**, *37,* 84.

6.5   L.-L. Fan, C. -J. Li, Z. -S. Meng, M. -L. Tong, *Eur. J. Inorg. Chem.* **2008**, 3905.

6.6   Z. Han, Y. Zhao, J. Peng, C. J. Gomez-Garcia, *Inorg. Chem.* **2007**, *46*, 5453.

6.7   (a) D. -L. Long, R.Tsunashima, L. Cronin, *Angew. Chem. Int. Ed.*   **2010**, *49*, 1736. (b) A. Muller, S. Q. N. Shah, H. Bogge, M. Schmidtmann, *Nature.* **1999**, *397*, 48.

6.8   G. R. Desiraju, T. Steiner, *The Weak Hydrogen Bond In Structural Chemistry and Biology, Oxford University Press, Oxford*, **2001**.

6.9   (a) J. W. Tye, Z. Weng, R. Giri, J. F. Hartwig, *Angew. Chem.* **2010**, *122*, 2231; *Angew. Chem. Int. Ed.* **2010**, *49*, 2185– 2189. (b) K. Latham, K. F. White, K. B. Szpakolski, C. J. Rix, J. M. White, *Inorg. Chim. Acta.* **2009**, *362*, 1872.

6.10   (a) R. Neumann, M. Dahan, *Nature*, **1997**, *388*, 353. (b) N. Mizuno, M. Misono, *Chem. Rev.* **1998**, *98*, 199– 217. (c) M. V. Vasylyev, R. Neumann, *J. Am. Chem. Soc.* **2004**, *126*, 884.

6.11   (a) J. P. Zhao, B. W. Hu, F. Lloret, J. Tao, Q. Yang, X. F. Zhang, X. H. Bu, *Inorg. Chem.*, **2010**, *49*, 10390.   (b) O. Kahn, *Molecular Magnetism, VCH, New York*, **1993**. (c) J. S. Miller, M. Drillon, *Magnetism: Molecules to Materials I–V, Wiley-VCH, Germany*, **2001**. (d) A. Escuer, G. Vlahopoulou, S. P. Perlepes, F. A. Mautner, *Inorg. Chem.* **2011**, *50*, 2468. (e) A. Aijaz, P. Lama, E. C.Sañudo, R.Mishra, P. K. Bharadwaj, *New J. Chem.* **2010**, *34*, 2502. (f) D. Maspoch, D. Ruiz-Molina, K. Wurst, C. Rovira, J. Veciana, *Chem. Commun.* **2002**, 2958. (g) Z. He, Z. –M. Wang, S. Gao, C. –H. Yan, *Inorg. Chem.* **2006**, *45*, 6694.

6.12   (a) J. A. R. Navarro, E. Barea, A. R. Dieguez, J. M. Salas, C. O. Ania, J. B. Parra, N. Masciocchi, S. Galli, A. Sironi, *J. Am. Chem. Soc.* **2008**, *130*, 3978. (b) D. Maspoch, D. Ruiz- Molina, K. Wurst, N. Domingo, M. Cavallini, F. Biscarini, J. Tejada, C. Rovira, J. Veciana, *Nat. Mater.* **2003**, *2*, 190.

6.13   P. Jain, V. Ramachandran, R. J. Clark, H. D. Zhou, B. H. Toby, N. S. Dalal, H. W. Kroto, A. K. Cheetham, *J. Am. Chem. Soc.* **2009**, *131*, 13625.

6.14   (a) H. L. Sun, Z. M. Wang, S. Gao, *Chem. Eur. J.* **2009**, *15*, 1757. (b) Y.L. Bai, J. Tao, W. Wernsdorfer, O. Sato, R.B. Huang, L.S. Zheng, *J. Am. Chem. Soc.* **2006**, *128*, 16428.

6.15   X. T. Liu, X. Y. Wang, W. X. Zhang, P. Cui, S. Gao, *Adv. Mater.* **2006**, *18*, 2852.

Note:

The results of this chapter have already been published in *ChemPhysChem*. **2013**, *14*, 1009–1015. with the title: "POM-Catalyzed In Situ Ligand Synthesis for the Construction of Metal Complexes and Their Use in the Formation of Coordination Polymers". This publication was the result Dr. Rahul Banerjee and his students Chandan Dey from the Physical/Materials Chemistry Division at CSIR-National Chemical Laboratory in Pune, India.

The results of this chapter also have already been published in *Chem. Commun.* **2011**, *47*, 11008–11010. with the title: "Design and in situ synthesis of a Cu-based porous framework featuring isolated double chain magnetic character ". This publication was the result of a collaboration between the group of Dr. Rahul Banerjee and his students Chandan Dey from the Physical/Materials Chemistry Division at CSIR-National Chemical Laboratory in Pune, India, Dr. Binoy Krishna Saha form Department of Chemistry, Pondicherry University in Pondicherry, India and the group of Dr. Pankaj Poddar with his student Raja Das from the Physical/Materials Chemistry Division at CSIR-National Chemical Laboratory in Pune, India. Dr. Binoy Krishna Saha helped to collect the single crystal data of Cu-LAD. Raja Das was involved in magnetic measurement of Cu-LAD.

Conclusion and Future Directive

7.1 Summary of the Chapters

First chapter is constructed with general informations regarding polyoxometalates (POMs). In this chapter polyoxometalates were defined first, then they were classified according to the constituent metals and hetero metals. The general synthesis procedures have been discussed accordingly for different POMs. Different application of POM based materials have been discussed briefly. Designing of smart materials using polyoxometalates has drawn current research attention due to their application in catalysis, magnetism, adsorption, separation, sensing etc. Different synthetic approaches to prepare POM based hybrid materials have been discussed finally.

POM based porous ionic crystals are easy to prepare and are advantageous over other porous materials due to their structural flexibility with respect to guest molecules. At the beginning of the chapter-II different POM based ionic crystals have been discussed for their potential application in sorption, separation and catalysis. We have synthesised a series of POM based ionic crystal using $[Co(en)_3]^{3+}$ cation and different POM anions. The salts have been characterized by single crystal X-ray diffraction and were used for selective adsorption of N_2 over H_2. This is first report of H_2 on POM based ionic salts.

Morphology of materials plays important role in determining the property of the materials. Changing morphology not only changes the surface area of the materials but also change the distribution of the active sites on surface. At the beginning of this chapter-III we have discussed the morphological diversity of different POM based hybrid materials and role of change in morphology was also discussed. We have prepared a vanadium cubane based coordination polymer in hydrothermal condition. The bulk compound shows two types of morphologies of same phase. We speculate that the needle type of morphology is the growth of crystal in three dimensions which is consists of two dimension sheet (flower morphology) of coordination polymer.

Proton conducting materials are important for fuel cell and bio-sensing application. Nafion is commonly used as proton conductor in fuel cell. Different metal oxide materials have been

used for proton conductivity at high temperature due to their high thermal stability. Metal organic frameworks (MOFs) being porous in nature provide opportunity to create a proton conducting path inside their porous matrix which contain inbuilt functionality inside the materials or loaded with different guest molecules such as water, imidazole, etc.I have described Strandberg type POM containing coordination polymer which thermally stable and holds one dimension parallel water channels to provide platform for proton conduction. The compound also shows reversible phase transformation (with distinct colour change) with respect to guest water molecules.

Metal organic frameworks (MOFs) are a class of porous materials which is built from metal ion and organic linkers. Although MOFs have been used for various applications such as adsorption, separation, magnetism, sensing, drug delivery, etc; but major application of MOFs are still limited in adsorption and separation. In this particular work (Chapter-V) we tried to incorporate metal oxide units inside MOFs to introduce catalytically active sites. We have tuned the synthetic condition to isolate pure metal oxide incorporated MOFs (MOZIF-1) from the mixture of ZIF-65 and MOZIF-1. Due to the presence of metal oxide units inside MOZIF-1 it was used for photocatalytic degradation of methyl orange and orange-II dye.

Preparation of ligand in situ is advantageous because it minimizes the difficulties of using hazardous chemical during the course of the process and reduces the problems of product separation each step. In chapter-VI we have studied oxidation of methyl group of neocuproine with Na_2MoO_4/MoO_3 catalyst in presence of HCl and Cu^{2+}. In hydrothermal condition by changing the pH of the medium we got different extent of oxidation of methyl group of neocuproine, even at high and temperature and pressure we found decarboxylation of oxidised carboxylic acid. The role of pH and concentration of reagent have been studied thoroughly through the process. When 1,3,5-benzene tricarboxylic acid was used as co-ligand, two coordination polymers were isolated at different pH. The coordination polymers were further studied for gas adsorption and magnetic properties.

7.2 Future Directives

7.2.1 Incorporation of POM inside metal organic framework

Metal organic frameworks (MOFs) are interesting class of porous network solids constructed form metal ions and organic linker. MOFs were mainly utilized for gas absorption in their

porous network for last two decades [7.1]. MOFs have systematic arrangement of pores in the network and the shape and size of pores can be controlled by changing the metal ions or organic ligands. MOFs have also shown some activity on catalysis [7.2], magnetism [7.3], ion exchange [7.4] etc, so far major activity of MOFs are limited in the area of absorption. The purpose of this proposal is to introduce functionality inside MOFs by incorporating polyoxometalates (POMs) [7.5] in the framework. A Keggin type POM encapsulated porous
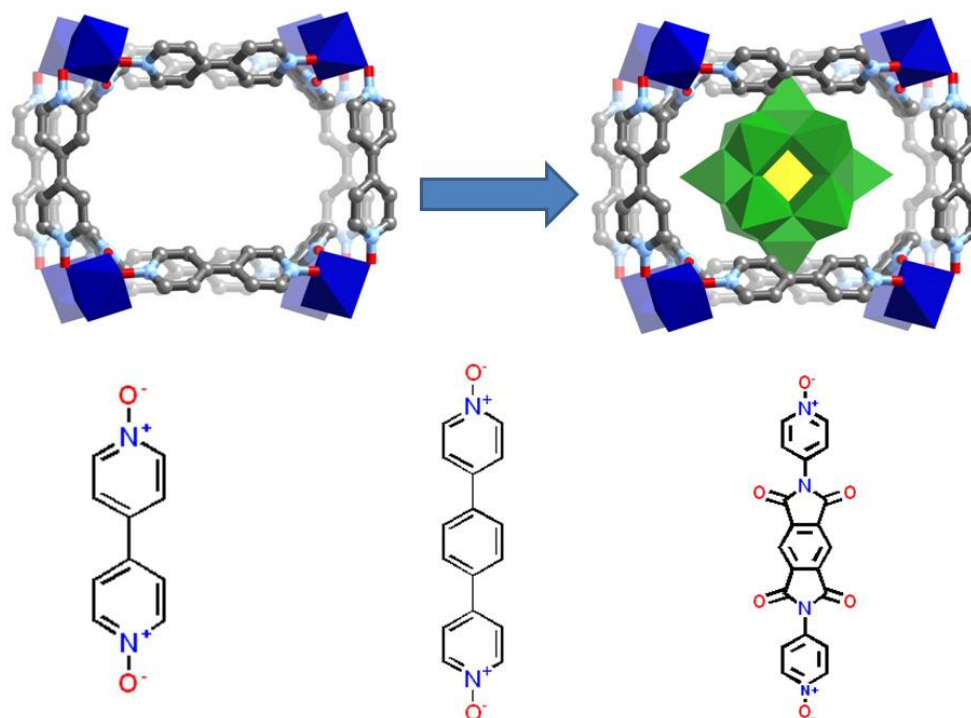

Figure 7.1: Keggin type POM has been incorporated inside MOF, $[Co_4(dpdo)_{12}][H(H_2O)_{27}(CH_3CN)_{12}][PW_{12}O_{40}]_3$. By varying the chain length of ligands it will be possible to increase free space inside POM loaded cavity which will be suitable for catalytic applications.

MOF, $[Co_4(dpdo)_{12}][H(H_2O)_{27}(CH_3CN)_{12}][PW_{12}O_{40}]_3$ was prepared by using $[PW_{12}O_{40}]^{3-}$ anion, 4,4′-bipyridine-*N*,*N*′-dioxide (dpdo) and Co^{2+}. The purpose of this proposal to use longer size *N*,*N*′-dioxide ligand to prepare POM incorporated MOFs with larger cavity inside the framework for better catalytic performance [7.6].

7.2.2 Incorporation of POM inside covalent organic frameworks (COFs)

Covalent organic frameworks (COFs) are two or three dimensional network structures constructed by organic monomeric units [7.7]. POMs are mostly soluble in polar solvents, but

the organic molecules (substrate for catalytic reaction) are soluble in organic solvent. The purpose of this proposal is built POM incorporated COFs as a biphasic medium for catalysis. COFs being hydrophilic in nature can interact with organic molecules even though the reaction in carried more environment friendly water medium. A COF material was prepared by the reaction of 1,3,5-triformylphloroglucinol with p-phenylenediamine in presence of 3 M acetic acid using 1:1 mesitylene/dioxane as the solvent [7.7b]. The aim of the proposal to incorporated POM inside COF via hydrothermal or mechanochemical process during the reaction or by post synthetic modifications.
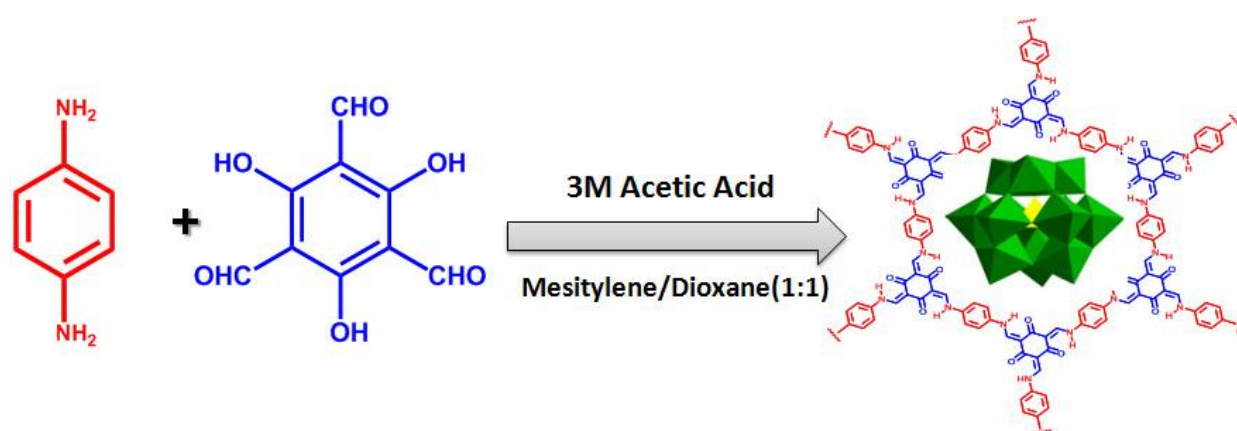

Figure 7.2: Scheme of synthesis of POM loaded COFs using 1,3,5-triformylphloroglucinol with *p*-phenylenediamine in presence of Keggin type POM.

7.2.3 POM Catalysed in situ ligand synthesis during formation of coordination polymer
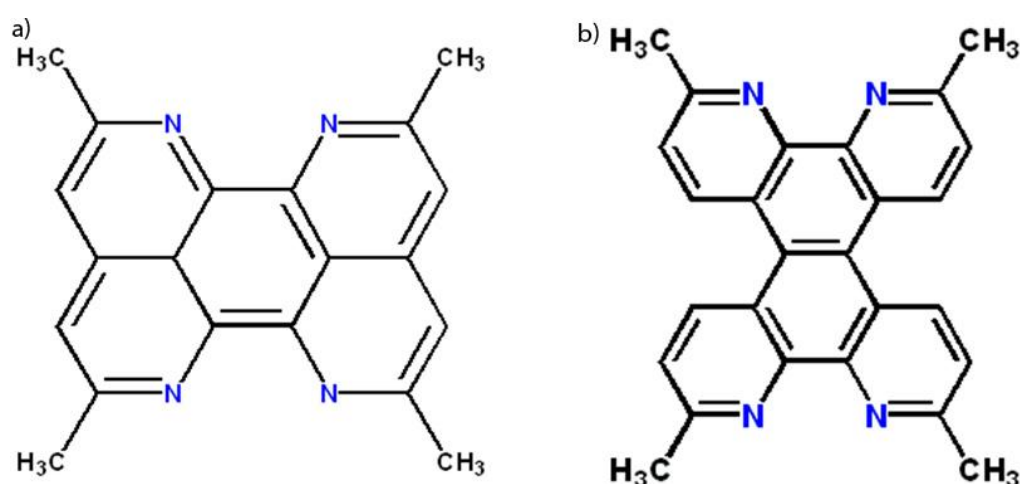

Figure 7.3: Scheme of substrates which could be used to produce multi-dented ligand in situ during the course of coordination polymer formation.

We have developed a synthesis strategy for preparation ligand in situ during formation of coordination polymer using Na_2MoO_4/MoO_3 in presence of HCl and Cu^{2+}. This synthesis method have been applied for preparation of coordination polymer in situ using 1,3,5-benzene tri carboxylic acid as co-ligand. Two coordination polymers were isolated using same ingredient just by changing the pH of the medium. The same methodology can be utilized further for preparing multi-dented ligand in situ during the course of reaction to construct more complex three dimensional structures.

7.3 Reference

7.1   (a) A. -C. Sudik, A. -P. Cote, A. G. Wong-Foy, M.; O'Keeffe, O. M. Yaghi, *Angew. Chem., Int.* Ed. **2006**, *45,* 2528. (b) A. Kondo, H. Noguchi, H. Kajiro, L. Carlucci, P. Mercandelli, D. -M. Proserpio, M. Respiration, *J. Phys. Chem. B.* **2006**, *110,* 25565. (c) M. Hong, *Cryst. Growth Des*. **2007**, *7,* 10. (d) C. Janiak, *Dalton Trans.* **2003**, *14,* 2781. (e) C. N. R. Rao, A. K. Cheetham, A. Thirumurugan, *J. Phys.:Condens. Matter* **2008**, *20,* 083202. (f) R. Robson, *Dalton Trans.* **2008**, 5113.

7.2   (a) C. D. Wu, A. Hu, L. Zhang, W. B. Lin, *J. Am. Chem. Soc.* **2005**, *127,* 8940. (b) W. B. Lin, *J. Solid State Chem.* **2005**, *178,* 2486. (c) M. Fujita, Y. J. Kwon, S. Washizu, K. Ogura, *J. Am. Chem. Soc*. **1994**, *116*, 1151. (d) J. S. Seo, D. Whang, H. Lee, S. I. Jun, J. Oh, Y. J. Jeon, K. Kim, *Nature*. **2000**, *404*, 982. (e) O. Ohmori, M. Fujita, *Chem. Commun*. **2004**, *10,* 1586. (f) W. Lin, *MRS Bull.* **2007**, *32,* 544.

7.3   (a) R. -D. Poulsen, A. Bentien, M. Chevalier, B. -B. Iversen, *J. Am. Chem. Soc.* **2005**, *127,* 9156. (b) S. -K. Ghosh, J. Ribas, M. -S. Fallah, P. -K. Bharadwaj, *Inorg. Chem.* **2005**, *44,* 3856. (c) S. -C. Xiang, X. -T. Wu, J. -J. Zhang, R. -B. Fu, S. -M. Hu, X. -D. Zhang, *J. Am. Chem. Soc*. **2005**, *127,* 16352. (d) F. Luo, D. -X. Hu, L. Xue, Y. -X. Che, J. -M. Zheng, *Cryst. Growth Des.* **2007**, *7,* 851.

7.4   (a) O. M. Yaghi, H. Li, *J. Am. Chem. Soc.* **1996**, *118,* 295. (b) T. K. Maji, R. Matsuda, S. Kitagawa, *Nat. Mater.* **2007**, *6*, 142. (c) K. S. Min, M. P. Suh, *J. Am. Chem. Soc.* **2000**, *122,* 6834.

7.5   (a) P. Gouzerh, A. Proust, *Chem. Rev.* **1998**, *98*, 77. (b) K. Binnemans, *Chem. Rev.* **2009,** *109*, 4283. (c) D. –L. Long, R. Tsunashima, L. Cronin, *Angew. Chem., Int. Ed.* **2010**, *49,* 1736. (d) E. Coronado, C. L. Gomez-Garcia, *Chem. Rev*. **1998**, *98*, 273. (e) D. E. Katsoulis, *Chem. Rev*. **1998**, *98*, 359. (f) Y. P. Jeannin, *Chem. Rev*. **1998**, *98*, 51. (g) A. Muller, S. Q. N. Shah, H. Bogge, M. Schmidtmann, *Nature*. **1999**, *397*, 48. (h)

A.; Muller, E.; Beckmann, H.; Bogge, M. Schmidtmann, A. Dress, *Angew. Chem., Int. Ed.* **2002**, *41*, 1162.

7.6 C. Duan, M. Wei, D. Guo, C. He, Q. Meng, *J. Am. Chem. Soc.* **2010**, *132*, 3321.

7.7 (a) A. P. Cote, A. I. Benin, N. W. Ockwig, M. O'Keeffe, A. J. Matzger, O. M. Yaghi, *Science*. **2005**, *310*, 1166. (b) S. Kandambeth, A. Mallick, B. Lukose, M. V. Mane, T. Heine, R. Banerjee, *J. Am. Chem. Soc.* **2012**, *134*, 19524.

7.8 C. Dey, R. Banerjee, *ChemPhysChem*. **2013**, *14*, 1009.

List of Publications

1. Synthesis and structural comparisons of five new fluorinated metal organic frameworks (F-MOFs). Pradip Pachfule, **Chandan Dey**, Tamas Panda and Rahul Banerjee. *CrystEngComm*. **2010**, *12*, 1600.

2. Structural diversity in a series of metal–organic frameworks (MOFs) composed of divalent transition metals, 4,4'-bipyridine and a flexible carboxylic acid. Pradip Pachfule, Tamas Panda, **Chandan Dey** and Rahul Banerjee, *CrystEngComm*. **2010**, *12*, 2381.

3. Structural Diversity in Partially Fluorinated Metal Organic Frameworks (F-MOFs) Composed of Divalent Transition Metals, 1,10-Phenanthroline, and Fluorinated Carboxylic Acid. Pradip Pachfule, **Chandan Dey**, Tamas Panda, Kumar Vanka and Rahul Banerjee, *Cryst. Growth Des*. **2010**, *10*, 1351.

4. Structural and Selective Gas Adsorption Studies of Polyoxometalate and Tris(ethylenediamine) Cobalt(III) Based Ionic Crystals. **Chandan Dey**, Raja Das, Pradip Pachfule, Pankaj Poddar, and Rahul Banerjee *Cryst. Growth Des*. **2011**, *11*, 139.

5. Design and In situ Synthesis of Cu-Based Porous Framework Featuring Isolated Double Chain Magnetic Character. **Chandan Dey**, Raja Das, Binoy K. Saha, Pankaj Poddar and Rahul Banerjee. *Chem. Commun*. **2011**, *47*, 11008.

6. Reversible Phase Transformation in Proton Conducting Strandberg-type POM Based Metal Organic Material. **Chandan Dey**, Tanay Kundu, and Rahul Banerjee *Chem. Commun*. **2012**, *48*, 266.

7. Solid phase Morphological Diversity of a Rare Vanadium Cubane(V4O16) Based Metal Organic Framework. **Chandan Dey**, Raja Das, Pankaj Poddar and Rahul Banerjee. *Cryst. Growth & Design*. **2012**, *12*, 12.

8. POM Catalyzed In Situ Ligand Synthesis for Construction of Metal Complexes to Coordination Polymers. **Chandan Dey** an Rahul Banerjee. *ChemPhysChem*. **2013**, *14*, 1009.

9. Controlled Synthesis of a Catalytically Active Hybrid Metal-Oxide Incorporated Zeolitic Imidazolate Framework (MOZIF). **Chandan Dey** and Rahul Banerjee. *Chem. Commun*. **2013**, *49*, 6617.

10. A high stereocontrolled asymmetric total synthesis of epimer of (+)-7-deoxypancratistatin. Subhash P. Chavan, Sumanta Garai, **Chandan Dey**, Rajesh G. Gonnade. *Tetrahedron Lett*. **2013**, *54*, 5562.

11. Ligand-free one-step synthesis of {001} faceted semiconducting BiOCl single crystals and their photocatalytic activity. Anupam Biswas, Raja Das, **Chandan Dey**, Rahul Banerjee, Poddar Pankaj. *Cryst. Growth Des*. **2014**, *14*, 236.

12. Crystalline Metal Organic Frameworks (MOFs): Synthesis, Structure and Function. **Chandan Dey**, Tanay Kundu, Bishnu P. Biswal, Arijit Mallick, Rahul Banerjee. *Acta Cryst*. **2014**, *B70*, 3.

Comments and Suggestions

Comments and Suggestions

CSIR-National Chemical Laboratory
Pune, India